INL/EXT-20-59906

Light Water Reactor Sustainability Program

Risk-Informed ATF and FLEX Analysis for an Enhanced Resilient BWR Under Design-Basis and Beyond-Design-Basis Accidents

September 2020

U.S. Department of Energy

Office of Nuclear Energy

INL/EXT-20-59906

Risk-Informed ATF and FLEX Analysis for an Enhanced Resilient BWR Under Design-Basis and Beyond-Design-Basis Accidents

Zhegang Ma
Sai Zhang
Hongbin Zhang
Jooyoung Park
Jianguo Yu
Cole Blakely
Thomas Ulrich
Ronald Boring

September 2020

Prepared for the
U.S. Department of Energy
Office of Nuclear Energy

EXECUTIVE SUMMARY

This report documents the activities performed by the Idaho National Laboratory (INL) during fiscal year (FY) 2020 for the U.S. Department of Energy (DOE) Light Water Reactor Sustainability (LWRS) Program, Risk-Informed Systems Analysis (RISA) Pathway, Enhanced Resilient Plant (ERP) Systems research. The purpose of the RISA Pathway research and development is to support plant owner-operator decisions with the aim to improve the economics, reliability, and maintain the high levels of safety of current nuclear power plants over periods of extended plant operations. The concept of ERP refers to the combinations of accident-tolerant fuel (ATF), optimal use of diverse and flexible coping strategy (FLEX), enhancements to plant components and systems, and the incorporation of augmented or new passive cooling systems, as well as improved fuel cycle efficiency. The objective of the ERP research effort is to use the RISA methods and toolkit in industry applications, including methods development and early demonstration of technologies, in order to enhance existing reactors' safety features (both active and passive) and to substantially reduce operating costs through risk-informed approaches to plant design modifications to the plant and their characterization.

One main focus of the FY 2020 efforts documented in this report was to extend the analyses conducted in FYs 2018 and 2019 for a pressurized water reactor (PWR) to a boiling water reactor (BWR). The same analysis process, risk analysis approaches, and analysis tools as in the previous work for PWR were used for a generic BWR with near-term ATF cladding (i.e., Iron-Chromium-Aluminum [FeCrAl] cladding and Chromium [Cr]-coated cladding) designs under the postulated station blackout (SBO) and medium loss-of-coolant (MLOCA) accident scenarios. In addition, a FLEX model was developed and incorporated into a generic BWR probabilistic risk assessment (PRA) model using the INL-developed software tool, Systems Analysis Programs for Hands-on Integrated Reliability Evaluations (SAPHIRE), to assess the risk impact from FLEX. The other main focus of the FY 2020 efforts was to advance analysis methods, including developing dynamic approach for FLEX human reliability analysis (HRA) using the INL-developed software tool, Event Modeling Risk Assessment using Linked Diagrams (EMRALD), as well as developing a multicriterion benefit evaluation (MCBE) method for evaluating costs and benefits of safety enhancements in nuclear power plants (NPPs). As a case study, the MCBE method was applied to evaluate the costs and benefits brought by FLEX implementation.

In the BWR ATF SBO analysis, nine SBO scenarios were developed and analyzed using Reactor Excursion and Leak Analysis Program 5-3D (RELAP5-3D) for thermal hydraulic analysis with traditional fuel design and near-term ATF designs. Due to the spectral shift operations of BWRs, the axial power shapes tend to be bottom peaked near the beginning-of-the-cycle (BOC), cosine shaped in the middle-of-the-cycle (MOC), and top-peaked in the end of the cycle (EOC). The RELAP5-3D simulations were performed using bottom-peaked, cosine, and top-peaked power shapes to represent the operating state at BOC, MOC, and EOC, respectively. The RELAP5-3D simulation results, including the time-to-core-damage (CD) and the production of hydrogen for traditional fuel design (Zircaloy, or Zry) and two near-term ATF designs (FeCrAl and Cr-coated), are presented in Tables ES-1 and ES-2 for BOC. The results show that the gain of coping time, or the delay of time to CD due to the ATF designs, is less than 20 minutes for most SBO scenarios. At BOC, for FeCrAl, eight of the nine analyzed SBO scenarios have a gain of coping time from 4 to 20 minutes. The other scenario has a gain of coping time of 50 minutes. For Chromium-coated cladding, eight of the nine analyzed SBO scenarios have a gain of coping time from 1 to 15 minutes. The other scenario has a gain of coping time of 42 minutes. The coping time gains at MOC and EOC are similar to, albeit a bit less, than those at BOC. The MOC and EOC results can be found in the corresponding sections of the report.

Table ES-1. Time-to-Core-Damage Comparison for SBO Scenarios with ATF Designs at BOC.

Scenario	Scenario Description				Time to CD t_{CD} (hh:mm)			Time to CD t_{CD} (hh:mm)		
					Zry	Cr-coated	Δt	Zry	FeCrAl	Δt
SBO-1	No SRV stuck open	RCIC available	HPCI not available	AC power not recovered in 4 hrs	6:59	7:11	0:12	6:59	7:19	0:20
SBO-1-1	No SRV stuck open	RCIC not available	HPCI available	AC power not recovered in 4 hrs	8:21	8:30	0:09	8:21	8:49	0:18
SBO-1-2	One SRV stuck open	RCIC available	HPCI not available	AC power not recovered in 4 hrs	7:31	7:38	0:07	7:31	7:47	0:16
SBO-1-3	One SRV stuck open	RCIC not available	HPCI available	AC power not recovered in 4 hrs	10:37	10:52	0:15	10:37	10:53	0:16
SBO-2	No SRV stuck open	RCIC not available	HPCI not available	AC power not recovered in 4 hrs	1:14	1:19	0:05	1:14	1:24	0:10
SBO-2-1	One SRV stuck open	RCIC not available	HPCI not available	AC power not recovered in 4 hrs	1:02	1:07	0:05	1:02	1:11	0:09
SBO-3	All SRVs stuck open	RCIC not available	HPCI not available	AC power not recovered in 4 hrs	0:31	0:32	0:01	0:31	0:35	0:04
SBO-4	No SRV stuck open	RCIC available HPCI not available	AC power recovered in 4 hrs	DEP success SPC failed	10:20	10:21	0:01	10:20	10:33	0:13
SBO-4-1	No SRV stuck open	RCIC available HPCI not available	AC power recovered in 4 hrs	DEP failed SPC failed	11:56	12:38	0:42	11:56	12:46	0:50

* Acronyms include: SRV = safety relief valve, RCIC = reactor core isolation cooling, HPCI = high-pressure core injection, AC = alternating current, DEP = depressurization, SPC = suppression pool cooling.

Table ES-2. Comparing H_2 Productions for SBO Scenarios with ATF Designs at BOC.

Scenario	Scenario Description				Total H_2 (kg)			H_2 %	
					Zry	Cr-coated	FeCrAl	Cr-coated	FeCrAl
SBO-1	No SRV stuck open	RCIC available	HPCI not available	AC power not recovered in 4 hrs	31.02	6.05	0.55	19.5	1.8
SBO-1-1	No SRV stuck open	RCIC not available	HPCI available	AC power not recovered in 4 hrs	32.24	6.23	0.65	19.3	2.0
SBO-1-2	One SRV stuck open	RCIC available	HPCI not available	AC power not recovered in 4 hrs	26.35	11.11	0.33	42.2	1.3
SBO-1-3	One SRV stuck open	RCIC not available	HPCI available	AC power not recovered in 4 hrs	26.20	5.19	0.41	19.8	1.6
SBO-2	No SRV stuck open	RCIC not available	HPCI not available	AC power not recovered in 4 hrs	24.08	4.11	0.30	17.1	1.2
SBO-2-1	One SRV stuck open	RCIC not available	HPCI not available	AC power not recovered in 4 hrs	46.25	5.44	0.44	11.8	1.0
SBO-3	All SRVs stuck open	RCIC not available	HPCI not available	AC power not recovered in 4 hrs	10.30	1.12	0.07	10.9	0.7
SBO-4	No SRV stuck open	RCIC available HPCI not available	AC power recovered in 4 hrs	DEP success SPC failed	13.07	1.91	0.13	14.6	1.0
SBO-4-1	No SRV stuck open	RCIC available HPCI not available	AC power recovered in 4 hrs	DEP failed SPC failed	34.05	7.25	1.10	21.3	3.2

With only a marginal increase of the time-to-core-damage with the FeCrAl and Cr-coated designs, the risk-benefit on behalf of the core damage frequency (CDF) as the risk metrics would be very small for the generic BWR. A simplified approach using a multiplication factor developed in previous ERP work was adopted in this report to estimate the risk impact of the ATF design with the small increase of the coping time. The BWR SBO SAPHIRE model was quantified using the coping time gains at BOC, MOC, EOC,

respectively. The SAPHIRE model quantification results, as presented in Tables ES-3 and ES-4 for BOC, show that the marginal coping time increase would lead to about 5% and 3% weather-related loss-of-offsite-power (LOOP) CDF reductions for the FeCrAl and Cr-coated designs at BOC, respectively. These CDF reductions are relatively small; however, this should not be misinterpreted as no benefits from the ATF. In fact, RELAP5-3D simulation results showing a clear benefit in adopting ATFs with much less hydrogen produced at the time of CD. It can be a few times lower for the Cr-coated cladding, and up to two orders of magnitude lower for FeCrAl cladding than with Zircaloy cladding cases. The CDF reductions at MOC and EOC are similar to, albeit slightly less than those at BOC. The MOC and EOC results can be found in the corresponding sections of the report.

Table ES-3. Weather-related SBO CDF Estimation for FeCrAl at BOC.

	Time to CD t_{CD} (hh:mm)			Power Recovery	CDF_0	F_{CT}	CDF'	ΔCDF	$\Delta CDF\%$
	Zr	FeCrAl	Δt						
SBO-1	6:59	7:19	0:20	4hrs No	2.77E-07	0.95	2.64E-07	-1.27E-08	-5%
SBO-1.1	8:21	8:49	0:28	4hrs No	4.10E-08	0.94	3.84E-08	-2.59E-09	-6%
SBO-1.2	7:31	7:47	0:16	4hrs No	2.65E-08	0.96	2.55E-08	-9.81E-10	-4%
SBO-1.3	10:37	10:53	0:16	4hrs No	3.80E-09	0.96	3.66E-09	-1.40E-10	-4%
SBO-2	1:14	1:24	0:10	0.5hrs Yes	1.68E-12	0.96	2.09E-12	4.15E-13	25%
SBO-2	1:14	1:24	0:10	0.5hrs No	1.27E-08	0.95	1.20E-08	-6.62E-10	-5%
SBO-2.1	1:02	1:11	0:09	--	3.44E-09	--	3.44E-09	0.00E+00	0%
SBO-3	0:31	0:35	0:04	--	2.85E-09	--	2.85E-09	0.00E+00	0%
SBO-4	10:20	10:33	0:13	4hrs Yes	2.22E-11	0.98	2.27E-11	5.00E-13	2%
SBO-4.1	11:56	12:46	0:50	4hrs Yes	3.15E-12	0.93	3.40E-12	2.55E-13	8%
Total					3.67E-07		3.50E-07	-1.71E-08	-5%

Table ES-4. Weather-related SBO CDF Estimation for Cr-coated at BOC.

	Time to CD t_{CD} (hh:mm)			Power Recovery	CDF_0	F_{CT}	CDF'	ΔCDF	$\Delta CDF\%$
	Zr	Cr-coated	Δt						
SBO-1	6:59	7:11	0:12	4hrs No	2.77E-07	0.97	2.69E-07	-7.75E-09	-3%
SBO-1.1	8:21	8:30	0:09	4hrs No	4.10E-08	0.98	4.01E-08	-8.66E-10	-2%
SBO-1.2	7:31	7:38	0:07	4hrs No	2.65E-08	0.98	2.61E-08	-4.37E-10	-2%
SBO-1.3	10:37	10:52	0:15	4hrs No	3.80E-09	0.97	3.67E-09	-1.32E-10	-3%
SBO-2	1:14	1:19	0:05	0.5hrs Yes	1.68E-12	0.98	1.89E-12	2.14E-13	13%
SBO-2	1:14	1:19	0:05	0.5hrs No	1.27E-08	0.97	1.23E-08	-3.43E-10	-3%
SBO-2.1	1:02	1:07	0:05	--	3.44E-09	--	3.44E-09	0.00E+00	0%
SBO-3	0:31	0:32	0:01	--	2.85E-09	--	2.85E-09	0.00E+00	0%
SBO-4	10:20	10:21	0:01	4hrs Yes	2.22E-11	1.00	2.22E-11	3.94E-14	0%
SBO-4.1	11:56	12:38	0:42	4hrs Yes	3.15E-12	0.94	3.36E-12	2.17E-13	7%
Total					3.67E-07		3.58E-07	-9.52E-09	-3%

Sensitivity analyses were performed for traditional fuel design and two near-term ATF designs under two SBO scenarios to examine how the combination of ATF and certain advanced technologies or

operations could postpone the time to CD and increase the coping time. Three sensitivity calculations were conducted, including increased reactor core isolation cooling (RCIC) operation time, FLEX equipment startup time, and RCIC blackstart operations. The results show an almost linear relationship between the time to CD and the RCIC operation time, significant effects of the FLEX startup time on the SBO mitigation, and considerable coping time gains provided by the combination of RCIC blackstart and ATF.

In the BWR ATF MLOCA analysis, four MLOCA scenarios were developed and analyzed using RELAP5-3D for thermal hydraulic analysis with traditional fuel design and near-term ATF designs. The RELAP5-3D simulations were also performed at BOC, MOC, and EOC. The RELAP5-3D simulation results, as presented in Tables ES-5 and ES-6 for BOC, show that for Cr-coated cladding, the gain of coping time, or the delay of time to CD, ranges from 2 minutes to 4 minutes for MLOCA-4, and less than 2 minutes for other MLOCA scenarios. For FeCrAl cladding, the gain on coping time ranges from 3 minutes to 11 minutes for the MLOCA scenarios. Although the relatively small increase of the time to CD from the RELAP5-3D simulation results would bring some margin of time for associated operator actions, a change to the general MLOCA PRA model is not warranted. The ATF designs would bring risk benefits to the plants even though the benefits are small and not quantified for MLOCA. Also, the RELAP5-3D simulation results show the clear benefit in adopting ATFs with much less hydrogen produced at the time of CD, which can be a few times lower for the Cr-coated cladding, and up to two orders of magnitude lower for FeCrAl cladding than that with Zircaloy cladding cases.

Table ES-5. Time-to-Core-Damage Comparison for MLOCA Scenarios with ATF Designs at BOC.

Scenario	Scenario Description	Time-to-Core-Damage t_{CD} (s)					
		Zry	Cr-coated	Δt	Zry	FeCrAl	Δt
MLOCA-1	VSS, No HPCI, No DEP, No LPI/VA	854	911	57	854	1127	273
MLOCA-2	VSS, No HPCI, DEP, No LPI/VA	809	922	113	809	1111	302
MLOCA-3	No VSS, No HPCI, No DEP, No LPI/VA	834	938	104	834	1139	305
MLOCA-4	VSS, HPCI, No LPI/VA	1914	2133	219	1914	2564	650

* Acronyms include: VSS = vapor suppression system, HPCI = high-pressure core injection, DEP = depressurization, LPI = low pressure injection, VA = alternate low pressure injection.

Table ES-6. Comparing H2 Productions for MLOCA Scenarios with ATF Designs at BOC.

Scenario	Scenario Description	Total H_2 (kg)			H_2 %	
		Zry	Cr-coated	FeCrAl	Cr-coated	FeCrAl
MLOCA-1	VSS, No HPCI, No DEP, No LPI/VA	21.9	1.9	0.2	8.6	1.1
MLOCA-2	VSS, No HPCI, DEP, No LPI/VA	16.6	2.2	0.2	13.4	1.4
MLOCA-3	No VSS, No HPCI, No DEP, No LPI/VA	17.8	2.0	0.2	11.1	1.3
MLOCA-4	VSS, HPCI, No LPI/VA	40.3	10.2	2.4	25.4	5.9

In the FLEX PRA analysis, FLEX equipment, including portable diesel generators and reactor pressure vessel makeup pumps, and associated human actions were modeled and incorporated into the generic BWR SAPHIRE model. Table ES-7 shows that the total LOOP CDF with FLEX from the generic model is 1.45E-6 per year, which is a 15% reduction when compared with the total LOOP CDF with no FLEX (1.71E-6 per year). Note that these results represent the risk impact on a generic BWR plant. Plant-specific analysis would have different results due to different structure, system, and component configurations, different risk profiles, and different structure, system, and component (SSC) risk contributions and significance. Plant-specific FLEX analyses should be conducted to evaluate specific risk impacts from the planned or implemented FLEX equipment and strategies.

Table ES-7. FLEX BWR PRA Model Quantification Results.

LOOP ET	CDF No FLEX	CDF with FLEX	ΔCDF	ΔCDF%
LOOPGR	4.97E-07	4.52E-07	-4.44E-08	-8.94%
LOOPPC	7.36E-08	7.34E-08	-2.00E-10	-0.27%
LOOPSC	5.79E-07	5.41E-07	-3.75E-08	-6.48%
LOOPWR	5.61E-07	3.86E-07	-1.75E-07	-31.19%
LOOP Total	1.71E-06	1.45E-06	-2.57E-07	-15.03%

In the FLEX HRA analysis, dynamic simulation approaches were explored to account for contextual and time uncertainties that have been missing in traditional HRA. Two FLEX HRA models with different approaches were developed using EMRALD. One FLEX HRA model is mainly developed on the basis of procedure contexts, while the other one depends on PRA/HRA modeling approaches. Benefits of EMRALD HRA modeling versus traditional HRA include: (1) evaluating HRA uncertainty by inclusively considering error probabilities, time-related factors, and equipment failures; (2) improving consideration of the dynamic context between human actions with statistic time distributions; and (3) modeling operator actions in a more nuanced and realistic manner. These first efforts were for proof of concept and still require additional fidelity to accurately capture realistic conditions; however, the initial modeling effort success was observed in demonstrating the feasibility of modeling FLEX-related human actions dynamically using EMRALD.

In the MCBE analysis, a comprehensive costs and benefits evaluation scope was established using multiple evaluation criteria (including public risk, occupational risk, plant revenue, and plant cost) and multiple contexts (including plant normal operations, incidents, and accidents). The MCBE method also reflects a decision maker's preferences toward hazard likelihood and consequence into cost and benefit estimations using cumulative prospect theory. The MCBE was applied to the FLEX implementation in a generic PWR plant as a case study. Preliminary, proof-of-concept results were obtained, indicating that, if FLEX were implemented at the reference plant for 20 years, the benefits of FLEX implementation are expected to outweigh the costs. The results also suggested that although FLEX was originally designed to cope with accidents, it would be beneficial to explore additional FLEX credit in plant operation and maintenance-efficiency improvement.

In evaluating the potential for fuel-rod bursts using BISON, simulations were carried out for Zircaloy and FeCrAl claddings under the SBO-2 scenario. The simulation results indicate that the evolution of the full-length BWR fuel-rod behavior is mainly determined by the cladding or coolant temperature. The results also strongly suggest that, although the clad melting temperature or peak cladding temperature may be a direct indicators of fuel-rod failures, it is more realistic to use a cladding failure criterion due to the cladding burst to determine the coping time. The simulated time to failure is about 5000 and 3900 seconds for FeCrAl and Zircaloy cladding, respectively. Thus, an increase of 1100 seconds in coping time may be reached using FeCrAl cladding.

CONTENTS

FIGURES

TABLES

ACRONYMS

AC	alternating current
ADS	automatic depressurization system
ATF	accident-tolerant fuel
BC	boundary condition
BCR	benefit-to-cost ratio
BDBEE	beyond-design-basis external event
BOC	beginning of the cycle
BWR	boiling water reactor
CBA	cost-benefit analysis
CCDP	conditional core damage probability
CCF	common-cause failure
CD	core damage
CDF	core damage frequency
CFR	Code of Federal Regulations
CLD	causal-loop diagram
CPT	cumulative prospect theory
Cr	Chromium
CRDHS	control rod drives hydraulic system
CS	core spray
CSS	containment spray system
CST	condensate storage tank
CT	completion time
CVS	containment venting system
DBA	design-basis accident
DC	direct current
DG	diesel generator
DID	defense in depth
DM	decision maker
DOE	Department of Energy
DW	drywell
ECCS	emergency core cooling system
EDG	emergency diesel generator
EIA	economic impact analysis

ELAP	extended loss of AC power
EOC	end of the cycle
EPRI	Electric Power Research Institute
EPS	emergency power system
ERP	enhanced resilient plant
ESD	event-sequence diagram
ET	event tree
FeCrAl	Iron-Chromium-Aluminum
FLEX	diverse and flexible coping strategy
FT	fault tree
FTLR	fail-to-load-and-run
FTR	fail-to-run
FTS	fail-to-start
FY	fiscal year
GE	General Electric
GNF	Global Nuclear Fuel
GOMS	goals, operators, methods, and selection
GUI	graphical user interface
HEP	human error probabilities
HFE	human failure event
HPCI	high pressure core injection
HRA	human reliability analysis
HX	heat exchanger
INL	Idaho National Laboratory
ISI	in-service inspection
IST	in-service testing
LER	large early release
LERF	large early release frequency
LI	late injection
LOCA	loss-of-coolant accident
LOOP	loss of offsite power
LPCI	low pressure core injection
LPCS	low pressure core spray
LPI	low pressure injection
LTSBO	long-term station blackout

LWR	light water reactor
LWRS	light water reactor sustainability
MCBE	multicriterion benefit evaluation
MCR	main control room
MLOCA	medium loss-of-coolant
MOC	middle of the cycle
MSIV	main steam isolation valves
NEI	Nuclear Energy Institute
NOED	notice of enforcement discretion
NOV	notice of violation
NPP	nuclear power plant
NPSH	net positive suction head
NPSHA	available net positive suction head
NPSHR	required net positive suction head
NRC	Nuclear Regulatory Commission
NUREG	nuclear regulatory report
O&M	operation and maintenance
OS	overstress
PCT	peak clad temperature
PI	plasticity instability
PRA	probabilistic risk assessment
PWR	pressurized water reactor
PWROG	PWR Owners Group
R&D	research and development
RA	risk assessment
RAVEN	Risk Analysis and Virtual Control Environment
RCIC	reactor core isolation cooling
RCP	reactor coolant pump
RELAP5-3D	Reactor Excursion and Leak Analysis Program 5–3D
RFO	refueling outage
RHR	residual heat removal
RISA	risk-informed systems analysis
ROM	reduced order model
RPS	reactor protection system
RPV	reactor pressure vessel

SAPHIRE	Systems Analysis Programs for Hands-on Integrated Reliability Evaluations
SBO	station blackout
SDP	significance determination process
SG	steam generator
SGP	steam generator pump
SLCS	standby liquid control system
SP	suppression pool
SPAR-H	standardized plant analysis risk – human reliability analysis
SRV	safety relief valve
SSC	structure, system, and component
STSBO	short-term station blackout
TBV	turbine bypass valve
TH	thermal-hydraulic
TM	testing and maintenance
TS	technical specification
TSSD	technical specification-required reactor shutdown
U.S.	United States
UTS	ultimate tensile strength
VSS	vapor suppression
WW	wetwell

RISK-INFORMED ATF AND FLEX ANALYSIS FOR AN ENHANCED RESILIENT BWR UNDER DESIGN-BASIS AND BEYOND-DESIGN-BASIS ACCIDENTS

1. INTRODUCTION

This report documents the activities performed by Idaho National Laboratory (INL) during fiscal year (FY) 2020 for the U.S. Department of Energy (DOE) Light Water Reactor Sustainability (LWRS) Program, Risk-Informed Systems Analysis (RISA) Pathway, Enhanced Resilient Plant (ERP) Systems research (Idaho National Laboratory, 2018). The LWRS Program is a research and development (R&D) program that provides technical foundations for the continued operation of the nation's nuclear power plants (NPPs), develops methods to support safe and economical long-term management and operation of existing NPPs, and investigates new technologies to address enhanced nuclear power plant performance, economics, and safety. With the continuing economic challenges faced by NPPs, the LWRS Program has redirected some of its R&D efforts to consider how to leverage the results from other ongoing R&D activities to improve the economic performance of LWRs in current and future energy markets. The RISA Pathway is one of the primary technical areas of R&D under the LWRS Program. This pathway supports decision-making related to economics, reliability, and safety by providing integrated plant system analysis and solutions through collaborative demonstrations to enhance economic competitiveness of operating NPPs. The purpose of RISA Pathway R&D is to support plant owner-operator decisions to improve economics and reliability, and to maintain the high levels of safety of current NPPs over periods of extended plant operations. The goals of the RISA Pathway are:

- To demonstrate risk-assessment methods coupled to safety margin quantification that can be used by decision-makers as a part of their margin recovery strategies
- To apply the "RISA toolkit" to enable more accurate representations of safety margins for the long-term benefit of nuclear assets.

One of the research efforts under the RISA Pathway is the ERP system analysis, which supports the DOE and industry initiatives including accident-tolerant fuel (ATF), diverse and flexible coping strategy (FLEX), and passive cooling system designs, in order to improve the safety and economic performance of the current fleet of NPPs. The ATF, combined with the optimal use of FLEX, the enhancements to plant components and systems, the incorporation of augmented or new passive cooling systems, and the improved fuel cycle efficiency are called ERP Systems. The objective of the ERP research effort is to use the RISA methods and toolkit in industry applications, including methods development and early demonstration of technologies, in order to enhance existing reactors' safety features (both active and passive) and to substantially reduce operating costs through risk-informed approaches.

One main focus area in FY 2020 for the ERP R&D efforts was to extend the analyses conducted in FYs 2018 and 2019 (Ma & al., 2018; Ma, et al., 2019a; Ma, et al., 2019b) for a pressurized water reactor (PWR) to a boiling water reactor (BWR). The same analysis process, risk analysis approaches, and analysis tools as in the previous work for PWR were used for a generic BWR with near-term ATF cladding (i.e., Iron-Chromium-Aluminum [FeCrAl] cladding and Chromium [Cr]-coated cladding) designs under the postulated station blackout (SBO) and medium loss-of-coolant (MLOCA) accident scenarios. In addition, a FLEX model was developed and incorporated into a generic BWR probabilistic risk assessment (PRA) model using the INL-developed software tool, Systems Analysis Programs for Hands-on Integrated Reliability Evaluations (SAPHIRE), to assess the risk impact from FLEX for BWR. The other main focus area in FY 2020 was to advance analysis methods, including developing a dynamic approach for FLEX human reliability analysis (HRA) with Event Modeling Risk Assessment using Linked Diagrams (EMRALD) (Prescott, Smith, & Vang, 2018) and developing a multicriterion benefit evaluation (MCBE) method for evaluating the costs and benefits of safety enhancements in NPPs. As a case study, the MCBE method was applied to evaluate costs and benefits brought by FLEX implementation at a generic PWR plant.

The remaining sections of the report are organized as below: Section 2 presents the analysis tools used in this work. Section 3 provides a description for a generic BWR model used in this work. Section 4 provides risk-informed analysis of SBO scenarios for near-term ATF designs. Section 0 provides risk-informed analysis of MLOCA scenarios for near-term ATF designs. Section 6 provides a FLEX BWR PRA using updated failure probability data and describes two dynamic approaches for FLEX HRA. Section 7 introduces the MCBE method and presents a case study of FLEX implementation cost and benefit evaluation. Section 8 presents the fuel performance analysis for the ATF designs with the BISON code. Section 9 provides a summary and the future work planning for ERP.

2. RISK-INFORMED ANALYSIS TOOLS

This section provides summarized descriptions of the computational tools used in the report. Although most of them were introduced in FYs 2018 and 2019 (Ma & al., 2018; Ma, et al., 2019a; Ma, et al., 2019b), the tools are described here in order for this report to be independent and complete.

2.1 SAPHIRE

SAPHIRE is a probabilistic risk and reliability assessment software tool developed and maintained by INL for the U.S. Nuclear Regulatory Commission (NRC) (Smith & Wood, 2011). SAPHIRE can be used to model NPP response to both internal hazards (for example general transients, loss of offsite power [LOOP], loss of feedwater, etc.) and external hazards (for example, seismic, fire, external flooding, high wind). SAPHIRE 8, the current version, can be used to develop Level 1 PRA for core damage frequency (CDF) quantification, Level 2 PRA for containment failure and release category frequency (including large early release frequency [LERF]) evaluation for severe accidents in which core damage (CD) has occurred, and limited Level 3 PRA for release consequence analysis. SAPHIRE 8 is a powerful PRA software that has both the basic PRA modeling capabilities such as creating event trees (ETs) and fault trees (FTs), defining and assigning basic event failure data, linking and solving ETs and FTs, documenting and reporting the results, and the advanced capabilities such as integrated Level 1 and Level 2 PRA analysis, performing sensitivity and uncertainty analyses, and conducting specialized analyses for the NRC's Accident Sequence Precursor Program and Significance Determination Process (SDP). Figure 2-1 shows the graphic user interface for SAPHIRE 8.

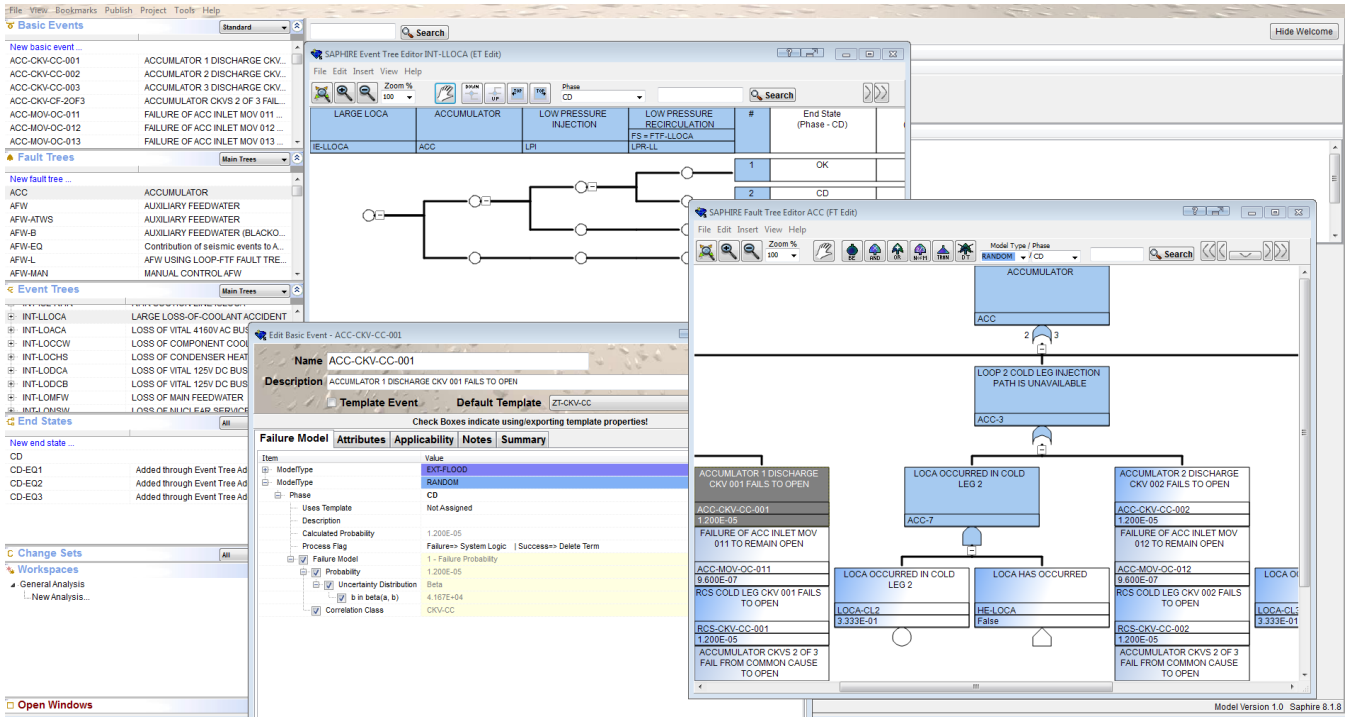

Figure 2-1. SAPHIRE 8 Graphic User Interface.

2.2 RELAP5-3D

RELAP5-3D code (RELAP5-3D Code Development Team, 2018) is the INL-developed best-estimate system thermal-hydraulic (TH) code of the RELAP5 family. It is capable of performing transient simulations of light water reactor systems during normal and accidental conditions (SBO, both large and small loss-of-coolant accidents [LOCAs], anticipated transient without scram, loss of feedwater, main steam line break, etc.). RELAP5-3D has also been successfully used for modeling and simulations of the following systems: fusion reactors, space reactors, gas and liquid metal reactors, and cardiovascular systems.

The code solves a non-homogeneous and non-equilibrium model (unequal velocities, unequal temperatures) for the two-phase flow using a fast, partially implicit numerical scheme. RELAP5-3D differs from the other RELAP5 versions thanks to a multi-dimensional TH, a 3D neutron kinetic modeling capability, and an extensive library of different fluids properties. The code development and validation is based on an extensive set of experimental data and its applicability to best-estimate plus uncertainty technology (Schultz, 2015). In the ERP activities, the code is applied for the calculations of SBO and MLOCA accident scenarios. Simulations are run inside the code applicability range (i.e. until the code predicts the onset of the extensive fuel damage). The applicability range of RELAP5-3D is shown in Figure 2-2.

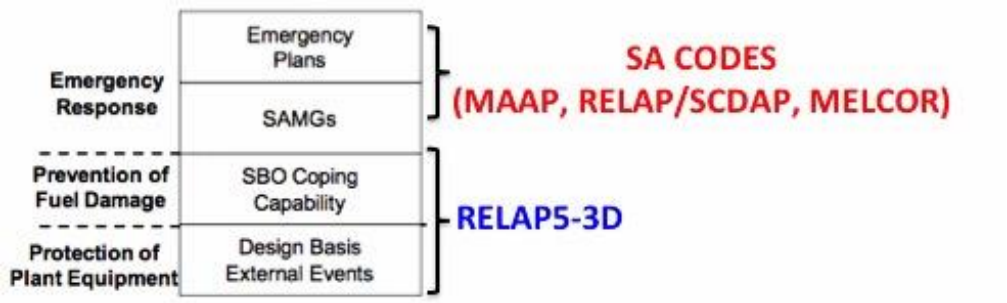

Figure 2-2. RELAP5-3D Role in LOOP and SBO Calculations.

References to the applicability of RELAP5 codes in simulating the above scenarios can be found in the open literature, for example (Prosek & Cizelj, 2013) and (Matev, 2006). For SBO and LOCA, the clad temperature failure criteria reported in Table 2-1 were adopted. It should be noted that for ATF, there are still not available fuel failure criteria. Therefore, for ATF it was decided to adopt the oxide shell failure temperatures as fuel failure criterion (Robb, Howell, & Ott, 2017). For Zircaloy the established criterion for the emergency core cooling system (ECCS) from 10 Code of Federal Regulations (CFR) Part 50.46 (U.S. Nuclear Regulatory Commission, 2017) is that peak clad temperature (PCT) should not exceed 1477 K. However, for the purpose of having consistent comparisons, the fuel failure criterion for Zircaloy is also set as the oxide shell failure temperature.

Table 2-1. Failure Criteria for Different Fuel Clads.

Clad Type	Failure Criteria	
	LOCA	SBO
Zircaloy	PCT>2100 K	PCT>2100 K
ATF - FeCrAl	PCT>1804 K	PCT>1804 K
ATF – Cr-coated	PCT>1804 K	PCT>1804 K

Concerning ATF modeling and simulation, it should be noted that MELCOR (Gauntt, et al., 2005), MAAP (EPRI, 2012), and TRACE (U.S. Nuclear Regulatory Commission, 2012) codes have been utilized previously to estimate the performance of various candidate ATF designs including FeCrAl and Cr-coated cladding materials. For instance, (Wu & Shirvan, 2019) used TRACE to analyze near-term ATF claddings under BWR short-term

and long-term SBO accidents. (Wang, Dailey, & Corradini, 2019) used MELCOR to evaluate the performance of ATF and reactor core isolation cooling (RCIC). In order to perform an effective study of the ATF candidate with the RELAP5-3D code for a BWR, additional code modifications to the oxidation model had to be implemented in FY 2020. The following paragraphs provide a description of the new oxidation model.

The capability of modeling a thin coating layer to the outside of fuel cladding was added to RELAP5-3D in this project. This coding change affects cylindrical heat structures for the fuel rods and rectangular heat structures for the fuel channels. The coating layer in the ATF designs is meant to protect the fuel cladding from oxidizing and degrading under high-temperature conditions. This oxidation reaction is of concern because it weakens the Zirconium cladding and also releases additional heat, which can increase the temperature in the reactor. The coating is designed to react instead of the cladding. A slow-reacting coating material should protect the cladding in the reactor and lengthen the lifetime of the reactor.

Note that the change in outer fuel radius does not affect the flow geometry in the reactor core. The additional thickness in the cladding does not contribute to the heat conduction through the cladding. This change will protect the outer layer of the cladding from oxidation, the amount of heat generated due to the chemical reaction will be added to the heat structure, and the amount of chemical reaction product generated will be calculated.

A correlation developed by (Cathcart & et al., 1977) is used to model the metal-water reaction model in RELAP5-3D which uses a parabolic rate law. This default correlation was developed for the Zirconium-Steam reaction. The code has been generalized to allow the user to model coolant-structure chemical interactions for which the parabolic rate law applies. The Cathcart correlation used in RELAP5-3D to calculate the thickness of the cladding converted to oxide is shown in Equation (2-1).

$$\Delta r^{n+1} = \left[(\Delta r^{n})^2 + (K\Delta t)e^{-(\Delta E/RT)}\right]^{1/2} \qquad (2\text{-}1)$$

where:

$(\cdot)^{n+1}$	=	New time value
$(\cdot)^{n+1}$	=	Old time value
K	=	Reaction rate constant (9.166 x 10-7 m2/s, derived from the Cathcart model)
Δt		Time step size (s)
ΔE	=	Activation energy (35,890 cal/mole for the Cathcart model)
R	=	Gas constant (1.986 cal/K-mole)
T	=	Cladding temperature (K)

The amount of heat added (Q) to the outer surface of the cladding due to oxidation is calculated as follows.

$$Q = \rho\pi[(r_o - \Delta r^{n})^2 - (r_o - \Delta r^{n+1})^2]\frac{H}{W} \qquad (2\text{-}2)$$

where:

r_o	=	Initial radius of unreacted cladding (cladding outer radius)
ρ	=	Cladding density (6,500 kg/m3 for Zirconium)
H	=	Reaction heat release (5.94 x 108 J/(kg-mole))
W		Molecular weight of cladding (91.22 kg/(kg-mole) for Zirconium)

Finally, the total Hydrogen mass generated by the metal-water reaction is calculated by multiplying the mass of Zirconium reacted by the ration of the molecular weight of 4 Hydrogen atoms to 1 Zirconium atom.

For the coating, the calculation of the thickness of the coating converted to oxide matches what is done for the cladding. The user can enter an initial coating thickness, material density, activation energy, reaction rate

constant, reaction heat release, coating material molecular weight, and the molecular weight of the reaction product (typically Hydrogen) divided by the coating material molecular weight.

At higher temperatures, the oxidation parameters can change significantly for both coated cladding and other ATF cladding types (e.g., full FeCrAl cladding). To account for this, additional input was added. The user can input a threshold temperature at which a transition occurs, followed by the usual input of material density, activation energy, reaction rate constant, reaction heat release, coating material molecular weight (although this should be a constant), and the molecular weight of the reaction product divided by the coating material molecular weight. Additional input was also added to allow the user to specify a transition temperature for the base-cladding or the full ATF cladding (FeCrAl). However, this option only allows the user to input a transition reaction rate constant.

The logic path for the metal-water reaction coding is shown in Figure 2-3, one potential logic path described here. When a coating layer is applied to the cladding, the coding first checks if the coating has oxidized through the entire thickness. If that is the case, the code will switch to performing the metal-water reaction calculations for the cladding material only. If the clad has broken, the metal-water reaction will be calculated for both the inner and outer surfaces of the cladding. If the outer surface heat structure temperature is greater than the specified transition temperature then the coding will switch to using the high-temperature parameters for the calculations. Other logic paths behave as shown in the figure.

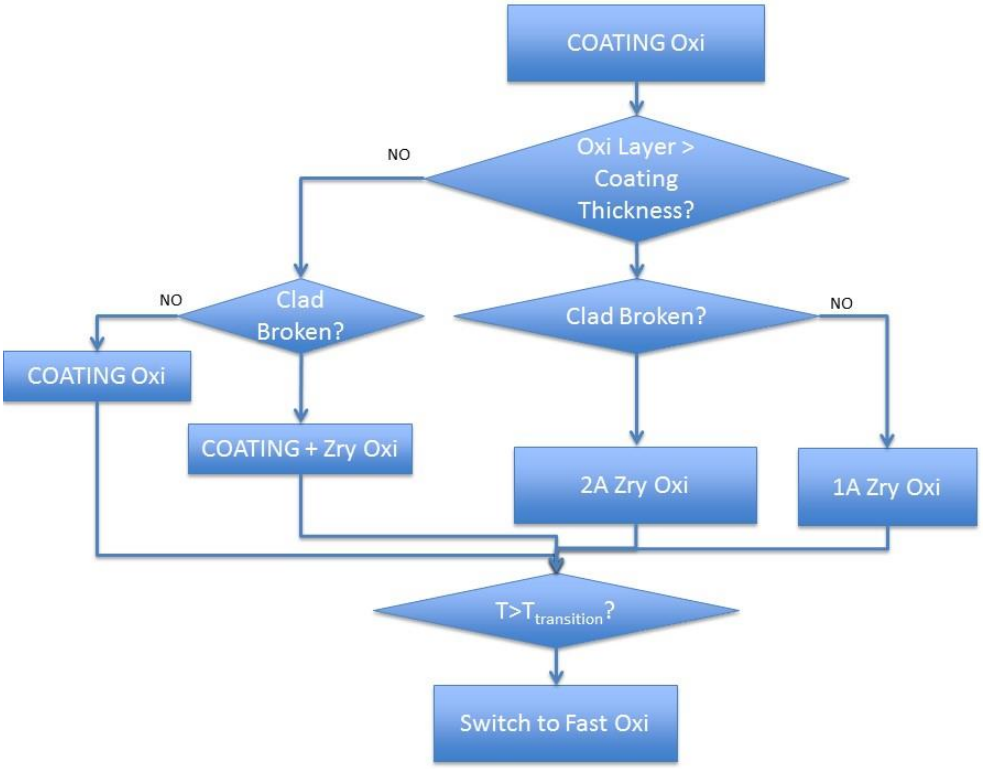

Figure 2-3. Logic Path for the Metal-Water Reaction Model Coding.

The changes to the input are as follows:

1CCCG002 Card, Coating Metal-Water Reaction Control	
W1(R)	Initial unreacted coating thickness on cladding's outer surface (m, ft).
W2(R)	Coating material density (kg/m^3). This quantity is optional, if not entered or 0.0 the default value for Zirconium (6,500 kg/m^3) is used.
W3(R)	Coating activation energy (cal/mole). This quantity is optional, if not entered or 0.0 the default value for the Cathcart model (35,890 cal/mole) is used.
W4(R)	Coating reaction rate constant (variable K) (m^2/s). This quantity is optional, if not entered or 0.0 the default value for the Cathcart model (2.252×10^{-6} m^2/s) is used.
W5(R)	Coating reaction heat release (J/kg-mole). This quantity is optional, if not entered or 0.0 the default value for the Zirconium-Steam reaction (5.94×10^8 J/kg-mole) is used.
W6(R)	Coating material molecular weight (kg/kg-mole). This quantity is optional, if not entered or 0.0 the default value for Zirconium (91.22 kg/kg-mole) is used.
W7(R)	Molecular weight of reaction product divided by Word 6. This quantity is optional, if not entered or 0.0 the default value for the Zirconium-Steam reaction (0.0442) is used.
W8(R)	Inner surface coating oxidation (for rectangular geometries only). To activate this option a real value greater than zero must be entered. Note that W8 of the 1CCCG003 Card must also be used to activate this option.
1CCCG005 Card, High-Temperature Coating Metal-Water Reaction Control	
W1(R)	Coating material transition temperature (K, F).
W2(R)	Coating material density (kg/m^3). This quantity is optional, if not entered or 0.0 the default value for Zirconium (6,500 kg/m^3) is used.
W3(R)	Coating activation energy (cal/mole). This quantity is optional, if not entered or 0.0 the default value for the Cathcart model (35,890 cal/mole) is used.
W4(R)	Coating reaction rate constant (variable K) (m^2/s). This quantity is optional, if not entered or 0.0 the default value for the Cathcart model (2.252×10^{-6} m^2/s) is used.
W5(R)	Coating reaction heat release (J/kg-mole). This quantity is optional, if not entered or 0.0 the default value for the Zirconium-Steam reaction (5.94×10^8 J/kg-mole) is used.
W6(R)	Coating material molecular weight (kg/kg-mole). This quantity is optional, if not entered or 0.0 the default value for Zirconium (91.22 kg/kg-mole) is used.
W7(R)	Molecular weight of reaction product divided by Word 6. This quantity is optional, if not entered or 0.0 the default value for the Zirconium-Steam reaction (0.0442) is used.
1CCCG003 Card, Cladding Metal-Water Reaction Control	
W8(R)	Initial oxide thickness on cladding's inner surface (m, ft). This quantity is optional for rectangular heat structures. This word must be entered to activate the calculation of the oxide thickness on the inner surface of a rectangular heat structure. The code sets this value to 0.0 for cylindrical or spherical heat structures. To activate this option a value less than or greater than zero must be entered. When less than zero, the initial oxide thickness is set to 0.0 m. When a value greater than zero is entered, the initial oxide thickness is the specified value. If 0.0 is entered, this option is ignored.
W9(R)	Cladding material transition temperature (K, F).
W10(R)	Cladding reaction rate constant (variable K) (m^2/s) at high-temperatures. This quantity is optional, if not entered or 0.0 the default value for the Cathcart model (2.252×10^{-6} m^2/s) is used.

2.3 EMRALD

EMRALD (Prescott, Smith, & Vang, 2018) is a dynamic PRA tool being developed at INL based on three-phase discrete event simulation. Traditional PRA modeling techniques are effective for many scenarios, but it is hard to capture time dependencies and any dynamic interactions using conventional techniques. EMRALD modeling methods are designed around traditional methods, yet enable an analyst to probabilistically model sequential procedures and see the progression of events through time that caused the outcome. Compiling the simulation results can show probabilities or patterns of time correlated failures.

An open communication protocol using the Extensible Messaging and Presence Protocol (XMPP) allows for easy coupling with other engineering tools. This coupling allows for direct interaction between the PRA model and physics based simulations, so that simulated events can drive the PRA model and sampled PRA parameters can affect the simulation environment. The capabilities included in EMRALD permit PRA models to more easily and realistically account for the dynamic conditions associated with the progression of plant transient and accident sequences including accounting for the occurrence of modeled operator actions taken to mitigate the event.

2.4 BISON

BISON (Hales, J. D. et al., 2015) is a finite element-based nuclear fuel performance code applicable to a variety of fuel forms including LWR fuel rods, tristructural isotopic particle fuel, and metallic rod and plate fuel. This advanced fuel performance code is being developed at INL and offers distinctive advantages over FRAPCON/FRAPTRAN such as 3D simulation capability, etc. BISON solves the fully coupled equations of thermo-mechanics and species diffusion, for either 1D spherical, 2D axisymmetric or 3D geometries. Fuel models are included to describe temperature and burnup dependent thermal properties, fission product swelling, densification, thermal and irradiation creep, fracture, and fission gas production and release. Plasticity, irradiation growth, and thermal and irradiation creep models are implemented for clad materials. Models also are available to simulate gap heat transfer, mechanical contact, and the evolution of the gap/plenum pressure with plenum volume, gas temperature, and fission gas addition. BISON has been coupled to the mesoscale fuel performance code, MARMOT (Idaho National Laboratory, 2020), demonstrating its fully coupled multiscale fuel performance capability. BISON is based on the Multiphysics Object-Oriented Simulation Environment (MOOSE) framework (Idaho National Laboratory, 2020); therefore, BISON can efficiently solve problems using standard workstations or very large high-performance computers.

3. GENERIC BWR MODEL

This section presents risk-informed analyses on ATF with a generic BWR plant SAPHIRE PRA model and an INL Generic BWR RELAP5-3D model. BWR SBO and MLOCA accident scenarios were developed by reviewing the PRA model and then analyzed by RELAP5-3D code for near-term ATF designs, FeCrAl, and Cr-coated cladding.

The generic RELAP5-3D BWR model used in this study is based on a GE BWR/4 design with Mark I containment, representative of the U.S. BWR fleet and is shown in Figure 3-1 (U.S. Nuclear Regulatory Commission, 2012). The rated thermal power for this generic BWR is 3,293 MWth with 764 fuel assemblies (or bundles) in the core. The reactor pressure vessel (RPV), jet pumps, separator/dryer unit, main steam lines, main feedwater lines, recirculation loops, and the safety relief valves (SRVs) are modeled. Figure 3-2 shows the RELAP5-3D nodalization diagram for the generic BWR plant model. The base model can simulate the TH parameters of the primary side and of some parts of the containment. The reference base model with Zircaloy clad was modified to include FeCrAl and Cr-coated as additional cladding material based on parameters from (Holzwarth & Stamm, 2002) and (Field, Snead, Yamamoto, & Terrani, 2017).

Table 3-1. Major Parameters for the Generic BWR.

	Value (SI Unit)
Rated Thermal Power (MWth)	3,293
Number of Fuel Assemblies (Bundles)	764
Core Mass Flow Rate (Kg/s)	11510
RPV Dome Normal Operating Pressure (MPa)	7.02
Feedwater Mass Flow Rate (Kg/s)	1681.3
Recirculation pump flow (Kg/s)	4278.6
Core mass flow rate (Kg/s)	11065.1
Bypass flow (Kg/s)	1266.2
Steam mass flow rate (Kg/s)	1681.3
Feedwater Temperature (^{o}K)	464.394
Feedwater Water Pressure (Mpa)	7.2
RPV Inner Diameter (m)	6.38
RCIC Rated Flow (Kg/s)	37.8

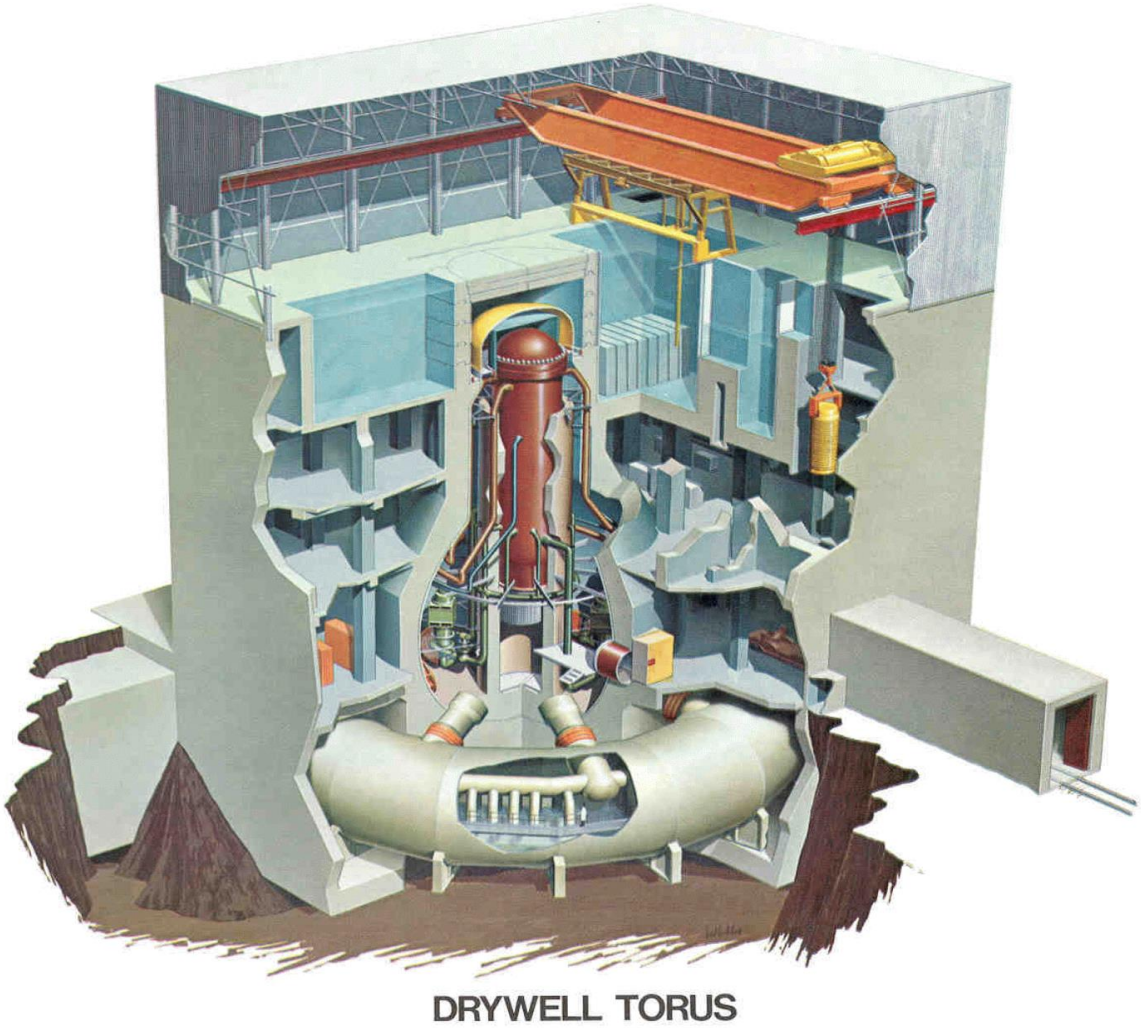

Figure 3-1. Cutaway Drawing of a BWR Mark I Containment Showing the Configuration of RPV, Recirculation Loop, Drywell, and Suppression Pool Torus (U.S. Nuclear Regulatory Commission, 2012).

The RELAP5-3D model developed for analyzing transient events is based on an input-deck describing:

- RPV
- Main feedwater line
- Main steam line
- Jet pumps
- Recirculation loops
- Reactor core
- Steam separator
- Steam dryer
- Automatic depressurization system (ADS)
- SRVs

- High pressure core injection (HPCI)
- RCIC
- Core spray (CS)
- Low pressure core injection (LPCI)
- Firehose injection
- Control rod drive hydraulic system (CRDHS)
- Standby liquid control system (SLCS)
- Wetwell (WW)
- Drywell (DW)
- Vent lines from WW to DW

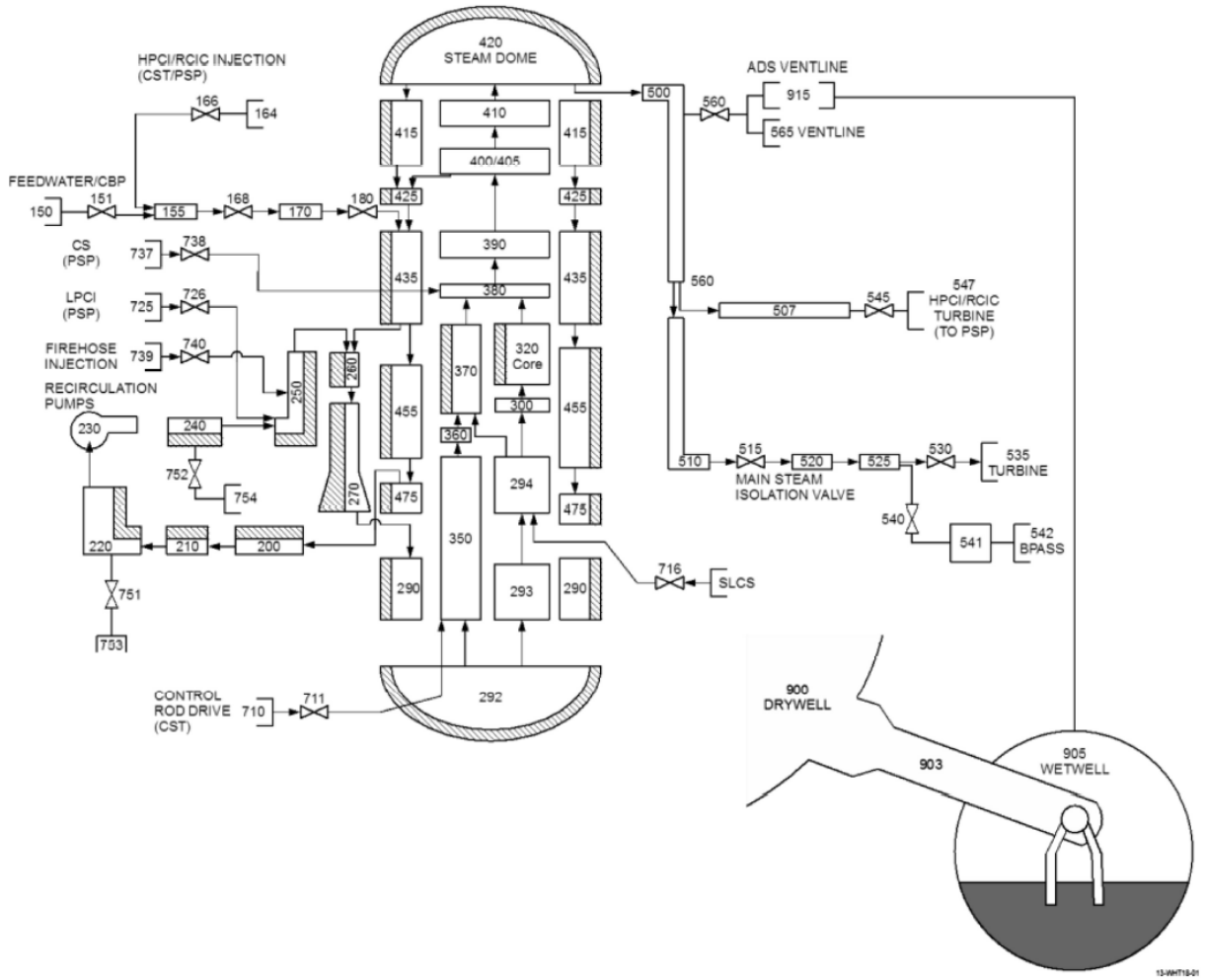

Figure 3-2. RELAP5-3D Nodalization Diagram.

3.1 TH Components

The modeling of the RPV includes the downcomer, lower plenum, core, upper plenum, standpipes, separator, dryer, and steam dome. The downcomer is modeled with a series of "Annulus" component. The steam separator unit is modeled with the "Simple Separator" component. The recirculation loops are lumped into one loop and it includes a jet pump, a recirculation pump with pipes from pump suction/discharge. The recirculation pumps and jet pumps allow the operator to vary coolant flow through the core and hence change the power of the nuclear reactor. The jet pump components are located in the region between the core shroud and the vessel wall, submerged in coolant. In order to limit the number of penetrations into the reactor vessel, the recirculation loops also serve as the residual heat removal (RHR) system. When the reactor is shut down, the core will continue to generate decay heat, which is removed by bypassing the turbine and dumping the steam directly to the condenser. RHR system provides shutdown cooling when pressure decreases to approximately 0.45 Mpa.

The main feedwater lines are lumped into one. The feedwater systems are modeled using a series of "Pipe" components connected by junctions. The flow rates in the main feedwater line are controlled to maintain the desired downcomer water level in the RPV. High pressure safety systems such as HPCI and RCIC will inject coolant through the main feedwater line. Finally, the main steam lines are lumped into one from three original steam lines. The main steam line has one main steam isolation valve (MSIV), turbine bypass valve (TBV), turbine stop valve, with turbine modeled with boundary conditions (BCs).

The generic BWR model also includes a Mark I containment which consists of a dry well (DW), a wet well (WW), and vacuum breakers. The WW represents the suppression pool (SP) and the vapor space above it, which jointly form the torus in a typical BWR-4 design. The DW contains steam or liquid released from SBO, LOCA, etc., and minimizes radioactive leakage.

The WW is essentially a large tank of water which resides within containment of some BWR designs. WW refers to a pressure vessel which contains both a water pool and a non-condensable gas space. The WW water pool is commonly referred to as an SP because excess steam is condensed into this pool in order to suppress possible overpressure events. The SP is also called a suppression chamber or a pressure SP. It contains a large volume of fresh water and serves as heat sink for SRV discharged steam and exhaust steam from turbines in the high pressure safety systems (i.e., HPCI and RCIC). The WW plays a vital safety role in SBO and other BWR accident scenarios in that it condenses released high-temperature steam vented from the DW to reduce containment pressure and provides a backup source of water for safety injection systems (the initial default is condensate storage tank [CST]). Steam can vent through the SRVs and/or the RCIC turbine exhaust into the WW where it condenses. The RCIC pump suction line draws water near the bottom of the WW pool to supply makeup water to the core. The steam injection and condensation taking place in the WW create momentum-induced mixing and buoyancy-induced thermal stratification. These two opposing phenomena determine the thermodynamic conditions of the WW and have a large effect on the overall performance of the RCIC System.

3.2 Safety Systems

The safety systems mainly involve coolant injection into RPV to prevent fuel damage under accident conditions and they can be categorized into high-pressure and low-pressure safety systems. In a typical BWR/4 plant, high-pressure safety systems include HPCI, RCIC, and ADS. Low pressure safety systems include LPCI, low pressure CS, Firewater, SLCS, and CRDHS.

The RCIC system, as shown in Figure 3-3, provides makeup water to the RPV for core cooling when it is isolated from the secondary plant and the normal water supply to the RPV is lost, and as a standby system for safe shutdown of the plant. It consists of a steam-driven turbine, turbine-driven pump, piping, and valves that are necessary to deliver core makeup water to the RPV at operating and accident conditions. The RCIC turbine is driven by high-pressure steam from the main steam lines and the exhaust is discharged to the SP. The RCIC pump supplies makeup coolant from the CST, or alternatively from the SP once the CST is drained, to the reactor via

the main feedwater lines. CST contains a large volume of fresh water that can be used to cool the core. The RCIC system is nearly passive with the exception of requiring battery for control function. The functionality of RCIC is determined by a combination of factors, including the availability of direct current (DC) power, heat capacity temperature limits, RPV water level, and RPV pressures. When DC power is available, RCIC water injection is initiated automatically with a low core water level signal or manually by the plant operator, and it is stopped automatically with a high core water level signal or manually by the plant operator. When DC power is not available, RCIC can also be blackstarted and blackrun.

After a normal reactor shutdown, the RCIC turbine is driven by decay heat-generated steam and exhausts to the WW. The RCIC operates in this way until the vessel pressure and temperature are reduced sufficiently to the point that the RHR system can come into operation. The RCIC system is actuated when: (1) The RPV is isolated from the main turbine and condenser, (2) SBO occurs and other systems are not available, or (3) Feedwater flow is disrupted, and high pressure prohibits shutdown cooling system action. The RCIC system operates for a wide range of system pressures, from normal operating pressure (~1135 psig) down to 150 psig. It is noted that RCIC is not considered as a part of the ECCS and does not have an LOCA function; however, it does play an important safety role. LOCA accidents usually depressurize the RPV quickly, thereby disabling the RCIC system.

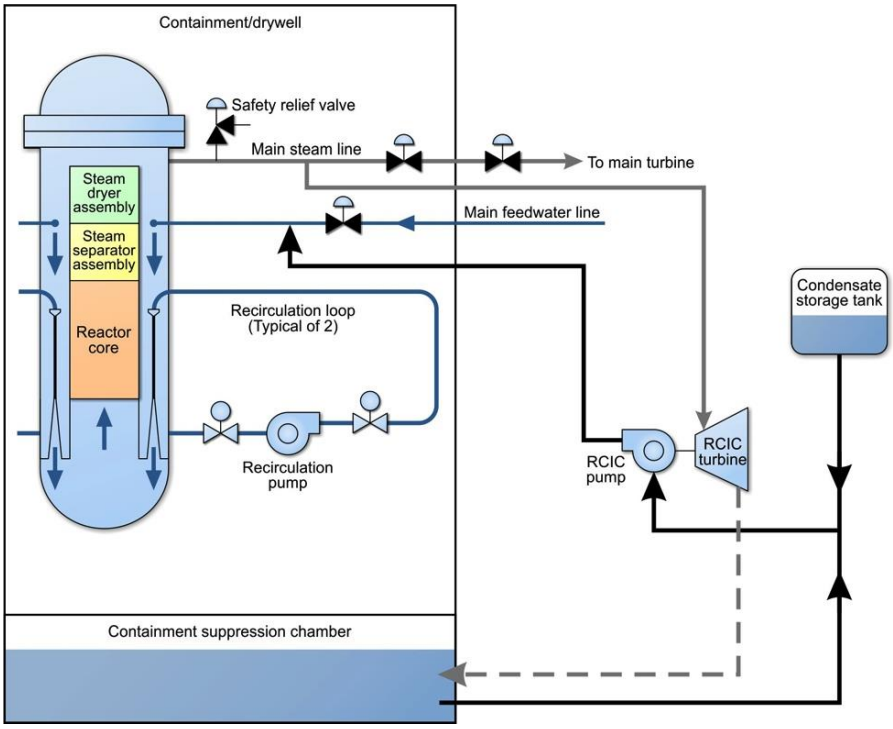

Figure 3-3. Schematic Illustration of RCIC System (U.S. Nuclear Regulatory Commission, 2012).

The HPCI system works in a similar way with RCIC but it provides greater water injection rate (about 10 times greater than that of RCIC). It consists of a steam turbine-driven pump, valves and valve operators, and associated piping, including that from the normal and alternate pump suction sources and the pump discharge up to the penetration of the main feedwater line. It is a single-train system actuated by either a low reactor water level or a high DW pressure. Just like RCIC, HPCI initially operates in an open loop mode, taking suction from the CST. When the level in the CST reaches a low-level setpoint, the HPCI system is aligned to the SP. HPCI is an independent ECCS system that requires no auxiliary alternating current (AC) power to provide makeup water to the core under small to intermediate size LOCA accidents. The main difference between HPCI and RCIC is that the operation of HPCI will rapidly depressurize the RPV due to its large steam release rate, while the steam-driven turbines of HPCI rely on high pressure steam to operate.

There are 13 SRVs connected on the steam exit pipe of the main steam line. SRVs can be manually controlled with DC power to limit the RPV pressure in a prescribed range or obtain the controlled depressurization of the reactor. Following a normal reactor shutdown, or reactor scram under accident scenarios, the decay heat continues to generate steam, albeit at a reduced rate. The turbine bypass system diverts the steam to the condenser if the RPV is not isolated from the secondary plant, or the steam will be vented to the SP through operation of the SRVs when the RPV is isolated. Among the 13 SRVs, five valves also serve in the ADS which can be employed to complete depressurizing the RPV in a short period of time. Once the RPV is completely depressurized by ADS, no core cooling is available unless AC power is recovered.

Low-pressure ECCS systems such as LPSI, low-pressure core spray (LPCS), and firewater can be aligned to the RPV to inject coolant to the core when AC power is available and the RPV is depressurized. LPCI is the dominant mode of the RHR system. It takes water from the SP and discharges to the RPV to maintain the coolant inventory at a relatively low pressure. LPCS is capable of pumping water from the SP and spray it on top of fuel assemblies.

3.3 Reactor Core Modeling

The reactor core modeling consists of flow channels simulating the coolant flow within the fuel assembly channel boxes and heat structures attached to flow channels simulating the heat transfer within the fuel rods. There are two independent TH channels representing the coolant flow in the core—one hot channel and one average channel. The hot channel represents the flow in the fuel assembly with highest power and the average channel represents the flow for the remaining 763 fuel assemblies.

The fuel design used in the core modeling is a representation of state-of-the-art fuel design for BWRs based on publicly available GE14 design data. Figure 3-4 shows the side view of the GE14 fuel assembly design. The fuel assembly geometry is a 10×10 lattice. The cross-sectional view of the fuel assembly is shown in Figure 3-5. The basic fuel rod is comprised of a column of right circular cylinder fuel pellets enclosed by a cladding tube and sealed gas-tight by plugs inserted in each end of the cladding tube. The fuel pellets consist of sintered uranium-dioxide (UO2) or UO2-gadolinia solid solution ((U,Gd)O2) with a ground cylindrical surface, flat ends, and chamfered edges. Each full-length UO2 fuel rod may include natural enrichment UO2 pellets at each end of the fuel pellet column. The fuel rod cladding tube is comprised of Zircaloy-2 with a metallurgically bonded inner Zirconium layer. Each fuel rod includes a plenum at the top of the fuel rod to accommodate the release of gaseous fission products from the fuel pellets. This gas plenum includes a compression spring to minimize fuel column movement during fuel assembly shipping and handling operations while permitting fuel column axial expansion during operation. The GE14 fuel assembly contains 14 fuel rods, which are reduced in length relative to the remaining fuel rods. These rods are called part length rods. Fuel rods are internally pressurized with helium to reduce the compressive hoop stress induced in the cladding tube by the coolant pressure and to improve the fuel to cladding heat transfer. With the absence of known data, the fuel rod internal pressure is assumed to be 1 MPa.

Table 3-2. Fuel Parameters (Nuclear Engineering International, 2007)

Parameters	Values
Bundle assembly lattice	10 x 10
Number of full-length rods	78
Number of part length rods	14
Number of water rods	2
Active fuel length (cm)	368.91
Part length rod length (cm)	213.36
Rod to rod pitch (cm)	1.295

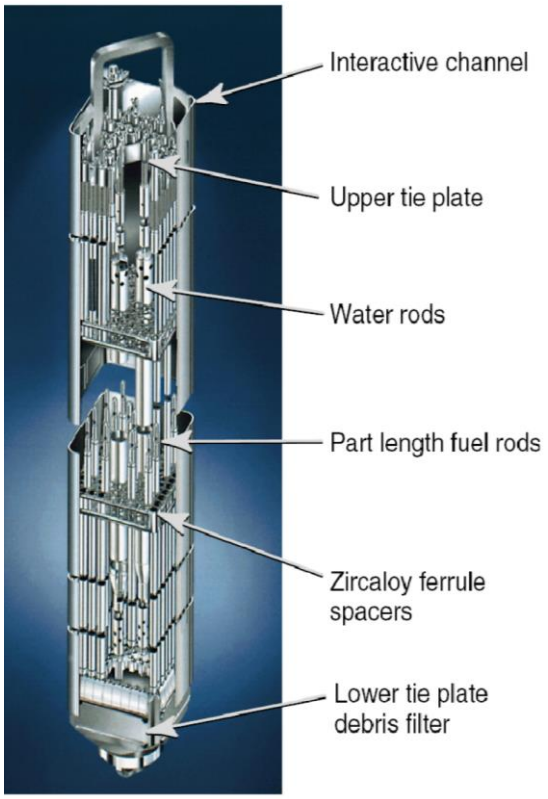

Figure 3-4. Side View of GE14 Fuel Assembly (U.S. Nuclear Regulatory Commission, 2011)

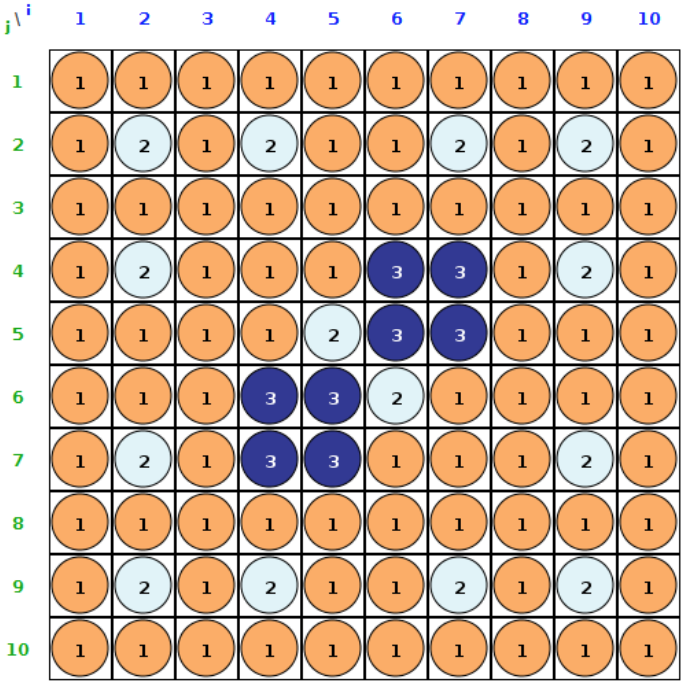

Figure 3-5. Cross-sectional View of the 10×10 Fuel Assembly Design. 1 Denotes Fuel Length Rods, 2 Denotes Part Length Rods and 3 Denotes Water Rods.

Since the reactor core has 764 fuel assemblies, with 92 fuel rods within each assembly, the total number of fuel rods in the core is 70,288, which renders tracking individual fuel rods impractical in systems transient analyses. Therefore, homogenization techniques would be used to lump fuel rods and flow channels into manageable number. Different homogenization approaches are used for thermal fluid dynamics calculations for the two-phase flow in the fuel assemblies than for the heat conduction and clad oxidation calculations in the fuel rods. For the thermal fluid dynamics calculations, two flow channels dare built to simulate the active flow within the fuel assemblies—the hot channel and the average channel. The hot channel represents the active flow within the hot assembly and the average channel represents the active flow in the remaining assemblies of the core. Hot assembly is the assembly with highest assembly power in the core.

For heat conduction and clad oxidation calculations, three sets of heat structures are built—one set represents the hot rod (highest power rod) in the hot assembly, another set represents the remaining 91 fuel rods in the hot assembly, and the third set represents the average of all the fuel rods in the remaining 763 fuel assemblies.

These homogenization approaches are reasonable as they: (1) greatly speedup the simulation time, and (2) capture the flow behaviors in the hot channel as well as the temperature profiles and oxidation behaviors in the hot rod. As a result, heat structures for the hot rod in the hot assembly and the heat structures for the remaining fuel rods in the hot assembly are attached to the flow in the hot channel, as shown in Figure 3-6. Analogously, the heat structures for all the fuel rods in the remaining 763 assemblies are lumped into one set and are attached to the flow in the average channel, as shown in Figure 3-7.

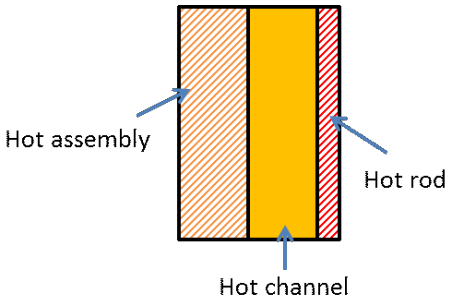

Figure 3-6. Schematic Illustration of the Heat Structure Mapping for the Hot Assembly and its Hot Rod with the Hot Channel.

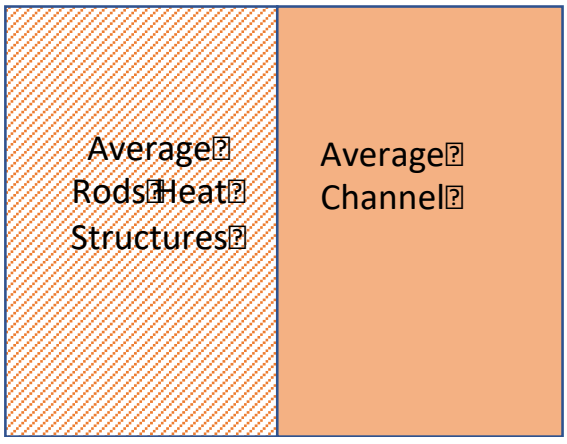

Figure 3-7. Schematic Illustration of the Heat Structure Mapping for the Average Assemblies and the Average Flow Channel.

The neutron energy spectrum can vary during an operation cycle to generate and utilize more plutonium from the non-fissile U-238 by changing the void fraction in the core through control of the core coolant flow rate. This operation method, which is called a spectral shift operation, is practiced in BWRs to save natural uranium. The core power shapes, as a function of cycle burnup state, have significant impact on the temperature distributions in the core. For a typical BWR core, the power shapes tend to be bottom peaked near the beginning of the cycle (BOC). As the cycle depletion progresses, the power shapes gradually evolve into cosine shape near the middle of the cycle (MOC). Toward the end of the cycle (EOC), the power shapes tend to be top peaked. In this analysis, operating conditions, in the form of maximum power verses exposure envelopes for GE14 are postulated which cover the conditions anticipated during normal steady-state operation and accident conditions. An example power-exposure envelope is shown in Figure 3-8, which is reproduced from the Global Nuclear Fuel's licensing topical report for GE14 fuel rod thermal-mechanical design report (Global Nuclear Fuel, 2006). The power shapes shown in Figure 3-8 represent the maximum power verses exposure envelopes that cover conditions anticipated during normal steady-state operation and anticipated operational occurrences. The fuel rod axial power shape is changed three times during each cycle, BOC, MOC, EOC, and simulates the distribution effects of burnup. The three power shapes should provide bounding conditions for the evolving power shapes in the cycle.

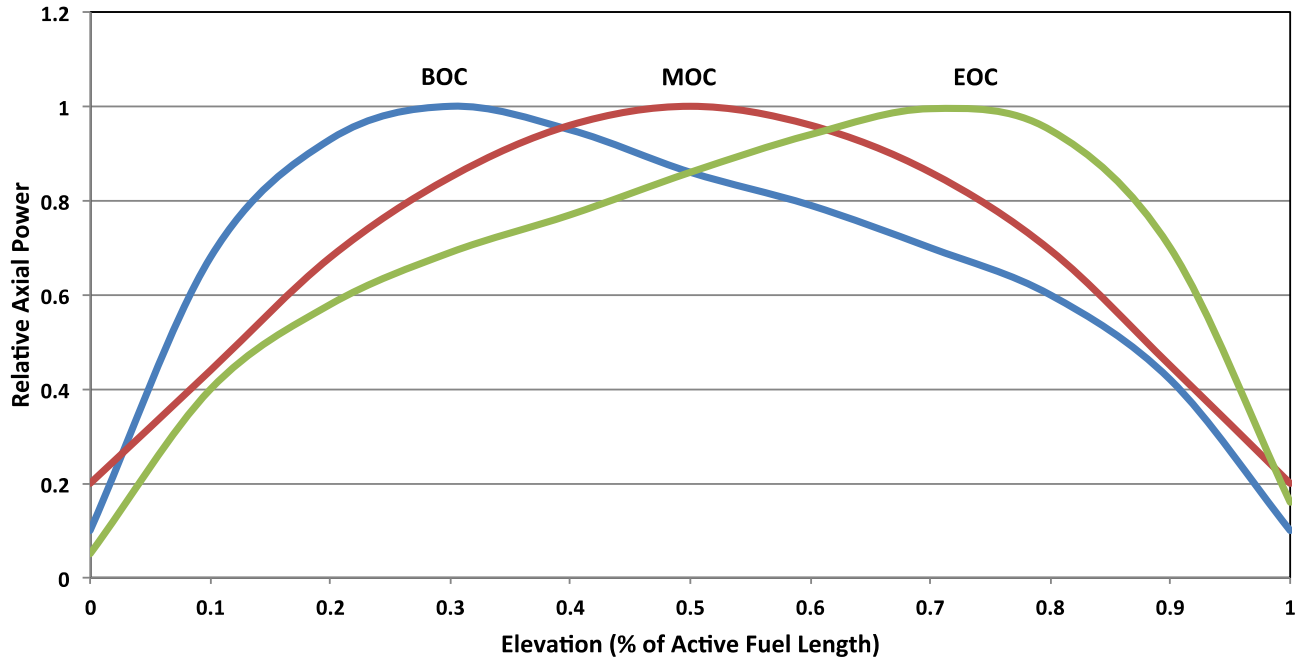

Figure 3-8. Core Axial Power Shapes Used in the RELAP5-3D Calculations (Global Nuclear Fuel, 2006).

3.4 Fuel Rod Geometry and Cladding Oxidation Kinetics

The specific fuel-rod parameters used are shown in Table 3-3. The Zircaloy cladding is the baseline fuel design cladding. The outer radius of the fuel rod is identical for Zry and FeCrAl. For the Chromium-coated cladding design, 15 microns in thickness of Cr-coating is applied to the outside surface of the baseline Zircaloy cladding, therefore, the outer radius of the Cr-coated cladding is 0.015 mm thicker than that of Zry and FeCrAl. Due to the higher neutron absorption rate of FeCrAl cladding, the thickness of FeCrAl cladding is reduced to half of that of Zircaloy cladding. The pellet diameter is increased to keep the plenum gap size the same as that of the baseline fuel design with Zircaloy cladding.

Table 3-3. Fuel Rod Geometry for Reference and ATF Fuel Designs.

Cladding Type	Pellet Outer Radius (cm)	Cladding Inner Radius (cm)	Cladding Outer Radius (cm)
Zircaloy	0.438	0.45	0.513
Zircaloy + Cr-coating	0.438	0.45	0.5145
FeCrAl	0.4695	0.4815	0.513

The RELAP5-3D input deck uses the special cards developed for simulating the oxidation kinetics of ATF (both coated and non-coated clads). The ATF oxidation parameters were obtained from selected publications and implemented in the RELAP5-3D input deck. The main parameters for the oxidation kinetics and the fuel pin geometries are reported in Table 3-4.

For the FeCrAl clad, a transition temperature of 1773 K was selected. When the code calculates such temperature, the oxidation kinetics parameters are switched to the stainless-steel oxidation parameter (i.e., rapid oxidation). The failure criterion for both Chromium and FeCrAl is the PCT reaching 1804 K. Additional to performing heat conduction and oxidation calculations in a fuel rod, RELAP5-3D performs a simplified clad deformation calculation. The empirical model included in RELAP5-3D was taken from the FRAP-T6 code. The purpose of the model is to consider a possible plastic deformation of the clad during an accident condition. The model can inform the user of a possible cladding rupture and of a possible flow blockage due to the hydraulic channel flow area reduction. Further investigation by specialized fuel pin mechanics codes, such as BISON, are needed if extensive plastic deformation or rupture of the clad are detected.

Table 3-4. RELAP5-3D Parameters for the Cladding Oxidation Kinetics.

Parameter	Cladding Type		
	Zry	Cr-coated	FeCrAl
Reaction Rate Constant (m^2 Metal/s)	9.166E-7	1.409E-5	2.444E-5
Reaction Heat Release (J/Kg mole)	5.94E+8	6.48E+7	6.73E+7
Activation Energy (cal/mole)	35,890	66,890	82,218
Clad Density (kg/m^3)	6,500	7,190	6,860
Clad Molecular Weight (kg/kg mole)	91.22	51.99	53.96
Ratio Molecular Weight Reactant/Clad	0.042	0.058	0.112

4. RISK-INFORMED ATF ANALYSIS OF BWR SBO SCENARIOS

The risk-informed analysis of near-term ATF designs for BWR SBO scenarios is presented in this section. The BWR SBO PRA model and scenarios are presented in Section 4.1. The RELAP5-3D analyses of ATF designs for the SBO scenarios are presented in Section 4.2. The results from sensitivity calculations are presented in Section 4.3. The analysis results are summarized in Section 4.4.

4.1 BWR SBO PRA Model and Scenarios

The generic BWR SBO SAPHIRE model starts with the occurrence of a LOOP event. There are four different LOOP categories: grid-related (GR), plant-centered (PC), switchyard-centered (SC), and weather-related or (WR) (Eide, Gentillon, Wierman, & Rasmuson, 2005). These have been analyzed separately by splitting the LOOP ET over these categories. Four LOOP ETs (LOOPGR, LOOPPC, LOOPSC, and LOOPWR) are developed in the PRA model for the corresponding LOOP categories. The ET structure is the same for all four LOOP ETs. The only differences are the initiating event frequencies and the AC power non-recovery probabilities.

The BWR SBO SAPHIRE model includes the LOOP-initiating ET (Figure 4-1), the SBO main ET (Figure 4-2), and three SBO sub-ETs: SBO-OP with AC power recovered and no SRV LOCA (Figure 4-3), SBO-extended loss-of-AC power (ELAP) for sequences with no AC power recovery and no SRV LOCA (Figure 4-4), and SBO-1 for sequences with one and only one SRV remains open (Figure 4-5). It should be noted that FLEX for ELAP operation is modeled in the SBO-ELAP sub-ET but not credited in this ATF analysis.

The four LOOP ETs (LOOPGR, LOOPPC, LOOPSC, LOOPWR) were quantified with SAPHIRE 8 using a truncation level of 1E-12. For each of the four LOOP ETs, there are 169 accident (or CD) sequences. 114 of the 169 LOOP accident sequences are SBO sequences in which onsite emergency diesel generators (EDGs) fail to supply emergency power to vital buses for the safety equipment. The total LOOP CDF is 1.71E-6/year, with LOOPGR, LOOPSC, and LOOPWR each contributes about 30%, and LOOPPC contributes less than 5% (see Table 4-1). The total SBO CDF is 6.76E-7/year, which is about 40% of the LOOP CDF. The weather-related SBO (SBOWR) contributes more than 50% of the total SBO CDF. The switchyard-centered SBO (SBOSC) and grid-related SBO (SBOGR) each contributes about 20%, while the plant-centered SBO (SBOPC) contributes less than 2% of the total SBO CDF (see Table 4-2).

Table 4-1. BWR LOOP ETs Quantification Results.

LOOP ET	Description	Sequence Count	CDF	CDF%
LOOPGR	LOOP-GRID RELATED	169	4.97E-07	29.1%
LOOPPC	LOOP-PLANT CENTERED	169	7.36E-08	4.3%
LOOPSC	LOOP-SWITCHYARD CENTERED	169	5.79E-07	33.8%
LOOPWR	LOOP-WEATHER RELATED	169	5.61E-07	32.8%
Total		676	1.71E-06	100.0%

Table 4-2. BWR SBO Sequences Quantification Results.

SBO	Description	Sequence Count	CDF	CDF%
SBOGR	SBO-GRID RELATED	114	1.46E-07	21.7%
SBOPC	SBO-PLANT CENTERED	114	1.06E-08	1.6%
SBOSC	SBO-SWITCHYARD CENTERED	114	1.51E-07	22.4%
SBOWR	SBO-WEATHER RELATED	114	3.67E-07	54.4%
Total		456	6.76E-07	100.0%

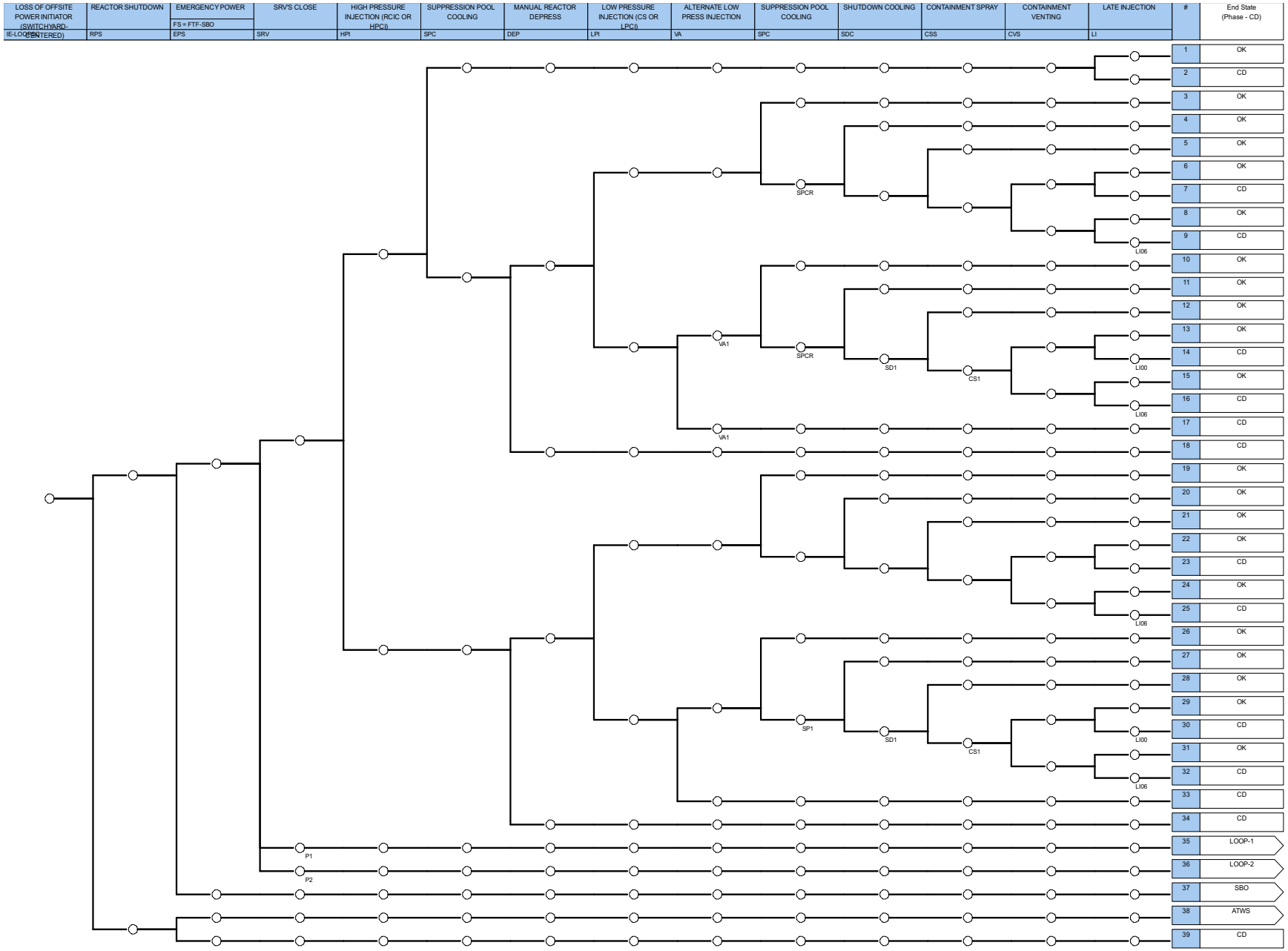

Figure 4-1. Generic BWR LOOP ET.

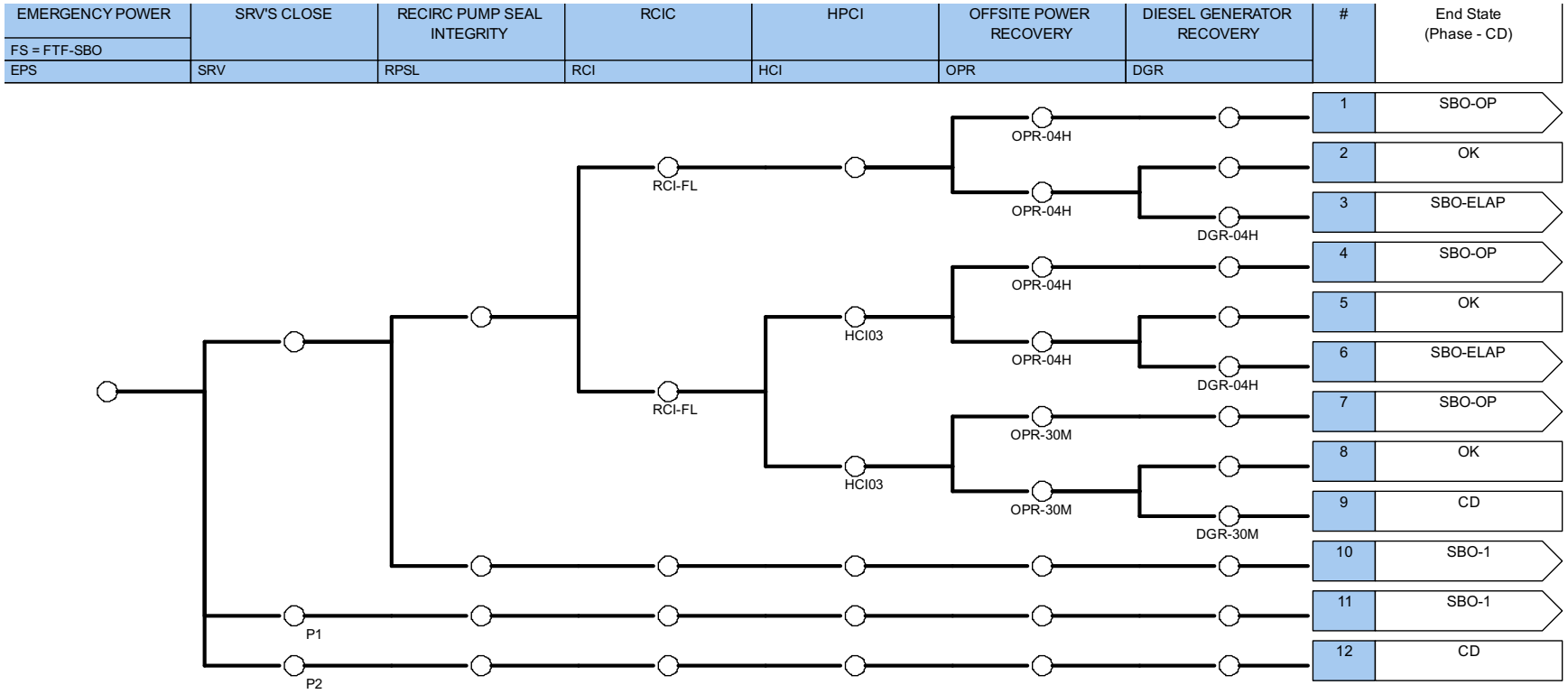

Figure 4-2. Generic BWR SBO ET.

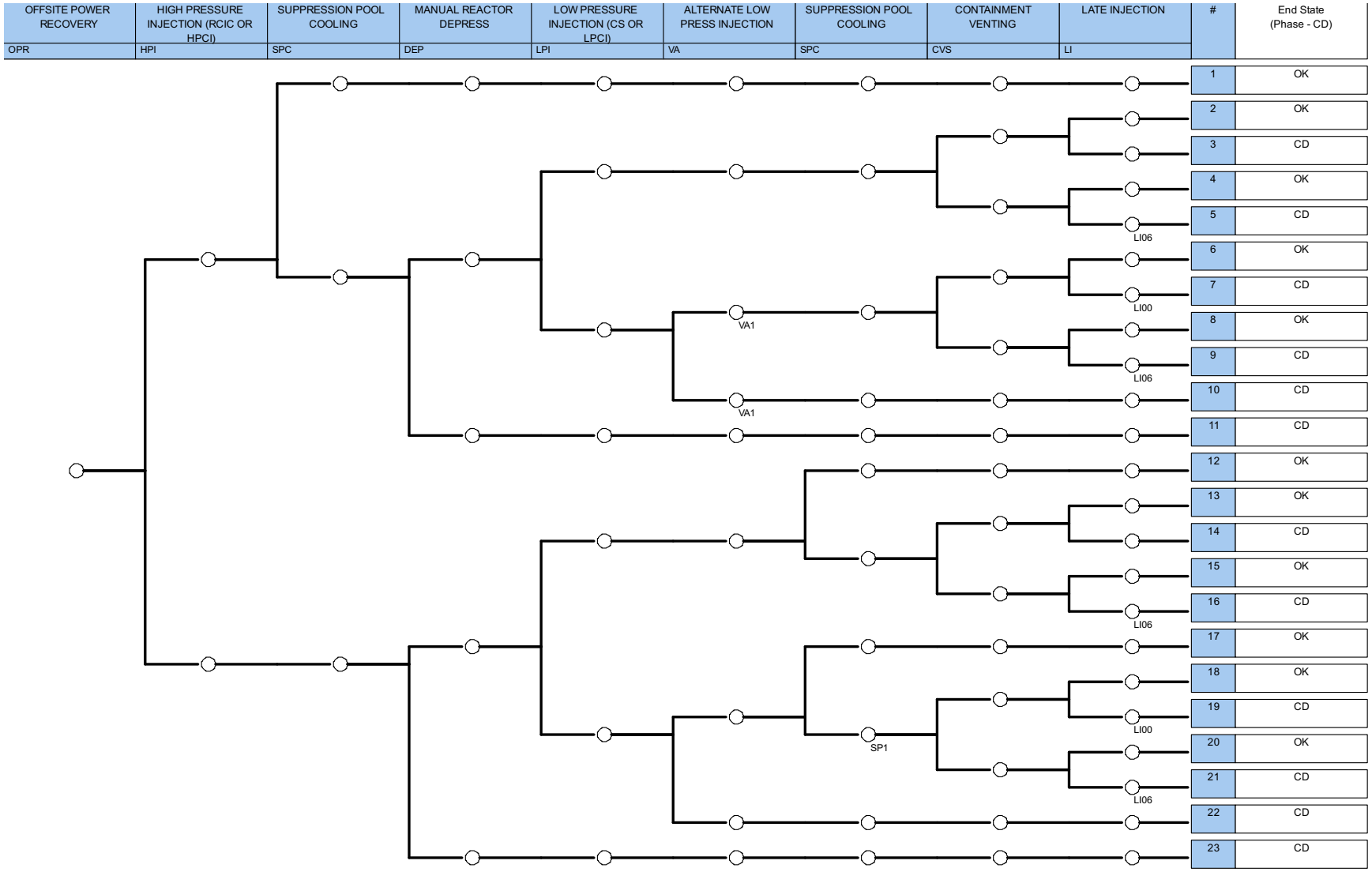

Figure 4-3. Generic BWR SBO-OP Sub-Tree.

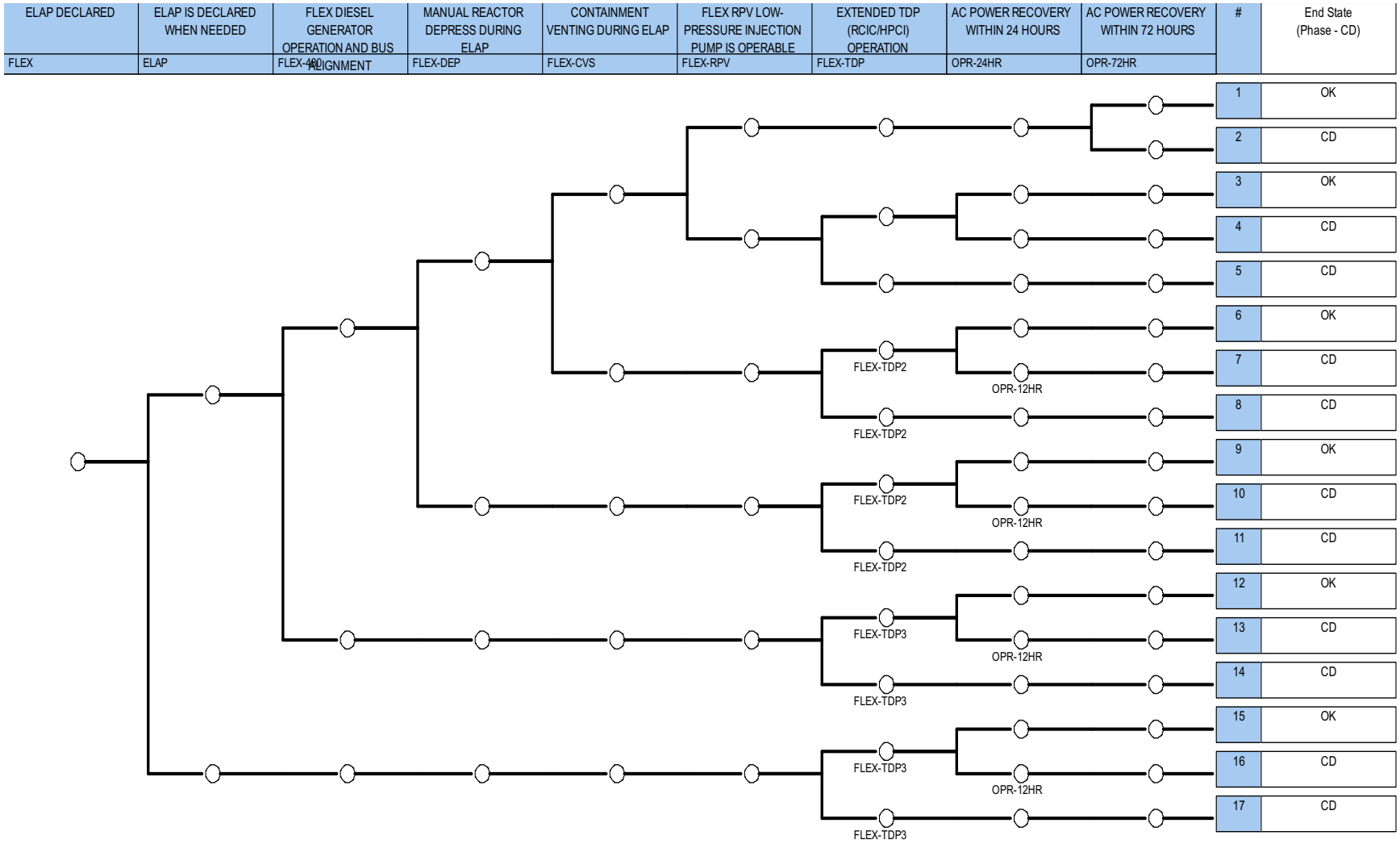

Figure 4-4. Generic BWR SBO-ELAP Sub-Tree.

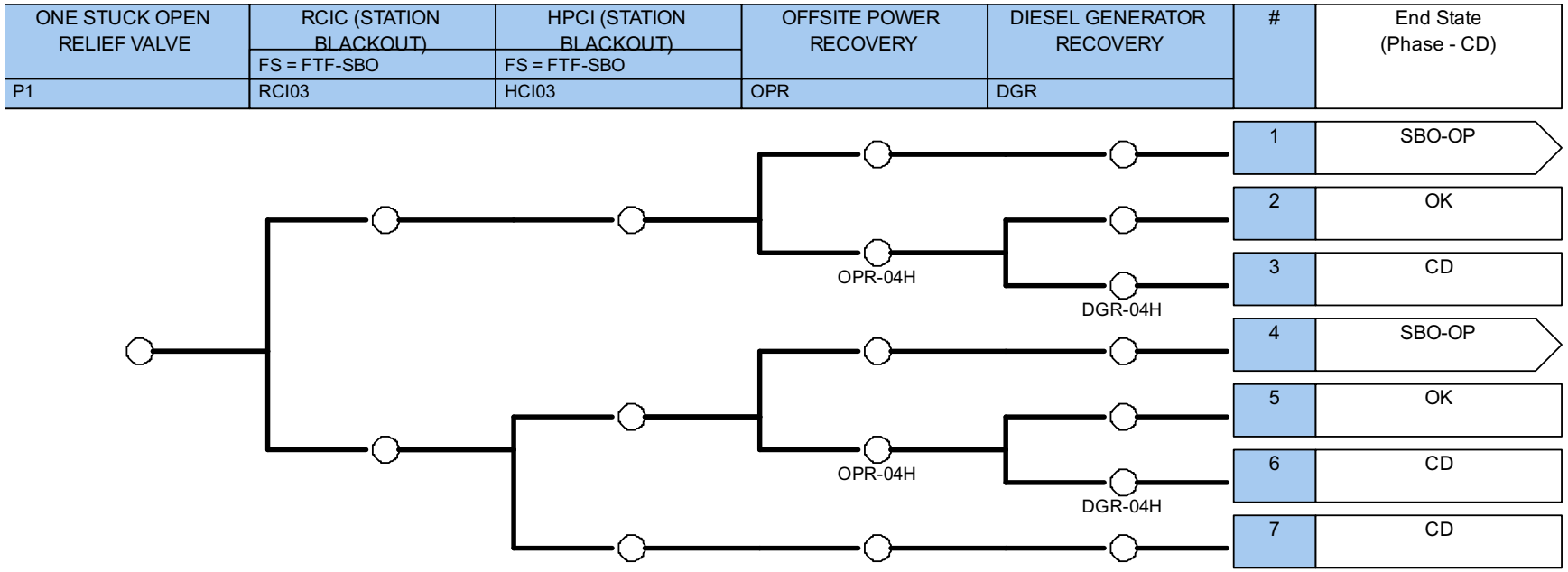

Figure 4-5. Generic BWR SBO-1 Sub-Tree.

A review of the 114 weather-related SBO accident sequences shows there are only 10 non-zero sequences (or sequence CDF greater than 1E-12/year, which was set as the quantification truncation level). The total weather-related SBO CDF is 3.67E-7/year. These 10 non-zero SBO sequences, as shown in Table 4-3, are described below in the order of their significances:

- LOOPWR:37-03-17, with a CDF of 2.77E-7/year contributing about 75% of the total weather-related CDF. In this SBO sequence, there is no SRV LOCA, no recirculation pump seal LOCA, RCIC is available, but no AC power recovery in 4 hours when the DC batteries deplete. CD occurred with no extended operation of RCIC or HPCI to remove the heat.
- LOOPWR:37-06-17, with a CDF of 4.10E-8/year contributing about 10% of the total weather-related SBO CDF. This sequence is similar to the first one (LOOPWR:37-03-17), with the difference in that RCIC is not available but HPCI is available to provide cooling water to the core before the batteries deplete.
- LOOPWR:37-11-3, with a CDF of 2.65E-8/year contributing about 7% of the total weather-related CDF. This sequence is similar to the first one (LOOPWR:37-03-17), with the difference that there is one SRV remaining open in the sequence.
- LOOPWR:37-09, with a CDF of 1.27E-8/year contributing about 3% of the total weather-related SBO CDF. This is a short-term station blackout (STSBO) as neither RCIC nor HPCI is available to mitigate the SBO event. There is no SRV LOCA in this sequence.
- LOOPWR:37-11-6, with a CDF of 3.80E-9/year contributing about 1% of the total weather-related CDF. This sequence is similar to the second one (LOOPWR:37-06-17), with the difference that there is one SRV remaining open in the sequence.
- LOOPWR:37-11-7, with a CDF of 3.44E-9/year contributing nearly 1% of the total weather-related SBO CDF. This is another STSBO sequence that is similar to LOOPWR:37-09. However, there is one SRV kept open through the event.
- LOOPWR:37-12, with a CDF of 2.85E-9/year contributing nearly 1% of the total weather-related SBO CDF. Two or more SRVs are kept open through the event for which the PRA model assumes CD.
- LOOPWR:37-01-05, a non-risk significant sequence with a very small CDF of 2.22E-11/year. In this SBO sequence, there is no SRV LOCA, no recirculation pump seal LOCA, RCIC is available, AC power is recovered in 4 hours before the DC batteries deplete. However, the SP cooling is not available, and although secondary side depressurization is success, the containment venting and late injection (LI) failed for long-term water injection. CD is expected.
- LOOPWR:37-01-11, a non-risk significant sequence with a very small CDF of 3.15E-12/year. This sequence is similar to the previous one (LOOPWR:37-01-05), with the difference in that both SP cooling and secondary side depressurization are not available. CD is assumed.
- LOOPWR:37-07-23, a non-risk significant sequence with a very small CDF of 1.68E-12/year. This is also an STSBO with neither RCIC nor HPCI being available before and after AC power recovery to mitigate the SBO event. There is no SRV LOCA in this sequence.

Table 4-3. BWR Non-Zero SBO Sequences.

None-Zero SBO Sequence	CDF	CDF%	Cut Sets
LOOPWR:37-03-17	2.77E-07	75.4%	473
LOOPWR:37-06-17	4.10E-08	11.2%	709
LOOPWR:37-11-3	2.65E-08	7.2%	242
LOOPWR:37-09	1.27E-08	3.5%	933
LOOPWR:37-11-6	3.80E-09	1.0%	260
LOOPWR:37-11-7	3.44E-09	0.9%	374
LOOPWR:37-12	2.85E-09	0.8%	144
LOOPWR:37-01-05	2.22E-11	0.0%	6
LOOPWR:37-01-11	3.15E-12	0.0%	1
LOOPWR:37-07-23	1.68E-12	0.0%	1
Total	3.67E-07	100.0%	3143

Nine SBO scenarios were developed for RELAP5-3D analysis based on the above BWR SBO PRA sequences, and were grouped into four categories:

1. Four long-term station blackout (LTSBO) with no AC power recovery scenarios, SBO-1 to SBO-1.3
2. Two STSBO with no RCIC/HPCI mitigation scenarios, SBO-2 and SBO-2.1
3. One SRV LOCA scenario, SBO-4
4. Two LTSBO with AC power recovery scenarios, SBO-4 and SBO-4.1, which are non-risk significant.

Table 4-4 shows the RELAP5-3D scenarios and their corresponding PRA sequences. Table 4-5 presents the details of each RELAP5-3D scenario.

Table 4-4. BWR Weather-Related SBO Scenarios for RELAP5-3D.

RELAP5-3D Scenario	Scenario Description	SBO PRA Sequence	CDF
SBO-1	No SRV Open, RCIC Success, but AC power not recovered in 4 hours, No RCIC/HPCI Black Run	LOOPWR:37-03-17	2.77E-07
SBO-1.1	No SRV Open, HPCI Success, but AC power not recovered in 4 hours, No RCIC/HPCI Black Run	LOOPWR:37-06-17	4.10E-08
SBO-1.2	One SRV Open, RCIC Success, but AC power not recovered in 4 hours	LOOPWR:37-11-3	2.65E-08
SBO-1.3	One SRV Open, HPCI Success, but AC power not recovered in 4 hours	LOOPWR:37-11-6	3.80E-09
SBO-2	No SRV Open, No RCIC/HPCI -> STSBO	LOOPWR:37-07-23	1.68E-12
SBO-2	No SRV Open, No RCIC/HPCI -> STSBO	LOOPWR:37-09	1.27E-08
SBO-2.1	One SRV Open, No RCIC or HPCI -> STSBO	LOOPWR:37-11-7	3.44E-09
SBO-3	Two or more SRV Open	LOOPWR:37-12	2.85E-09
SBO-4	No SRV Open, RCIC Success, AC Power Recovered, SPC Failed, DEP Success, containment venting system (CVS) failed, LI failed	LOOPWR:37-01-05	2.22E-11
SBO-4.1	No SRV Open, RCIC Success, AC Power Recovered, SPC Failed, DEP failed	LOOPWR:37-01-11	3.15E-12

Table 4-5. SBO Scenarios for RELAP-5 3D Analysis.

RELAP5 SBO Scenario		SBO Main ET & SBO-1				SBO-OP (AC Power Recovered)					SBO-ELAP
#	Description	Open SRVs	RCIC Available	HPCI Available	AC Power Recovery	RCIC/HPCI Available	SPC Available	Depress. Success	Containment Venting	LI	Extended RCIC/HPCI
SBO-1	No SRV Open, RCIC Success, but AC power not recovered in 4 hours, No RCIC/HPCI Black Run	0	Yes		4Hrs No						No
SBO-1.1	No SRV Open, HPCI Success, but AC power not recovered in 4 hours, No RCIC/HPCI Black Run	0	No	Yes	4Hrs No						No
SBO-1.2	One SRV Open, RCIC Success, but AC power not recovered in 4 hours	1	Yes		4Hrs No						
SBO-1.3	One SRV Open, HPCI Success, but AC power not recovered in 4 hours	1	No	Yes	4Hrs No						
SBO-2	No SRV Open, No RCIC/HPCI -> STSBO	0	No	No							
SBO-2.1	One SRV Open, No RCIC or HPCI -> STSBO	1	No	No							
SBO-3	Two or more SRV Open	>=2									
SBO-4	No SRV Open, RCIC Success, AC Power Recovered, SPC Failed, DEP Success, CVS failed, LI failed	0	Yes		4Hrs Yes	Yes	No	Yes	No	No	
SBO-4.1	No SRV Open, RCIC Success, AC Power Recovered, SPC Failed, DEP failed	0	Yes		4Hrs Yes	Yes	No	No			

4.2 BWR SBO RELAP5-3D Analysis

SBO scenarios are triggered by an initiating event (e.g., fire, flood, or seismic event) that causes the complete loss of AC electric power to the essential and nonessential switchgear buses in an NPP. This happens with the loss of the offsite electric power system concurrent with turbine trip and unavailability of the onsite emergency AC power system. Because many safety systems required for reactor core cooling, decay heat removal, and containment heat removal are dependent on AC power, the consequence of an SBO could be a severe CD accident, as indicated in the PRA analysis presented in the previous subsection.

When an initiating event causes the loss of all onsite and offsite AC power, the reactor protection system (RPS) would scram the reactor, tripping the turbines. The TBVs close. MSIVs close due to low RPV water level and the RPV becomes isolated. Due to the loss of AC power, the recirculation pumps stop, and the main feedwater pumps also stop pumping water into RPV. The LPCI mode of the RHR system and LPCS are not available. Containment cooling and containment spray systems are also not available. Additionally, SLCS as well as the CRHDS are not available.

In the SBO scenarios, SRVs are functioning because the valves can be lifted by steam to release steam from RPV and reduce pressure in it. If the onsite DC power is available, the turbine-driven systems, such as RCIC and HPCI, that rely on control power for their operations, would work until the DC power is exhausted. In the PRA analysis shown in Section 4.1, it is assumed the DC power lasts for 4 hours before it is exhausted. The availability of DC power delays the occurrence of CD and hence it is named as LTSBO.

Additionally, if the DC power is lost, it will result in the loss of turbine-driven systems (RCIC and HPCI) or other safety systems that rely on control power. This scenario proceeds to CD more rapidly and hence it is named as STSBO. An STSBO has a lower CDF (as shown in Table 4-4) because it requires a more severe initiating event and more extensive system failures.

The following presents the RELAP5-3D analyses for each of the scenarios described in Table 4-5.

4.2.1 SBO-1: LTSBO with RCIC Available for 4 Hours

In this scenario, the station batteries are assumed to provide DC power for 4 hours before it is exhausted following the loss of all AC power. Therefore, the RCIC system is available for 4 hours after the accident initiation. The DC power-controlled components and systems can operate as required for this period, such as the RPV water level instrumentation. As a result, RCIC operations can be controlled so that the RPV water level will remain between12.0914 m and 14.7828 m. RCIC starts to inject water to RPV once water level falls below the lower bound and stops once the water level rises above the upper bound. Once the station batteries are exhausted at 4 hours, RCIC system will cease operation. It is also assumed that the RCIC system will not blackrun (manual operation) once the DC power is exhausted after 4 hours. It is further assumed in this scenario that the AC power is not recovered after 4 hours, and consequently all water injections to the RPV are lost after 4 hours and the core proceeds to fuel failure and CD. Because the decay power is at a much lower level than that of an STSBO, the accident progression would be slower, and time-to-core-damage would be longer.

The differences between calculations due to the different claddings were negligible prior to the onset of core uncovery and were relatively small after the onset of core uncovery. The calculations were terminated when the hottest cladding in each RELAP5-3D run reached its failure temperature. The termination times varied by less than 20 minutes. The calculated amount of hydrogen produced during the transients varied significantly between claddings.

Figure 4-6 shows the RCIC mass flow rate to RPV. The RCIC works between 0 and 4 hours with the water injection at rated mass flow rate. Figure 4-7 shows the collapsed water level in the RPV and it is shown that in the first 4 hours, the RPV core water level is controlled to stay within a proper range due to the availability of core water level monitoring and regulated water injection into the RPV by RCIC. The collapsed water level starts to drop after RCIC stops injecting water to the RPV due to boil-off caused by decay heat. The RPV dome pressure is maintained in a prescribed range as shown in Figure 4-8, with the automatic operations of SRV, as shown in

Figure 4-9. The RCIC steam flow is shown in Figure 4-10 and the void fraction for one control volume in the hot channel is shown in Figure 4-11. The void fraction is kept at a fairly low range in the first 4 hours when RCIC water injection to the RPV is available. After RCIC stops injecting water, the water level starts to drop, and the void fraction is going up and reaches dryout conditions. As SRVs releases high-pressure and high-temperature steam into the SP, the suppression temperature goes up as shown in Figure 4-12. The PCT comparisons for Zry, Cr-coating, and FeCrAl claddings are shown in Figure 4-13. It can be seen that the PCTs are kept low for 6 hours until dryout starts to happen and the PCTs start to rise exponentially until the cladding reaches melting temperature.

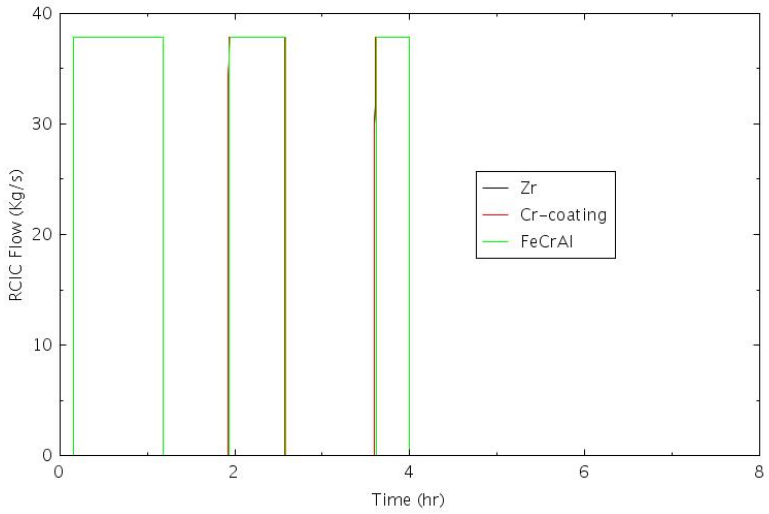

Figure 4-6. RCIC Mass Flow Rate to RPV at BOC for SBO-1.

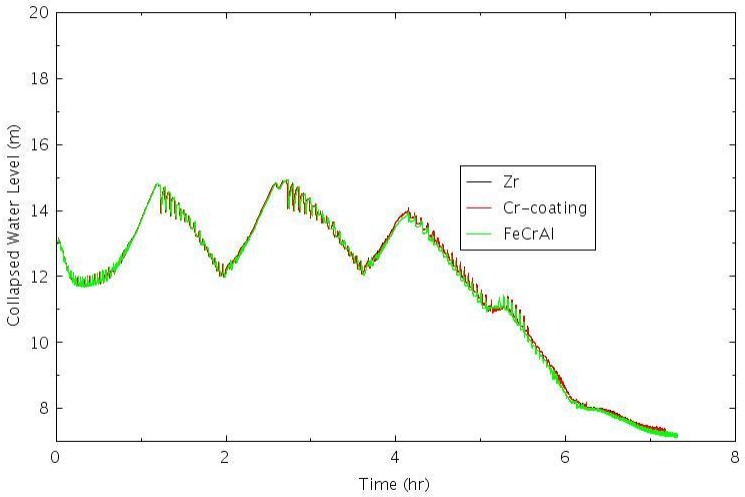

Figure 4-7. Collapsed Water Level in the RPV at BOC for SBO-1.

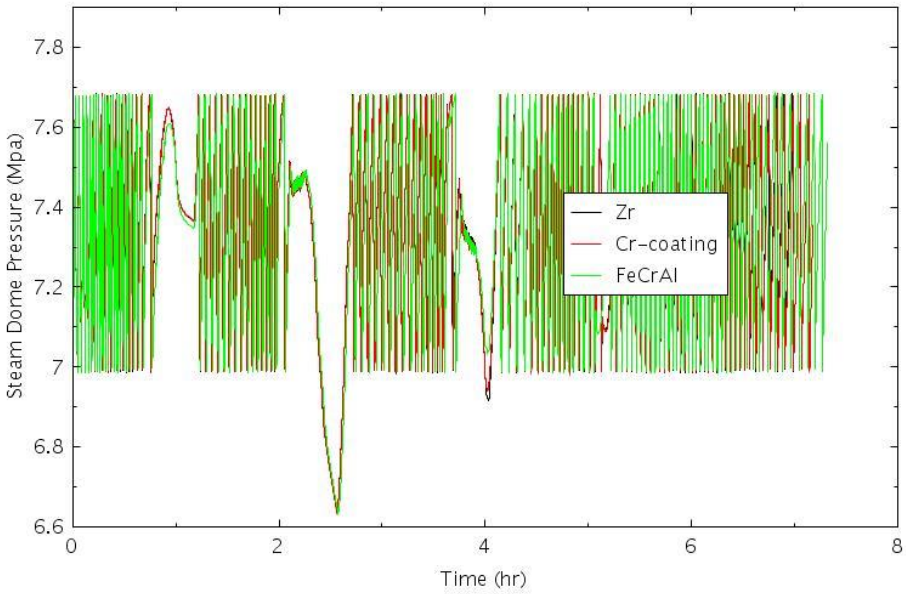

Figure 4-8. Dome Pressure at BOC for SBO-1.

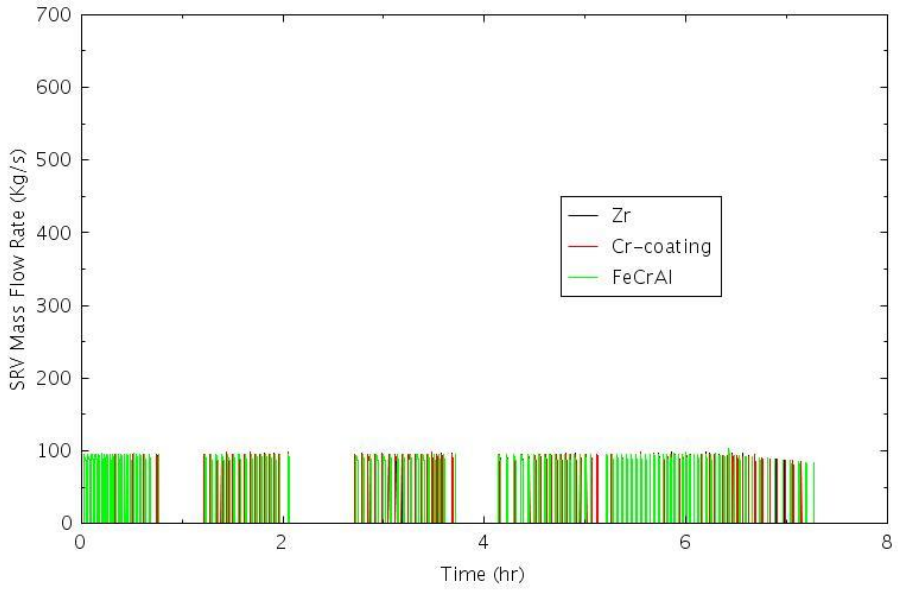

Figure 4-9. SRV Mass Flow Rate at BOC for SBO-1.

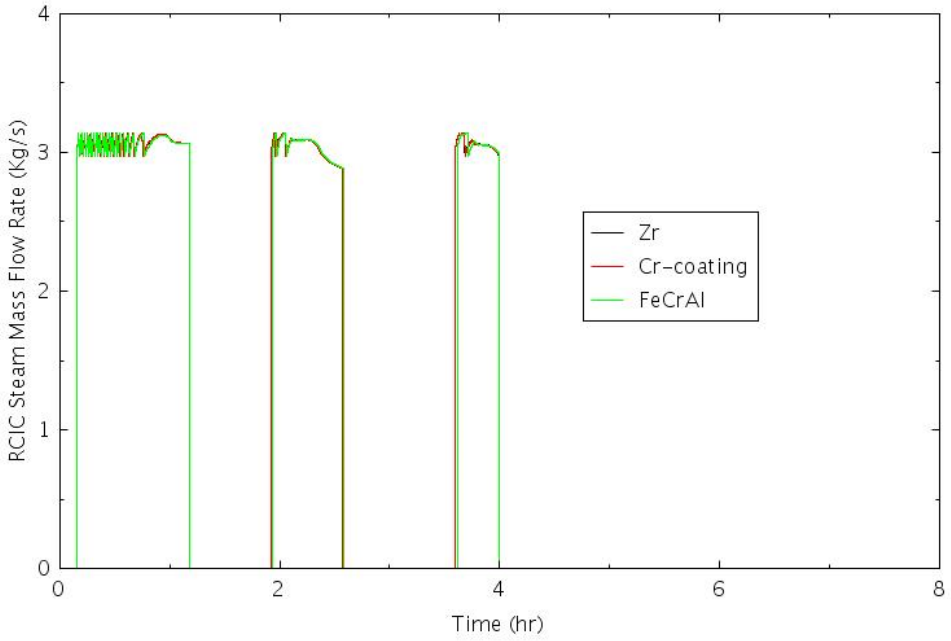

Figure 4-10. RCIC Steam Mass Flow Rate at BOC for SBO-1.

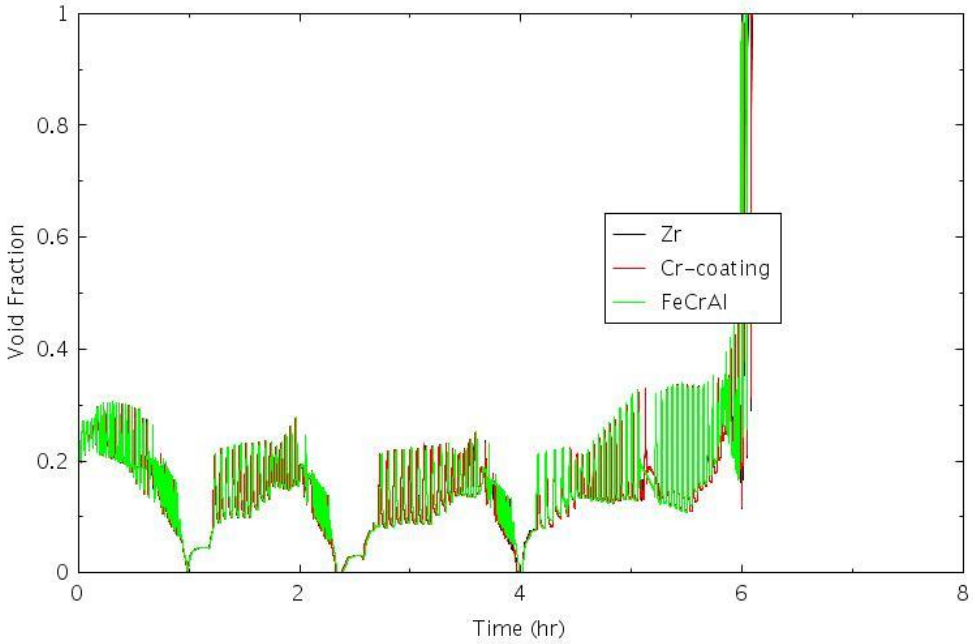

Figure 4-11. Void Fraction for One Element in the Hot Channel at BOC for SBO-1.

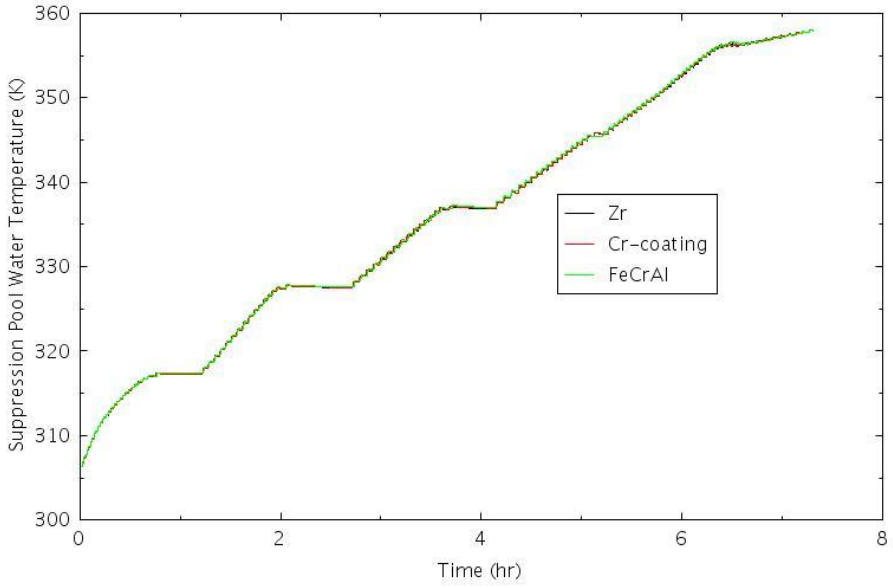

Figure 4-12. SP Water Temperature at BOC for SBO-1.

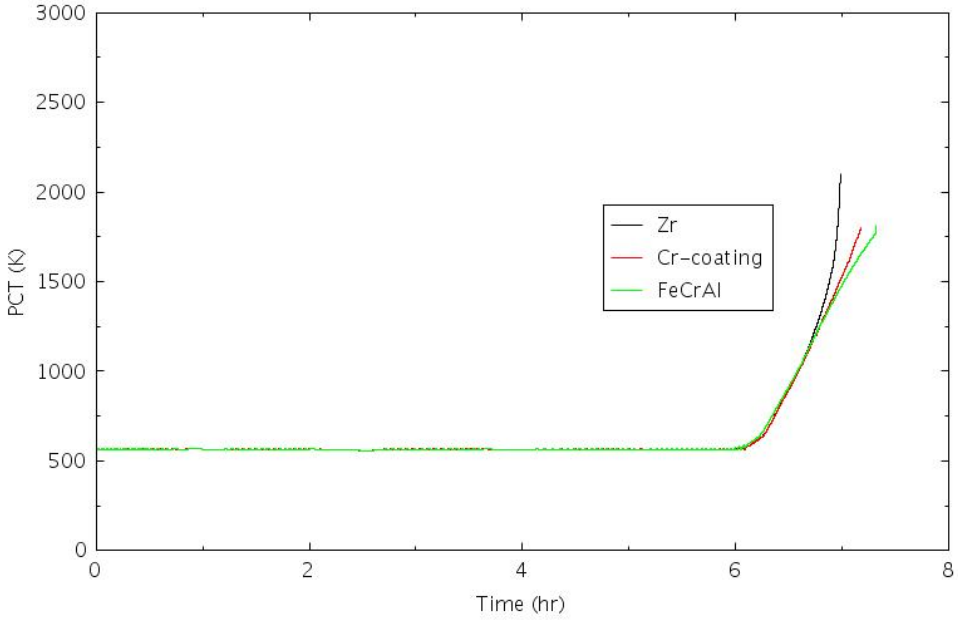

Figure 4-13. PCT at BOC for SBO-1.

4.2.2 SBO-1.1: LTSBO with HPCI Available for 4 Hours

In this scenario, the station batteries are assumed to provide DC power for 4 hours following the loss of all AC power. It is further assumed that HPCI system is available for 4 hours while RCIC system is not available after the accident initiation. Same as that in SBO-1, the DC power controlled components and systems can operate as required for this period, such as the RPV water level instrumentation. As a result, HPCI operations can be controlled so that the RPV water level will remain between 12.0914 m and 14.7828 m. HPCI starts to inject water to RPV once water level falls below the lower bound and stops once the water level rises above the upper bound. Once the station batteries are exhausted at 4 hours, HPCI system will cease operation. It is also assumed that the HPCI (and RCIC) systems will not blackrun (manual operation) once the DC power is exhausted after 4 hours. Just like that in SBO-1, it is further assumed in this scenario that the AC power is not recovered after 4 hours, and consequently all water injections to the RPV are lost after 4 hours and the core proceeds to fuel failure and CD. In this scenario, the decay heat power is at a much lower level compared to that of STSBO, the accident progression would be slower, and time-to-core-damage would also be longer.

HPCI has much higher water injection rate than that of RCIC. Figure 4-14 shows the HPCI mass flow rate to RPV, which is about nine times higher than that of RCIC as shown in Figure 4-6. The HPCI works between 0 and 4 hours. Figure 4-15 shows the collapsed water level in the first 4 hours and it is shown that the RPV core water level is controlled to stay within a proper range due to the availability of core water level monitoring. The RPV dome pressure is maintained in a prescribed range as shown in Figure 4-16, with the automatic operations of SRV, as shown in Figure 4-17. The HPCI steam flow is shown in Figure 4-18 and the void fraction for one control volume in the hot channel is shown in Figure 4-19. The void fraction is kept at a fairly low range in the first 4 hours when RCIC water injection to the RPV is available. After HPCI stops injecting water, the water level starts to drop, and the void fraction is going up and reaches dryout conditions. As SRVs releases high-pressure and high-temperature steam into the SP, the suppression temperature goes up as shown in Figure 4-20. The PCT comparisons for Zry, Cr-coating, and FeCrAl claddings are shown in Figure 4-21.

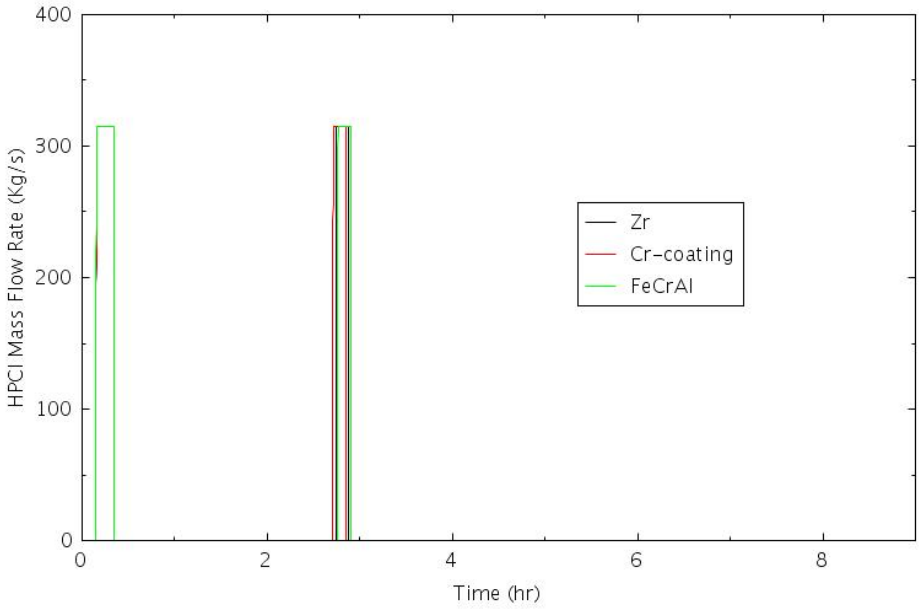

Figure 4-14. HPCI Mass Flow Rate at BOC for SBO-1.1.

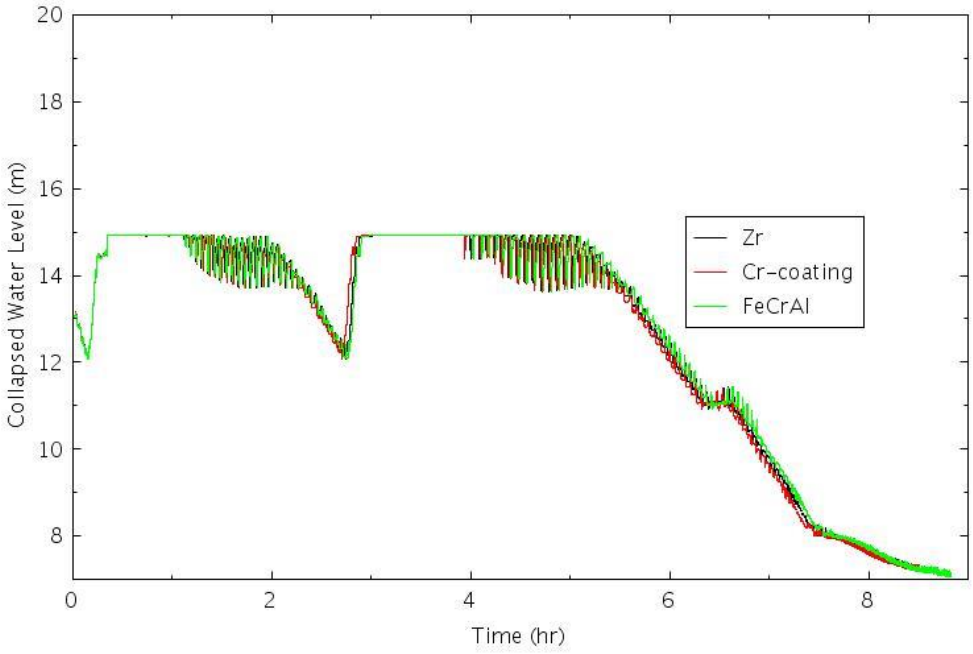

Figure 4-15. RPV Collapsed Downcomer Water Level at BOC for SBO-1.1.

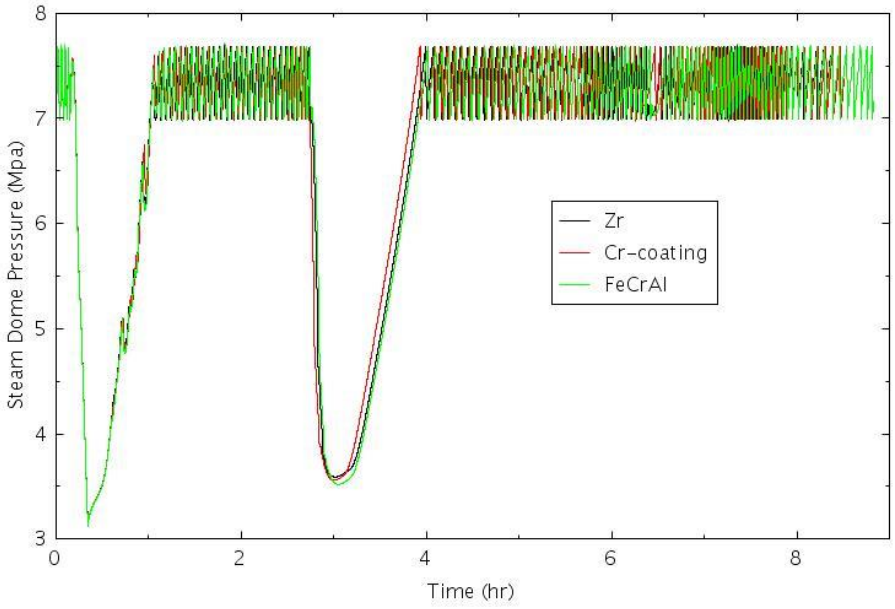

Figure 4-16. Dome Pressure at BOC for SBO-1.1.

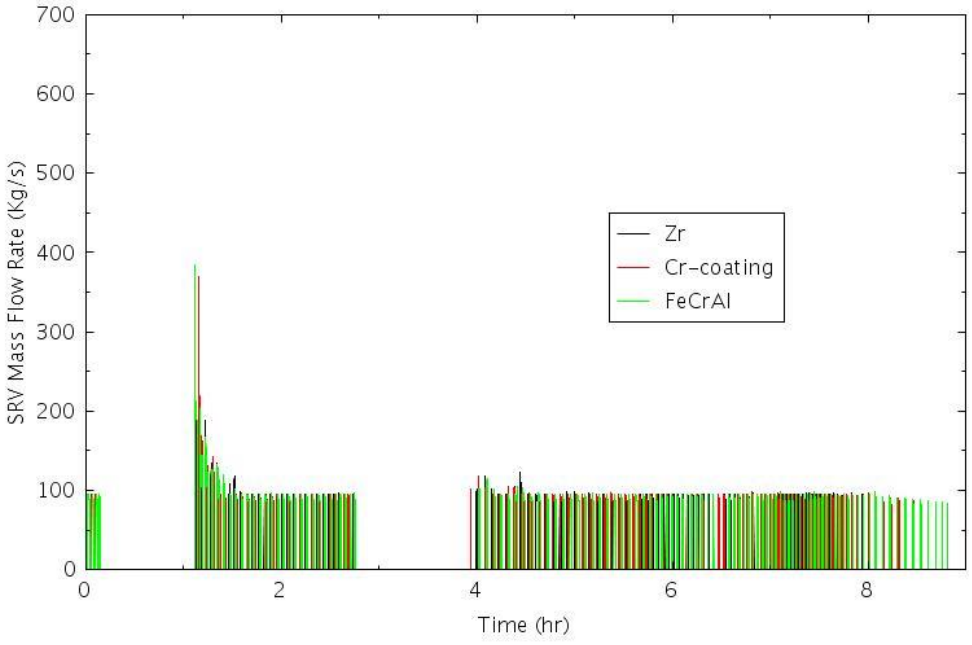

Figure 4-17. SRV Mass Flow Rate at BOC for SBO-1.1.

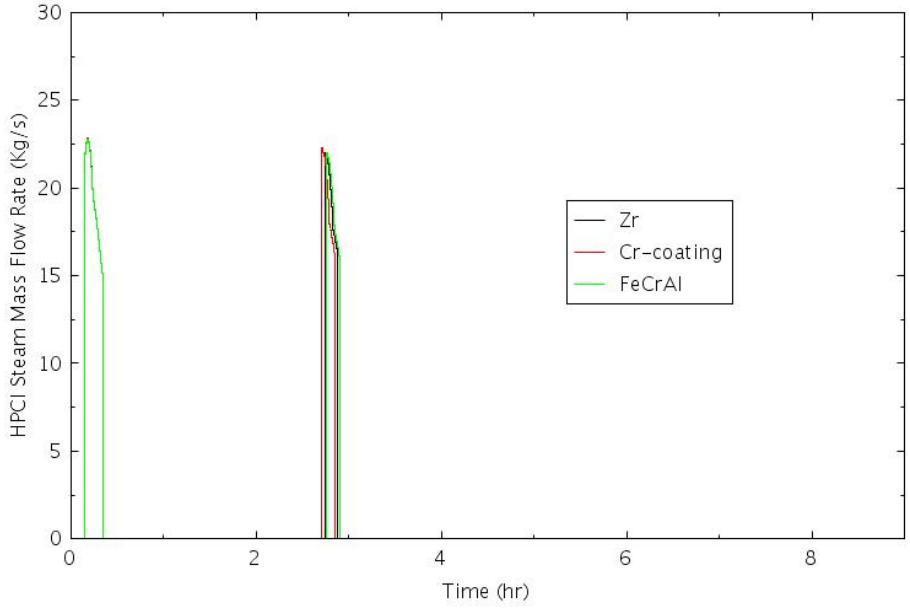

Figure 4-18. Steam Mass Flow Rate for HPCI System at BOC for SBO-1.1.

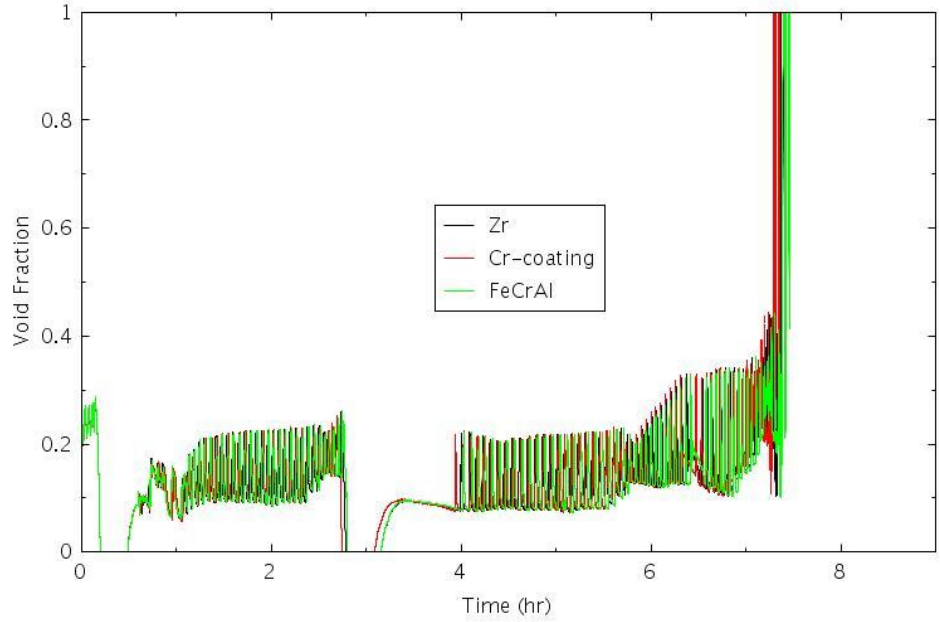

Figure 4-19. Void Fraction in One Element of the Hot Channel at BOC for SBO-1.1.

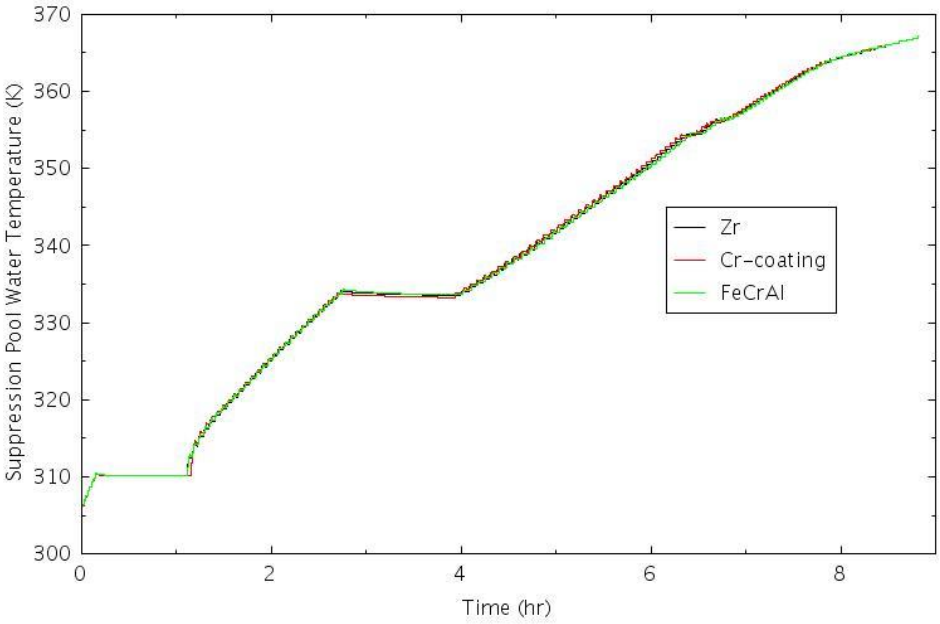

Figure 4-20. SP Water Temperature at BOC for SBO-1.1.

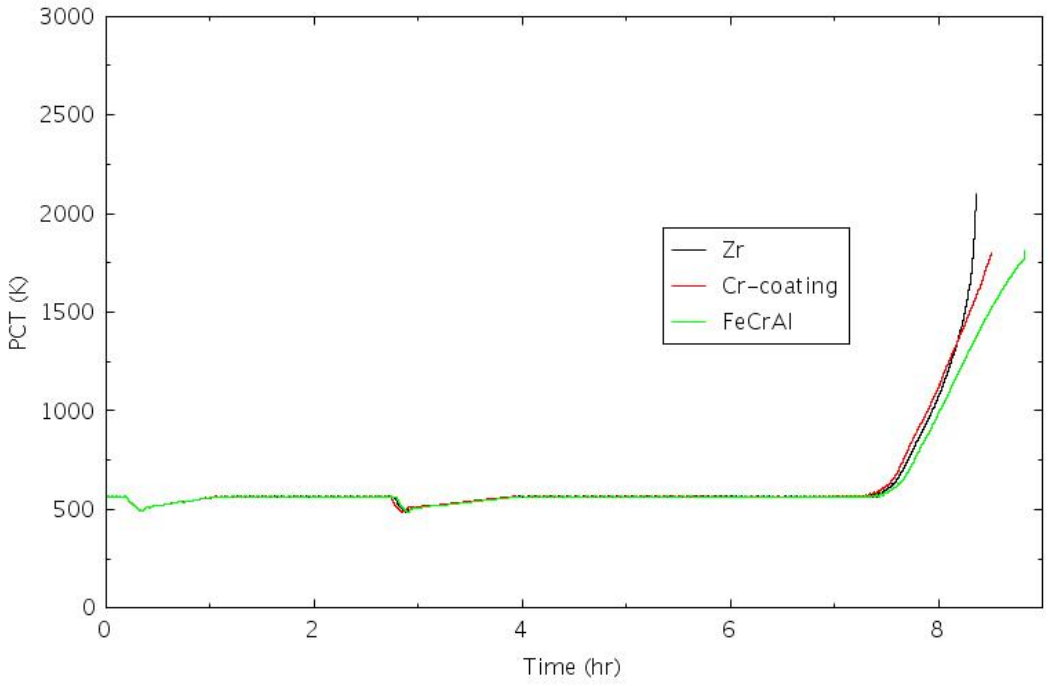

Figure 4-21. PCT at BOC for SBO-1.1.

4.2.3 SBO-1.2: LTSBO with RCIC Available for 4 Hours and One SRV Stuck Open

In this scenario, the station batteries are assumed to provide DC power for 4 hours following the loss of all AC power. The RCIC system is available for 4 hours after the accident initiation. However, one SRV is assumed to stick open once it is activated. Therefore, the RPV depressurizes rapidly. The DC-power-controlled components and systems can operate as required for this period, such as the RPV water level instrumentation. As a result, RCIC operation can be controlled so that the RPV water level will remain between 12.0914 m and 14.7828 m. RCIC starts to inject water to RPV once water level falls below the lower bound and stops once the water level rises above the upper bound. Once the station batteries are exhausted at 4 hours, the RCIC system will cease operation. It is also assumed that the RCIC system will not blackrun (manual operation) once the DC power is exhausted after 4 hours. It is further assumed in this scenario that the AC power is not recovered after 4 hours, and consequently all water injections to the RPV are lost after 4 hours and the core proceeds to fuel failure and CD. Because the decay power is at a much lower level than that of STSBO, the accident progression would be slower, and time-to-core-damage would be longer.

Figure 4-22 shows the RCIC mass flow rate to RPV. The RCIC works between 0 and 3 hours before the high water level setpoint is reached even though the DC power is available for 4 hours. Figure 4-23 shows the collapsed water level which is controlled to stay within a proper range when the core water level monitoring is available in the first 4 hours. The water level drops initially due to the loss of the RPV inventory resulting from the one SRV being stuck open. The water level starts to rise at about 1 hour due to the water injection from RCIC. The RCIC water injection stops at slightly over 2.5 hours, when the water level reaches the upper bound. After that, the water level drops continuously due to the steam release from a stuck-open SRV. Due to the continuous release of steam from the one stuck-open SRV, the RPV pressure is depressurized rapidly in the first hour and stays low for the remaining transient time, as shown in Figure 4-24. The SRV steam mass flow rate is shown in

Figure 4-25. The RCIC steam flow is shown in Figure 4-26 and the void fraction for one control volume in the hot channel is shown in Figure 4-27. The void fraction is kept at a fairly low range in the first 6 hours due to the availability of RCIC water injection to the RPV in the first 4 hours. After 6 hours, the void fraction goes up rapidly and reaches dryout conditions. As SRVs release high-pressure and high-temperature steam into the SP, the suppression temperature goes up as shown in Figure 4-28. The PCT comparisons for Zry, Cr-coating, and FeCrAl claddings are shown in Figure 4-29.

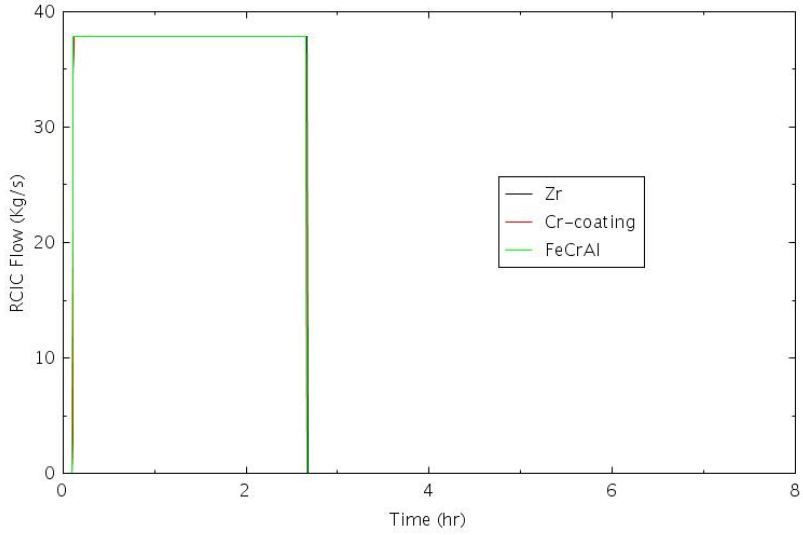

Figure 4-22. RCIC Water Injection Mass Flow Rate at BOC for SBO-1.2.

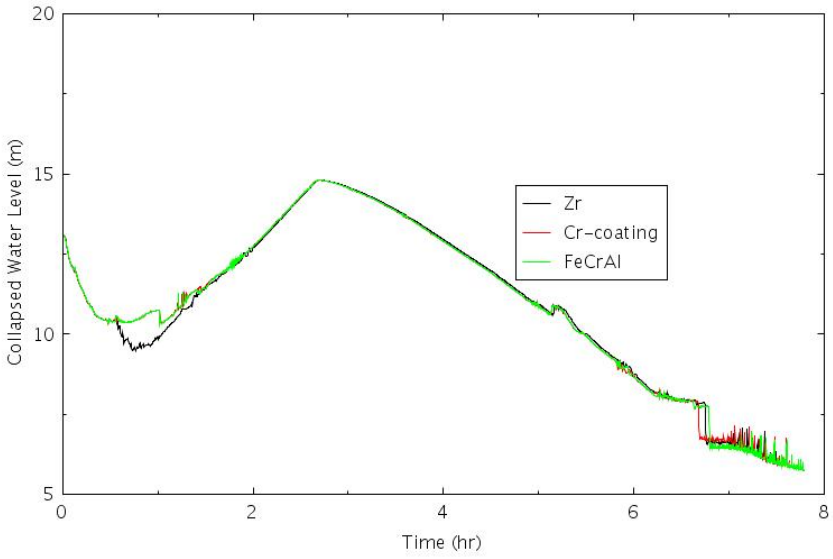

Figure 4-23. RPV Downcomer Collapsed Water Level at BOC for SBO-1.2.

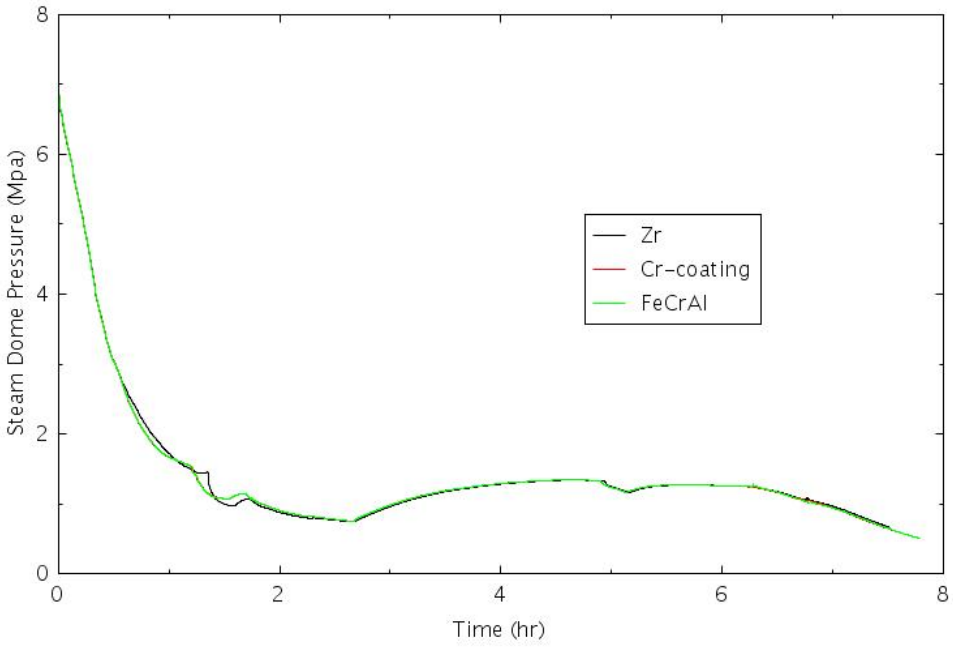

Figure 4-24. RPV Dome Pressure at BOC for SBO-1.2.

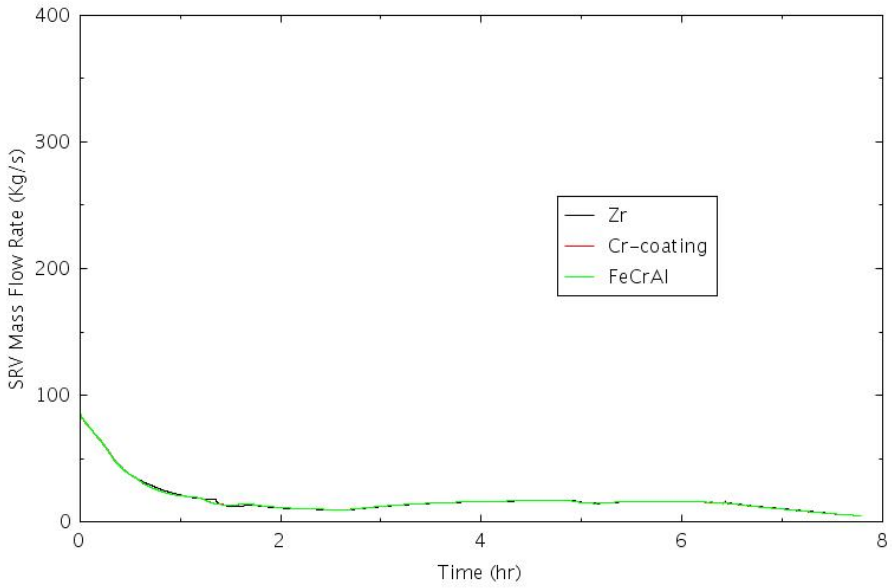

Figure 4-25. SRV Mass Flow Rate at BOC for SBO-1.2.

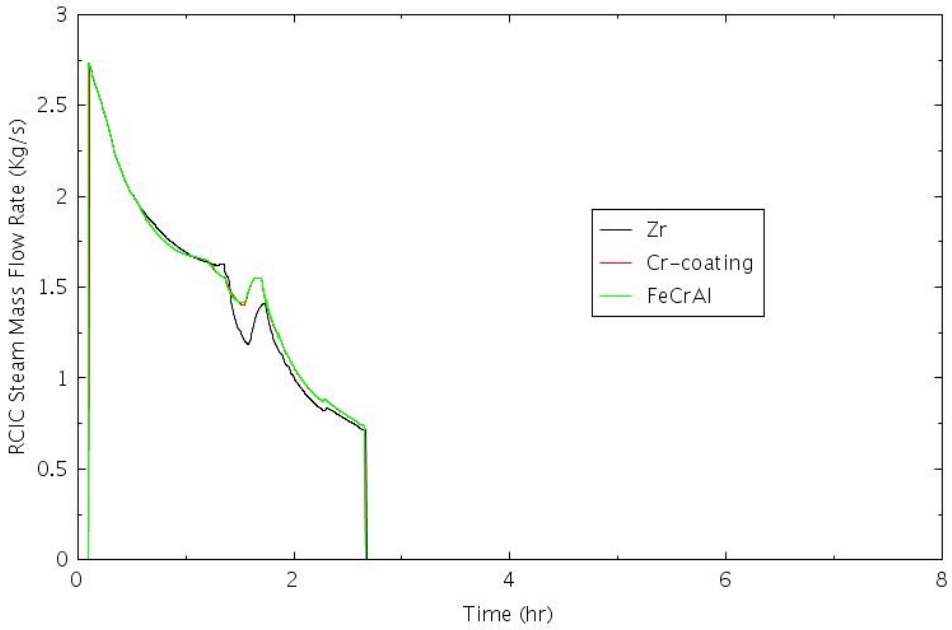

Figure 4-26. RCIC Steam Mass Flow Rate at BOC for SBO-1.2.

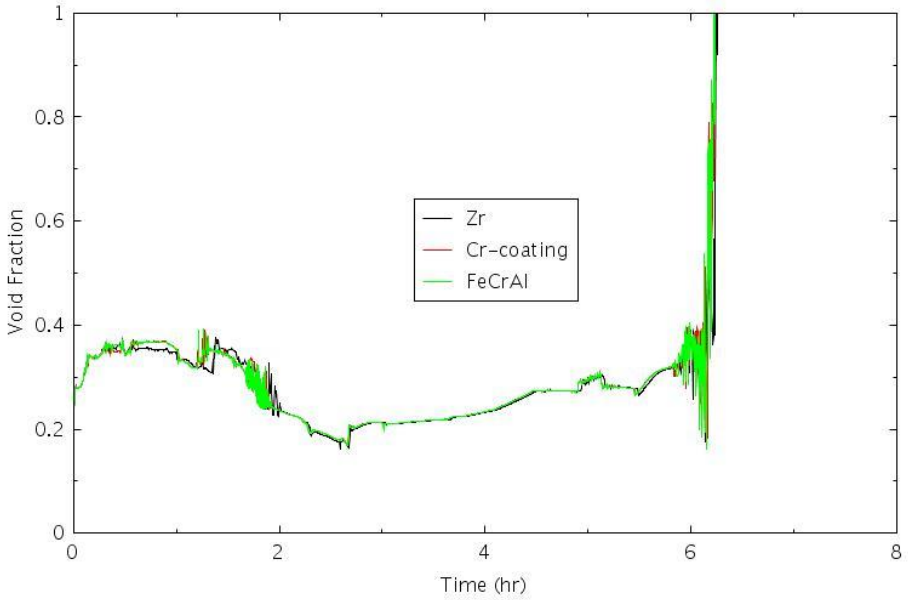

Figure 4-27. Void Fraction in One Element of the Hot Channel at BOC for SBO-1.2.

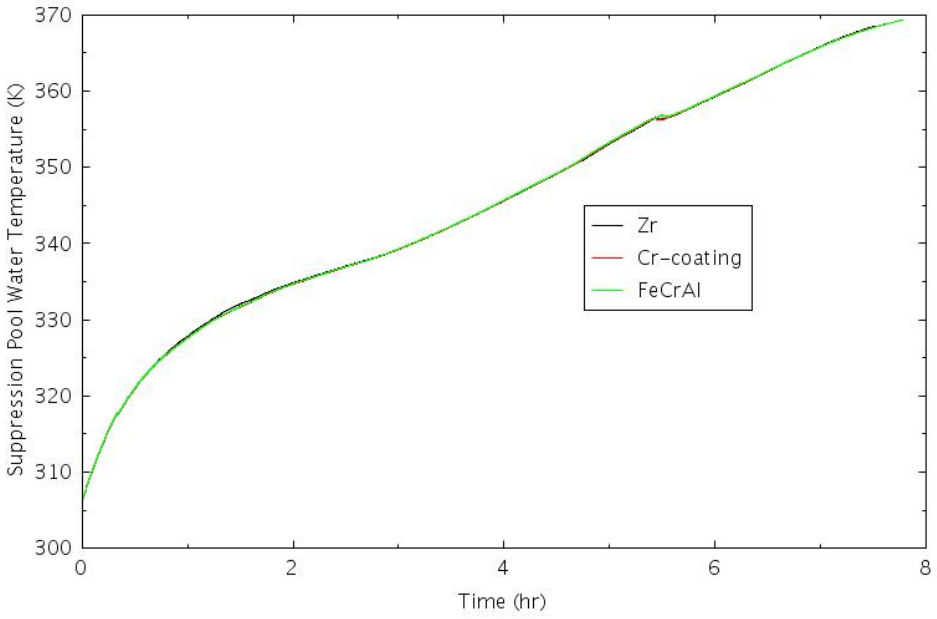

Figure 4-28. SP Water Temperature at BOC for SBO-1.2.

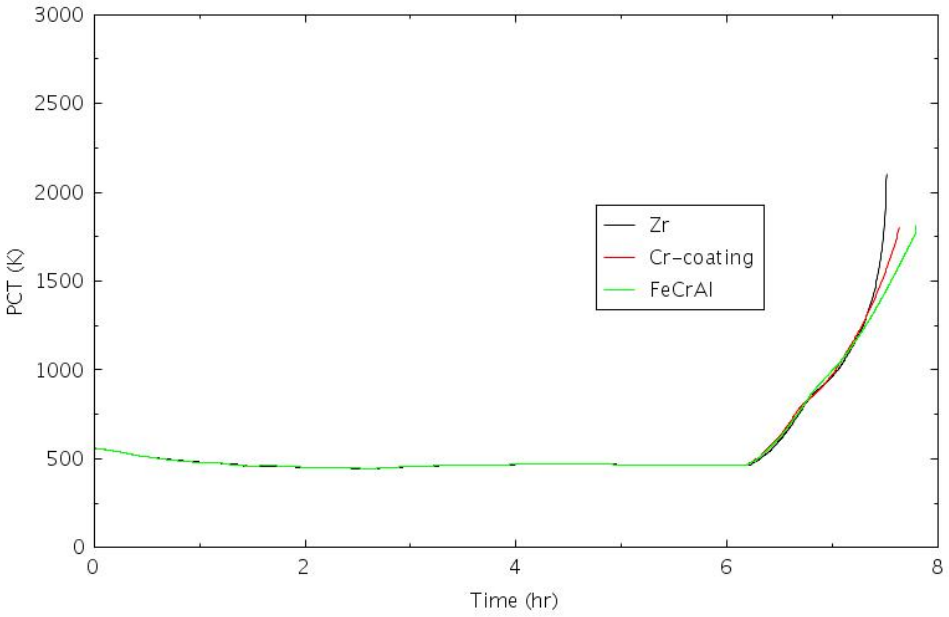

Figure 4-29. PCT at BOC for SBO-1.2.

4.2.4 SBO-1.3: LTSBO with HPCI Available for 4 Hours and One SRV Stuck Open

In this scenario, the station batteries are assumed to provide DC power for 4 hours following the loss of all AC power. The HPCI system is available for 4 hours after the accident initiation. However, one SRV is assumed to stick open once it is activated. Therefore, the RPV depressurizes rapidly. The DC power controlled components and systems can operate as required for this period, such as the RPV water level instrumentation. As a result, HPCI operation can be controlled so that the RPV water level will remain between 12.0914 m and 14.7828 m. HPCI starts to inject water to RPV once water level falls below the lower bound and stops once the water level rises above the upper bound. Once the station batteries are exhausted at 4 hours, HPCI system will cease operation. It is also assumed that the HPCI system will not blackrun (manual operation) once the DC power is exhausted after 4 hours. It is further assumed in this scenario that the AC power is not recovered after 4 hours, and consequently all water injections to the RPV are lost after 4 hours and the core proceeds to fuel failure and CD. Because the decay power is at a much lower level than that of STSBO, the accident progression would be slower, and time-to-core-damage would be longer.

Figure 4-30 shows the HPCI mass flow rate to RPV. Due to the high mass flow rate of HPCI, the HPCI system is turned on for a short period of time before it is turned off twice between 0 and 4 hours. Figure 4-31 shows the collapsed water level which is controlled to stay within a proper range due to the availability of HPCI injection and core water level monitoring. The collapsed water level starts to drop continuously at about 6 hours. The RPV dome pressure, as shown in Figure 4-32, decreases rapidly within the first half an hour of the transient due to the stuck open of one SRV and stays at a low level for the remaining of the transient. The SRV steam flow is shown in Figure 4-33. The steam mass flow rate through HPCI is shown in Figure 4-34. The void fraction for one control volume in the hot channel is shown in Figure 4-35. The void fraction is kept at a fairly low range in the first 8 hours due to the availability of HPCI water injection in the first 4 hours. After 8 hours, the void fraction is going up and reaches dryout conditions. As SRVs releases high-pressure and high-temperature steam into the SP, the suppression temperature goes up as shown in Figure 4-36. The PCT comparisons for Zry, Cr-coating, and FeCrAl claddings are shown in Figure 4-37.

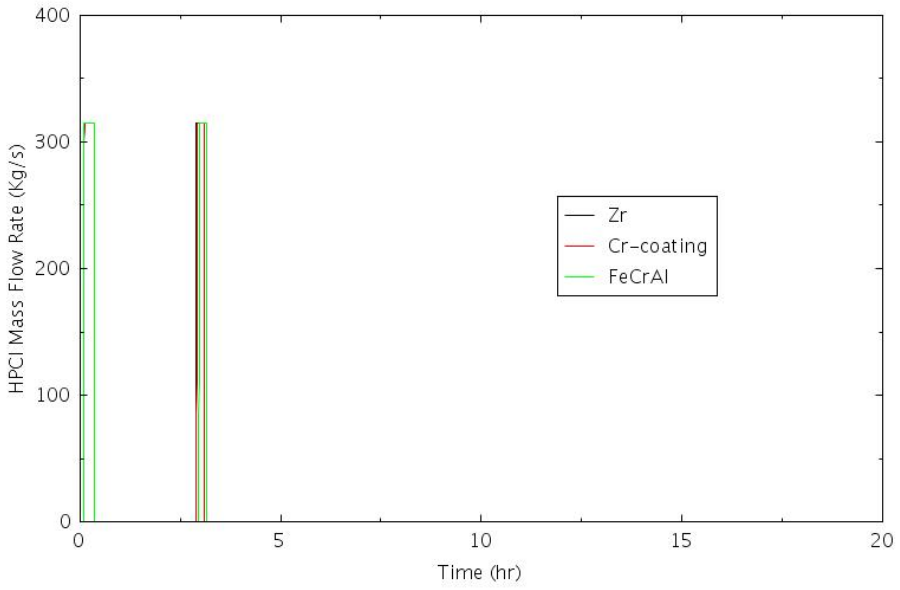

Figure 4-30. HPCI Water Injection Mass Flow Rate at BOC for SBO-1.3.

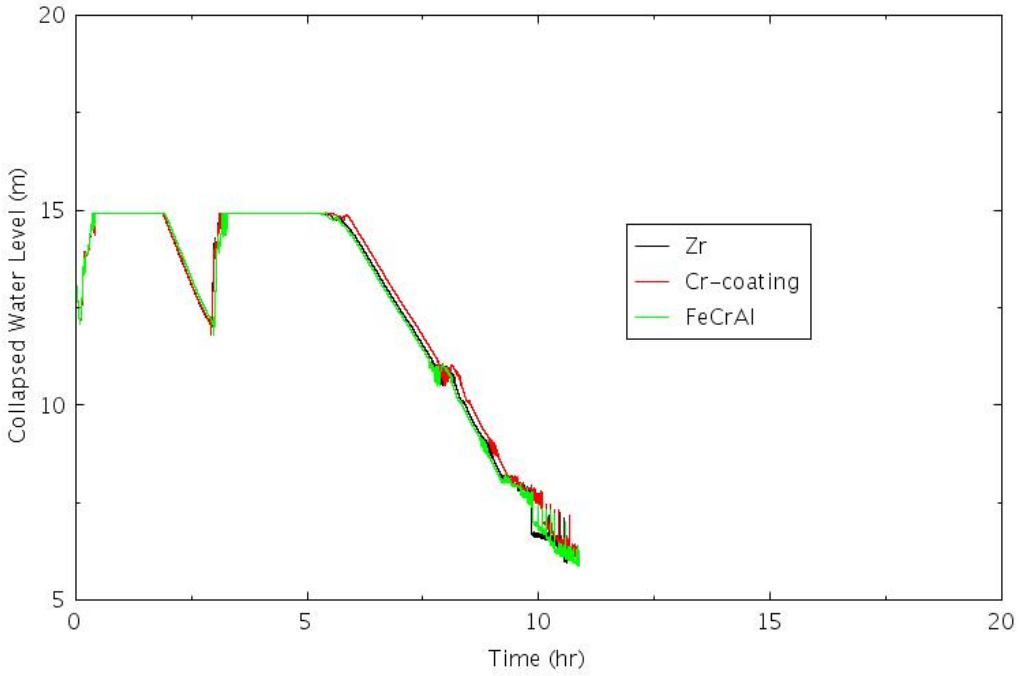

Figure 4-31. RPV Downcomer Collapsed Water Level at BOC for SBO-1.3.

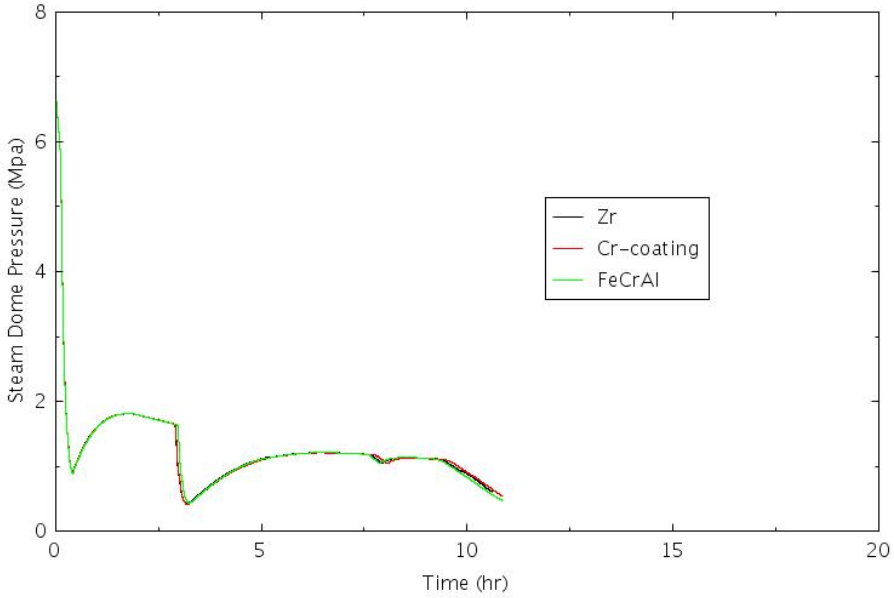

Figure 4-32. RPV Dome Pressure at BOC for SBO-1.3.

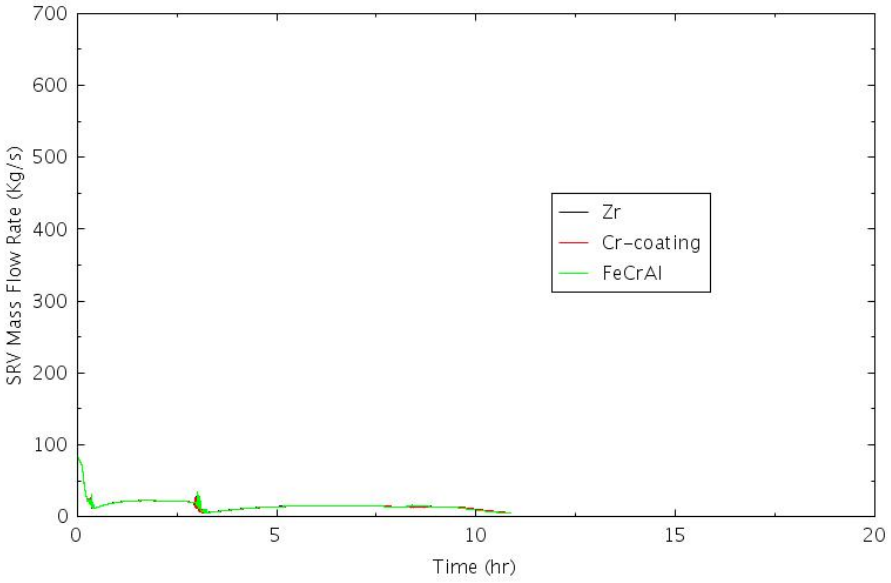

Figure 4-33. SRV Mass Flow Rate at BOC for SBO-1.3.

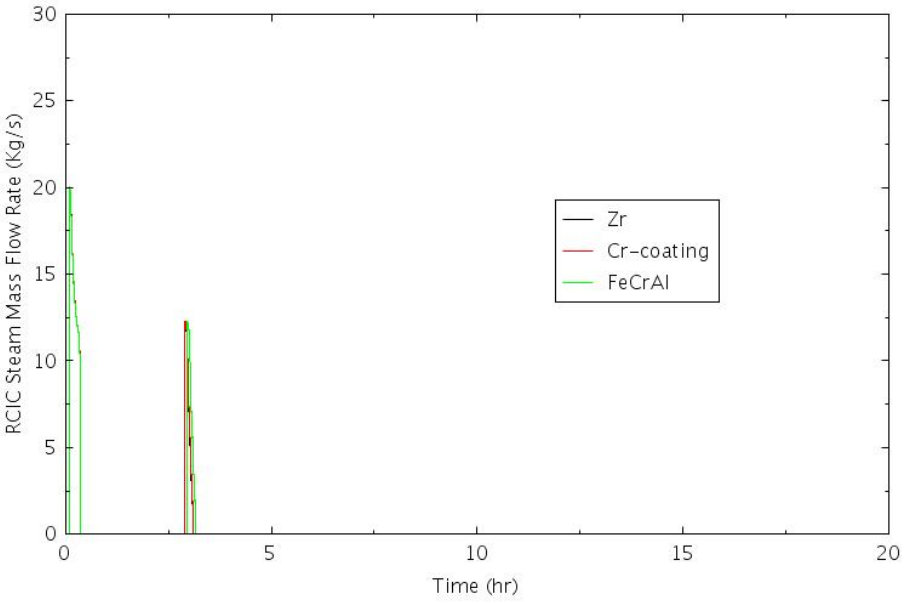

Figure 4-34. Steam Mass Flow Rate for HPCI at BOC for SBO-1.3.

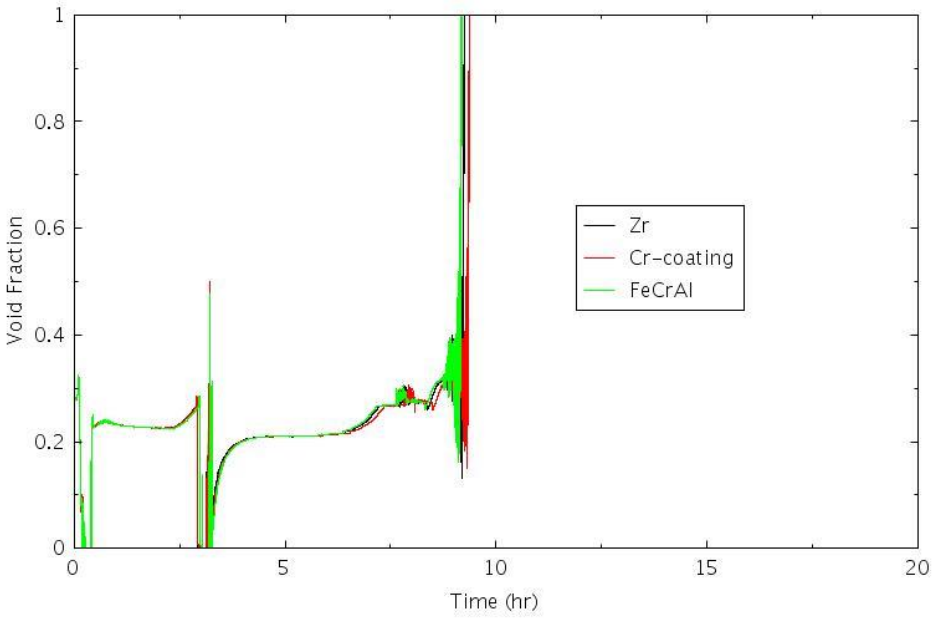

Figure 4-35. Void Fraction in One Element of the Hot Channel at BOC for SBO-1.3.

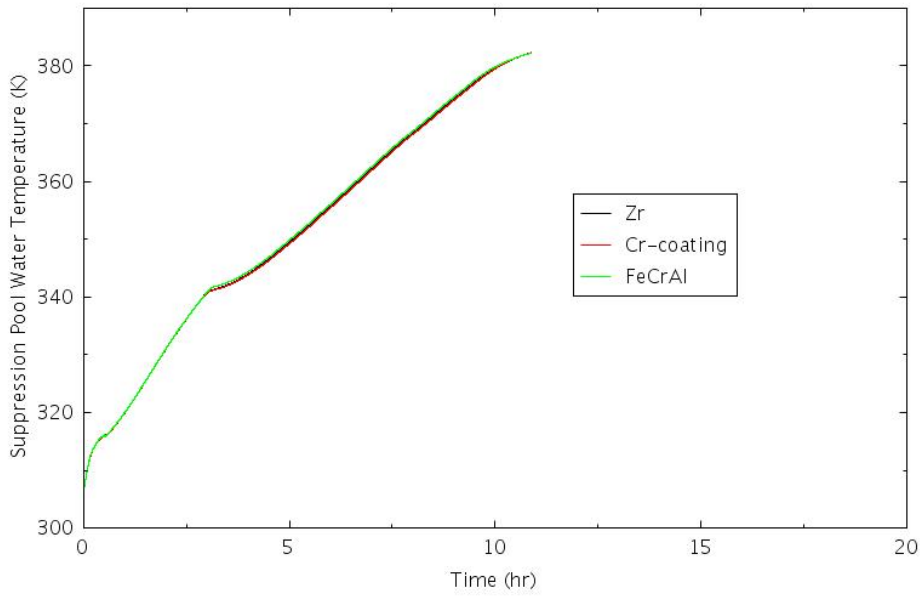

Figure 4-36. SP Water Temperature at BOC for SBO-1.3.

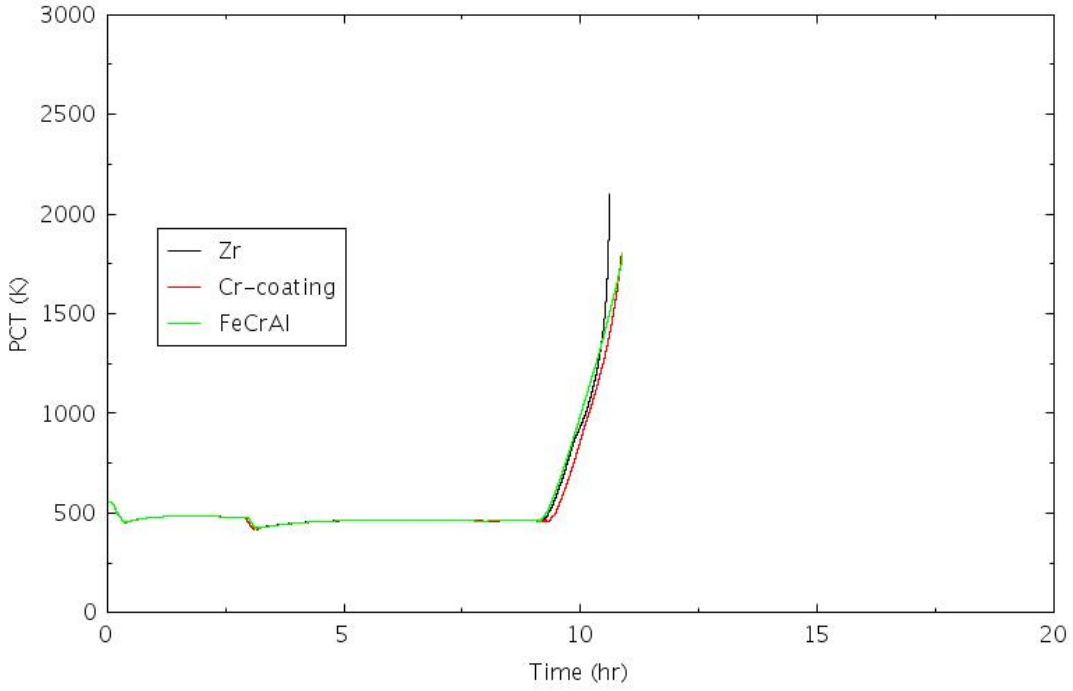

Figure 4-37. PCT at BOC for SBO-1.3.

4.2.5 SBO-2: Short-Term Station Blackout

STSBO is initiated by the same spectrum of events that leads to LTSBO, but is more extensive in the damage to plant equipment. Besides a total loss of offsite AC power from power grids and onsite AC power from diesel generators (DGs), all onsite DC power from station batteries is also assumed to fail. All plant components dependent on control or motive power for startup and operation are disabled, including steam-driven emergency coolant makeup systems such as RCIC and HPCI. It is further assumed that manual control of reactor pressure relief valves also fails. Plant operators will attempt to blackstart RCIC in STSBO condition. Several manual actions are required to blackstart RCIC, including opening normally closed valves to admit steam from the main steam lines to the steam-driven turbines of RCIC system and pump discharge valves so that water can be directed to the RPV. However, in this scenario, it is assumed that RCIC blackstart is not successful. Consequently, all coolant injections are lost so that the temperature of fuel and cladding will keep increasing until the cladding melts.

Figure 4-38 shows the collapsed water level which decreases continuously following the initiation of the SBO due the RPV keeping losing its coolant inventory by the opening/closing of the SRVs. The SRV total fluid mass flow rate is shown in Figure 4-39. The RPV dome pressure is shown in Figure 4-40. The oscillations of the RPV pressure are caused by the cycling of the SRVs. The SRVs open when the pressure of the main-line pipe where the SRVs are connected reaches opening threshold values, and close when the pressure drops to closing threshold values. In this way, the RPV pressure is kept in a safe range. The void fraction for one control volume in the hot channel is shown in Figure 4-41. The void fraction is kept at a fairly low range in the first half hour, then goes up fairly rapidly until dryout happens. As SRVs release high-pressure and high-temperature steam into the SP, the

suppression temperature goes up, as shown in Figure 4-42. The PCT comparisons for Zry, Cr-coating, and FeCrAl claddings are shown in Figure 4-43. The CD happens between 1.2 hour and 1.5 hours for these three types of cladding materials.

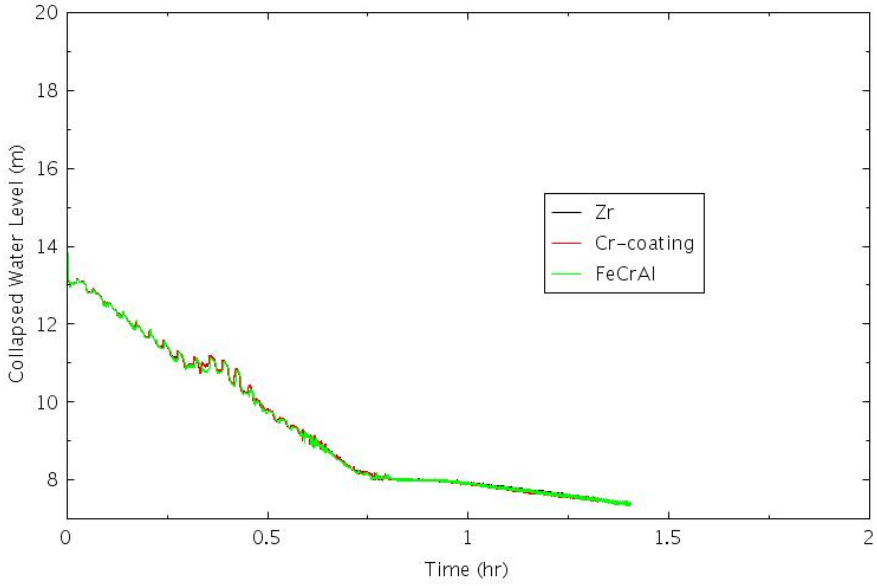

Figure 4-38. RPV Downcomer Collapsed Water Level at BOC for SBO-2.

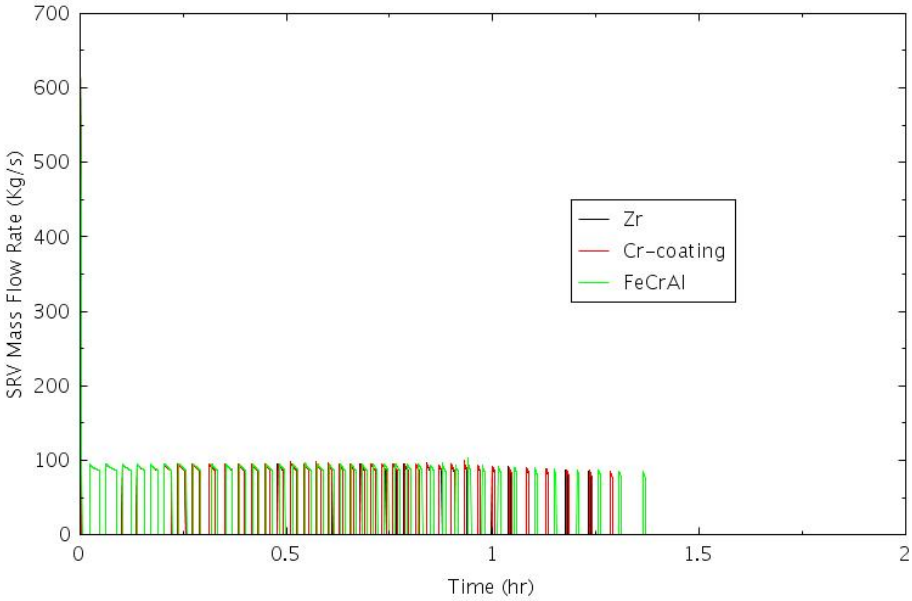

Figure 4-39. SRV Mass Flow Rate at BOC for SBO-2.

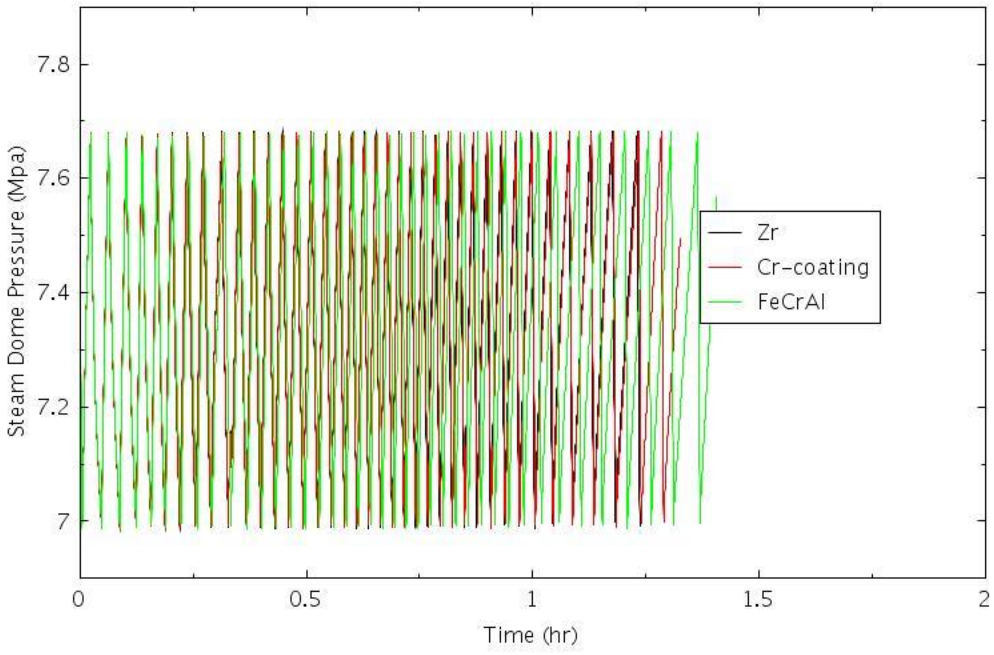

Figure 4-40. RPV Dome Pressure at BOC for SBO-2.

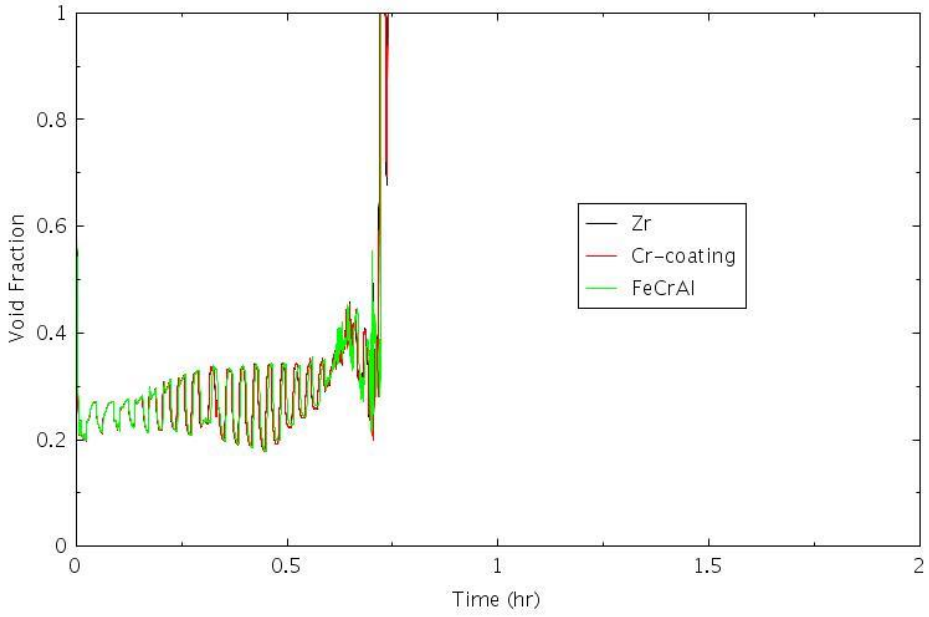

Figure 4-41. Void Fraction in One Element of the Hot Channel at BOC for SBO-2.

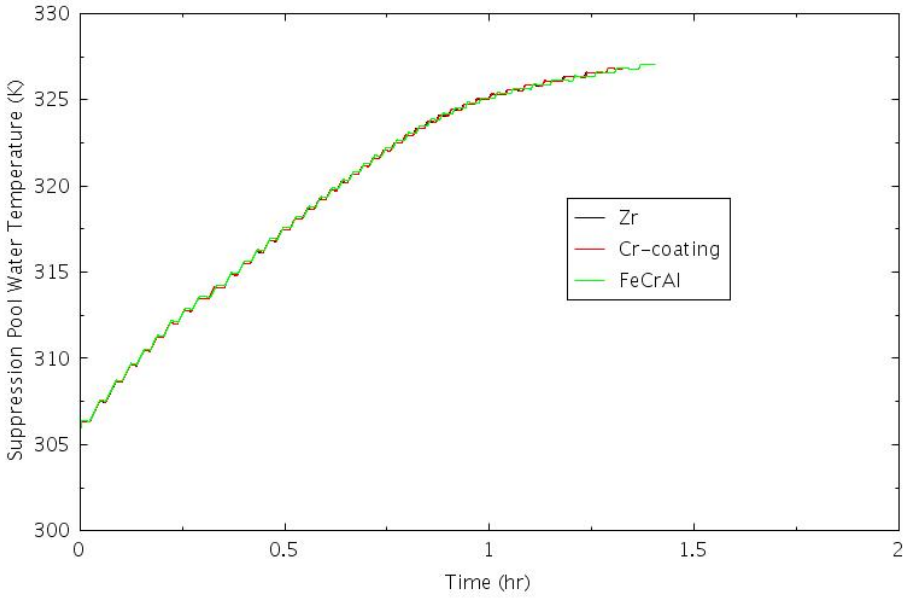

Figure 4-42. SP Water Temperature at BOC for SBO-2.

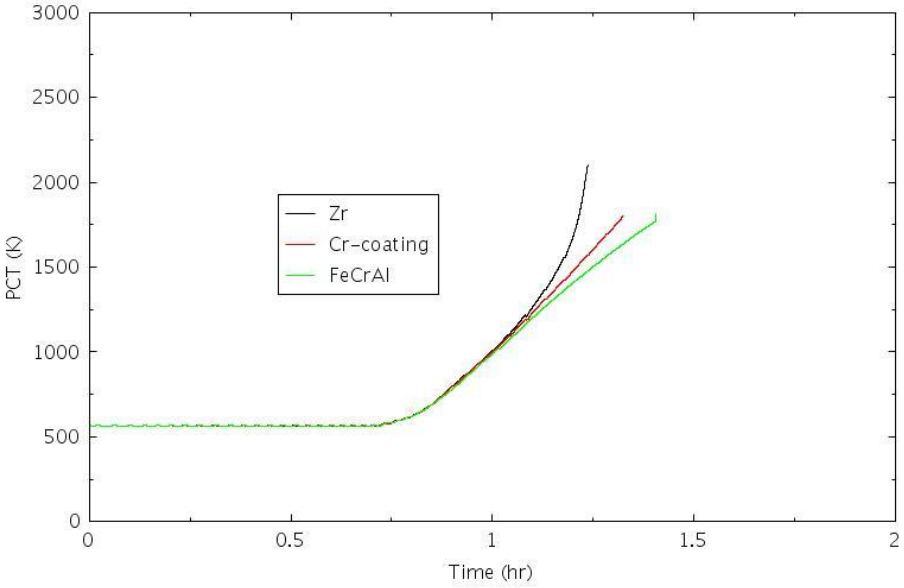

Figure 4-43. PCT at BOC for SBO-2.

4.2.6 SBO-2.1: STSBO with One SRV Open

This STSBO scenario is similar to the one described in SBO-2, with one major difference—one SRV sticks open once it is activated. Similar to SBO-2, in this STSBO scenario, besides a total loss of offsite AC power from power grids and onsite AC power from DGs, all onsite DC power from station batteries also fails. All plant components dependent on control or motive power for startup and operation are disabled, including steam-driven emergency coolant makeup systems (e.g., RCIC and HPCI), as well as manual control of reactor pressure relief valves. Plant operators will attempt to blackstart RCIC in STSBO condition. Several manual actions are required to blackstart RCIC, including opening normally closed valves to admit steam from the main steam lines to the steam-driven turbines of RCIC system and pump discharge valves so that water can be directed to the RPV. However, in this scenario, it is assumed that RCIC blackstart is not successful. Consequently, all coolant injections are lost so that the temperature of fuel and cladding will keep increasing until the cladding melts.

Figure 4-44 shows the dome pressure in this scenario. One SRV is stuck open so the RPV pressure decreases rapidly and continuously throughout the duration of the transient. The downcomer collapsed water level, as shown in Figure 4-45, also decreases rapidly and continuously due to the loss of the coolant inventory in the RPV from the stuck-open SRV. The SRV coolant mass flow rate is shown in Figure 4-46. As the RPV pressure decreases, the coolant mass flow rate also decreases. The void fraction for one control volume in the hot channel is shown in Figure 4-47. The void fraction is kept at a fairly low range in the first half hour and then goes up rapidly and reaches dryout conditions. As SRVs releases high-pressure and high-temperature steam into the SP, the suppression temperature goes up as shown in Figure 4-48. The PCT comparisons for Zry, Cr-coating, and FeCrAl claddings are shown in Figure 4-49. The CD happens within less than 1 hour for these three types of cladding materials. The stuck open one SRV induces more severe coolant loss from the RPV and hence core uncover happens sooner than that of SBO-2. Consequently, the CD happens sooner than that of SBO-2.

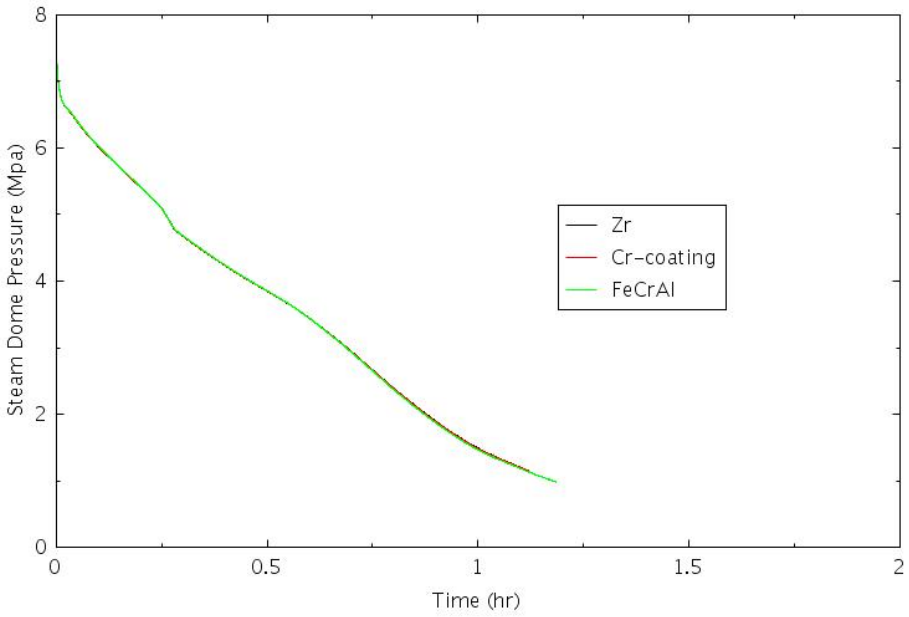

Figure 4-44. RPV Dome Pressure at BOC for SBO-2.1.

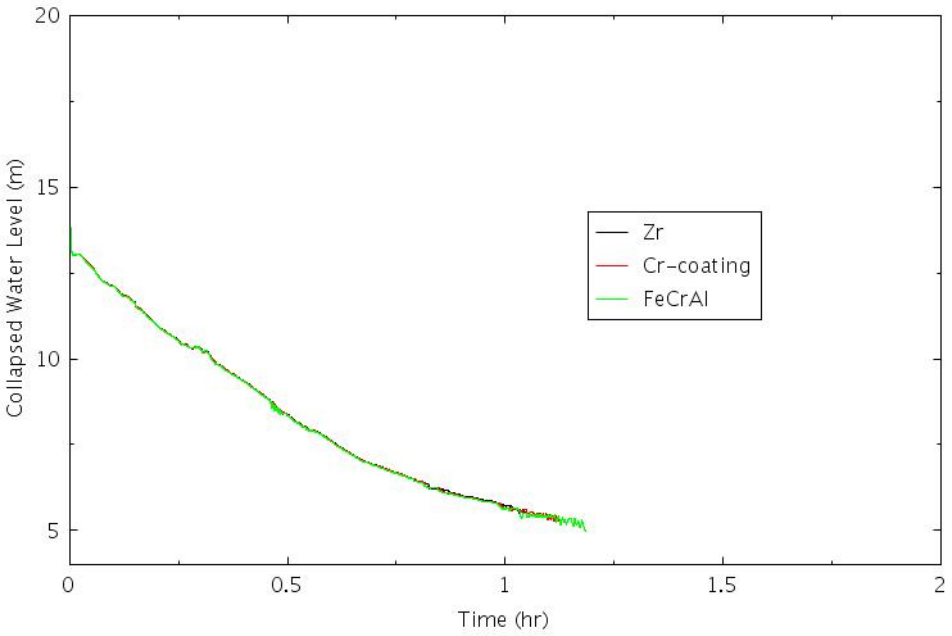

Figure 4-45. RPV Downcomer Collapsed Water Level at BOC for SBO-2.1.

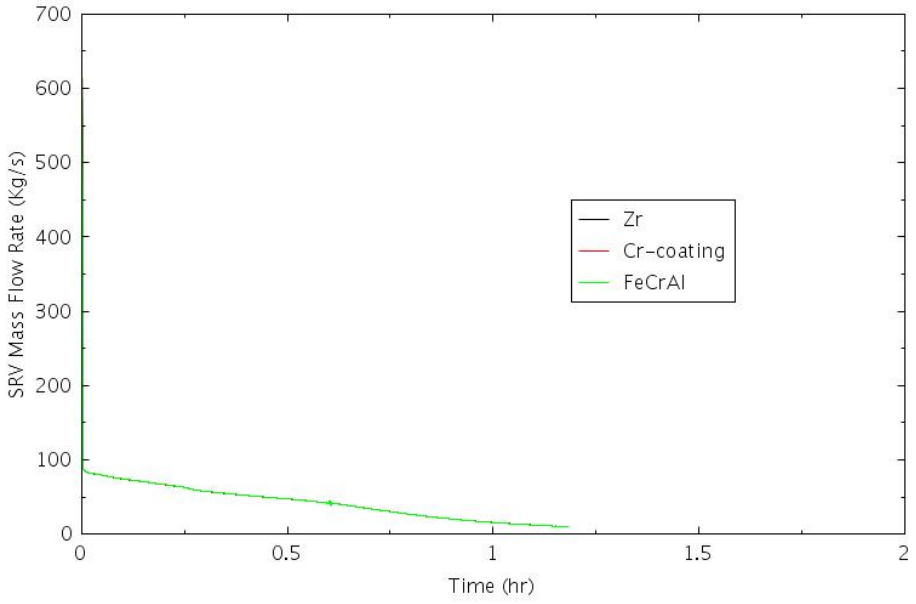

Figure 4-46. SRV Mass Flow Rate at BOC for SBO-2.1.

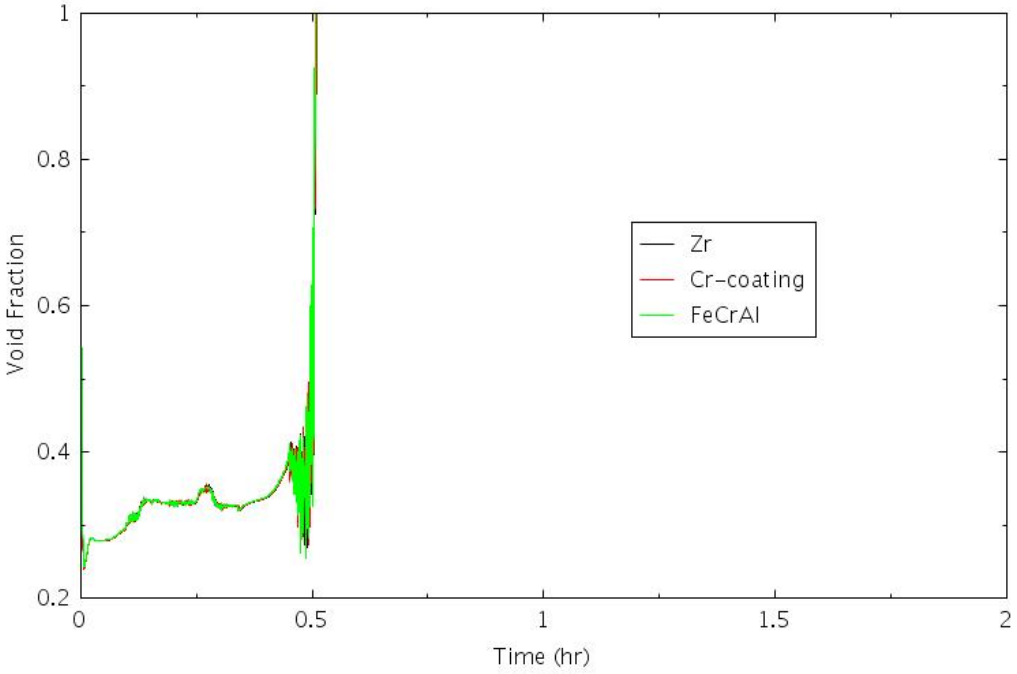

Figure 4-47. Void Fraction in One Element of the Hot Channel at BOC for SBO-2.1.

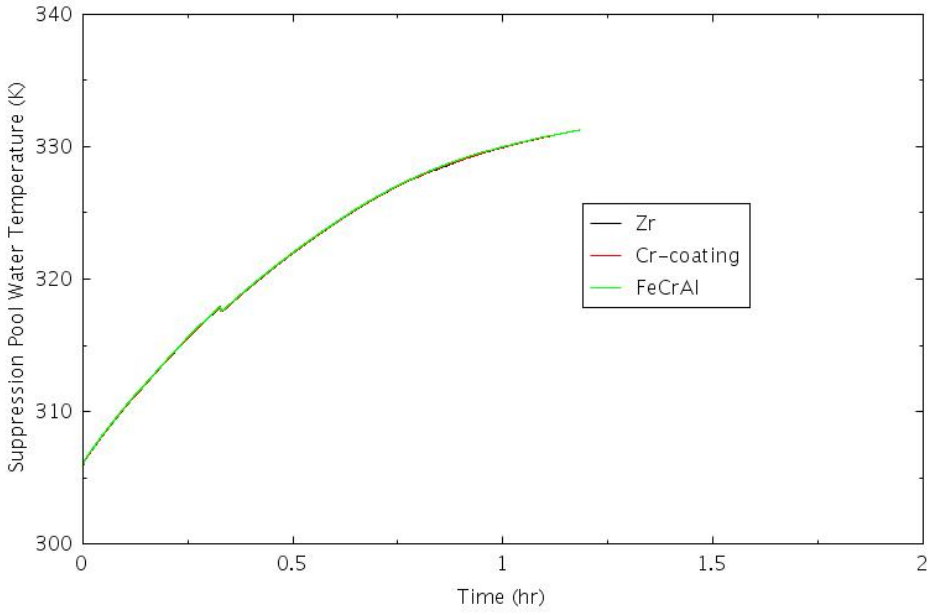

Figure 4-48. SP Water Temperature at BOC for SBO-2.1.

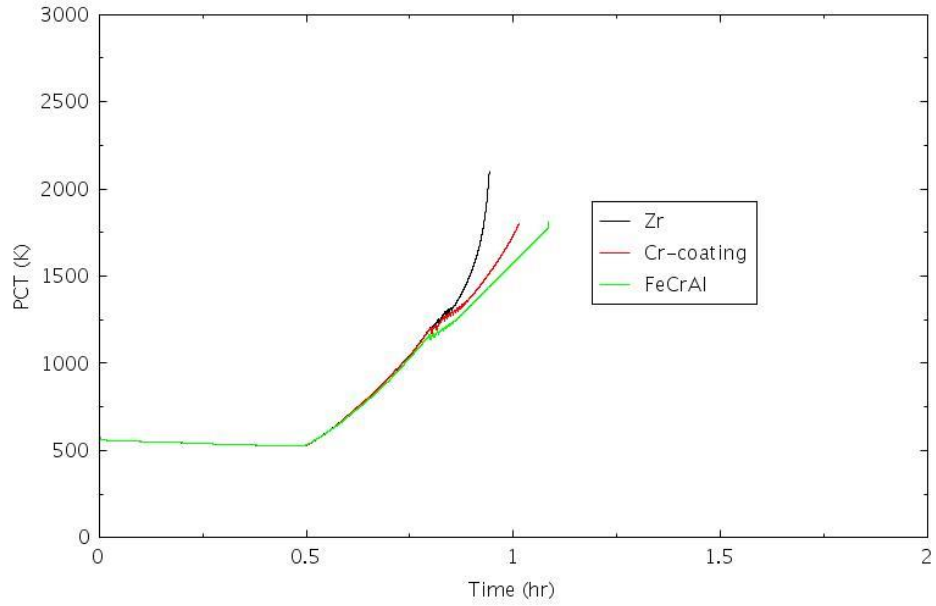

Figure 4-49. PCT at BOC for SBO-2.1.

4.2.7 SBO-3: STSBO with Two or More SRV Open

This SBO scenario is similar to that described in SBO-2.1 with one major difference, all the SRVs are activated at the initiation of the SBO and stay open for the duration of the transient. It is assumed in this scenario that with certain extreme external event such as fire coupled with simultaneous STSBO scenario caused all the SRVs stuck open. In this scenario, a total loss of offsite AC power from power grids and onsite AC power from DGs happen, all onsite DC power from station batteries also fail. All plant components dependent on control or motive power for startup and operation are disabled, including steam-driven emergency coolant makeup systems (e.g., RCIC and HPCI), as well as manual control of reactor pressure relief valves. Plant operators will attempt to blackstart RCIC in this STSBO condition. Several manual actions are required to blackstart RCIC, including opening normally closed valves to admit steam from the main steam lines to the steam-driven turbines of RCIC system and pump discharge valves so that water can be directed to the RPV. However, in this scenario, it is assumed that RCIC blackstart is not successful. Consequently, all coolant injections are lost so that the temperature of fuel and cladding will keep increasing until the cladding melts.

Figure 4-50 shows the RPV dome pressure. Due to stuck open of all the SRVs, the RPV pressure decreases more rapidly than that in SBO-2.1. The coolant mass flow rate through all the SRVs is shown in Figure 4-51. The RPV downcomer collapsed water level is shown in Figure 4-52. Due to the significant coolant loss through all the stuck open SRVs, the water level drops more rapidly than that in SBO-2.1. The downcomer collapsed water level is shown in Figure 4-52. Due to severe loss of the coolant inventory in the RPV, the void fraction goes up rapidly quickly and reaches dryout conditions at about 0.2 hours. As SRVs release high-pressure and high-temperature steam into the SP, the suppression temperature goes up as shown in Figure 4-53. The PCT comparisons for Zry, Cr-coating, and FeCrAl claddings are shown in Figure 4-54. Among all the SBO scenarios analyzed, the time to CD is shortest in this scenario. The CD happens in less than 0.6 hours for all three cladding materials.

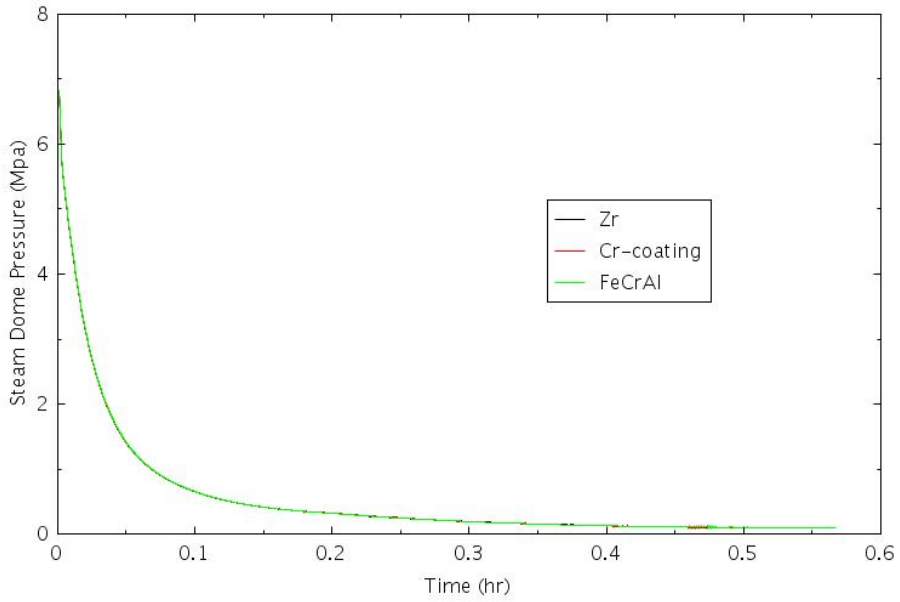

Figure 4-50. RPV Dome Pressure at BOC for SBO-3.

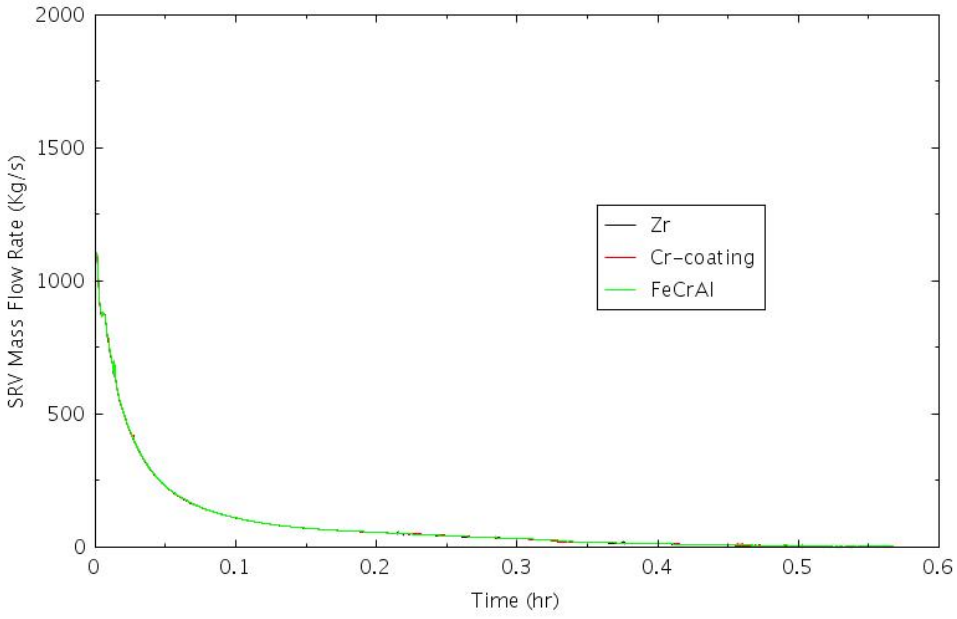

Figure 4-51. SRV Mass Flow Rate at BOC for SBO-3.

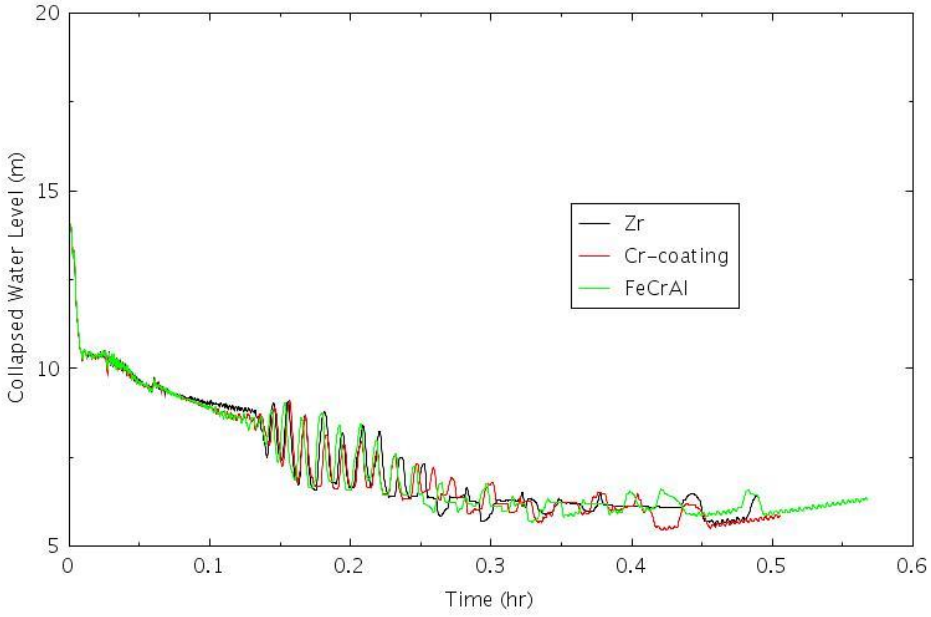

Figure 4-52. RPV Downcomer Collapsed Water Level at BOC for SBO-3.

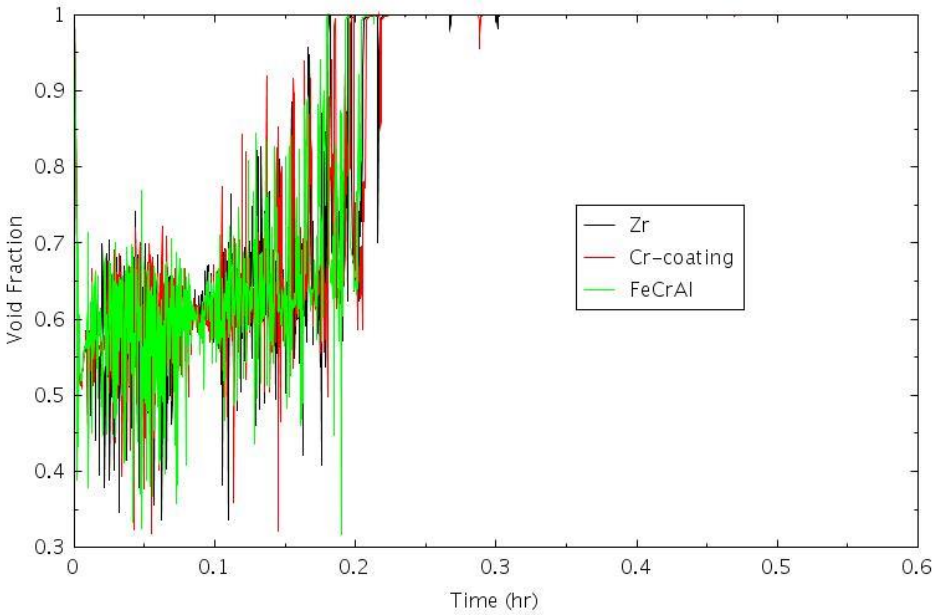

Figure 4-53. Void Fraction in One Element of the Hot Channel at BOC for SBO-3.

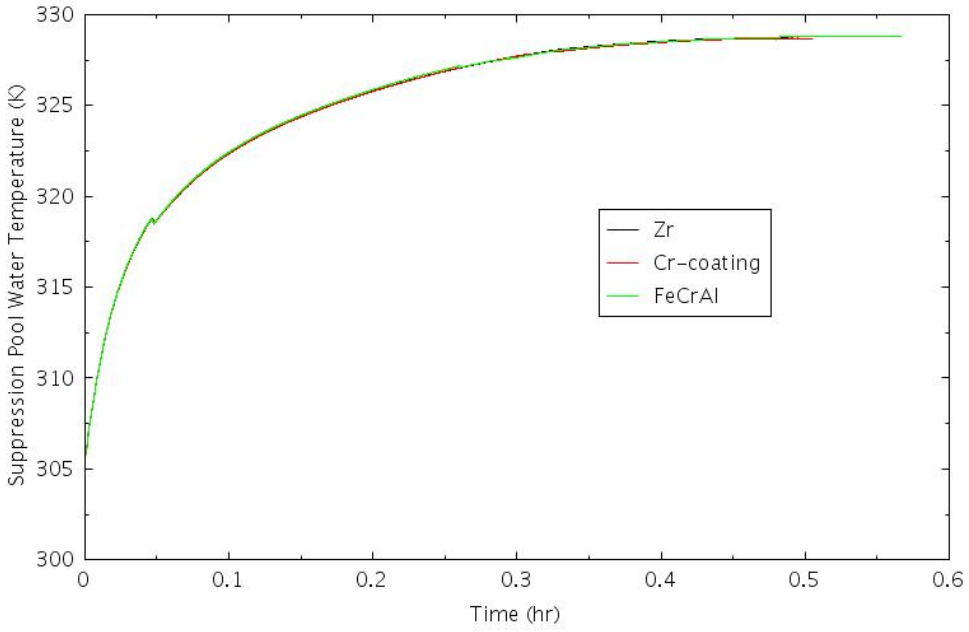

Figure 4-54. SP Water Temperature at BOC for SBO-3.

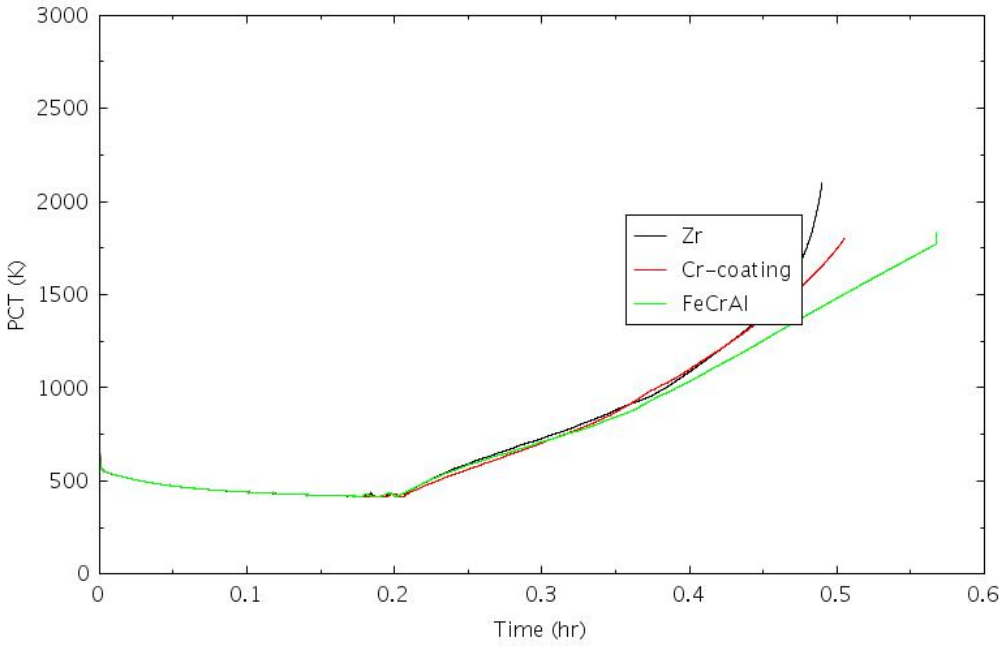

Figure 4-55. PCT at BOC for SBO-3.

4.2.8 SBO-4: LTSBO with AC Power Recovery

In this scenario, it is assumed that the RCIC operates successfully in the first 4 hours after the initiation of the SBO. The AC power is successfully recovered after 4 hours and consequently RCIC can continue to inject water to RPV after 4 hours in a regulated manner controlled by the high- and low-water-level setpoints. The SP cooling is assumed to fail such that the pressure and temperature in the SP would rise continuously after the initiation of SBO. It is further assumed that no SRVs are stuck open; however, five SRVs are manually opened to depressurize the RPV when the net-positive suction head (NPSH) margin goes to zero for the RCIC turbopump. Under such a condition, cavitation in the RCIC turbopump would occur and cause the turbopump to stop pumping water into the RPV. Cavitation is the formation of vapor bubbles in a flowing fluid due to the local static pressure decrease below the vapor pressure of the pumped liquid. The formation of this vapor and the following rapid condensation can produce damage and adversely affect the operation of a centrifugal pump. Consequently, the RPV loses water injection and the water level starts to drop continuously to cause fuel to uncover and eventually fuel failure. In this scenario, it is assumed that when NPSH margin goes down to zero, the five SRVs that constitute ADS will be manually opened to depressurize the RPV. It is further assumed no low pressure safety injection system works to allow LI of water into the RPV.

NPSH, which is generally used to describe the concept of cavitation, represents the total (or stagnation) pressure at the pump suction point relative to the vapor pressure of the liquid. The NPSH margin is defined as the difference between available NPSH (NPSHA) and required NPSH (NPSHR).

$$NPSH\ Margin = NPSHA - NPSHR \qquad (4\text{-}1)$$

The NPSH margin should be no less than zero, otherwise, noise, cavitation erosion of the pump's parts (mainly the impeller) and pump performance degradation will occur. NPSHR is a property of the pump itself. It corresponds to an acceptable level of pump cavitation, here we choose a conservative value as 8.114 m (26.62 ft) (U.S. Nuclear Regulatory Commission, 2010) The NPSHA is the head difference available at the pump suction, which can be determined by the following equation,

$$NPSHA = H_{suf} - H_{v,suc} + \Delta H - H_{loss} = \frac{P_{suf}}{\rho_{avg} g} - \frac{P_{v,suc}}{\rho_{l,suc} g} + \frac{\int_{z_{pump\_inlet}}^{z_{water\_surface}} \rho(z) g dz}{\rho_{l,suc} g} - H_{loss} \qquad (4\text{-}2)$$

where, H_{suf} represents the liquid surface head resulting from the pressure in the air space above (P_{suf}); $H_{v,suc}$ represents the vapor head determined by the saturated pressure of the water temperature at the suction point ($P_{v,suc}$); ρ_{avg} is the averaging density of liquid; $\rho_{l,suc}$ is the liquid density at the suction point; ΔH is the elevation difference between the liquid surface in the pool and the pump suction flange, (m); H_{loss} is the pressure loss in the flow path from fluid suction point to pump suction flange, (m). P_{suf} consists of noncondensible gas pressure P_{nc} and the vapor pressure $P_{v,surf}$ determined by the pool surface temperature, while $P_{v,suc}$ is a function of liquid temperature at the suction point. When WW is simulated using a lumped parameter model, then $P_{v,surf} = P_{v,suc}$ and $\rho_{avg} = \rho_{l,suc}$. And the above equation could be re-written as,

$$NPSHA = \frac{P_{nc}}{\rho_l g} + \Delta H - H_{loss} \qquad (4\text{-}3)$$

If strong thermal stratification exists in the SP, the surface temperature could be much higher than the liquid temperature at the suction point, which greatly enlarges the difference between $P_{v,surf}$ and $P_{v,suc}$ and implies a potential larger margin for NPSHA. It is demonstrated that about 30% of margin increase could be obtained when thermal stratification is considered, which implies that detailed thermal stratification/mixing study should be performed in the BWR Mark I containment SBO analysis in order to accurately simulate the scenarios. Thermal stratification study of the SP is left for future work.

The calculations were carried out using the power shapes at BOC, MOC, and EOC. The figures shown in the following are for MOC only. Figure 4-56 shows the RCIC water injection mass flow rate at MOC. It can be seen that the RCIC water injection continues after 4 hours when the AC power is recovered. The RCIC system stops injecting water to the RPV when the NPSH margin goes down to zero as shown in Figure 4-57. The NPSH margin is a function of the SP pressure (as shown in Figure 4-58), temperature (as shown in Figure 4-59) and water density (as shown in Figure 4-60). The RPV collapsed water level is shown in Figure 4-61. The RPV water level is kept between the low-water-level setpoint and the high water level setpoint when the RCIC is working and it drops precipitously after RCIC stops injecting water to the RPV and the opening of ADS to depressurize the RPV. The RPV dome pressure is shown in Figure 4-62. The reactor vessel pressure is kept within a tight range of the operating pressure when RCIC is working. Once RCIC stops working and after the opening of the ADS, the RPV dome pressure drops to low values rapidly within a short period of time. Figure 4-63 shows the SRV mass flow rate during the transient. It can be seen the SRV mass flow rate took a significant jump when the ADS is manually opened. Figure 4-64 shows the void fraction in one control volume of the hot channel during the transient. Figure 4-65 shows the PCT comparison for the three types of cladding materials analyzed.

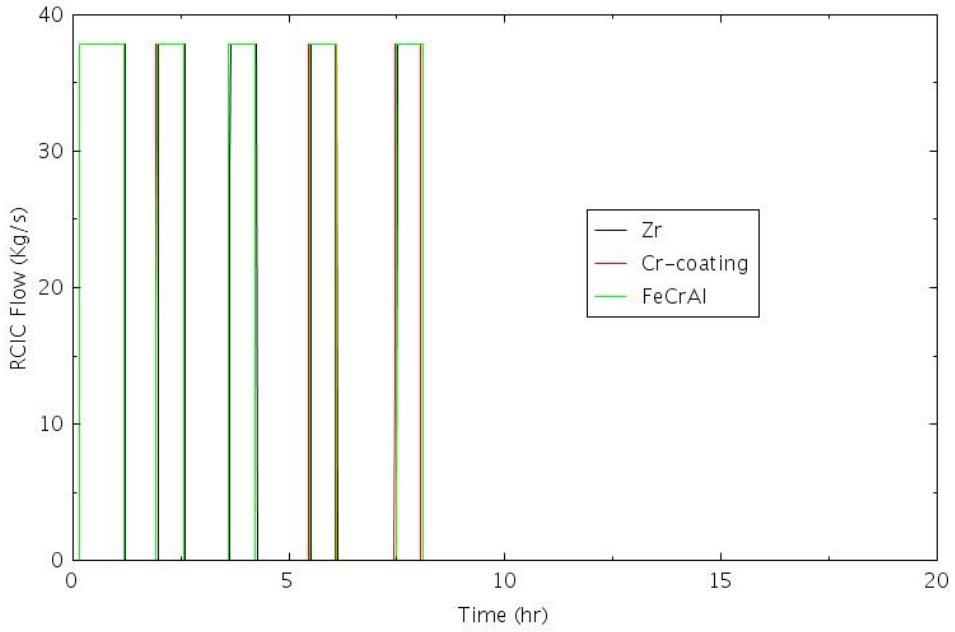

Figure 4-56. RCIC Water Injection Mass Flow Rate at MOC for SBO-4.

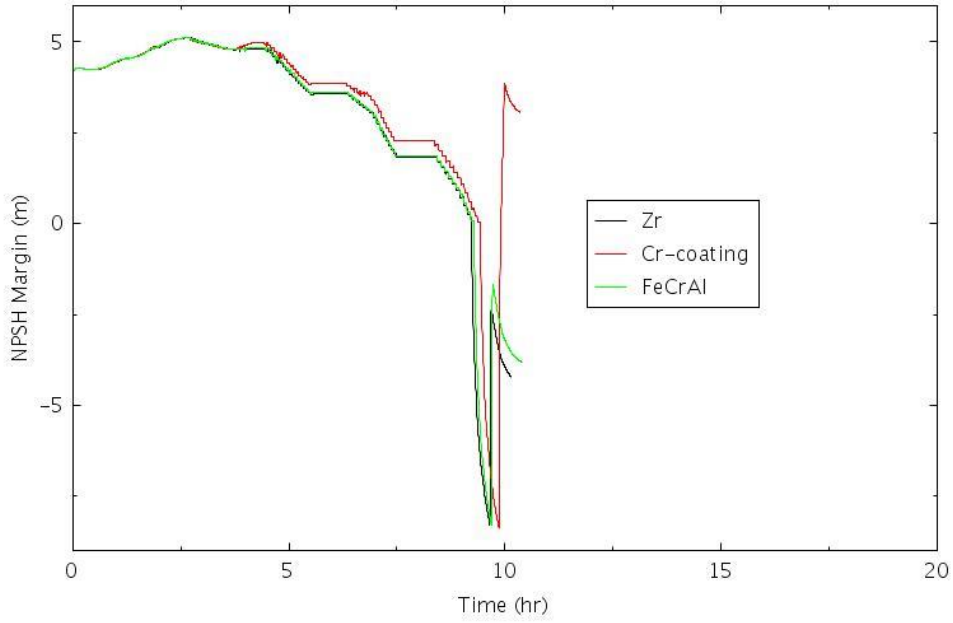

Figure 4-57. NPSH Margin at MOC for SBO-4.

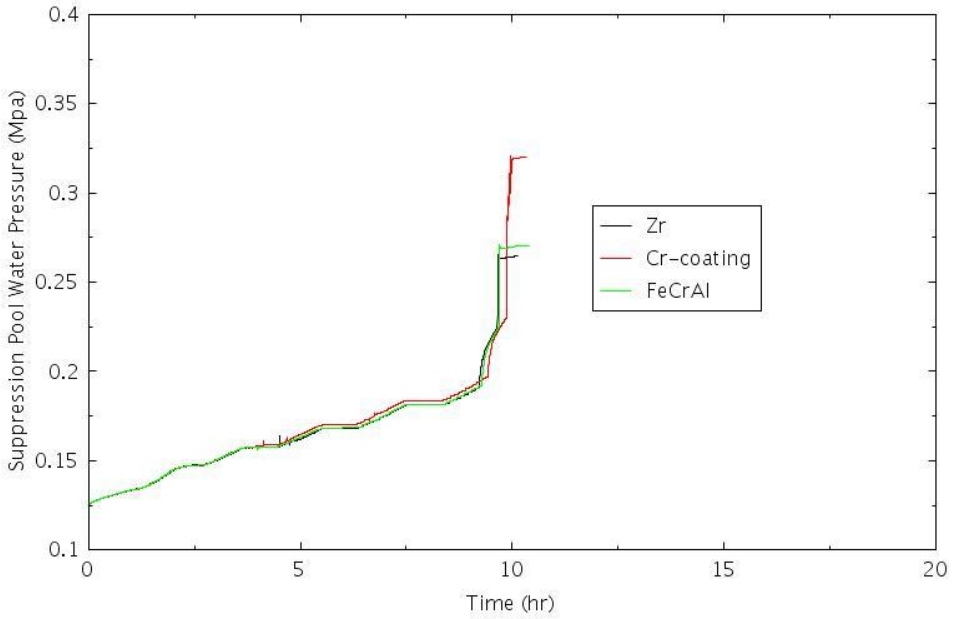

Figure 4-58. SP Water Pressure at MOC for SBO-4.

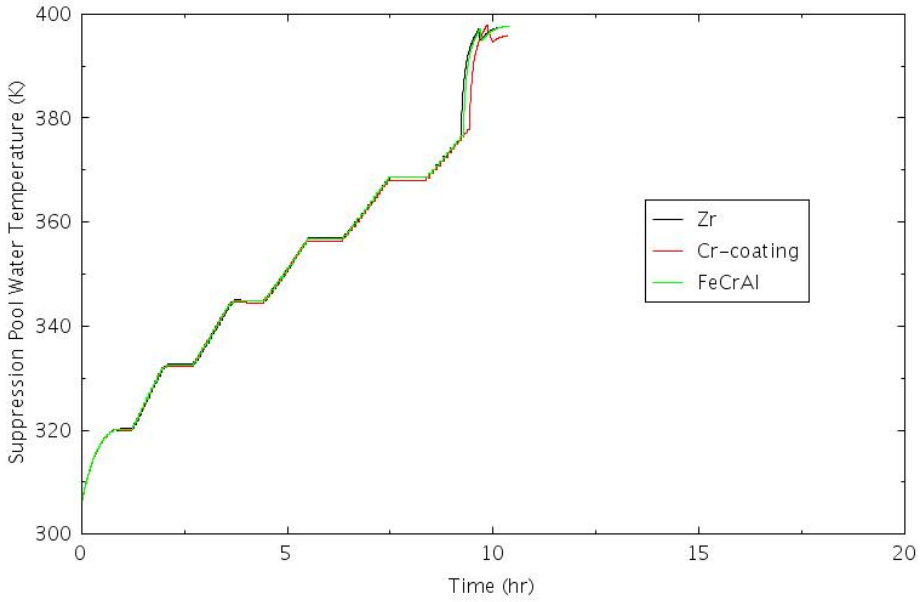

Figure 4-59. SP Water Temperature at MOC for SBO-4.

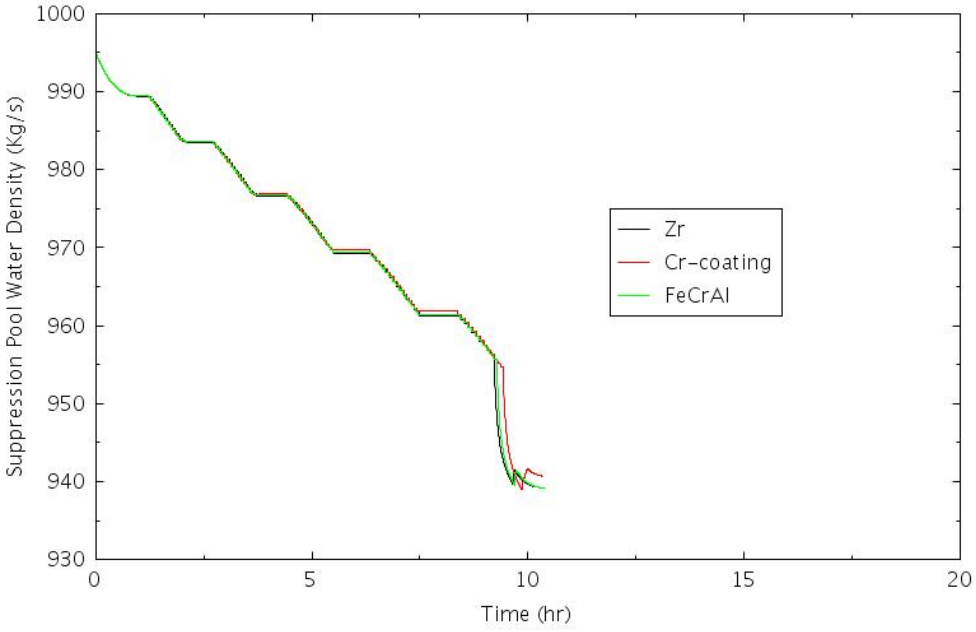

Figure 4-60. SP Water Density at MOC for SBO-4.

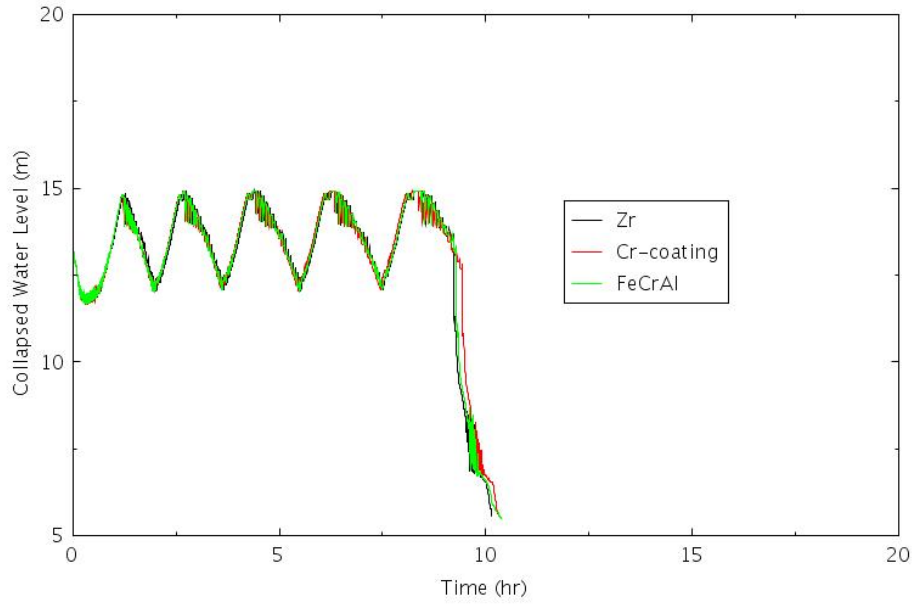

Figure 4-61. RPV Downcomer Collapsed Water Level at MOC for SBO-4.

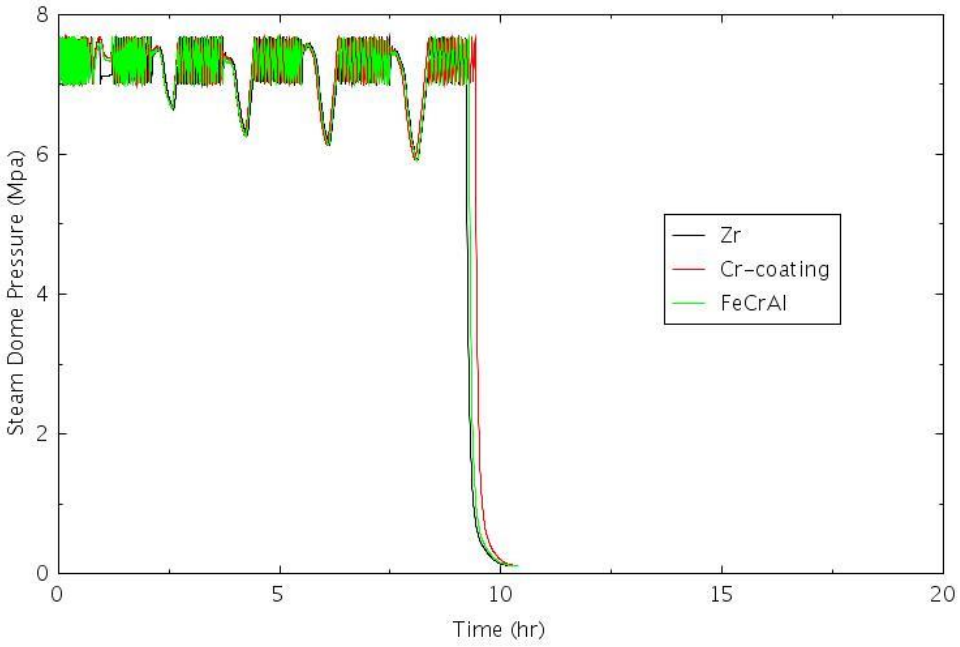

Figure 4-62. RPV Dome Pressure at MOC for SBO-4.

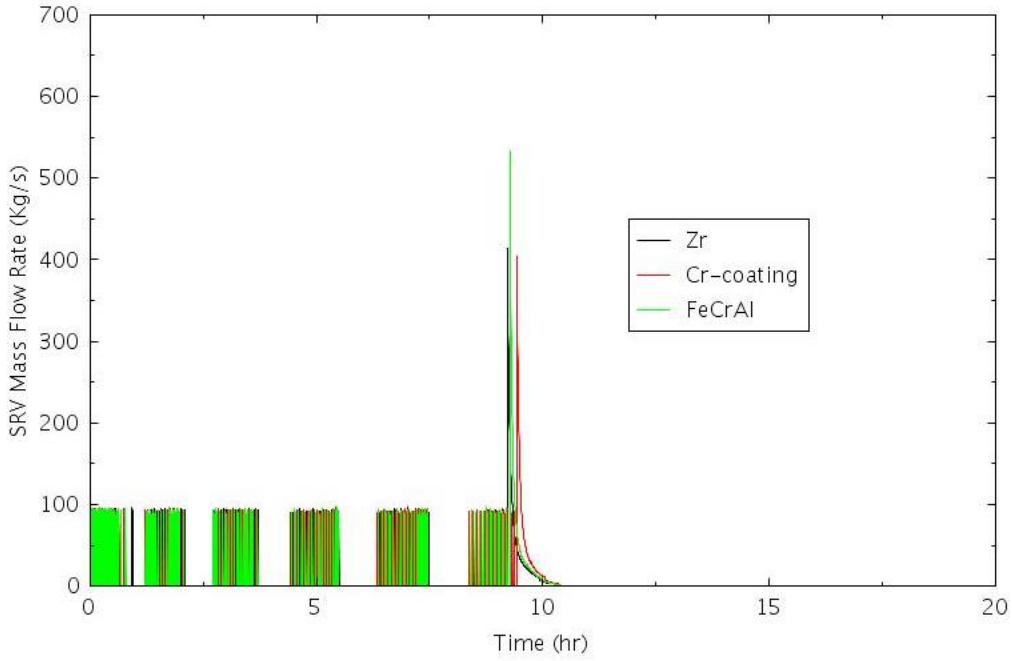

Figure 4-63. SRV Mass Flow Rate at MOC for SBO-4.

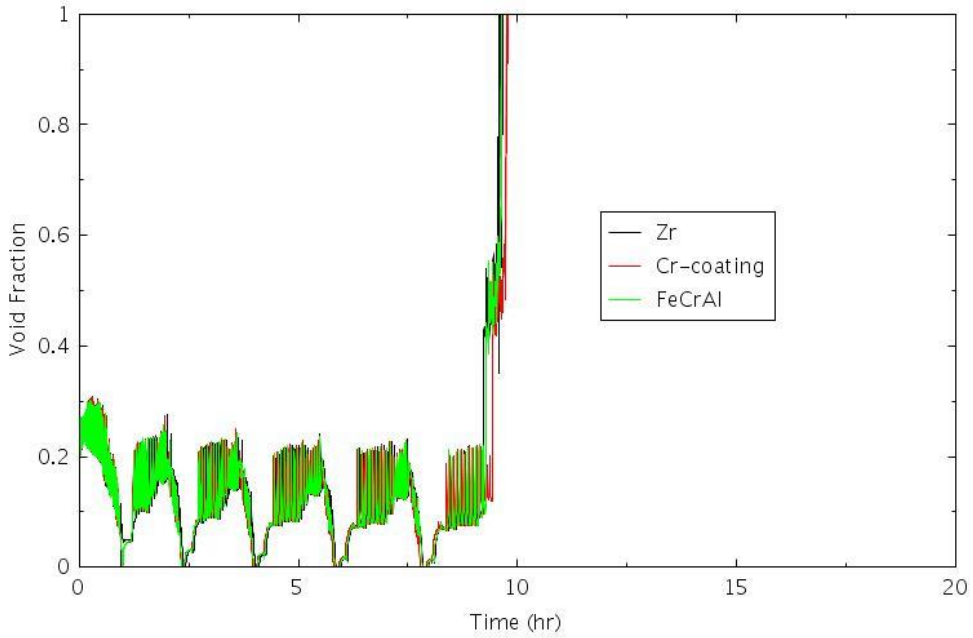

Figure 4-64. Void Fraction for One Element in the Hot Channel at MOC for SBO-4.

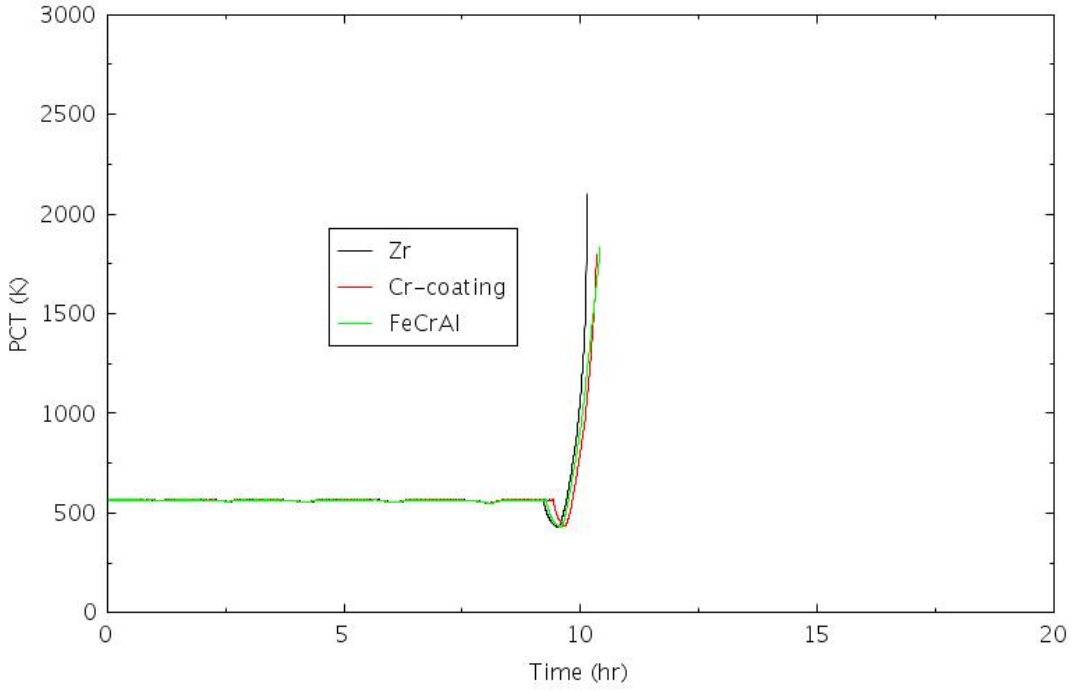

Figure 4-65. Comparison of PCT at MOC for SBO-4.

4.2.9 SBO-4.1: LTSBO with AC Power Recovery and Failure of Depressurization

In this scenario, it is assumed that the RCIC operates successfully in the first 4 hours after the initiation of the SBO. The AC power is successfully recovered after 4 hours and consequently RCIC can continue to inject water to RPV after 4 hours in a regulated manner controlled by the high- and low-water-level setpoints. The SP cooling is assumed to fail so the pressure and temperature in the SP would rise continuously after the initiation of SBO. It is further assumed that there are no SRVs stuck open and no SRVs are manually opened to depressurize the RPV so its pressure is kept within an appropriate range by the automatic opening and closing of SRVs controlled by the high- and low-pressure setpoints. As a result, the low-pressure safety systems such as core injection and core spray systems are not activated. In the RELAP5-3D calculations for this scenario, it is assumed that when the NPSH margin goes to zero, cavitation in the RCIC turbopump would occur and cause the turbopump to stop pumping water into the RPV. Cavitation is the formation of vapor bubbles in a flowing fluid due to the local static pressure decrease below the vapor pressure of the pumped liquid. The formation of this vapor and the following rapid condensation can produce damage and adversely affect the operation of a centrifugal pump. Consequently, the RPV loses water injection and the water level starts to drop continuously to cause fuel uncover and eventually fuel failure. The major difference between this scenario and that in SBO-4 is that there is no RPV depressurization in this scenario.

Figure 4-66 shows the RPV collapsed water level at MOC for SBO-4.1. It shows that RCIC system, with the RCIC water injection mass flow rate shown in Figure 4-67, could keep the vessel liquid level in a safe range in which the core can be fully covered while the RPV would not be flooded. The NPSH margin is shown in Figure 4-68. As the steam is condensed by water in the SP and leads to the increase of liquid temperature (as shown in

Figure 4-69) and pressure (as shown in Figure 4-70) and the decrease of liquid density (as shown in Figure 4-71), the NPSH margin decreases. When the NPSH margin decreases to zero at about 9 hours, the RCIC system fails. Figure 4-72 shows the RPV dome pressure. It can be seen from the figure that the RPV dome pressure is kept within a small range of the operating pressure with the automatic on and off of SRVs (as shown in Figure 4-73) throughout the entire SBO transient. Figure 4-74 shows the void fraction for one element in the hot channel and it shows that the void fraction is kept at a low value with the RCIC operations. When RCIC ceases operations, the water level starts to decrease, the core becomes uncovered, and the void fraction starts to go up quickly. Figure 4-75 shows the comparison of the PCT.

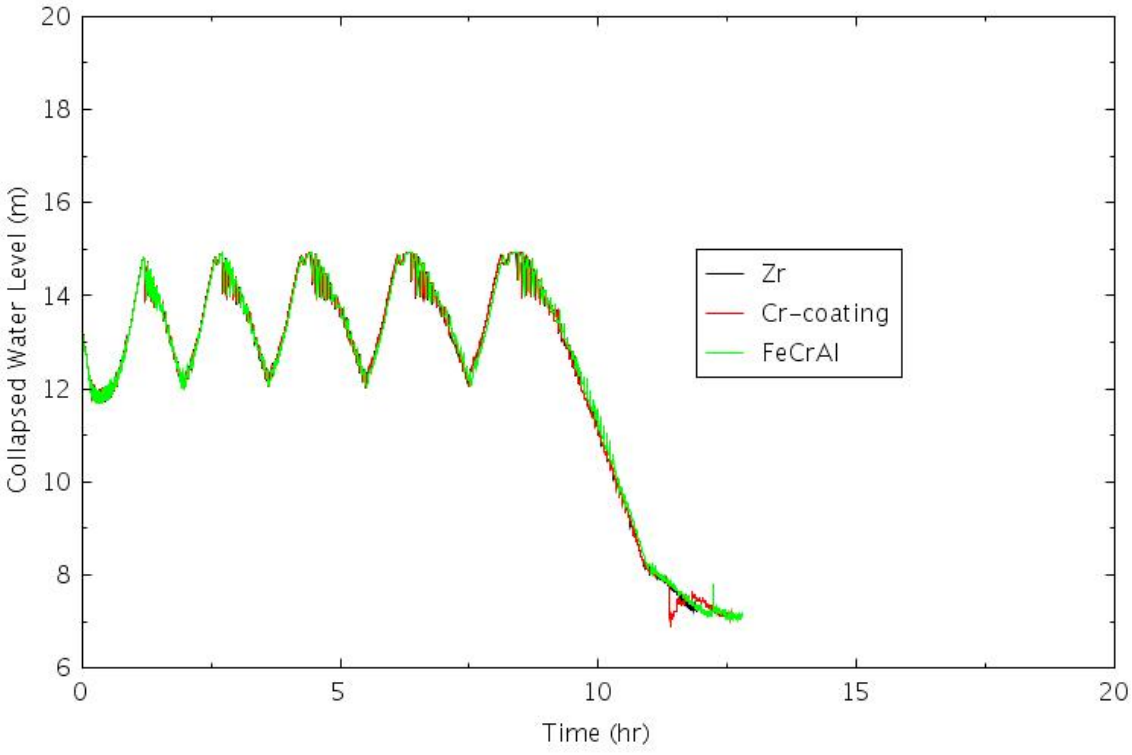

Figure 4-66. RPV Downcomer Collapsed Water Level at BOC for SBO-4.1.

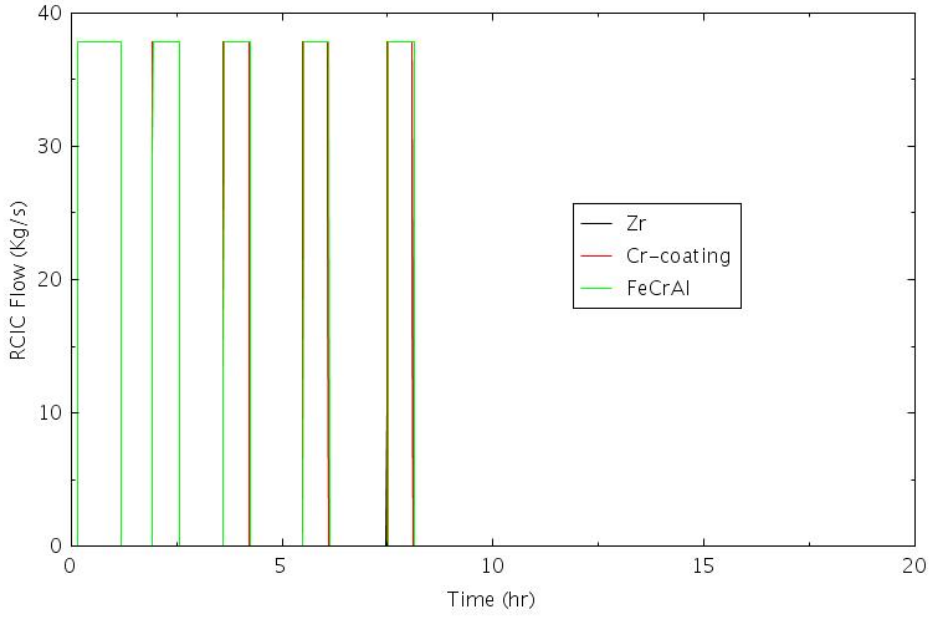

Figure 4-67. RCIC Water Injection Mass Flow Rate at BOC for SBO-4.1.

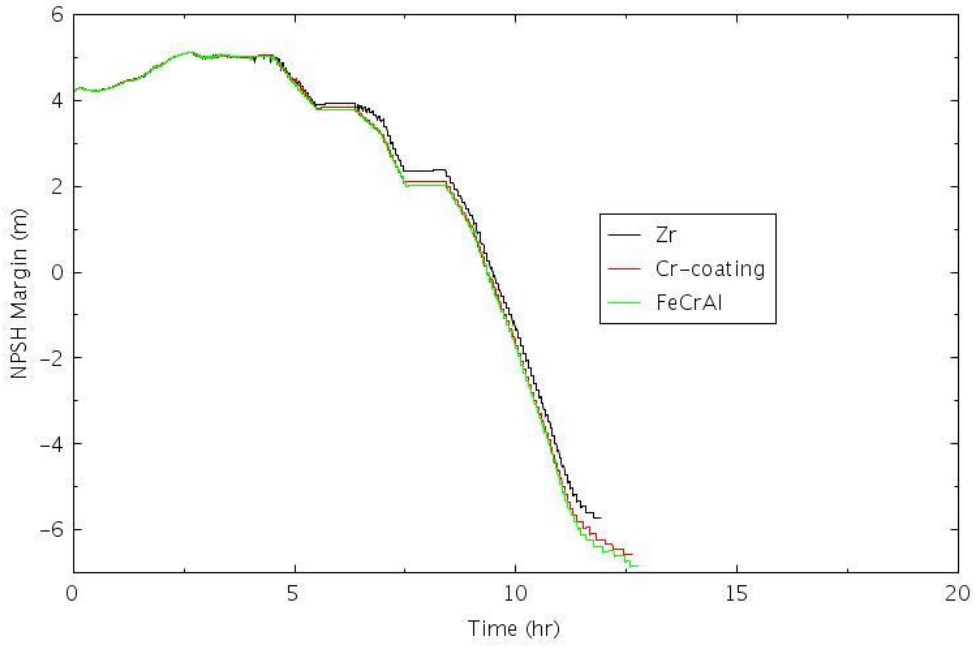

Figure 4-68. NPSH Margin at BOC for SBO-4.1.

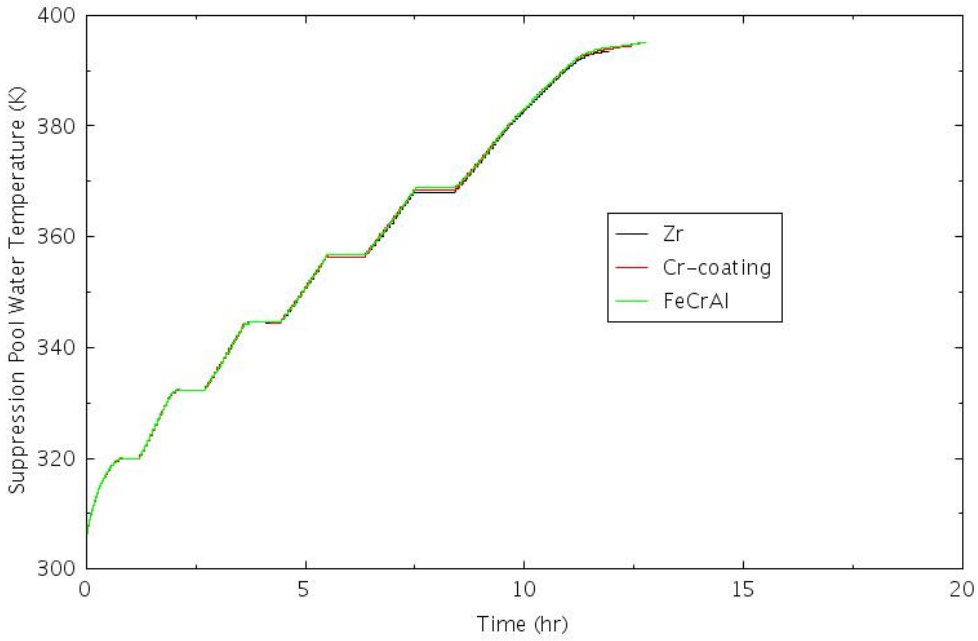

Figure 4-69. SP Water Temperature at BOC for SBO-4.1.

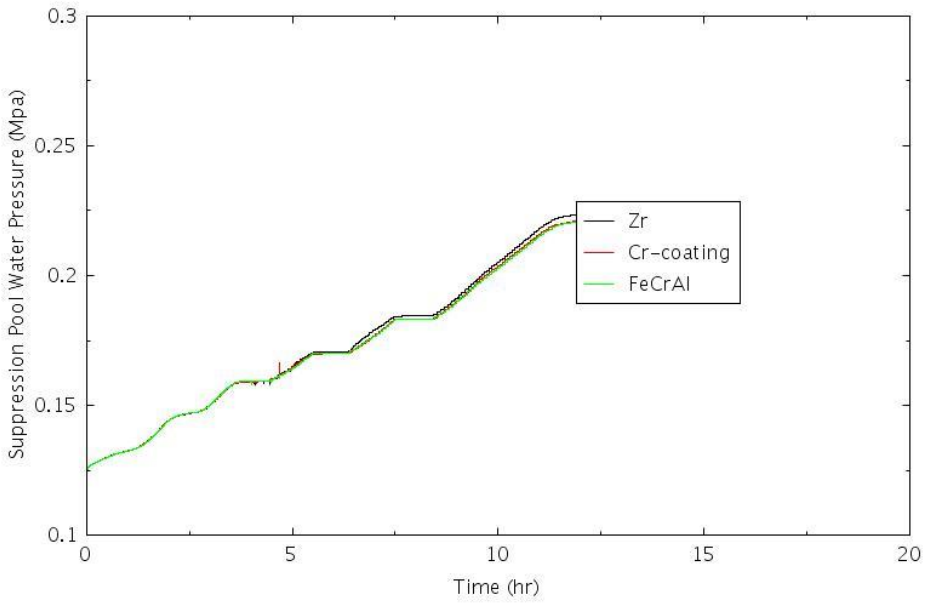

Figure 4-70. SP Water Pressure at BOC for SBO-4.1.

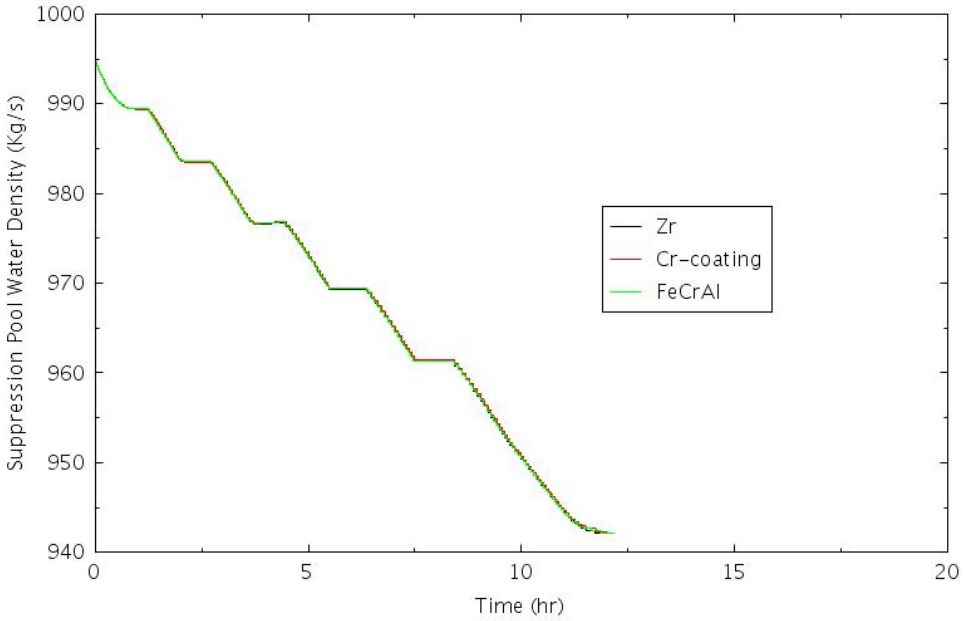

Figure 4-71. SP Water Density at MOC for SBO-4.1.

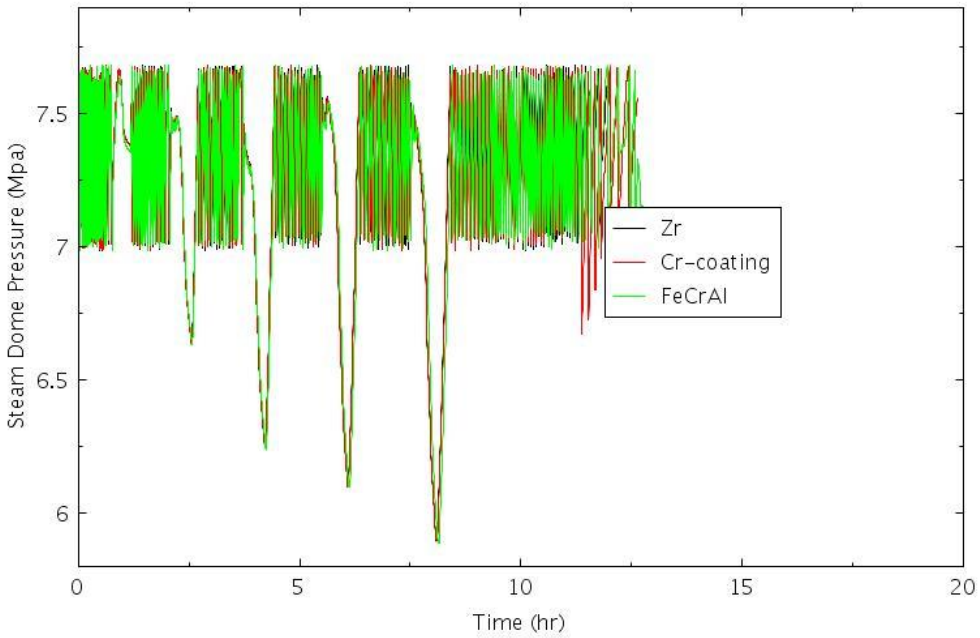

Figure 4-72. RPV Dome Pressure at BOC for SBO-4.1.

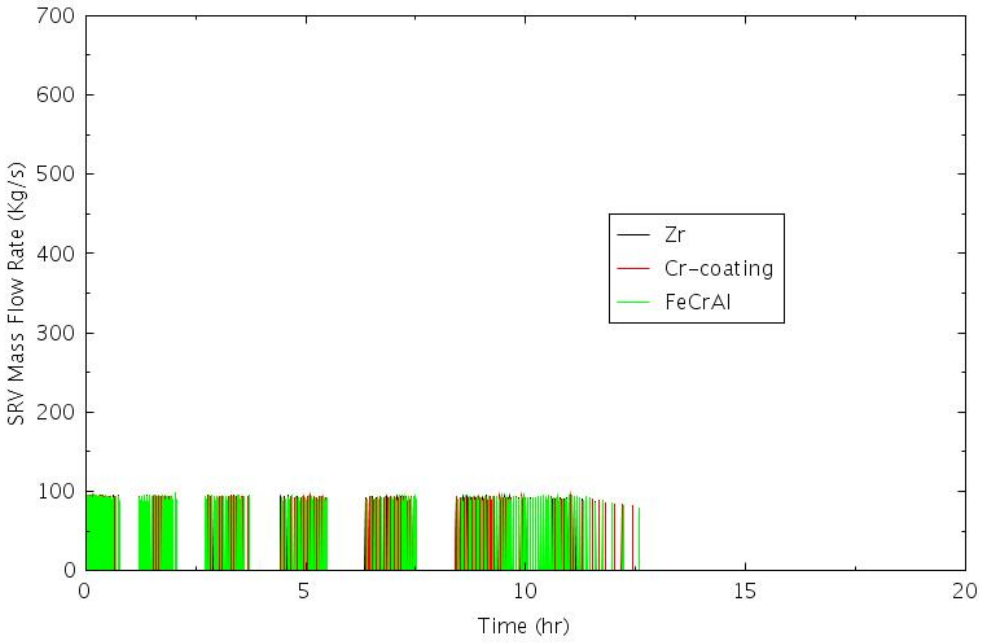

Figure 4-73. SRV Mass Flow Rate at BOC for SBO-4.1.

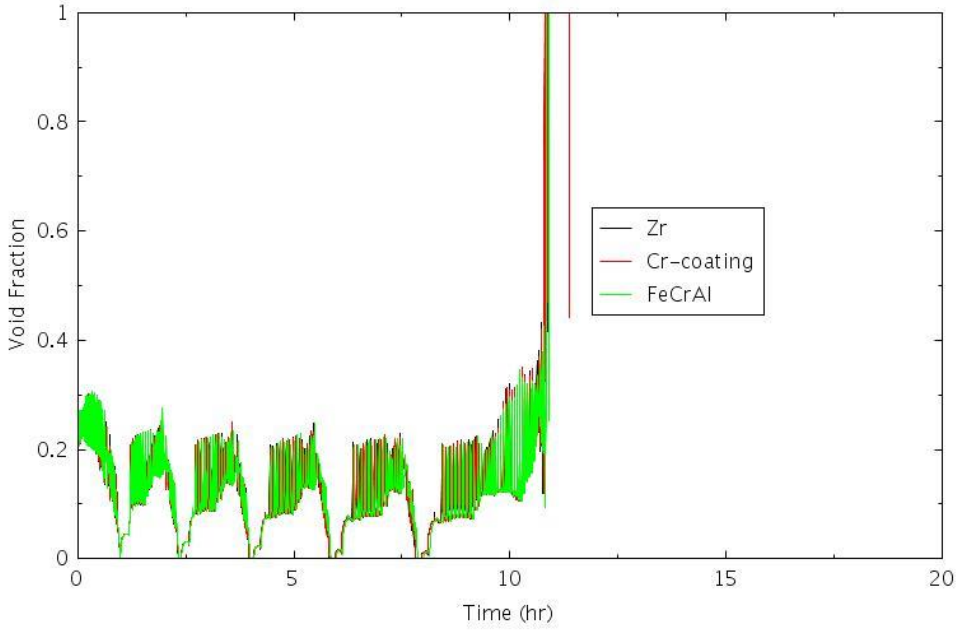

Figure 4-74. Void Fraction in One Element of the Hot Channel at BOC for SBO-4.1.

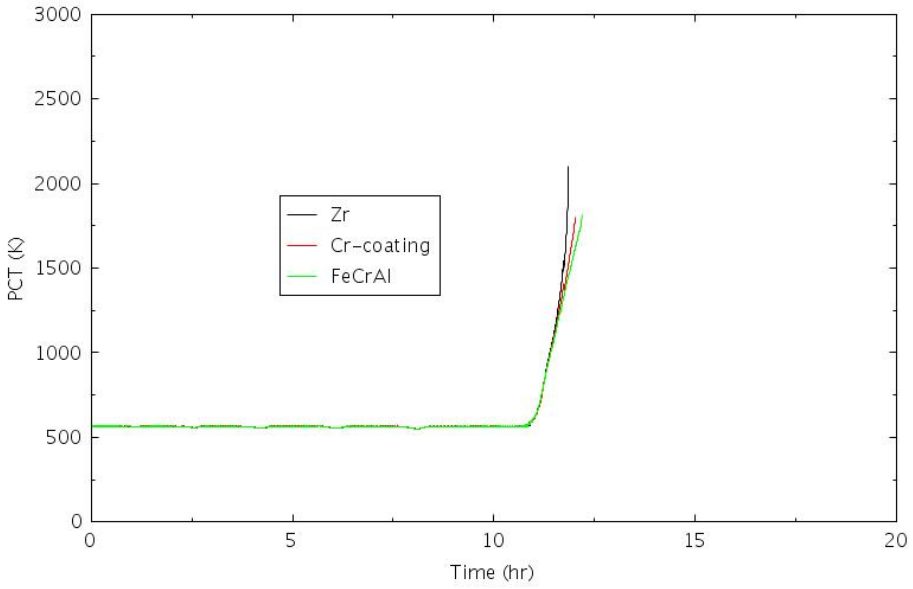

Figure 4-75. PCT at MOC for SBO-4.1.

4.3 Sensitivity Analysis

One of the most important metrics to enhance the resiliency of an NPP is to increase its coping time. Within the ERP Project, coping time is defined as "the available time for NPP operators to mitigate an event that has the potential to result in significant CD or a large early release of radioactive materials to the environment" (Zhang, Szilard, & Hess, 2018). The analysis results from the previous subsection indicate that the gain on coping time from ATF alone is modest. However, the combination of ATF and other advanced nuclear technologies could provide much longer coping time. In this subsection, sensitivity calculations are performed to demonstrate that the combination of ATF and certain advanced technologies or operations can significantly postpone the time to CD and increase the coping time. The sensitivity calculations include: (1) Increase RCIC operation time, (2) FLEX equipment startup time, and (3) RCIC blackstart operations.

4.3.1 Increase RCIC Operation Time

Sensitivity analysis is performed for the SBO-1 scenario—"LTSBO with RCIC Available for 4 Hours." In the calculations performed in the previous subsection, it is assumed that RCIC is available for 4 hours after the initiation of an SBO accident. However, in a real NPP, the actual time available for RCIC operations depends on the capacity of the onsite battery. In order to analyze the effect on varying battery capacity, sensitivity calculations are performed with RCIC operation time ranges from 4 hours to 10 hours. Specifically, six calculations are performed for RCIC operations of 5, 6, 7, 8, 9, and 10 hours, respectively. The calculations are performed at BOC only. It is further assumed in the calculations that the AC power is not recovered after RCIC ceases operations, and consequently all water injections to the RPV are lost after RCIC stops working and the core proceeds to fuel failure and CD. The time to CD versus the RCIC operation time from these calculations is plotted in Figure 4-76.

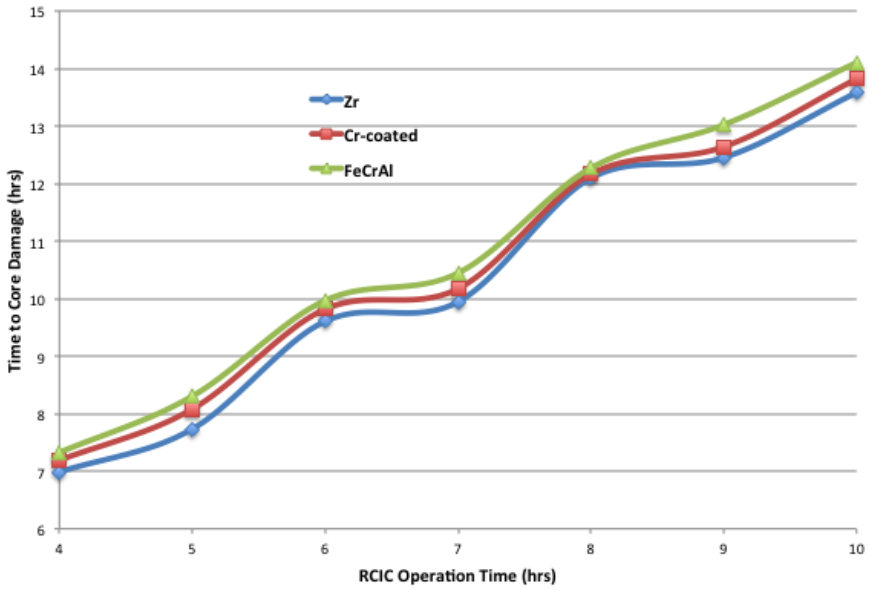

Figure 4-76. Time to CD vs. RCIC Operation Time for LTSBO Scenario.

It is found that the prolonged operations of RCIC can delay the time to CD. Hence, the extended RCIC operation provides longer coping time for operators to mitigate the SBO accident. Figure 4-76 shows that the relationship between the time to CD and RCIC operation time is almost linear, which indicates that the time to extend the RCIC operations is directly attributable to the gain on coping time. Therefore, extending the operation time and band of RCIC is one area that would contribute to enhancing the resilience of BWRs. One area is to increase the capacity of onsite battery. The increased battery capacity provides longer DC power time to control the RCIC operations. The other area is to better understand the true operating limits of the RCIC system. An accompanying project called "Enhanced Operation Strategies for System Components" within the RISA Pathway of the LWRS Program is collaborating with the U.S. nuclear industry and universities to perform experimental and simulation work to understand the true operating limits of Terry turbine systems and the "self-regulating" mode of operation of RCIC observed in the Fukushima Daiichi Unit 2 accident in order to credit RCIC in accident management. The self-regulating mode of operation of RCIC provides much longer operation time for RCIC to mitigate SBO accidents.

4.3.2 Effect of FLEX Equipment Startup Time

In this analysis, it is assumed that a FLEX portable generator is engaged to maintain a long-term supply of control power. Using the RPV water level information, which is available by use of a FLEX portable generator, operators can either position, align and start FLEX portable pump to replace RCIC as the water injection source, or manually control RCIC to maintain a stable water level in the RPV. It is assumed that FLEX portable pump is used to replace RCIC in this analysis. A series of RELAP5-3D calculations are performed to estimate the time required to get FLEX portable generator and pump started before the fuel experiences damage. The scenario studied is based on the SBO-1 scenario with which RCIC are available for 4 hours. After the RCIC system operates for 4 hours, it is assumed that FLEX equipment will be brought into service to replace the function of RCIC. The sensitivity calculations are performed with the assumption that the FLEX equipment can be started from 4 hours to longer time.

The calculations are performed at BOC only and the results show that if the FLEX generator and pump can be started within 6.9 hours after the initiation of an SBO, the SBO accident can be successfully mitigated. Figure 4-77 shows the PCT comparisons for the case with FLEX equipment started at 6.9 hours after the initiation of an SBO. The results indicate that even though the PCT rises rapidly after 6 hours, the FLEX injection is able to stop the PCT rise and turn it around before it reaches the clad failure temperature.

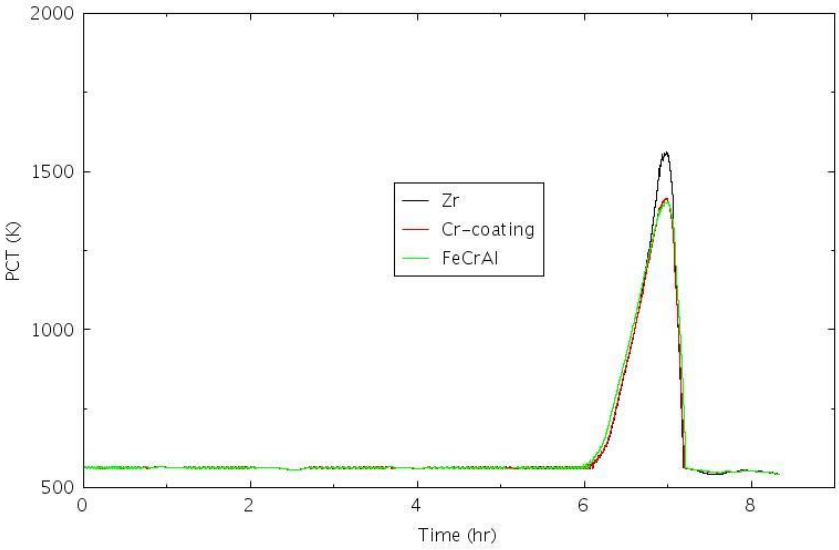

Figure 4-77. PCT Comparisons with FLEX Injection Starts at 6.9 Hours for LTSBO

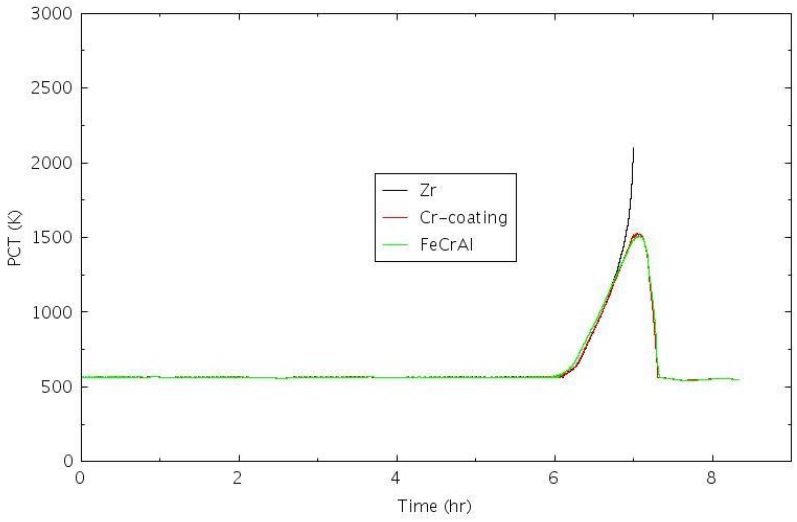

Figure 4-78. PCT Comparisons with FLEX Injection Starts at 7 Hours for LTSBO.

Figure 4-78 shows the PCT comparisons with FLEX generator and pump started at 7 hours. The Zircaloy cladding would experience fuel failure; however, both the Cr-coated and FeCrAl ATF cladding materials would survive the SBO accident. The slower temperature rise of the ATF cladding provides the time needed for FLEX injection to stop the cladding temperature rise and to cool the fuel in the core.

Figure 4-79 shows the PCT comparisons with FLEX generator and pump started at 7.2 hours. The results show that both Zircaloy and Chromium-coated cladding would experience failure during the SBO. However, the

FeCrAl cladding would survive the SBO accident given its slower temperature rise than that of Zircaloy and Chromium-coated claddings.

Figure 4-80 shows the PCT comparisons with FLEX generator and pump started at 7.3 hours. The results show that the FLEX water injection is brought on too late and all three cladding materials would experience fuel failure. Additional calculations for the FLEX startup time greater than 7.3 hours all indicate cladding failure for all the three cladding materials.

The sensitivity calculations indicate the FLEX startup time has significant effect on the SBO mitigation. The sooner the FLEX equipment can be brought online the higher the probability to mitigate an SBO. The additional coping time came with the ATF cladding materials can prevent the "cliff-edge" effect under certain circumstances as shown in Figure 4-78 and Figure 4-79. The analysis shows the benefit of combining FLEX and ATF to mitigate an SBO accident.

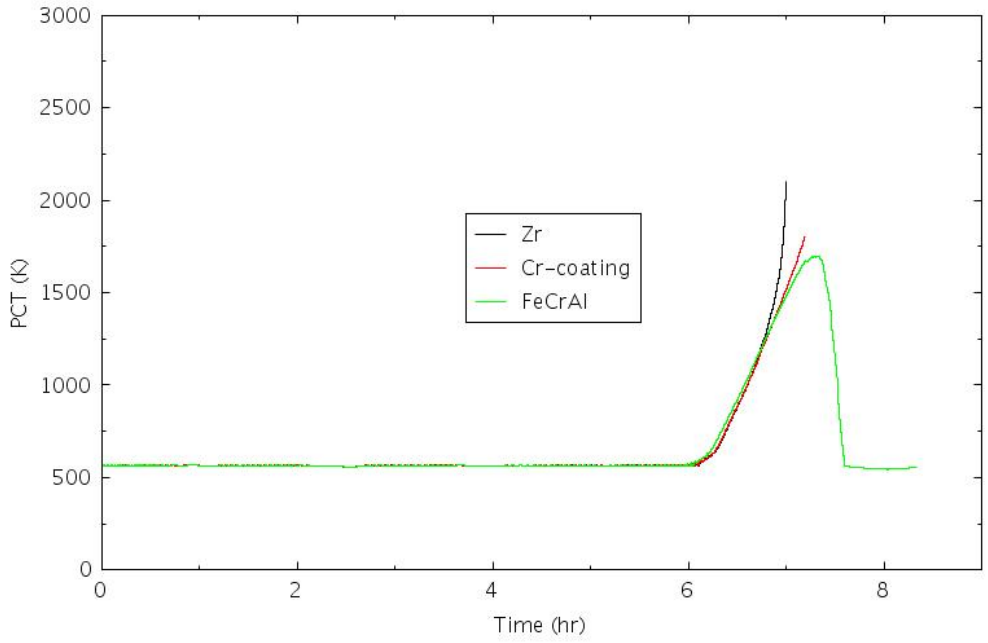

Figure 4-79. PCT Comparisons with FLEX Injection Starts at 7.2 Hours for LTSBO.

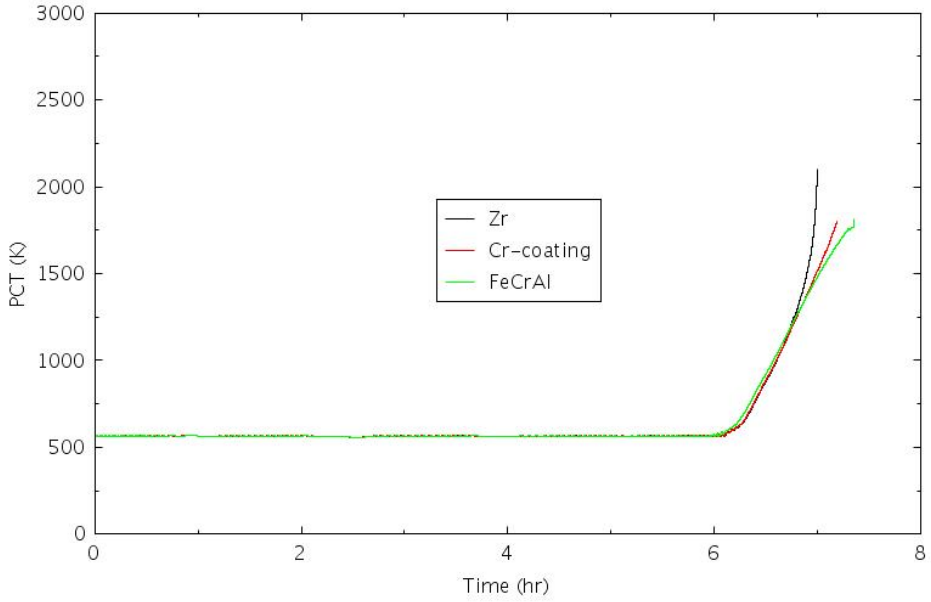

Figure 4-80. PCT Comparisons with FLEX Injection Starts at 7.3 Hours for LTSBO.

4.3.3 STSBO with RCIC Blackstart

In an STSBO, it is assumed that DC power fails immediately fails after the initiation of the SBO. This in turn significantly reduces the time available for operator intervention and accelerates the progression time to CD. The plant operators will attempt to start and operate the RCIC system without AC or DC control power. This is known as "RCIC blackstart." The STSBO scenario SBO-2 described in the previous section is used in the RCIC blackstart calculations here. The calculations were performed at BOC only. Similar to the analysis performed in (Wu & Shirvan, 2019), it is assumed that the attempt to blackstart RCIC is successful in 40 minutes rather than the 1 hour assumed in State-of-the-Art Reactor Consequence Analyses (U.S. Nuclear Regulatory Commission, 2012) after the initiation of the STSBO. Since the onsite DC power is assumed unavailable, the RPV water level measurement device is not functional and the steam flow into the RCIC Terry turbine is not regulated. As a result, RCIC system is assumed to operate at a rated capacity of 37.8 kg/s, which is higher than the rate required to make up for water boil-off losses. The RPV water level will rise above its nominal valve and eventually overfill the RPV. It is further assumed that once the main steam lines are flooded with the water from RPV overfilling, the RCIC system is disabled and ceases injecting water to the RPV. The calculations are performed at BOC only. Figure 4-81 shows the water mass flow rate to the RPV supplied by the RCIC system after it is successfully blackstarted. Figure 4-82 shows the collapsed water level in the RPV downcomer during the SBO scenario. It can be seen that before RCIC is blackstarted, the water level keeps dropping due to boil-off-driven decay heat and the absence of makeup water. With the successful blackstart of RCIC, the water level starts to rise until it reaches the main steam line level and RCIC ceases operating. After that, the water level starts to decrease until the cladding melts. Figure 4-83 shows the PCT for STSBO with RCIC blackstart scenario. Table 4-6 shows the comparison of time to CD for STSBO with and without RCIC blackstart. The simulation results show that with the successful blackstart of RCIC, the time to CD for all three cladding types is delayed by 4 hours. Additionally, compared to the baseline Zr cladding, the Chromium-coated and FeCrAl ATF cladding materials added 14 minutes and 24 minutes, respectively, to the time to CD. It can be concluded that the combination of RCIC blackstart and ATF provides a much longer coping time for plant operators to mitigate an STSBO accident.

Table 4-6. Time to CD Comparisons at BOC for STSBO Scenarios with ATF Designs and with and without RCIC Blackstart

Scenario	Scenario Description	Time to CD t_{CD} (hh:mm)					
		Zry	Cr-coated	Δt	Zry	FeCrAl	Δt
SBO-2	No SRV stuck open, RCIC/HPCI not Available, AC power not recovered in 4 hrs	1:14	1:19	0:05	1:14	1:24	0:10
SBO-2-RCIC-Blackstart	No SRV stuck open, RCIC Blackstart, HPCI not Available, AC power not recovered in 4 hrs	5:09	5:23	0:14	5:09	5:33	0:24

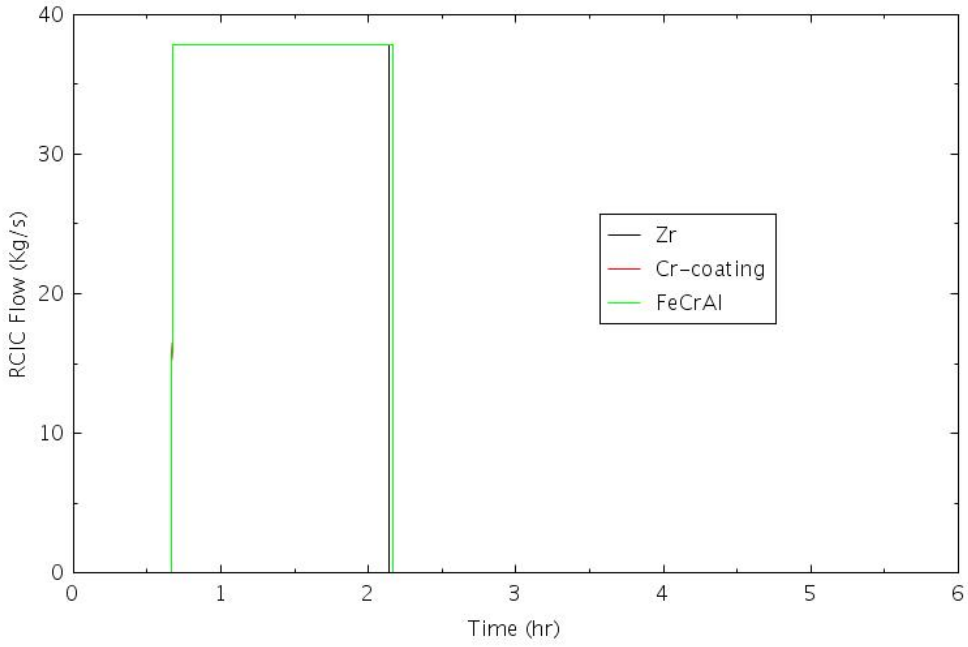

Figure 4-81. RCIC Water Injection Mass Flow Rate at BOC for STSBO with RCIC Blackstart.

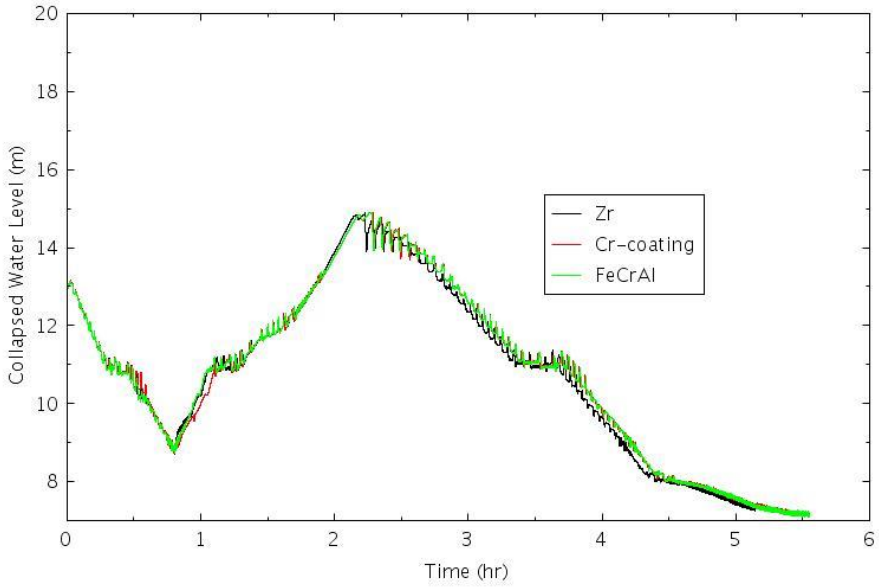

Figure 4-82. RPV Collapsed Water Level at BOC for STSBO with RCIC Blackstart.

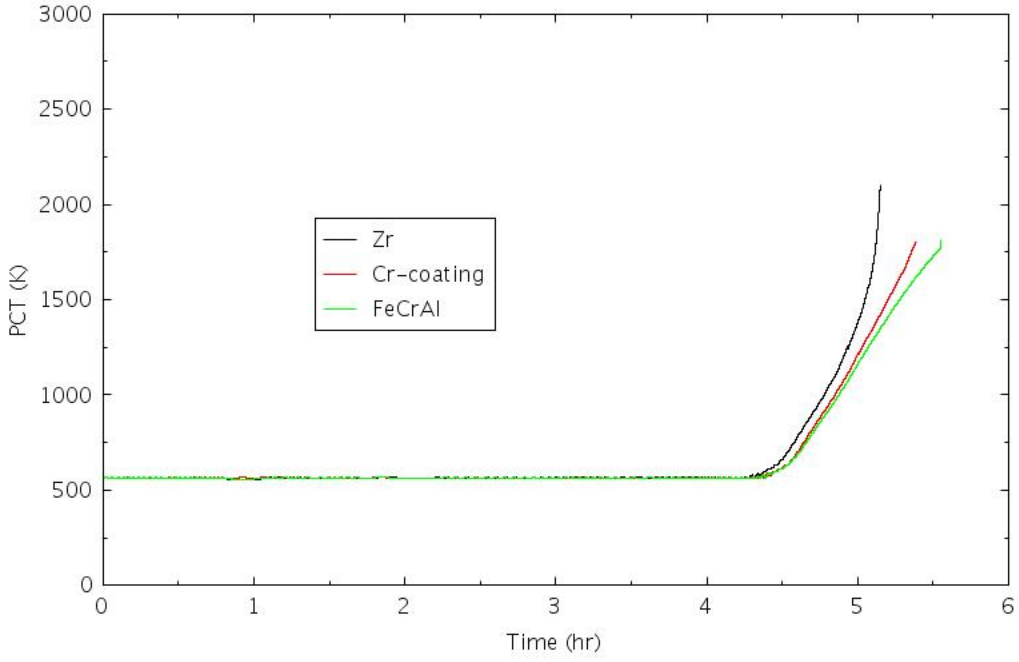

Figure 4-83. PCT at BOC for STSBO with RCIC Blackstart.

4.4 Summary of SBO Analyses

4.4.1 RELAP5-3D Results

Table 4-7 through Table 4-9 compare the times to CD for ATF designs (FeCrAl and Cr-coated) with those for existing Zircaloy clad design in different SBO scenarios at BOC, MOC, and EOC, respectively. The tables show that the gain of coping time, or the delay of time to CD, is less than or equal to 20 minutes for most scenarios. At BOC, for FeCrAl, eight of the nine analyzed SBO scenarios have a gain of coping time from 4 to 20 minutes. The other scenario has a gain of coping time of 50 minutes. For Chromium-coated cladding, eight of the nine analyzed SBO scenarios have a gain of coping time from 1 to 15 minutes, with the other scenario a gain of coping time of 42 minutes. The coping time gains at MOC and EOC are a bit less that those at BOC.

However, the RELAP5-3D simulation results show the clear benefit in adopting the ATF with much less hydrogen produced at the time of CD. Table 4-10 through Table 4-12 compare the hydrogen production for ATF designs (FeCrAl and Cr-coated) with that for existing Zircaloy clad design in different SBO scenarios at BOC, MOC, and EOC respectively. The tables show the hydrogen production can be a few times lower for the Cr-coated cladding, and up to two orders of magnitude lower for FeCrAl cladding than that with Zircaloy cladding cases.

Table 4-7. Time to CD Comparisons at BOC for SBO Scenarios with ATF Designs.

Scenario	Scenario Description				Time to CD t_{CD} (hh:mm)			Time to CD t_{CD} (hh:mm)		
					Zry	Cr-coated	Δt	Zry	FeCrAl	Δt
SBO-1	No SRV stuck open	RCIC available	HPCI not Available	AC power not recovered in 4 hrs	6:59	7:11	0:12	6:59	7:19	0:20
SBO-1-1	No SRV stuck open	RCIC not available	HPCI Available	AC power not recovered in 4 hrs	8:21	8:30	0:09	8:21	8:49	0:18
SBO-1-2	One SRV stuck open	RCIC available	HPCI not Available	AC power not recovered in 4 hrs	7:31	7:38	0:07	7:31	7:47	0:16
SBO-1-3	One SRV stuck open	RCIC not available	HPCI Available	AC power not recovered in 4 hrs	10:37	10:52	0:15	10:37	10:53	0:16
SBO-2	No SRV stuck open	RCIC not available	HPCI not Available	AC power not recovered in 4 hrs	1:14	1:19	0:05	1:14	1:24	0:10
SBO-2-1	One SRV stuck open	RCIC not available	HPCI not Available	AC power not recovered in 4 hrs	1:02	1:07	0:05	1:02	1:11	0:09
SBO-3	All SRVs stuck open	RCIC not available	HPCI not Available	AC power not recovered in 4 hrs	0:31	0:32	0:01	0:31	0:35	0:04
SBO-4	No SRV stuck open	RCIC available HPCI not available	AC power recovered in 4 hrs	DEP Success SPC Failed	10:20	10:21	0:01	10:20	10:33	0:13
SBO-4-1	No SRV stuck open	RCIC available HPCI not available	AC power recovered in 4 hrs	DEP Failed SPC Failed	11:56	12:38	0:42	11:56	12:46	0:50

Table 4-8. Time to CD Comparisons at MOC for SBO Scenarios with ATF Designs.

Scenario	Scenario Description				Time to CD t_{CD} (hh:mm)			Time to CD t_{CD} (hh:mm)		
					Zry	Cr-coated	Δt	Zry	FeCrAl	Δt
SBO-1	No SRV stuck open	RCIC available	HPCI not available	AC power not recovered in 4 hrs	6:54	7:03	0:09	6:54	7:09	0:15
SBO-1-1	No SRV stuck open	RCIC not available	HPCI available	AC power not recovered in 4 hrs	8:16	8:29	0:13	8:16	8:34	0:18
SBO-1-2	One SRV stuck open	RCIC available	HPCI not available	AC power not recovered in 4 hrs	7:22	7:33	0:11	7:22	7:41	0:19
SBO-1-3	One SRV stuck open	RCIC not available	HPCI available	AC power not recovered in 4 hrs	10:41	10:44	0:03	10:41	10:45	0:04
SBO-2	No SRV stuck open	RCIC not available	HPCI not available	AC power not recovered in 4 hrs	1:10	1:14	0:04	1:10	1:18	0:08
SBO-2-1	One SRV stuck open	RCIC not available	HPCI not available	AC power not recovered in 4 hrs	1:00	1:04	0:04	1:00	1:09	0:09
SBO-3	All SRVs stuck open	RCIC not available	HPCI not available	AC power not recovered in 4 hrs	0:29	0:31	0:02	0:29	0:33	0:04
SBO-4	No SRV stuck open	RCIC available HPCI not available	AC power recovered in 4 hrs	DEP success SPC failed	10:08	10:20	0:12	10:08	10:24	0:16
SBO-4-1	No SRV stuck open	RCIC available HPCI not available	AC power recovered in 4 hrs	DEP failed SPC failed	11:51	12:02	0:11	11:51	12:11	0:20

Table 4-9. Time to CD Comparisons at EOC for SBO Scenarios with ATF Designs.

Scenario	Scenario Description				Time to CD t_{CD} (hh:mm)			Time to CD t_{CD} (hh:mm)		
					Zry	Cr-coated	Δt	Zry	FeCrAl	Δt
SBO-1	No SRV stuck open	RCIC available	HPCI not available	AC power not recovered in 4 hrs	6:51	6:56	0:05	6:51	7:04	0:13
SBO-1-1	No SRV stuck open	RCIC not available	HPCI available	AC power not recovered in 4 hrs	8:11	8:14	0:03	8:11	8:27	0:16
SBO-1-2	One SRV stuck open	RCIC available	HPCI not available	AC power not recovered in 4 hrs	7:18	7:21	0:03	7:18	7:35	0:17
SBO-1-3	One SRV stuck open	RCIC not available	HPCI available	AC power not recovered in 4 hrs	10:13	10:21	0:08	10:13	10:33	0:20
SBO-2	No SRV stuck open	RCIC not available	HPCI not available	AC power not recovered in 4 hrs	1:08	1:10	0:02	1:08	1:15	0:07
SBO-2-1	One SRV stuck open	RCIC not available	HPCI not available	AC power not recovered in 4 hrs	0:56	1:00	0:04	0:56	1:05	0:09
SBO-3	All SRVs stuck open	RCIC not available	HPCI not available	AC power not recovered in 4 hrs	0:27	0:27	0:00	0:27	0:31	0:04
SBO-4	No SRV stuck open	RCIC available HPCI not available	AC power recovered in 4 hrs	DEP success SPC failed	10:11	10:17	0:06	10:11	10:23	0:12
SBO-4-1	No SRV stuck open	RCIC available HPCI not available	AC power recovered in 4 hrs	DEP failed SPC failed	11:41	11:48	0:07	11:41	12:02	0:21

Table 4-10. Hydrogen Production Comparisons at BOC for SBO Scenarios with ATF Designs.

Scenario	Scenario Description				Total H2 (kg)			H2 %	
					Zry	Cr-coated	FeCrAl	Cr-coated	FeCrAl
SBO-1	No SRV stuck open	RCIC available	HPCI not available	AC power not recovered in 4 hrs	31.02	6.05	0.55	19.5	1.8
SBO-1-1	No SRV stuck open	RCIC not available	HPCI available	AC power not recovered in 4 hrs	32.24	6.23	0.65	19.3	2.0
SBO-1-2	One SRV stuck open	RCIC available	HPCI not available	AC power not recovered in 4 hrs	26.35	11.11	0.33	42.2	1.3
SBO-1-3	One SRV stuck open	RCIC not available	HPCI available	AC power not recovered in 4 hrs	26.20	5.19	0.41	19.8	1.6
SBO-2	No SRV stuck open	RCIC not available	HPCI not available	AC power not recovered in 4 hrs	24.08	4.11	0.30	17.1	1.2
SBO-2-1	One SRV stuck open	RCIC not available	HPCI not available	AC power not recovered in 4 hrs	46.25	5.44	0.44	11.8	1.0
SBO-3	All SRVs stuck open	RCIC not available	HPCI not available	AC power not recovered in 4 hrs	10.30	1.12	0.07	10.9	0.7
SBO-4	No SRV stuck open	RCIC available HPCI not available	AC power recovered in 4 hrs	DEP success SPC failed	13.07	1.91	0.13	14.6	1.0
SBO-4-1	No SRV stuck open	RCIC available HPCI not available	AC power recovered in 4 hrs	DEP failed SPC failed	34.05	7.25	1.10	21.3	3.2

Table 4-11. Hydrogen Production Comparisons at MOC for SBO Scenarios with ATF Designs.

Scenario	Scenario Description				Total H_2 (kg)			H_2 %	
					Zry	Cr-coated	FeCrAl	Cr-coated	FeCrAl
SBO-1	No SRV stuck open	RCIC available	HPCI not available	AC power not recovered in 4 hrs	26.69	5.04	0.38	18.9	1.4
SBO-1-1	No SRV stuck open	RCIC not available	HPCI available	AC power not recovered in 4 hrs	26.27	5.13	0.40	19.5	1.5
SBO-1-2	One SRV stuck open	RCIC available	HPCI not available	AC power not recovered in 4 hrs	25.88	5.40	0.29	20.9	1.1
SBO-1-3	One SRV stuck open	RCIC not available	HPCI available	AC power not recovered in 4 hrs	33.14	5.66	0.36	17.1	1.1
SBO-2	No SRV stuck open	RCIC not available	HPCI not available	AC power not recovered in 4 hrs	18.45	3.05	0.22	16.5	1.2
SBO-2-1	One SRV stuck open	RCIC not available	HPCI not available	AC power not recovered in 4 hrs	40.45	6.13	0.67	15.2	1.7
SBO-3	All SRVs stuck open	RCIC not available	HPCI not available	AC power not recovered in 4 hrs	11.95	2.06	0.31	17.2	2.6
SBO-4	No SRV stuck open	RCIC available HPCI not available	AC power recovered in 4 hrs	DEP success SPC failed	9.57	2.05	0.11	21.4	1.1
SBO-4-1	No SRV stuck open	RCIC available HPCI not available	AC power recovered in 4 hrs	DEP failed SPC failed	31.46	5.51	0.46	17.5	1.5

Table 4-12. Hydrogen Production Comparisons at EOC for SBO Scenarios with ATF Designs.

Scenario	Scenario Description				Total H_2 (kg)			H_2 %	
					Zry	Cr-coated	FeCrAl	Cr-coated	FeCrAl
SBO-1	No SRV stuck open	RCIC available	HPCI not available	AC power not recovered in 4 hrs	20.58	4.07	0.30	19.8	1.5
SBO-1-1	No SRV stuck open	RCIC not available	HPCI available	AC power not recovered in 4 hrs	24.41	4.57	0.32	18.7	1.3
SBO-1-2	One SRV stuck open	RCIC available	HPCI not available	AC power not recovered in 4 hrs	29.28	4.23	0.29	14.4	1.0
SBO-1-3	One SRV stuck open	RCIC not available	HPCI available	AC power not recovered in 4 hrs	25.69	4.33	0.26	16.9	1.0
SBO-2	No SRV stuck open	RCIC not available	HPCI not available	AC power not recovered in 4 hrs	18.73	2.48	0.17	13.2	0.9
SBO-2-1	One SRV stuck open	RCIC not available	HPCI not available	AC power not recovered in 4 hrs	35.96	6.23	2.20	17.3	6.1
SBO-3	All SRVs stuck open	RCIC not available	HPCI not available	AC power not recovered in 4 hrs	11.20	1.51	0.08	13.5	0.7
SBO-4	No SRV stuck open	RCIC available HPCI not available	AC power recovered in 4 hrs	DEP success SPC failed	18.15	1.96	0.10	10.8	0.6
SBO-4-1	No SRV stuck open	RCIC available HPCI not available	AC power recovered in 4 hrs	DEP failed SPC failed	28.43	5.06	0.38	17.8	1.4

4.4.2 Risk Impact Evaluation

With only a marginal increase of the time-to-core-damage with FeCrAl and Cr-coated against the conventional Zry cladding design based on the RELAP5-3D simulation results (see Table 4-7 through Table 4-9), the risk-benefit on behalf of the CDF as the risk metrics would be very small. The less than an hour time difference does not warrant a change of the PRA SBO model (ET, FT, success criteria, or human reliability analysis). Instead, a simplified approach proposed in (Ma et al., 2018) using a multiplication factor, called coping time factor $F_{CT}(m/n)$, is adopted in this report to estimate the risk impact of the ATF design with the small increase of coping time. If an SBO sequence that includes top events of AC power recovery (either offsite power

recovery or DG recovery) within n hours has a base case CDF of CDF_0, with the increase of coping time for m hours with the ATF design, the time-to-core-damage is delayed by m hours, and the base case top events of AC power recovery within n hours become as AC power recovery within $(m+n)$ hours. The failure probability for operator to recover AC power is thus smaller which would lead to a reduced CDF of CDF', by the factor of $F_{CT}(m/n)$:

$$CDF' = F_{CT}(m/n) * CDF_0 \quad (4\text{-}4)$$

The coping time factor $F_{CT(m/n)}$ can be estimated from the ratio of the probabilities of operator fails to recover AC power within different time periods. The probability of operator fails to recover AC power within t hours, $P_{ACR}(t)$, is calculated as:

$$P_{ACR}(t) = P_{OPR}(t) \cdot P_{DGR}(t) \quad (4\text{-}5)$$

where:

$P_{OPR}(t)$ = Probability of operator failing to recover offsite power within t hours

$P_{DGR}(t)$ = Probability of operator failing to recover DGs within t hours

The recovery human error probabilities (HEPs), P_{OPR} and P_{DGR}, can be estimated based on :

$$P_{OPR}(t) = 1 - \Phi[\frac{ln(t)-\mu}{\sigma}] \quad (4\text{-}6)$$

$$P_{DGR}(t) = e^{-(\frac{t}{\beta})^{\alpha}} \quad (4\text{-}7)$$

where[1]:

μ, σ = Lognormal distribution parameters, $\mu = -0.45$, $\sigma = 1.51$ (LOOPPC), $\mu = 0.17$, $\sigma = 1.50$ (LOOPSC), $\mu = 0.80$, $\sigma = 1.17$ (LOOPGR), $\mu = 1.63$, $\sigma = 2.05$ (LOOPWR)

α, β = Weibull distribution parameters, $\alpha = 0.70$, $\beta = 20.77$

Table 4-13 shows the calculated values of P_{OPR} and P_{DGR} within specified time periods from 1 hour to 9 hours. The column of P(n+1)/P(n) in the table presents the ratio of P_{ACR} within n+1 hours to that of within n hours. The last two columns present the ratios if the coping time is increased by 0.5 hours or 0.25 hours. The coping time factor $F_{CT}(m/n)$ is estimated by rounding up these ratios with the results presented in

Table 4-14. The factor $F_{CT}(m/n)$ can then be applied to the PRA SBO sequence results.

Table 4-15 through Table 4-20 show the estimated CDF for the analyzed SBO sequences with FeCrAl and Cr-coated cladding designs at BOC, MOC, and EOC, respectively. The results show that the marginal coping time increase brought by the FeCrAl and Cr-coated designs would lead to about ~3–5% and ~1–3% reductions in CDF led by weather-related LOOP, respectively. For both ATF designs, the CDF reductions vary during the fuel cycle, exhibiting the greatest reduction at BOC and lowest reduction at EOC.

It is to be noted that, for three out of 10 scenarios (i.e., SBO-2.0 corresponding to PRA sequence LOOPWR:37-07-23, SBO-4 corresponding to PRA sequence LOOPWR:37-01-05, and SBO-4.1 corresponding to PRA sequence LOOPWR:37-01-11), their CDF' values are higher than the CDF_0 values. This is because the three scenarios involve successful recovery actions: the introduction of ATF designs provides coping time extension, which reduces the probability of recovery failure and increases the probability of recovery success. Also, for two out of 10 scenarios (i.e., SBO-2.1 corresponding to PRA sequence LOOPWR:37-11-7 and SBO-3 corresponding to PRA sequence LOOPWR:37-12), their CDF' values are the same as the CDF_0 values, since these two scenarios

1. These distribution parameter values were the latest versions when the generic BWR PRA model was developed. Please note that these values are being updated annually. As of September 2020, the most recent versions are provided in INL/EXT-19-54699, "Analysis of Loss-of-Offsite-Power Events: 1987-2018" (Johnson & Ma, 2019), and INL/EXT-19-54609, "Enhanced Component Performance Study: Emergency Diesel Generators 1998-2018" (Ma Z. , 2019).

do not involve recovery actions. Even though, the impact of CDF reduction overwhelms the impact of CDF increase and the total CDF led by weather-related LOOP shows a decreasing trend.

Although the CDF reductions seem trivial, this should not be misinterpreted to suggest ATF brings no risk benefits since there are observed clear benefits from ATF slowing down the hydrogen production. As stated in Section 4.4.1, the hydrogen production can be a few times lower for the Cr-coated cladding, and up to two orders of magnitude lower for FeCrAl cladding than with Zircaloy cladding cases.

Table 4-13. Failure Probabilities for Operator to Recover AC Power.

Operator Action	P_{OPR}	P_{DGR}	P_{ACR}	P(n+1)/P(n)	P(n+0.5)/P(n)	P(n+0.25)/P(n)
Operator Fails to Recover in n = 1 hr	7.87E-01	8.87E-01	6.98E-01	80%	90%	95%
Operator Fails to Recover in n = 2 hrs	6.76E-01	8.24E-01	5.57E-01	84%	92%	96%
Operator Fails to Recover in n = 3 hrs	6.02E-01	7.73E-01	4.65E-01	86%	93%	96%
Operator Fails to Recover in n = 4 hrs	5.47E-01	7.30E-01	3.99E-01	87%	94%	97%
Operator Fails to Recover in n = 5 hrs	5.04E-01	6.92E-01	3.49E-01	88%	94%	97%
Operator Fails to Recover in n = 6 hrs	4.69E-01	6.58E-01	3.08E-01	89%	95%	97%
Operator Fails to Recover in n = 7 hrs	4.39E-01	6.27E-01	2.75E-01	90%	95%	97%
Operator Fails to Recover in n = 8 hrs	4.13E-01	5.99E-01	2.48E-01	91%	95%	98%
Operator Fails to Recover in n = 9 hrs	3.91E-01	5.73E-01	2.24E-01			

Table 4-14. Estimated Coping Time Factor.

Coping Time Factor	$F_{CT}(1.0/n)$	$F_{CT}(0.5/n)$	$F_{CT}(0.25/n)$
Operator Fails to Mitigate Accident in n = 1 hr	0.80	0.90	0.95
Operator Fails to Mitigate Accident in n = 2 hrs	0.85	0.95	1.00
Operator Fails to Mitigate Accident in n = 3 hrs	0.90	0.95	1.00
Operator Fails to Mitigate Accident in n = 4 hrs	0.90	0.95	1.00
Operator Fails to Mitigate Accident in n = 5 hrs	0.90	0.95	1.00
Operator Fails to Mitigate Accident in n = 6 hrs	0.90	0.95	1.00
Operator Fails to Mitigate Accident in n = 7 hrs	0.90	0.95	1.00
Operator Fails to Mitigate Accident in n = 8 hrs	0.95	0.95	1.00

Table 4-15. CDF Estimation for FeCrAl at BOC.

	Time to CD t_{CD} (hh:mm)			Power Recovery	CDF_0	F_{CT}	CDF'	ΔCDF	$\Delta CDF\%$
	Zr	FeCrAl	Δt						
SBO-1	6:59	7:19	0:20	4hrs No	2.77E-07	0.95	2.64E-07	-1.27E-08	-5%
SBO-1.1	8:21	8:49	0:28	4hrs No	4.10E-08	0.94	3.84E-08	-2.59E-09	-6%
SBO-1.2	7:31	7:47	0:16	4hrs No	2.65E-08	0.96	2.55E-08	-9.81E-10	-4%
SBO-1.3	10:37	10:53	0:16	4hrs No	3.80E-09	0.96	3.66E-09	-1.40E-10	-4%
SBO-2[a]	1:14	1:24	0:10	0.5hrs Yes	1.68E-12	0.96	2.09E-12	4.15E-13	25%
SBO-2[b]	1:14	1:24	0:10	0.5hrs No	1.27E-08	0.95	1.20E-08	-6.62E-10	-5%
SBO-2.1	1:02	1:11	0:09	--	3.44E-09	--	3.44E-09	0.00E+00	0%
SBO-3	0:31	0:35	0:04	--	2.85E-09	--	2.85E-09	0.00E+00	0%
SBO-4	10:20	10:33	0:13	4hrs Yes	2.22E-11	0.98	2.27E-11	5.00E-13	2%
SBO-4.1	11:56	12:46	0:50	4hrs Yes	3.15E-12	0.93	3.40E-12	2.55E-13	8%
Total					3.67E-07		3.50E-07	-1.71E-08	-5%

a Corresponds to PRA sequence LOOPWR:37-07-23

b Corresponds to PRA sequence LOOPWR:37-09

Table 4-16. CDF Estimation for Cr-Coated at BOC

	Time to CD t_{CD} (hh:mm)			Power Recovery	CDF_0	F_{CT}	CDF'	ΔCDF	$\Delta CDF\%$
	Zr	Cr-coated	Δt						
SBO-1	6:59	7:11	0:12	4hrs No	2.77E-07	0.97	2.69E-07	-7.75E-09	-3%
SBO-1.1	8:21	8:30	0:09	4hrs No	4.10E-08	0.98	4.01E-08	-8.66E-10	-2%
SBO-1.2	7:31	7:38	0:07	4hrs No	2.65E-08	0.98	2.61E-08	-4.37E-10	-2%
SBO-1.3	10:37	10:52	0:15	4hrs No	3.80E-09	0.97	3.67E-09	-1.32E-10	-3%
SBO-2[a]	1:14	1:19	0:05	0.5hrs Yes	1.68E-12	0.98	1.89E-12	2.14E-13	13%
SBO-2[b]	1:14	1:19	0:05	0.5hrs No	1.27E-08	0.97	1.23E-08	-3.43E-10	-3%
SBO-2.1	1:02	1:07	0:05	--	3.44E-09	--	3.44E-09	0.00E+00	0%
SBO-3	0:31	0:32	0:01	--	2.85E-09	--	2.85E-09	0.00E+00	0%
SBO-4	10:20	10:21	0:01	4hrs Yes	2.22E-11	1.00	2.22E-11	3.94E-14	0%
SBO-4.1	11:56	12:38	0:42	4hrs Yes	3.15E-12	0.94	3.36E-12	2.17E-13	7%
Total					3.67E-07		3.58E-07	-9.52E-09	-3%

Table 4-17. CDF Estimation for FeCrAl at MOC

	Time to CD t_{CD} (hh:mm)			Power Recovery	CDF_0	F_{CT}	CDF'	ΔCDF	$\Delta CDF\%$
	Zr	FeCrAl	Δt						
SBO-1	6:54	7:09	0:15	4hrs No	2.77E-07	0.97	2.67E-07	-9.62E-09	-3%
SBO-1.1	8:16	8:34	0:18	4hrs No	4.10E-08	0.96	3.93E-08	-1.70E-09	-4%
SBO-1.2	7:22	7:41	0:19	4hrs No	2.65E-08	0.96	2.54E-08	-1.16E-09	-4%
SBO-1.3	10:41	10:45	0:04	4hrs No	3.80E-09	0.99	3.76E-09	-3.60E-11	-1%
SBO-2[a]	1:10	1:18	0:08	0.5hrs Yes	1.68E-12	0.97	2.01E-12	3.36E-13	20%
SBO-2[b]	1:10	1:18	0:08	0.5hrs No	1.27E-08	0.96	1.21E-08	-5.37E-10	-4%
SBO-2.1	1:00	1:09	0:09	--	3.44E-09	--	3.44E-09	0.00E+00	0%
SBO-3	0:29	0:33	0:04	--	2.85E-09	--	2.85E-09	0.00E+00	0%
SBO-4	10:08	10:24	0:16	4hrs Yes	2.22E-11	0.98	2.28E-11	6.12E-13	3%
SBO-4.1	11:51	12:11	0:20	4hrs Yes	3.15E-12	0.97	3.25E-12	1.08E-13	3%
Total					3.67E-07		3.54E-07	-1.31E-08	-4%

Table 4-18. CDF Estimation for Cr-Coated at MOC

	Time to CD t_{CD} (hh:mm)			Power Recovery	CDF_0	F_{CT}	CDF'	ΔCDF	$\Delta CDF\%$
	Zr	Cr-coated	Δt						
SBO-1	6:54	7:03	0:09	4hrs No	2.77E-07	0.98	2.71E-07	-5.85E-09	-2%
SBO-1.1	8:16	8:29	0:13	4hrs No	4.10E-08	0.97	3.98E-08	-1.24E-09	-3%
SBO-1.2	7:22	7:33	0:11	4hrs No	2.65E-08	0.97	2.58E-08	-6.81E-10	-3%
SBO-1.3	10:41	10:44	0:03	4hrs No	3.80E-09	0.99	3.77E-09	-2.71E-11	-1%
SBO-2[a]	1:10	1:14	0:04	0.5hrs Yes	1.68E-12	0.98	1.85E-12	1.73E-13	10%
SBO-2[b]	1:10	1:14	0:04	0.5hrs No	1.27E-08	0.98	1.24E-08	-2.77E-10	-2%
SBO-2.1	1:00	1:04	0:04	--	3.44E-09	--	3.44E-09	0.00E+00	0%
SBO-3	0:29	0:31	0:02	--	2.85E-09	--	2.85E-09	0.00E+00	0%
SBO-4	10:08	10:20	0:12	4hrs Yes	2.22E-11	0.98	2.27E-11	4.63E-13	2%
SBO-4.1	11:51	12:02	0:11	4hrs Yes	3.15E-12	0.98	3.21E-12	6.03E-14	2%
Total					3.67E-07		3.59E-07	-8.07E-09	-2%

Table 4-19. CDF Estimation for FeCrAl at EOC

	Time to CD t_{CD} (hh:mm)			Power Recovery	CDF_0	F_{CT}	CDF'	ΔCDF	$\Delta CDF\%$
	Zr	FeCrAl	Δt						
SBO-1	6:51	7:04	0:13	4hrs No	2.77E-07	0.97	2.69E-07	-8.37E-09	-3%
SBO-1.1	8:11	8:27	0:16	4hrs No	4.10E-08	0.96	3.95E-08	-1.52E-09	-4%
SBO-1.2	7:18	7:35	0:17	4hrs No	2.65E-08	0.96	2.55E-08	-1.04E-09	-4%
SBO-1.3	10:13	10:33	0:20	4hrs No	3.80E-09	0.95	3.62E-09	-1.74E-10	-5%
SBO-2[a]	1:08	1:15	0:07	0.5hrs Yes	1.68E-12	0.97	1.97E-12	2.96E-13	18%
SBO-2[b]	1:08	1:15	0:07	0.5hrs No	1.27E-08	0.96	1.22E-08	-4.73E-10	-4%
SBO-2.1	0:56	1:05	0:09	--	3.44E-09	--	3.44E-09	0.00E+00	0%
SBO-3	0:27	0:31	0:04	--	2.85E-09	--	2.85E-09	0.00E+00	0%
SBO-4	10:11	10:23	0:12	4hrs Yes	2.22E-11	0.98	2.27E-11	4.63E-13	2%
SBO-4.1	11:41	12:02	0:21	4hrs Yes	3.15E-12	0.97	3.26E-12	1.13E-13	4%
Total					3.67E-07		3.56E-07	-1.16E-08	-3%

Table 4-20. CDF Estimation for Cr-Coated at EOC

	Time to CD t_{CD} (hh:mm)			Power Recovery	CDF_0	F_{CT}	CDF'	ΔCDF	$\Delta CDF\%$
	Zr	Cr-coated	Δt						
SBO-1	6:51	6:56	0:05	4hrs No	2.77E-07	0.99	2.74E-07	-3.28E-09	-1%
SBO-1.1	8:11	8:14	0:03	4hrs No	4.10E-08	0.99	4.07E-08	-2.92E-10	-1%
SBO-1.2	7:18	7:21	0:03	4hrs No	2.65E-08	0.99	2.63E-08	-1.89E-10	-1%
SBO-1.3	10:13	10:21	0:08	4hrs No	3.80E-09	0.98	3.73E-09	-7.14E-11	-2%
SBO-2[a]	1:08	1:10	0:02	0.5hrs Yes	1.68E-12	0.99	1.76E-12	8.76E-14	5%
SBO-2[b]	1:08	1:10	0:02	0.5hrs No	1.27E-08	0.99	1.25E-08	-1.41E-10	-1%
SBO-2.1	0:56	1:00	0:04	--	3.44E-09	--	3.44E-09	0.00E+00	0%
SBO-3	0:27	0:27	0:00	--	2.85E-09	--	2.85E-09	0.00E+00	0%
SBO-4	10:11	10:17	0:06	4hrs Yes	2.22E-11	0.99	2.24E-11	2.34E-13	1%
SBO-4.1	11:41	11:48	0:07	4hrs Yes	3.15E-12	0.99	3.19E-12	3.87E-14	1%
Total					3.67E-07		3.63E-07	-3.97E-09	-1%

5. RISK-INFORMED ATF ANALYSIS OF MLOCA SCENARIOS

The risk-informed analysis for ATF under MLOCA scenarios is performed in this section. Section 5.1 presents the PRA model and scenarios for a BWR MLOCA accident. Section 5.2 presents the RELAP5-3D analysis of the baseline fuel and ATF under MLOCA scenarios and Section 5.3 presents the summary of the analysis results.

5.1 BWR MLOCA PRA Model and Scenarios

The generic BWR MLOCA ET is shown in Figure 5-1. The ET includes the following top events:

- RPS: success or failure of the RPS to shut down the reactor by inserting control rods
- VSS: success or failure of vapor suppression
- HCI02: success or failure of the HPCI system to inject flow from both the SP and the CST to the reactor vessel
- DEP: success or failure of manual depressurization with ADS valves for low pressure injection
- LPI: success or failure of low pressure injection, either by core spray system or RHR system
- VA: success or failure of the alternate low pressure injection through RHR service water booster pump
- SPC: success or failure of the SP cooling mode of RHR
- CSS: success or failure of the containment spray mode of RHR
- PCSR: success or failure of main condenser recovery
- CVS: success or failure of containment venting
- LI: success or failure of LI through control rod drive, condensate, or RHR service water system.

The MLOCA ET was quantified with SAPHIRE 8 using a truncation level of 1E-12. There are 13 MLOCA accident (or CD) sequences. The total MLOCA CDF is 1.43E-7/year (see Table 5-1).

Table 5-1. BWR MLOCA ETs Quantification Results.

Name	CDF	CDF%
MLOCA:31	1.30E-07	90.45%
MLOCA:30	9.07E-09	6.32%
MLOCA:32	4.07E-09	2.84%
MLOCA:33	2.21E-10	0.15%
MLOCA:07	2.04E-10	0.14%
MLOCA:15	1.30E-10	0.09%
MLOCA:22	2.34E-11	0.02%
Total	1.43E-07	100.0%

A review of the 13 MLOCA accident sequences shows there are only seven non-zero sequences (or sequence CDF greater than 1E-12/year, which was set as the quantification truncation level):

- MLOCA:31, with a CDF of 1.30E-7/year contributing about 90% of the total MLOCA CDF. In this sequence (/RPS, /VSS, HCI02, DEP), the reactor is shut down; vapor suppression is successful; however, HPCI fails to provide injection and manual depressurization fails. With no inventory control, core damage occurs.
- MLOCA:30, with a CDF of 9.07E-9/year contributing about 6% of the total MLOCA CDF. In this sequence (/RPS, /VSS, HCI02, /DEP, LPI, VA), the reactor is shut down; vapor suppression is successful; however,

HPCI fails to provide injection, although manual depressurization is successful, LPI and VA fail. With no inventory control, core damage occurs.

- MLOCA:32, with a CDF of 4.07E-9/year contributing about 3% of the total MLOCA CDF. In this sequence (/RPS, VSS), the reactor is shut down, but vapor suppression fails, core damage occurs.
- The remaining four sequences including the anticipated transient without scram sequence (MLOCA:33) and the other three sequences (MLOCA:07, MLOCA:15, and MLOCA:22) have negligible risk contributions, about 0.1% or smaller, and will not discussed further in the analysis.

Four RELAP5-3D scenarios were developed based on the BWR SBO PRA sequences (see Table 5-2). **Error! Reference source not found.** presents the details of each RELAP5-3D scenario.

Table 5-2. BWR MLOCA Scenarios for RELAP5-3D.

RELAP5-3D Scenario	Scenario Description	MLOCA PRA Sequence	CDF
MLOCA-1	Reactor Shutdown, Vapor Suppression Success, but HPCI and DEP Fail	MLOCA:31	1.30E-07
MLOCA-2	Reactor Shutdown, Vapor Suppression Success, HPCI Fails, DEP Success, but LPI and VA Fail	MLOCA:30	9.07E-09
MLOCA-3	Reactor Shutdown, Vapor Suppression Fails	MLOCA:32	4.07E-09
MLOCA-4	Reactor Shutdown, Vapor Suppression Success, HPCI Success, but LPI and VA Fail	MLOCA:15	1.30E-10

Table 5-3. MLOCA Scenarios for RELAP-5 3D Analysis.

RELAP5-3D Scenario	Scenario Description	RPS	VSS	HPCI	DEP	LPI & VA
MLOCA-1	Reactor Shutdown, Vapor Suppression Success, but HPCI and DEP Fail	Success	Success	Fail	Fail	
MLOCA-2	Reactor Shutdown, Vapor Suppression Success, HPCI Fails, DEP Success, but LPI and VA Fail	Success	Success	Fail	Success	Fail
MLOCA-3	Reactor Shutdown, Vapor Suppression Fails	Success	Fail			
MLOCA-4	Reactor Shutdown, Vapor Suppression Success, HPCI Success, but LPI and VA Fail	Success	Success	Success		Fail

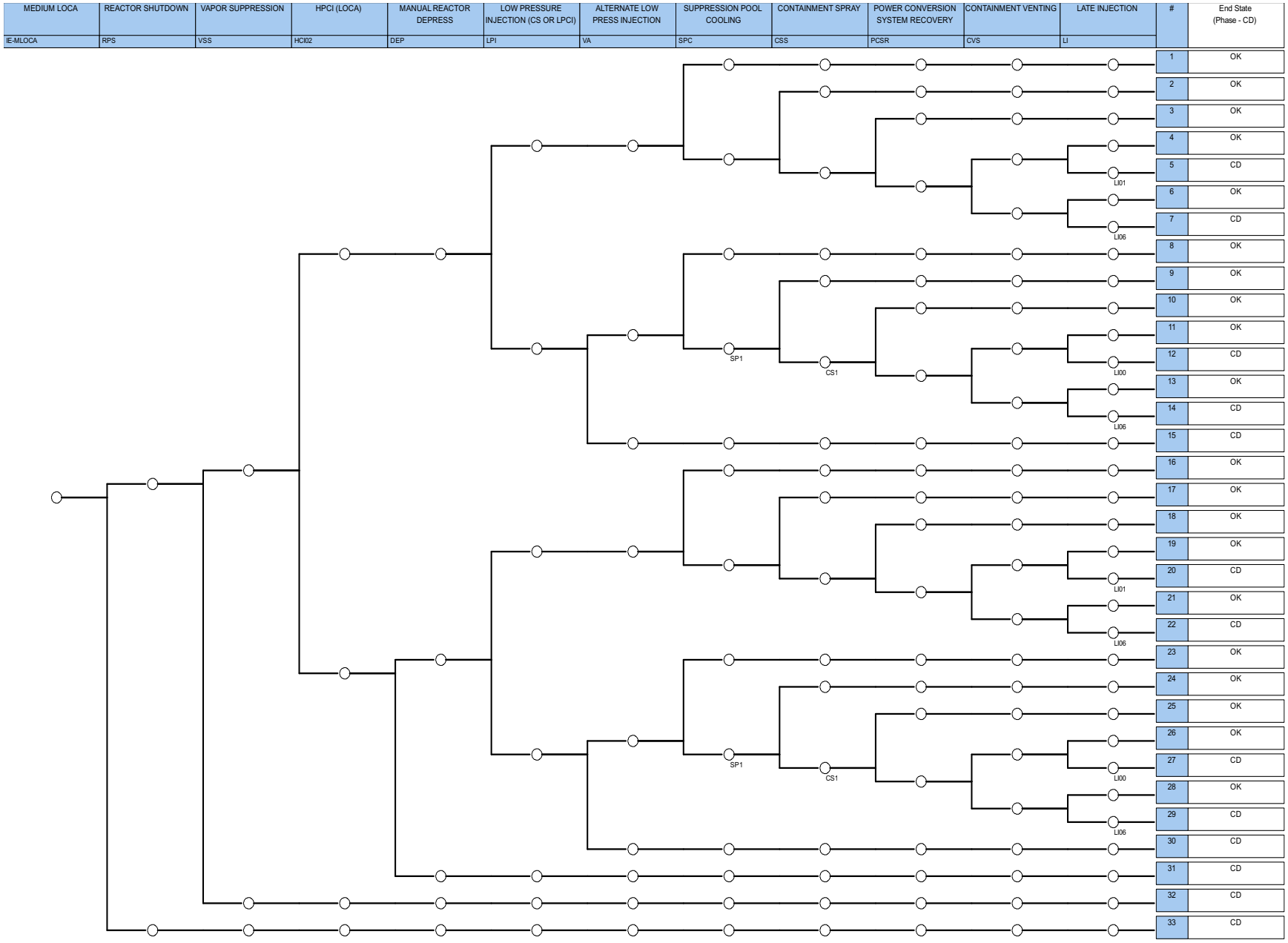

Figure 5-1. Generic BWR MLOCA ET.

5.2 RELAP5-3D Analysis of MLOCA Scenarios

Previous studies on BWR LOCA from open literatures indicate that the most limiting LOCA case of a BWR/4 reactor is a break on the recirculation suction line. In this study, the break is assumed to happen on the recirculation suction line between RPV and the recirculation pump. The break size is assumed to be 8 inches in diameter with a break area of 0.3491 ft^2, representing about 9% of the recirculation suction line. This break size falls within the conventional definition of medium break size between 0.1 ft^2 to 1 ft^2 (note this MLOCA definition may be different from those assumed in PRA, and sensitivity analysis may be considered in the future work). A BWR/4 plant has two recirculation loops. However, the RELAP5-3D plant model used in the SBO analyses presented in the previous section lumped the two recirculation loops into one. In order to provide a more realistic simulation of LOCA behaviors in a BWR/4, the RELAP5-3D plant model used in the SBO analyses has been expanded to include two recirculation loops. It is assumed that the break only happens at one of the recirculation loops while the other loop stays intact.

The reactor is successfully scrammed with the ensuing initiation of LOCA. The reactor scram can be triggered by the signals from high DW pressure, or low reactor water level, or high-vessel pressure, or high flux, etc. For LOCA, the high DW pressure or low-water-level are the most important. The scram signal of the DW high pressure is found to be activated earlier than the other scram signals.

5.2.1 MLOCA-1 - Reactor Shutdown, Vapor Suppression Success, but HPCI and DEP Fail

In this scenario, the reactor power is shutdown after LOCA happens. The vapor suppression is successful to ensure the integrity of the containment DW. It is further assumed HPCI fails to provide water injection to the RPV and manual depressurization of RPV fails such that LPCI systems are not able to provide water injection to the RPV. As a result, with an absence of makeup water for the RPV after the initiation of LOCA, the coolant inventory will boil off due to the decay heat and eventually lead to fuel damage.

The calculations were done at BOC, MOC, and EOC. To save space, only the results at MOC are shown in the following figures. Figure 5-2 shows the mass flow rate at the break area at MOC for this scenario. Figure 5-3 shows the collapsed water level in the RPV. Figure 5-4 shows the RPV dome pressure. Figure 5-5 shows the PCT during MLOCA-1. The coping time gain with respect to Zircaloy is 1.5 minutes for Chromium-coated cladding and 4 minutes for FeCrAl cladding, respectively.

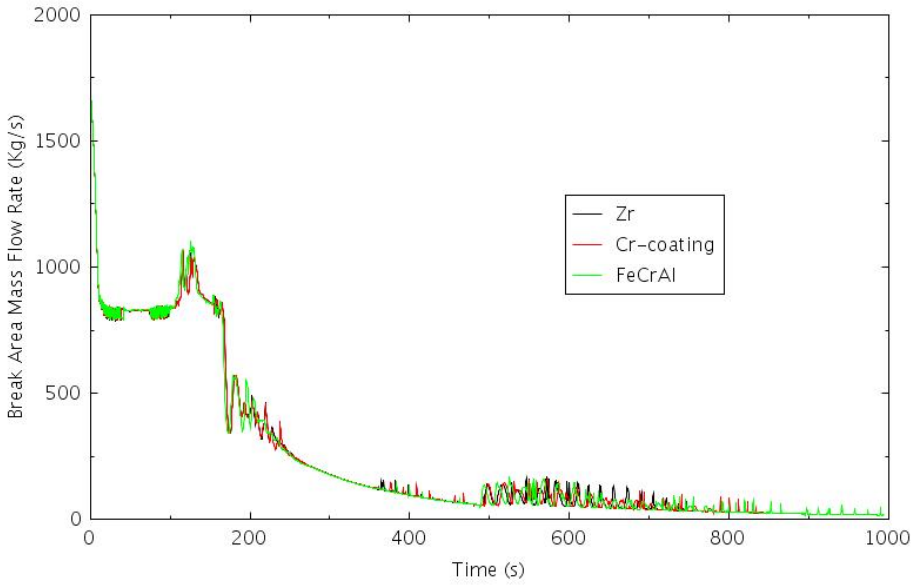

Figure 5-2. Break Area Mass Flow Rate at MOC for MLOCA-1.

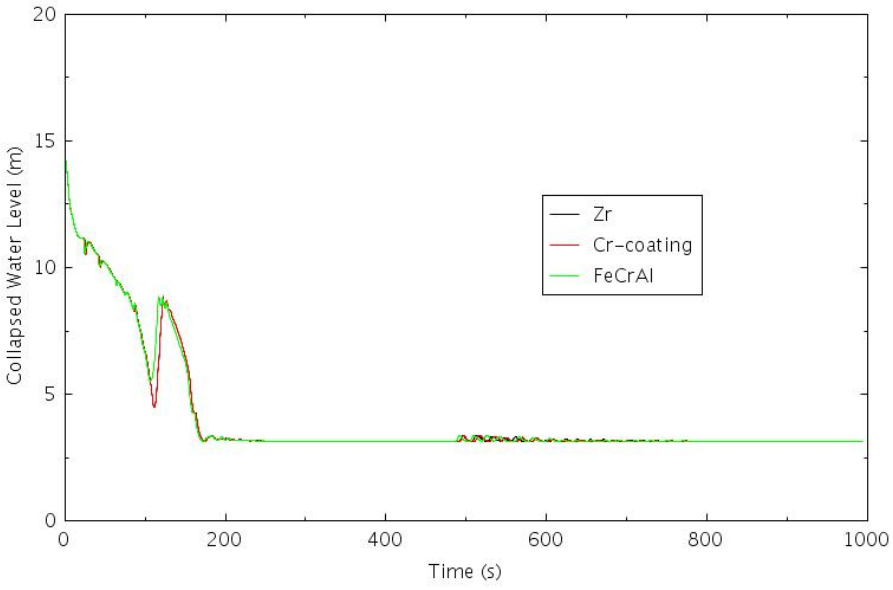

Figure 5-3. RPV Downcomer Collapsed Water Level at MOC for MLOCA-1.

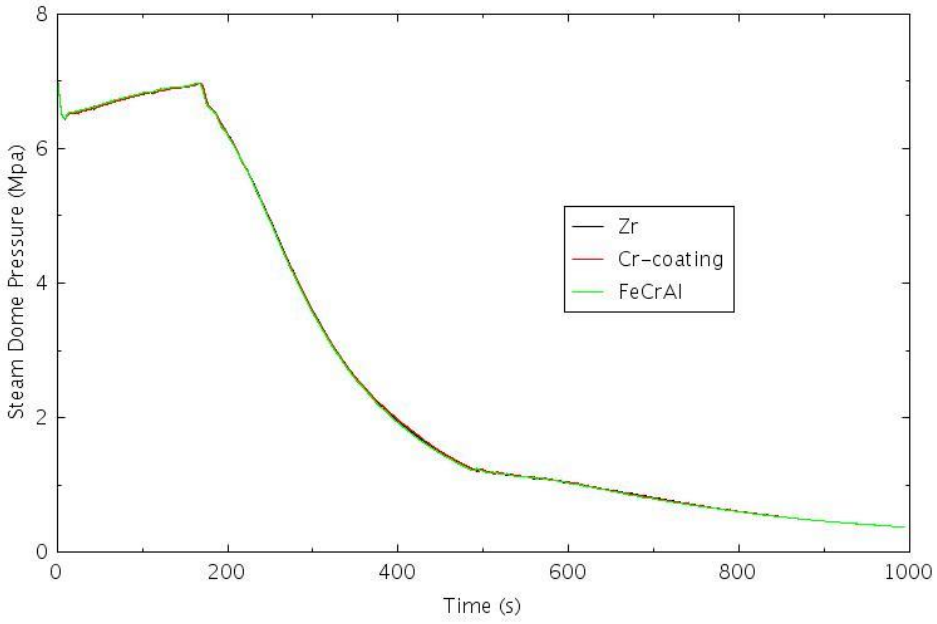

Figure 5-4. RPV Dome Pressure at MOC for MLOCA-1.

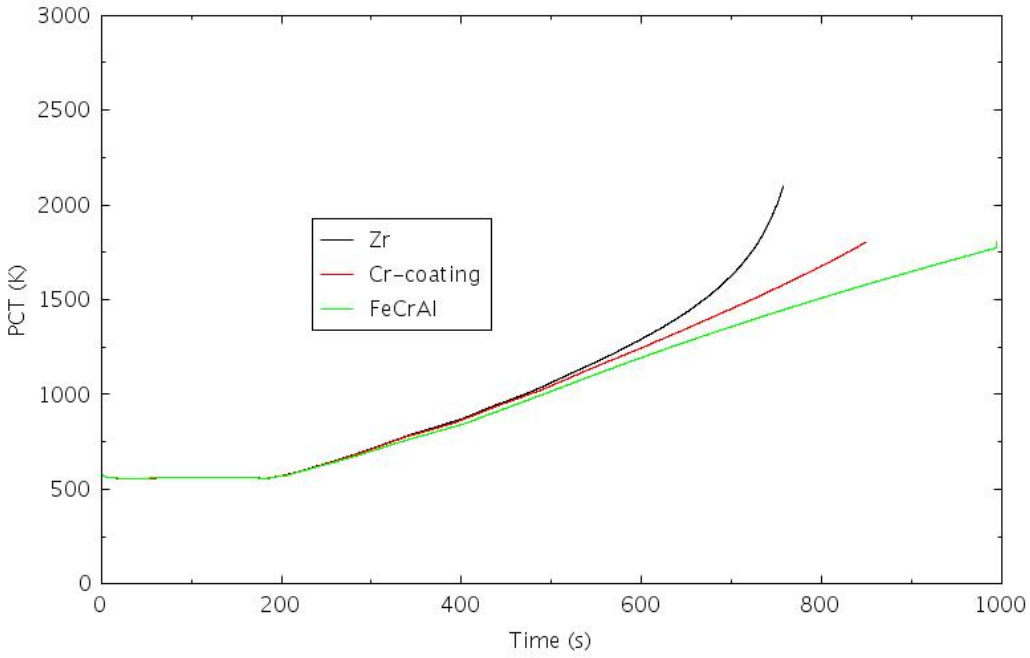

Figure 5-5. PCT at MOC for MLOCA-1.

5.2.2 MLOCA-2 - Reactor Shutdown, Vapor Suppression Success, HPCI Fails, DEP Success, but LPI and VA Fail

In this scenario, the reactor scram is triggered by the DW high-pressure signal following the initiation of medium LOCA. The vapor suppression is successful to ensure the integrity of the containment DW. It is further assumed HPCI fails to provide water injection to the RPV and manual depressurization of RPV is successful. However, LPCI systems such as LPI or alternate low pressure injection through RHR service water booster pump fail to provide water injection to the RPV. As a result, with absence of makeup water to the RPV after the initiation of LOCA, the coolant inventory will boil off due to the decay heat and lead to fuel damage.

The calculations were done at BOC, MOC, and EOC. To save space, only the results at MOC are showing in the following figures. Figure 5-6 shows the mass flow rate at the break area at MOC for this scenario. Figure 5-7 shows the collapsed water level in the RPV. Figure 5-8 shows the RPV dome pressure. Figure 5-9 shows the mass flow rate through the manual operation of ADS to depressurize the RPV. The manual opening of ADS is triggered at 66.8 seconds by the low-water-level setpoint of 9.766 m. Figure 5-10 shows the PCT during MLOCA-2. The coping time gain with respect to Zircaloy is 78 seconds for Chromium-coated cladding and 219 seconds for FeCrAl cladding, respectively.

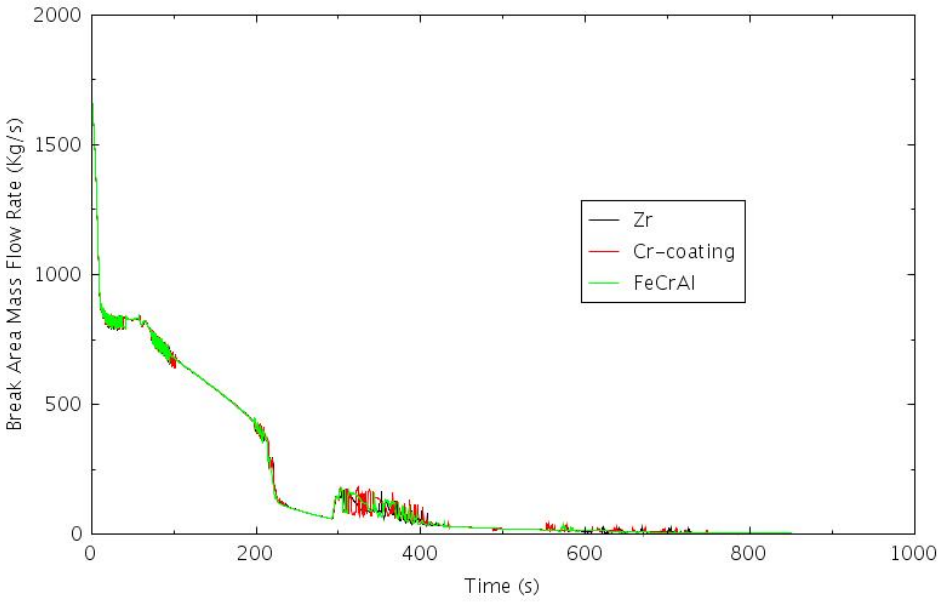

Figure 5-6. Break Area Mass Flow Rate at MOC for MLOCA-2.

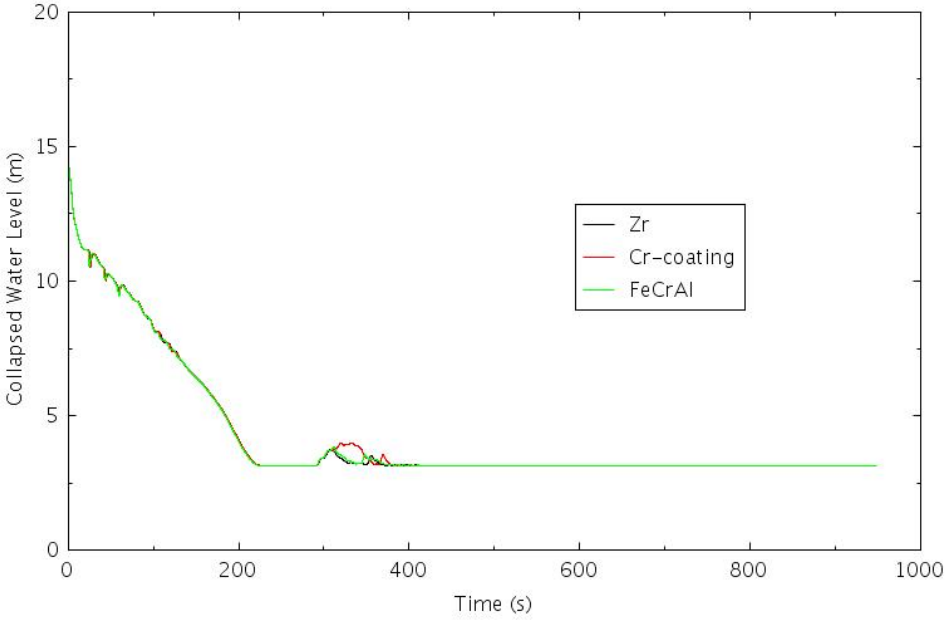

Figure 5-7. RPV Downcomer Collapsed Water Level at MOC for MLOCA-2.

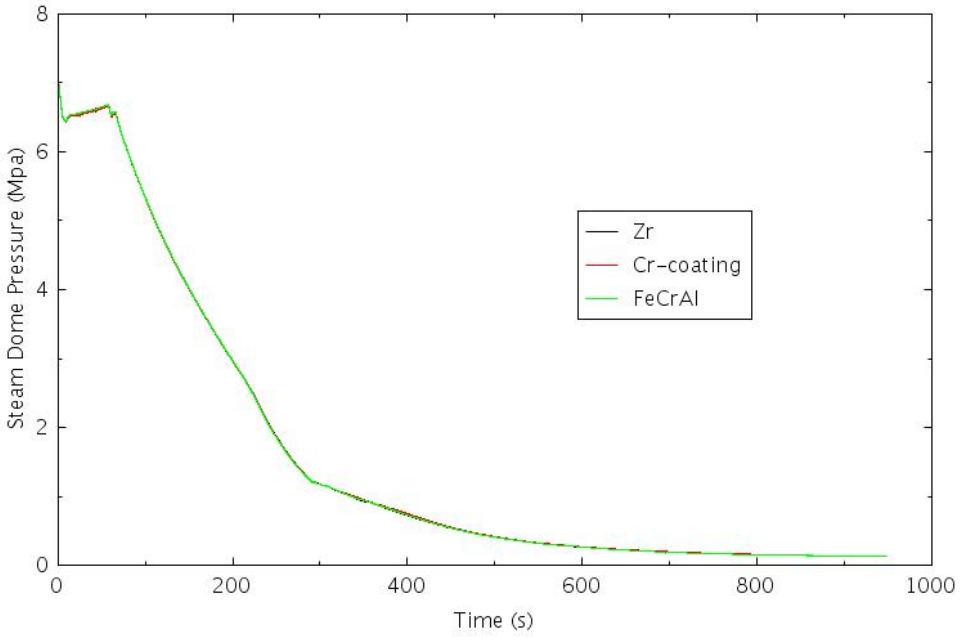

Figure 5-8. RPV Dome Pressure at MOC for MLOCA-2.

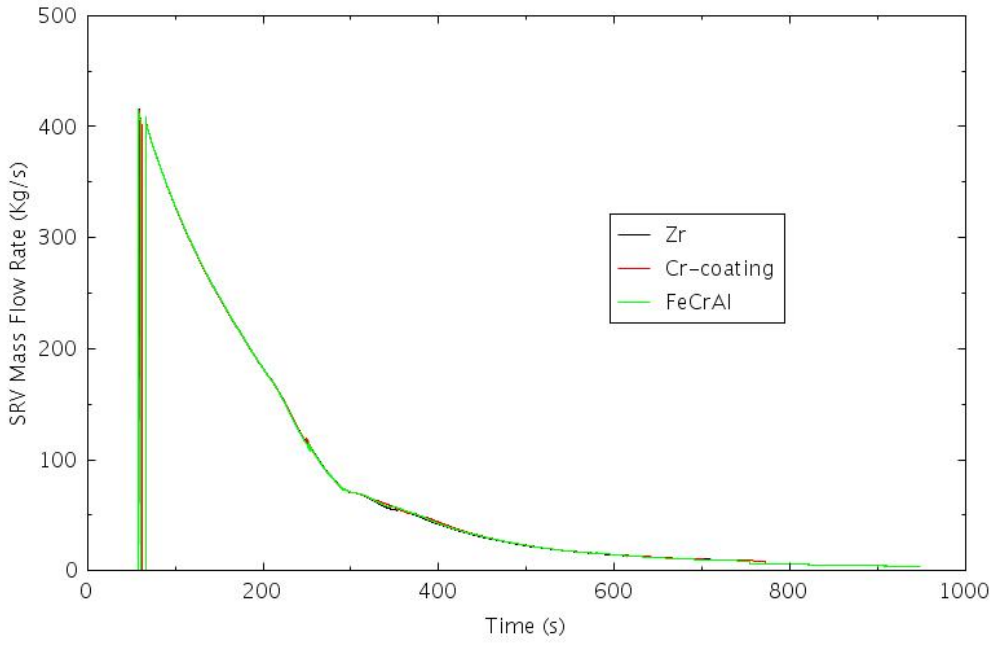

Figure 5-9. SRV Mass Flow Rate at MOC for MLOCA-2.

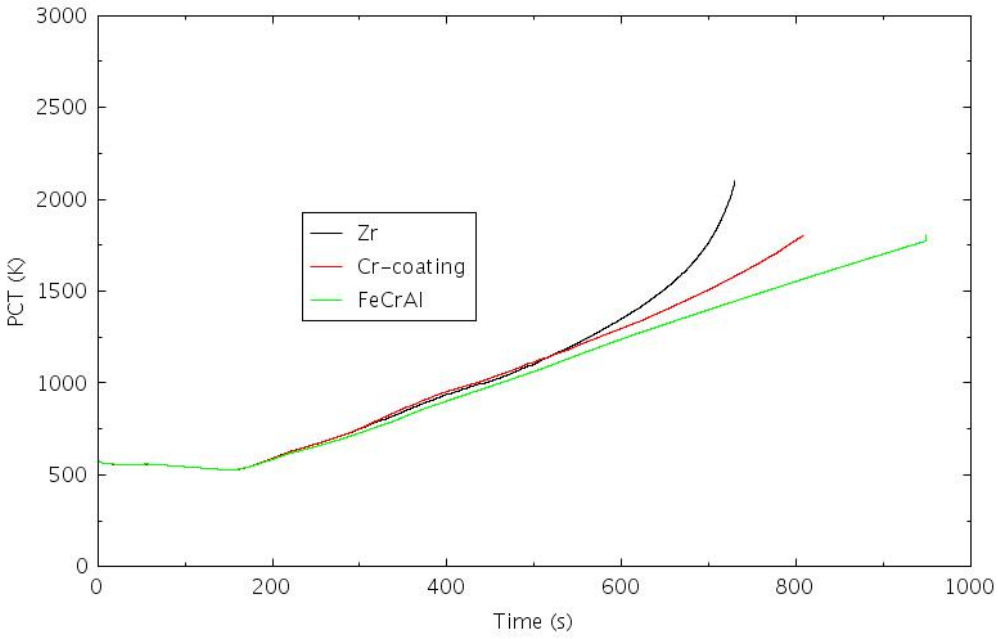

Figure 5-10. PCT at MOC for MLOCA-2.

5.2.3 MLOCA-3 - Reactor Shutdown, Vapor Suppression Fails

In this scenario, the reactor is successfully scrammed following the initiation of medium LOCA. It is assumed that vapor suppression fails and neither HPCI nor LPCI systems are able to provide water injection to the RPV. With the failure of vapor suppression, the drywell pressure reaches its design criterion of 0.49 MPa and leads to the drywell failure. Additionally, with absence of makeup water to the RPV, the coolant inventory will boil off due to the decay heat and lead to fuel damage.

The calculations were done at BOC, MOC, and EOC. To save space, only the results at EOC are showing in the following figures. Figure 5-11 shows the mass flow rate at the break area at EOC for this scenario. Figure 5-12 shows the collapsed water level in the RPV. Figure 5-13 shows the RPV dome pressure. Figure 5-14 shows the PCT during MLOCA-3. The coping time gain with respect to Zircaloy is 9 seconds for Chromium-coated cladding and 212 seconds for FeCrAl cladding, respectively.

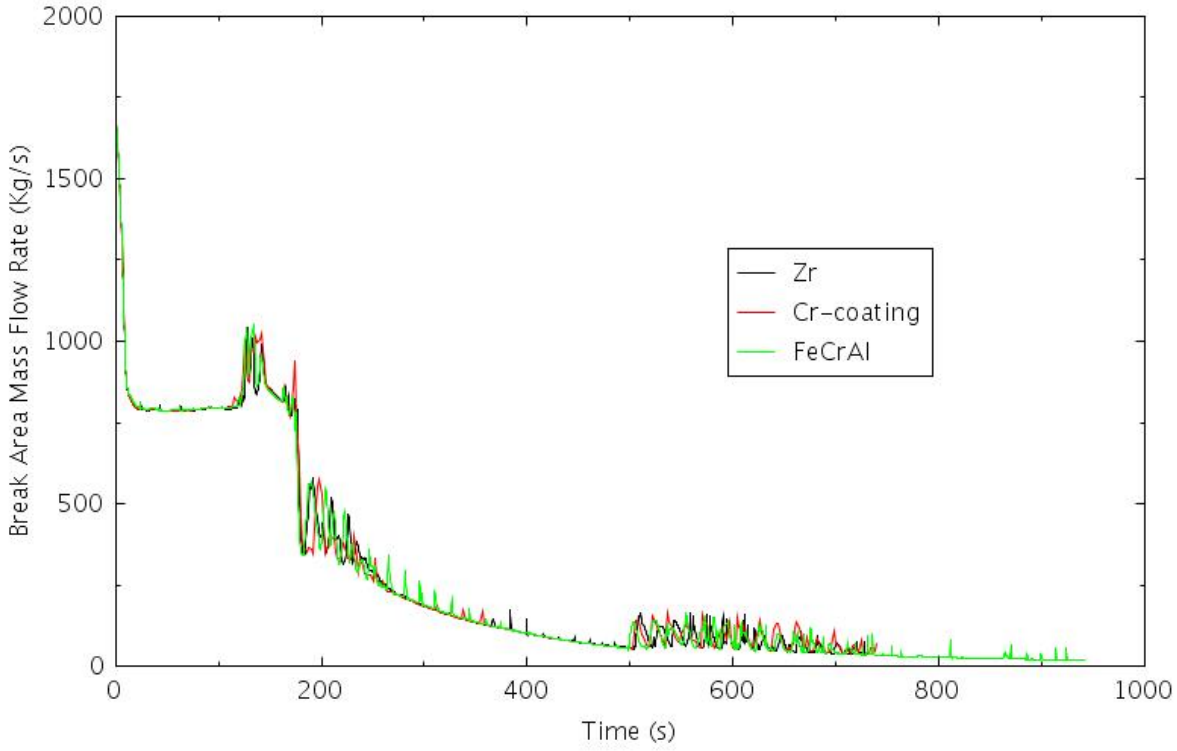

Figure 5-11. Break Area Mass Flow Rate at EOC for MLOCA-3.

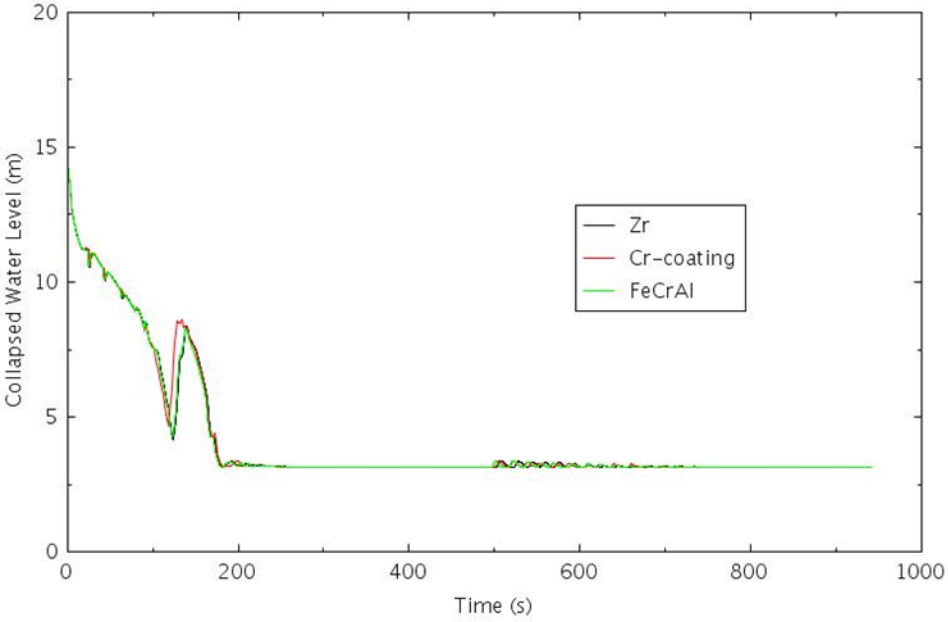

Figure 5-12. RPV Collapsed Water Level at EOC for MLOCA-3.

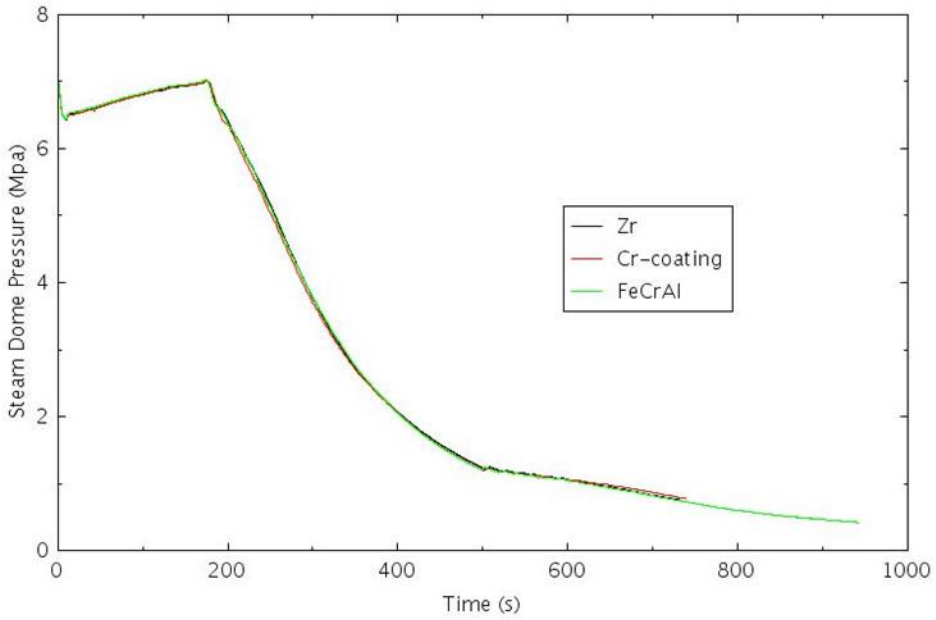

Figure 5-13. RPV Dome Pressure at EOC for MLOCA-3.

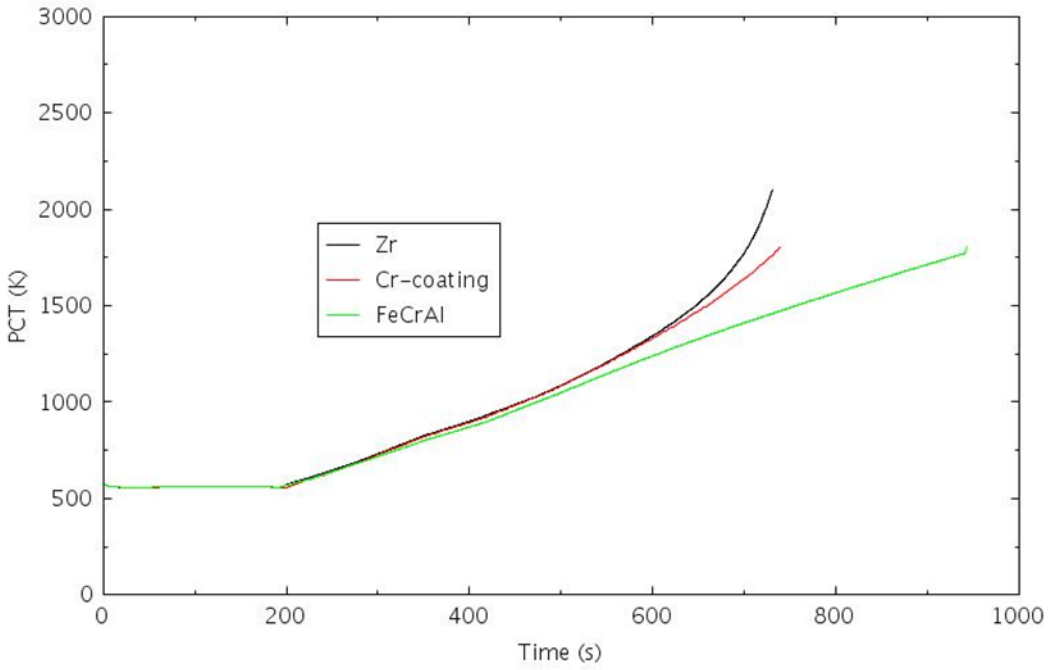

Figure 5-14. PCT at EOC for MLOCA-3.

5.2.4 MLOCA-4 - Reactor Shutdown, Vapor Suppression Success, HPCI Success, but LPI and VA Fail

In this scenario, the reactor is successfully scrammed by the DW high-pressure signal following the initiation of medium LOCA. The vapor suppression is successful to ensure the integrity of the containment DW. It is further assumed HPCI is able to provide water injection to the RPV and manual depressurization of RPV is not performed. The HPCI system is activated by low-water-level setpoint and it is stopped when the RPV pressure drops to 150 psia. However, LPCI systems such as LPI or alternate low-pressure injection through the RHR service water booster pump failed to provide water injection to the RPV. As a result, once the HPCI stops injecting water into the RPV, the coolant inventory will boil off due to the decay heat and lead to fuel damage.

The calculations were done at BOC, MOC, and EOC. To save space, only the results at MOC are showing in the following figures. Figure 5-15 shows the mass flow rate at the break area at MOC for this scenario. Figure 5-16 shows the HPCI water injection mass flow rate. HPCI is activated around 9 seconds and stopped at about 548 seconds by low RPV pressure. Figure 5-17 shows the RPV dome pressure and Figure 5-18 shows the collapsed water level in the RPV. Figure 5-19 shows the PCT during MLOCA-4. The coping time gain with respect to Zircaloy is 112 seconds for Chromium-coated cladding and 388 seconds for FeCrAl cladding, respectively. Compared with the previous three MLOCA scenarios in which HPCI is assumed to fail to provide water injection to the RPV, the time-to-core-damage is much delayed with HPCI functioning. However, HPCI alone is not enough to make up the water loss through the break and therefore is not able to prevent fuel damage.

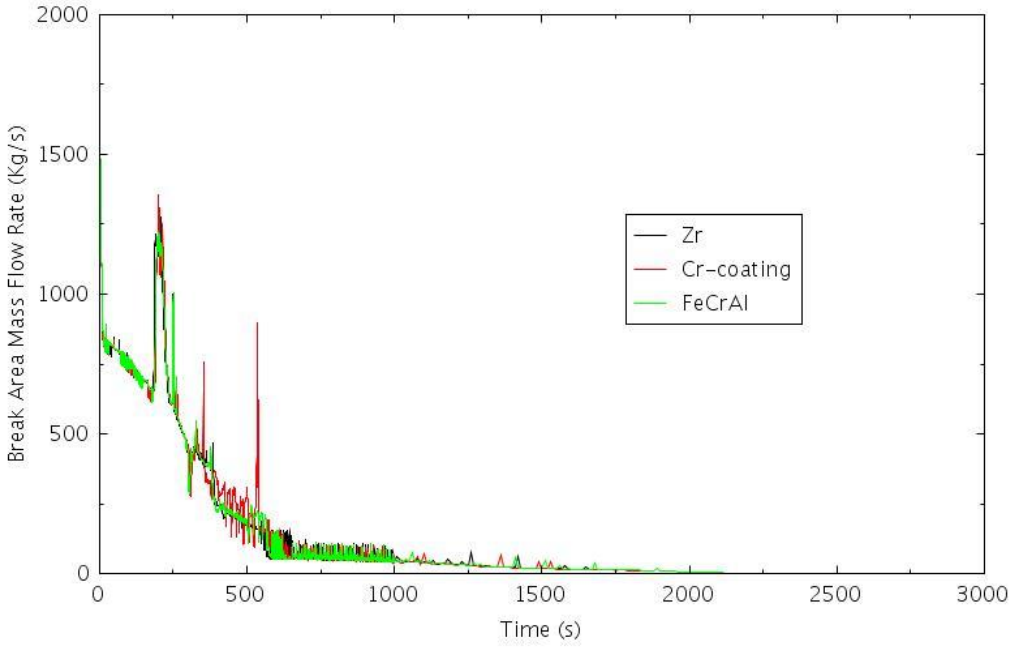

Figure 5-15. Break Area Mass Flow Rate at MOC for MLOCA-4.

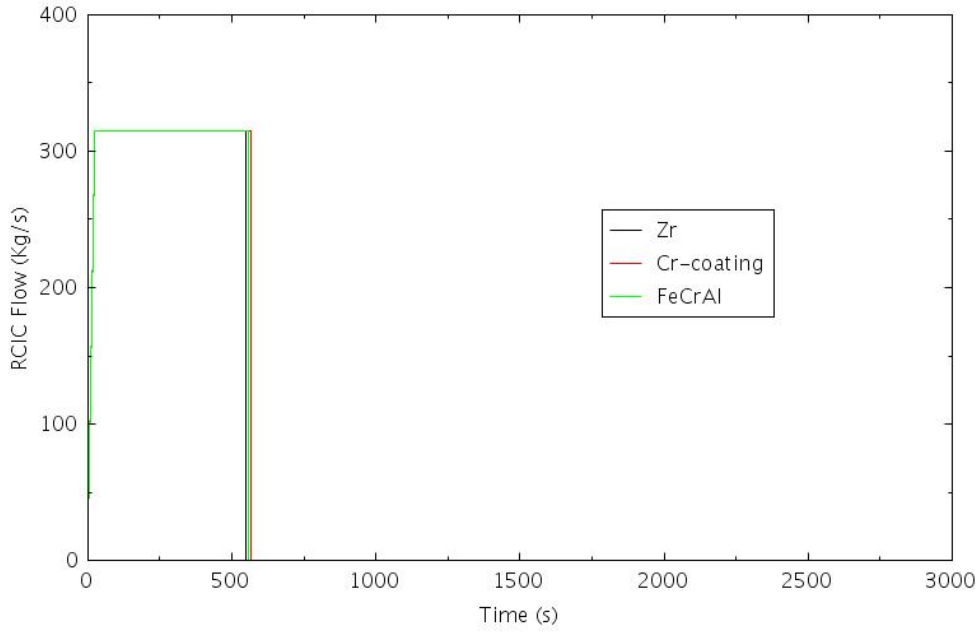

Figure 5-16. HPCI Water Injection Mass Flow Rate at MOC for MLOCA-4.

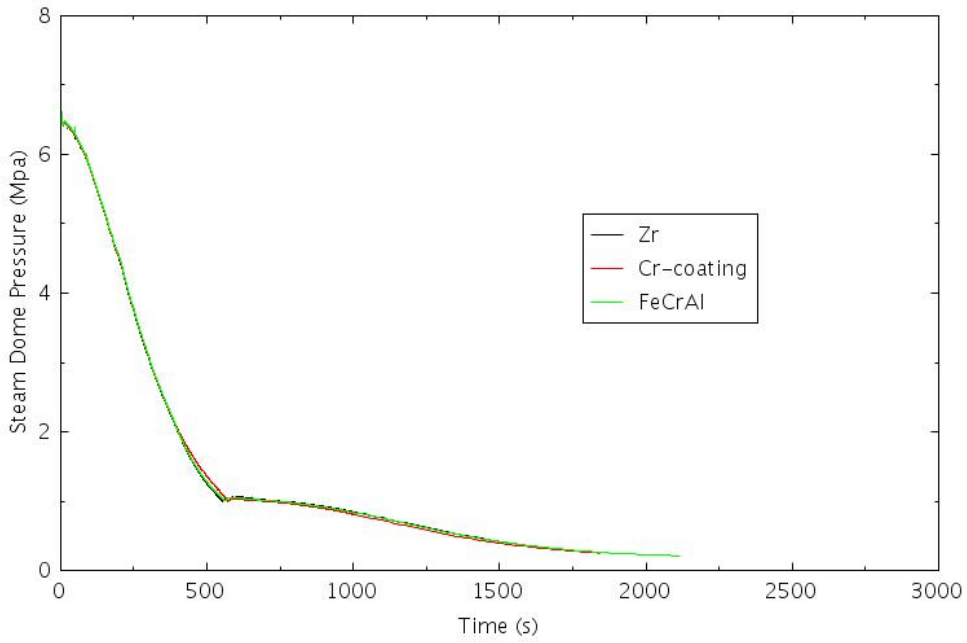

Figure 5-17. RPV Dome Pressure at MOC for MLOCA-4.

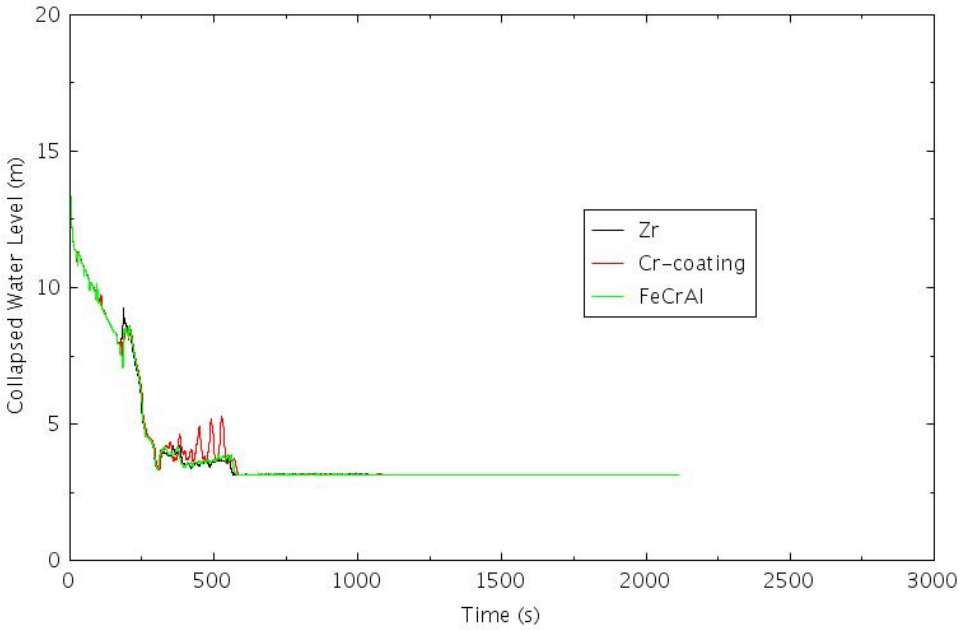

Figure 5-18. RPV Downcomer Collapsed Water Level at MOC for MLOCA-4.

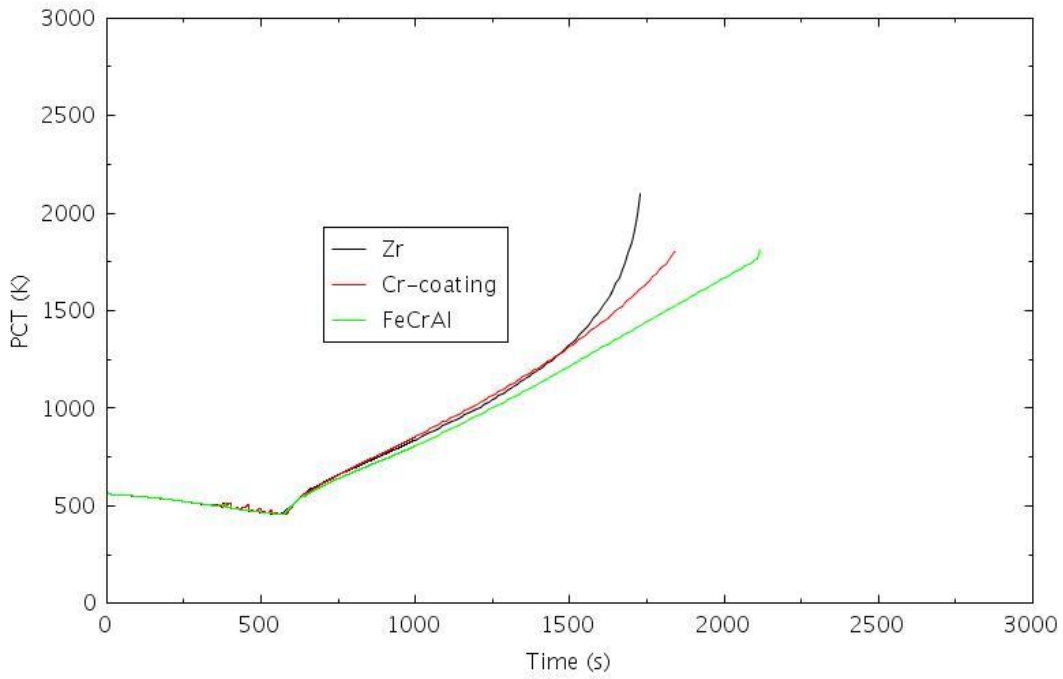

Figure 5-19. PCT at MOC for MLOCA-4.

5.3 Summary of Analysis for MLOCA Scenarios

Table 5-4 through Table 5-6 compare the times to core damage for ATF designs (FeCrAl and Cr-coated) with those for existing Zircaloy clad design in different MLOCA scenarios at BOC, MOC, and EOC respectively. The tables show that for Chromium-coated cladding, the gain of coping time, or the delay of time to CD ranges from 2 minutes to 4 minutes for MLOCA-4, and less than 2 minutes for other MLOCA scenarios. For FeCrAl cladding, the gain on coping time ranges from 3 minutes to 11 minutes for the MLOCA scenarios. Although the relatively small increase of the time-to-core-damage from the RELAP5-3D simulation results would bring a little time margin for associated operator actions, a change to the general MLOCA PRA model is not warranted. The ATF designs would bring risk benefits to the plants even though the benefits are small and not quantified for MLOCA.

However, the RELAP5-3D simulation results show the clear benefit in adopting the ATF with much less hydrogen produced at the time of CD. Table 5-7 through Table 5-9 compare the hydrogen production for ATF designs (FeCrAl and Cr-coated) with those for existing Zircaloy clad design in different MLOCA scenarios at BOC, MOC, and EOC, respectively. The tables show the hydrogen production can be few times lower for the Cr-coated cladding, and two orders of magnitude lower than with Zircaloy cladding cases.

Table 5-4. Time to CD Comparisons at BOC for MLOCA Scenarios with ATF Designs

Scenario	Scenario Description	Time to CD t_{CD} (s)			Time to CD t_{CD} (s)		
		Zry	Cr-coated	Δt	Zry	FeCrAl	Δt
MLOCA-1	VSS, No HPCI, No DEP	854	911	57	854	1127	273
MLOCA-2	VSS, No HPCI, DEP, No LPI/VA	809	922	113	809	1111	302
MLOCA-3	No VSS, No HPCI, No DEP, No LPI/VA	834	938	104	834	1139	305
MLOCA-4	VSS, HPCI, No DEP, No LPI/VA	1914	2133	219	1914	2564	650

Table 5-5. Time to CD Comparisons at MOC for MLOCA Scenarios with ATF Designs

Scenario	Scenario Description	Time to CD t_{CD} (s)			Time to CD t_{CD} (s)		
		Zry	Cr-coated	Δt	Zry	FeCrAl	Δt
MLOCA-1	VSS, No HPCI, No DEP	757	849	92	854	994	237
MLOCA-2	VSS, No HPCI, DEP, No LPI/VA	730	808	78	730	949	219
MLOCA-3	No VSS, No HPCI, No DEP, No LPI/VA	792	842	50	792	1010	28
MLOCA-4	VSS, HPCI, No DEP, No LPI/VA	1730	1842	112	1730	2118	388

Table 5-6. Time to CD Comparisons at EOC for MLOCA Scenarios with ATF Designs

Scenario	Scenario Description	Time to CD t_{CD} (s)			Time to CD t_{CD} (s)		
		Zry	Cr-coated	Δt	Zry	FeCrAl	Δt
MLOCA-1	VSS, No HPCI, No DEP	730	779	49	730	926	196
MLOCA-2	VSS, No HPCI, DEP, No LPI/VA	689	713	24	689	880	191
MLOCA-3	No VSS, No HPCI, No DEP, No LPI/VA	730	739	9	730	942	212
MLOCA-4	VSS, HPCI, No DEP, No LPI/VA	1533	1668	135	1533	1938	405

Table 5-7. H2 Production Comparisons for MLOCA Scenarios at BOC with ATF Designs

Scenario	Scenario Description	Total H_2 (kg)			H_2 %	
		Zry	Cr-coated	FeCrAl	Cr-coated	FeCrAl
MLOCA-1	VSS, No HPCI, No DEP	21.9	1.9	0.2	8.6	1.1
MLOCA-2	VSS, No HPCI, DEP, No LPI/VA	16.6	2.2	0.2	13.4	1.4
MLOCA-3	No VSS, No HPCI, No DEP, No LPI/VA	17.8	2.0	0.2	11.1	1.3
MLOCA-4	VSS, HPCI, No DEP, No LPI/VA	40.3	10.2	2.4	25.4	5.9

Table 5-8. H2 Production Comparisons for MLOCA Scenarios at MOC with ATF Designs

Scenario	Scenario Description	Total H_2 (kg)			H_2 %	
		Zry	Cr-coated	FeCrAl	Cr-coated	FeCrAl
MLOCA-1	VSS, No HPCI, No DEP	14.4	2.2	0.1	15.3	1.0
MLOCA-2	VSS, No HPCI, DEP, No LPI/VA	14.4	4.9	0.1	33.7	1.0
MLOCA-3	No VSS, No HPCI, No DEP, No LPI/VA	16.8	2.0	0.1	11.9	0.8
MLOCA-4	VSS, HPCI, No DEP, No LPI/VA	33.1	5.1	2.1	15.5	6.4

Table 5-9. H2 Production Comparisons for MLOCA Scenarios at EOC with ATF Designs

Scenario	Scenario Description	Total H_2 (kg)			H_2 %	
		Zry	Cr-coated	FeCrAl	Cr-coated	FeCrAl
MLOCA-1	VSS, No HPCI, No DEP	15.1	1.5	0.1	9.9	1.0
MLOCA-2	VSS, No HPCI, DEP, No LPI/VA	14.6	2.9	0.1	20.0	0.8
MLOCA-3	No VSS, No HPCI, No DEP, No LPI/VA	12.5	1.3	0.1	10.4	1.0
MLOCA-4	VSS, HPCI, No DEP, No LPI/VA	28.0	4.9	2.1	17.6	7.4

6. RISK-INFORMED FLEX ANALYSIS

This section presents FLEX-related analysis, including an overview of FLEX (see Section 6.1), FLEX BWR PRA modeling and risk-impact quantification (see Section 0), as well as two dynamic approaches for FLEX HRA (see Section 6.3).

6.1 FLEX Overview

While a more detailed introduction on FLEX characterization and crediting FLEX in PRA can be found in (Ma, et al., 2019a) with risk-informed FLEX analysis for PWR, this subsection intends to briefly recap some essential background information on FLEX.

As a post-Fukushima safety enhancement, FLEX is added to U.S. NPPs to increase defense-in-depth for beyond-design-basis external events (BDBEEs) by providing support for obtaining power or water to maintain or restore key plant-safety functions. FLEX consists of pre-staged or portable FLEX equipment (such as pumps, generators, hoses, and tractors), and associated staging, protection, procedures and guidance, and programmatic controls (Nuclear Energy Institute, 2016; U.S. Nuclear Regulatory Commission, 2019b). FLEX equipment can be categorized in different ways, including:

- Locations (onsite or offsite)
- Connections (permanently installed, pre-staged, or portable)
- Mitigative functions (AC or DC power; makeup for reactor cooling system, steam generator [SG], reactor coolant pump (RCP) seal cooling or spent fuel pool)
- Accident scenarios that FLEX may mitigate: (1) currently credited: SBO/ ELAP, (2) potentially creditable: LOOP, LOCA, RCP seal cooling LOCA, etc.

FLEX can be designed as a plant-specific strategy and usually adopts a three-phase approach: Phase 1 relies on existing plant equipment; Phase 2 transits from plant equipment to onsite FLEX equipment; Phase 3 utilizes resources provided by offsite FLEX equipment, which is stored at three locations throughout the U.S. and can be delivered to any of domestic NPP sites within 24 hours. Being originally developed and implemented to address ELAP and loss of normal access to ultimate heat sink scenarios, FLEX is mostly credited in such SBO/ELAP scenarios in PRA. However, with substantial investments made on FLEX, the nuclear industry should, and could, investigate a more extended scope of FLEX credit in order to increase both safety and economic benefits from the FLEX investment.

When crediting FLEX equipment in a PRA model, the requirements differ according to FLEX equipment types. The offsite portable FLEX equipment is usually not credited in PRA due to the time required to transport the equipment to the site. The FLEX equipment permanently installed in the plant could be treated like a piece of normal plant equipment with proper data and HRAs. To credit onsite portable FLEX equipment in PRA, the following evaluations should be conducted, including capability and reliability, time, procedure and training, staffing and communication, tool, and environment conditions. The permanently staged, portable FLEX equipment could be treated either like permanently-installed FLEX equipment or onsite portable FLEX equipment, depending on with which type it shares more commonalities.

6.2 FLEX BWR PRA Analysis

This section presents FLEX BWR PRA analysis that incorporates portable 480V AC DGs (FLEX-480) and RPV makeup pumps (FLEX-RPV) into the generic SAPHIRE BWR model.

6.2.1 FLEX PRA Modeling

6.2.1.1 ET/FT

There are two approaches to crediting FLEX equipment and mitigating strategies in a PRA model. One is to add new top events (along with associated FTs to support the top events) to the ETs that represent the FLEX equipment and mitigating strategies. The other is to revise FTs by incorporating the FLEX equipment and mitigating strategies into the existing logic. Caution should be given in both approaches that FLEX is credited only to those identified applicable accident sequences. The underlying logic should also be developed to ensure that FLEX equipment credit is limited to only those applicable accident sequences.

This analysis incorporates FLEX into the SAPHIRE SBO-ELAP sub-ET (shown in Figure 4-4) through five FLEX-related top events:

- ELAP: a house event for operator failing to deploy FLEX equipment for SBO-ELAP scenario
- FLEX-480: whether the FLEX 480V DGs could be functional
- FLEX-DEP: whether manual reactor depressurization during ELAP could be successful
- FLEX-CVS: whether or not containment venting succeeds during FLEX
- FLEX-RPV: whether the FLEX RPV LPI pumps are operable.

The logic, or FTs, for FLEX-480 and FLEX-RPV are presented in Figure 6-1 and Figure 6-2, respectively. Two redundant FLEX 480V DG trains and two redundant FLEX RPV makeup pump trains are assumed in this study. Both independent and common-cause failures (CCFs) for the failure modes of fail-to-start (FTS), fail-to-run (FTR), and fail-to-load-and-run (FTLR) at early term are modeled. Equipment tests and maintenance as well as human actions (e.g., to stage FLEX diesel and pumps and to refill alternative water tank for FLEX pumps), are also modeled.

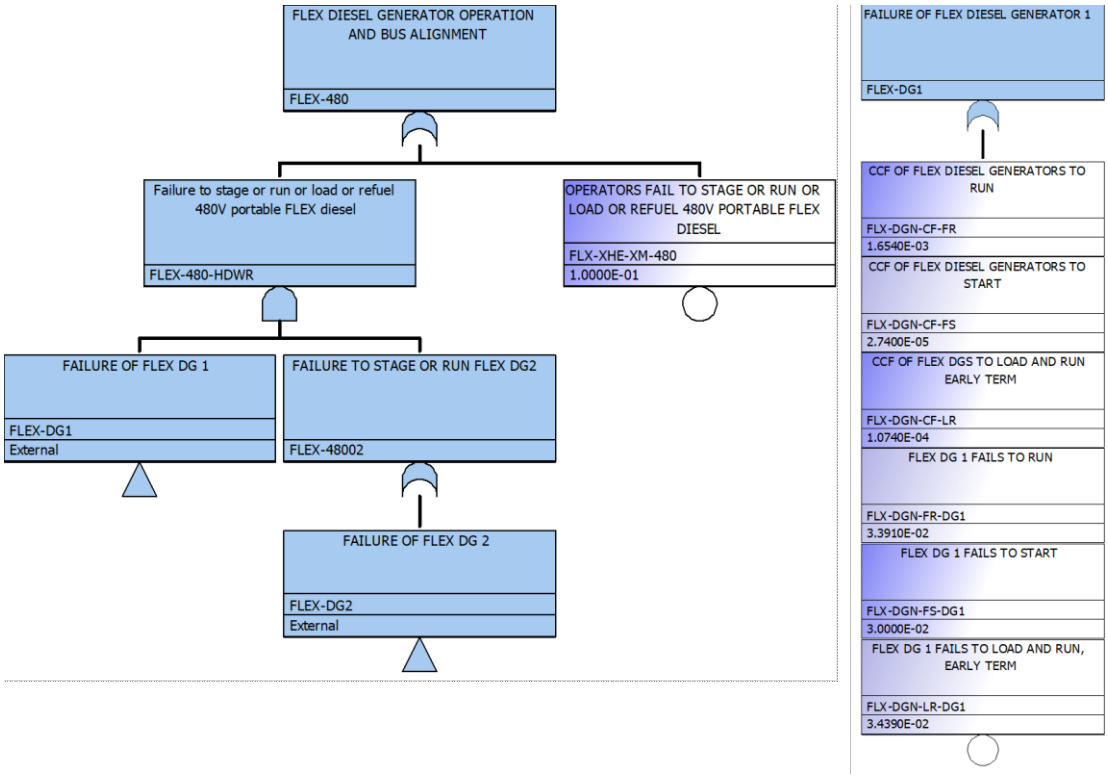

Figure 6-1. FLEX-480 FTs.

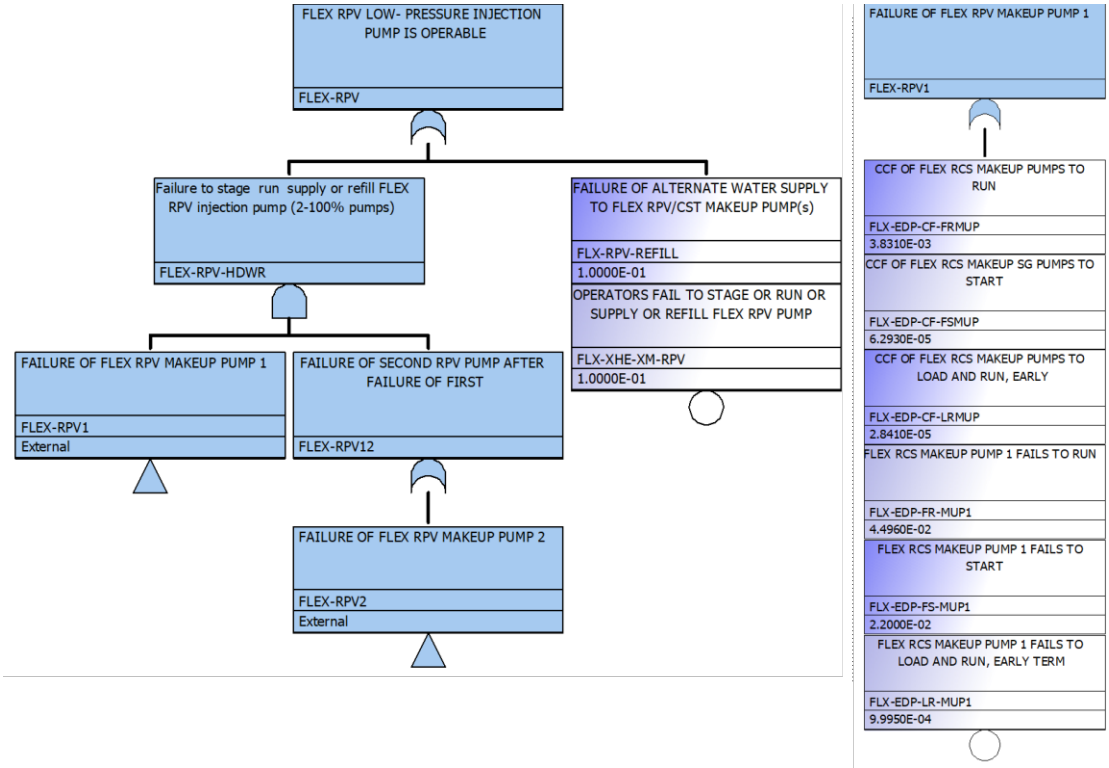

Figure 6-2. FLEX-RPV FTs.

6.2.1.2 Data

For FLEX portable equipment, since there is very limited failure data available for them, generic failure rates for permanently-installed equipment as well as engineering judgements may have to be used or referred to. With insufficient industry data available to estimate portable equipment failure rates, this analysis continues using the assumptions for the previous PWR FLEX PRA analysis (Ma, et al., 2019a), which were made based on the insights from the studies on FLEX equipment performance data conducted across nuclear power industry (EPRI, 2014; Linthicum & Powell, 2019). The assumptions include that the FLEX equipment FTS failure probability and the FLEX equipment FTLR failure rates are both 10 times the industry-average estimates for permanently-installed equipment, and the FLEX equipment FTR failure rate and the FLEX equipment unavailability during test or maintenance are the same of the industry-average estimates for permanently-installed PRA equipment. The latest industry-average estimates for permanently-installed PRA equipment can be found from the NRC Industry-Average Parameter Estimates 2015 Update (U.S. Nuclear Regulatory Commission, 2017) on the Reactor Operational Experience Results and Database website https://nrcoe.inl.gov/resultsdb/AvgPerf/. Sensitivity studies could be conducted as needed to evaluate the impact of the data assumption on the analysis results.

For CCF, it is likely that the FLEX equipment and permanently-installed equipment is not in the same common-cause group as they usually have different design characteristics, manufacturers, and operating and maintenance procedures. However, additional assessments should be conducted to make the final decision. Only the CCFs of the redundant FLEX DGs and RPV pumps are currently modeled.

Table 6-1 presents the FLEX equipment failure probabilities and failure rates used in this analysis. The template names such as EDG-FTS and EDP-FTS under the “Note” column refer to those in the NRC Industry-Average Parameter Estimates 2015 Update (U.S. Nuclear Regulatory Commission, 2017).

Table 6-1. FLEX Equipment Failure Probabilities/Rates.

Basic Event	Description	Failure Probability/Rate	Note
FLX-DGN-FS	FLEX DG fails to start	3.0E-02	Uses 10× of EDG-FTS
FLX-DGN-FR	FLEX DG fails to run	1.5E-03	Uses 1× of EDG-FTR
FLX-DGN-LR	FLEX DG fails to load and run, early term	3.5E-02	Uses 10× of EDG-FTLR
FLX-DGN-TM	FLEX DG unavailable during test or maintenance	1.5E-02	Uses 1× of EDG-TM
FLX-EDP-FS	FLEX RPV makeup pump fails to start	2.2E-02	Uses 10× of EDP-FTS
FLX-EDP-FR	FLEX RPV makeup pump fails to run	2.0E-03	Uses 1× of EDP-FTR
FLX-EDP-LR	FLEX RPV makeup pump fails to load and run, early term	1.0E-03	Uses 10× of EDP-FTLR
FLX-EDP-TM	FLEX RPV makeup pump unavailable during test or maintenance	1.6E-02	Uses 1× of EDP-TM

6.2.1.3 HRA

Other than FLEX data, FLEX HRA is another big issue the industry encounters during the FLEX PRA modeling. It is recognized that existing HRA methods were developed to evaluate and quantify HEPs associated with the operator actions taken in the control room. Yet, much of human actions in deploying, installing, and connecting FLEX equipment occur outside the control room, which may need innovative HRA methods for FLEX analysis. While Section 6.3 develops dynamic approaches for FLEX HRA and the industry is actively working on new HRA methods for FLEX analysis, a scoping value of 0.1 is used as the HEP in this FLEX BWR PRA analysis, which could certainly be revised and re-evaluated once FLEX HRA methods become more mature for use in the near future. Four FLEX human failure events (HFEs) are modeled, as shown in Table 6-2.

Table 6-2. FLEX HFEs in FLEX BWR PRA.

Basic Event	Description	Failure Probability
FLEX-XHE-XE-ELAP	Operators fail to declare ELAP when beneficial	1.0E-01
FLX-XHE-XM-480	Operators fail to stage/run/load/refuel FLEX DG	1.0E-01
FLX-XHE-XM-RPV	Operators fail to stage/run/supply/refill FLEX RPV makeup pump	1.0E-01
FLX-RPV-REFILL	Failure of alternate water supply to FLEX RPV/CST makeup pump(s)	1.0E-01

6.2.2 FLEX PRA Model Quantification

As introduced in Section 4.1, the generic BWR LOOP/SBO SAPHIRE model includes four LOOP ETs (i.e., LOOP GR, LOOPPC, LOOPSC, and LOOPWR). The ET structure is the same for all four LOOP ETs. The only differences are the initiating event frequencies and the AC power non-recovery probabilities. The above FLEX PRA model was implemented at the SBO-ELAP sub-ET level that would affect all four LOOP ETs. The four sub-ETs were quantified with FLEX-incorporated using SAPHIRE 8. The total LOOP CDF with FLEX is 1.45E-6 per year (Table 6-3). When compared with the total LOOP CDF with no FLEX (1.71E-06 per year), the implementation of FLEX represents about 15% risk reduction.

Table 6-3. FLEX BWR PRA Model Quantification Results.

LOOP ET	CDF No FLEX	CDF with FLEX	ΔCDF	ΔCDF%
LOOPGR	4.97E-07	4.52E-07	-4.44E-08	-8.94%
LOOPPC	7.36E-08	7.34E-08	-2.00E-10	-0.27%
LOOPSC	5.79E-07	5.41E-07	-3.75E-08	-6.48%
LOOPWR	5.61E-07	3.86E-07	-1.75E-07	-31.19%
LOOP Total	1.71E-06	1.45E-06	-2.57E-07	-15.03%

It should be noted that the above FLEX PRA analysis results represent the risk impact on a generic BWR plant. Plant-specific FLEX analysis should be conducted to evaluate plant-specific risk impact from the planned or implemented plant-specific FLEX equipment and strategies, which might be different from the results presented here due to different structure, system, and component (SSC) configurations, different plant risk profiles, and different SSC risk contributions and significance. In the meantime, FLEX reliability data and FLEX HRA included in this section could be improved with continuous industry efforts (see Section 6.3 for development of dynamic approaches for FLEX HRA conducted for this research).

6.3 FLEX Dynamic HRA

6.3.1 FLEX HRA Overview

Current HRA approaches for characterizing operator response with FLEX equipment to BDBEE (Nuclear Energy Institute, 2016) rely on traditional static methods (Boring et al., 2015; Park et al., 2019; Reid, 2018). These approaches acknowledge that BDBEE scenarios are not adequately modeled in existing PRA models. They largely use existing HRA methods, but these methods were designed primarily for design-basis events within the main control room (MCR). Recent guidance by Electric Power Research Institute (EPRI) has provided example analyses using existing HRA methods for the most common deployment scenarios of portable equipment (EPRI, 2018). Many questions remain about the suitability of these legacy methods to address FLEX events. To circumvent shortcomings associated with generalizing HRA methods beyond their intended scope, the U.S. NRC has relied on expert elicitation methods to arrive at HEPs (Kichline, 2018). However, these approaches to anchor HRA for FLEX with existing HRA methods are challenged by the wide variety of circumstances that can underlie a BDBEE scenario.

This section introduces a dynamic simulation approach to account for contextual and temporal uncertainties that have been missed in existing HRA methods. Two FLEX HRA models with different approaches have been developed using EMRALD (Prescott, Smith, & Vang, 2018), which is an INL-developed software tool for researching the capabilities of dynamic PRA. Of the two EMRALD HRA modeling examples, one FLEX HRA model is mainly developed by extracting operator tasks from procedures, while the other one depends on operator tasks derived from PRA/HRA event and FT modeling. This delineation of approaches corresponds to a more human factors driven approach (focusing foremost on human actions) vs. a more PRA driven approach (focusing on human actions that contribute to hardware failure). The major insights coming from each modeling approach are discussed in this section.

6.3.2 FLEX HRA Modeling Using EMRALD Software

6.3.2.1 EMRALD Software Overview

As was briefly introduced in Section 2.3, EMRALD was developed to support the increasing need for dynamic PRA models that can respond to evolving plant conditions through simulation (Prescott, Smith, & Vang,

2018). Historically, PRA models are completed in a static fashion in which a fixed plant state is defined, and models are based on those unchanged characteristics. EMRALD is one of a growing number of tools to support plant state variations through simulation to better model realistic event progressions. Many of the dynamic PRA tools in use today are scripting methods that are difficult to use and debug and do not possess a graphical user interface (GUI). EMRALD is a robust platform that can generate probabilistic findings, process variables, and timing of events for analysis by using a drag-and-drop GUI for creating models. This GUI enhances the usability and ease of model creation. EMRALD adopts an iterative method of building models and allows for continued improvement and modification of modeling structures.

6.3.2.2 Advantages of FLEX HRA Modeling Using EMRALD Software

Assessing the use cases of HRA deployment in a FLEX situation illustrates there are some key characteristics that mandate a more dynamic tool than the more common static HRA methods.

First, the entire purpose of FLEX processes is to respond to events that are, by definition, beyond the design basis of the current plant infrastructure. The few serious historic event occurrences within the nuclear industry were unpredicted and therefore unplanned. The variability of a FLEX deployment is such that a dynamic tool is required to give the model any sense of realism in its application to an actual event. EMRALD's GUI-based interface and quick spin-up time enables a more efficient demonstration and testing of ideas surrounding the actual interaction of FLEX procedures and human reliability.

Second, since the activities for FLEX occur outside the control room, it is important to adopt a tool that supports performing the actual simulation. EMRALD achieves this through events and their timing to form a structure for the simulation. Traditional activities are often coupled to thermohydraulic simulations such as RELAP5-3D (RELAP5-3D Code Development Team, 2018); however, for activities outside the control room, these simulations are less applicable. Though the time thresholds are based on values derived from simulations such as RELAP5-3D, the thermohydraulic code itself is not necessary. A self-contained simulation alternative is needed. EMRALD supports this structure and is therefore a suitable candidate for dynamic HRA.

6.3.2.3 FLEX HRA Modeling with Different Approaches

This section introduces two different approaches to develop FLEX HRA models using EMRALD software, as shown in Table 6-4.

Table 6-4. Differences between Procedure Context-Based and PRA/HRA-Based Modeling Approaches.

	Procedure Context-Based Modeling	PRA/HRA-Based Modeling
Description	Specifically, models procedure contexts	Models basic events that have been considered in existing PRA and HRA
Characteristics	This model is useful to account for context uncertainties that complicate determination of HEPs	Within existing PRA and HRA modeling, it could be used for validating time uncertainties that are not covered in existing PRA and HRA

First, the procedure context-based approach specifically models human actions at the procedure step level. Tasks modeled in this approach are extracted from the procedures used to perform the FLEX deployment. In a FLEX situation, there are modified roles for control room and field operators as the primary goals of each change to respond to the emergency. Control room operators move to a mitigation focus and away from the primary day-to-day goal of efficient power generation for the customer base. Field operators are the primary actors in a FLEX scenario and perform many of the prescriptive steps in procedures as well as respond to novel circumstances. From an HRA perspective, there is a level of variability and unpredictability that will need to be explored in order to adequately capture its effects in a quantitative model. The procedure context-based approach is useful to account for context uncertainties that complicate the determination of HEPs.

Second, PRA/HRA-based approaches primarily model those basic events associated with design-basis events. Tasks modeled in this approach are extracted from the human failure events defined in the PRA. Existing methods

have evaluated equipment and human failure in an integrated manner, but it is a challenge to see interactions between the failures over time. Furthermore, FLEX actions generally take a lot of time in comparison with human actions that have been considered in the existing PRA and HRA (e.g., short-duration control room activities). Within PRA and HRA modeling, this approach could be used for validating time uncertainties that are not covered in existing PRA and HRA.

6.3.3 Procedure Context-Based FLEX HRA Modeling

6.3.3.1 Modeling Overview

This model starts by assuming an ELAP scenario. This entry condition was assumed in order to limit the model considerations to responses of an ELAP rather than also considering the probabilities and ranges of entry for an ELAP occurrence. The original intent was to model the steps from the ELAP declaration to response and deployment. Therefore, a scenario that allowed for power restoration but required emergency core-cooling capabilities was selected in order to demonstrate the processes that operators step through involving several different procedures. The generic initial ELAP procedure guides operators to establishing makeup feed flow to SGs, which necessitates the deployment of an auxiliary FLEX pump. To deploy this FLEX pump, the procedures direct operators to the FLEX staging process. This process uses installation hard cards (i.e., field procedures) for the individual pieces of equipment including the pump itself, hoses, electrical connections, and a diesel generator to provide power.

For this specific model, as a proof of concept of dynamic HRA for FLEX, we make several assumptions to constrain the number of involved systems and potential actions:

- ELAP has been declared within the recommended timeline
- Assessment of plant systems has resulted in power to the control room, but loss of auxiliary feedwater to the SGs
- Staging of the FLEX makeup pump is required to deliver feedwater to steam generators.

The final bullet point explains the primary step that is modeled within this effort. It involves several variables of interest. From the procedures, there are three potential staging locations for the makeup auxiliary feedwater pump, and there are several prioritizations involving timing considerations. The realistic input to a decision-making step for an operator choosing between the various paths from the FLEX storage area to the staging locations is quantity of debris in the way of traversal. As FLEX policies are largely responses to varying natural disasters, it is assumed that regardless of the initiating weather event there will be large amounts of debris across the site. Utilities have planned for this by having bulldozers and other heavy equipment on site to accommodate debris clearing. This model assumes a time penalty depending on the presence of debris that could influence operator decision-making.

6.3.3.2 Model Details

The model itself is comprised of three primary hierarchical types of elements. The main model diagram defines the overall simulation (see Figure 6-3). The main model ties the underlying models together and initializes the simulation state (e.g., the state of the plant and environment in which the FLEX activities are begun). The plant state and level of debris present within each simulation run is initialized from the main model invoking the debris model (see Figure 6-4). During each simulation run, only one of the three staging areas is deemed usable for FLEX deployment, but the path to the one available staging area must still be cleared of debris. Furthermore, the highest priority staging area is assumed to be the closest, the second priority is the second closest, and the third is the farthest away. The distance magnitude then factors into the amount of time the debris-clearing action requires for each of the different staging areas, such that the third priority location requires the longest clearing time. Another critical function of the main model is tracking the overall simulation time against the allowed 74-minutes to deploy the FLEX pump to maintain sufficient water in the steam generator and support the

necessary heat removal to keep the core cool. Exceeding this 74-minute timespan consists of a system failure due to an inappropriate amount of time elapsing to perform the FLEX activities.

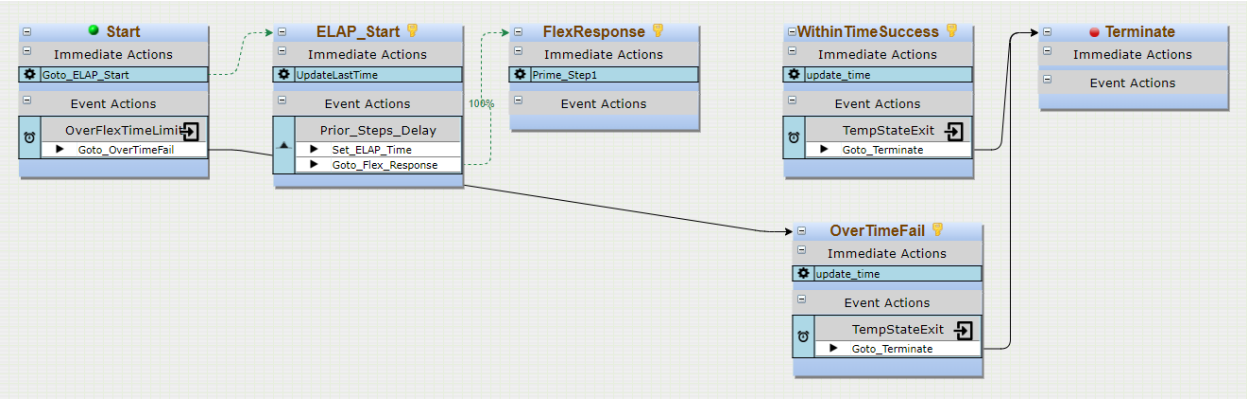

Figure 6-3. Main Model Governing the Procedure Context-based FLEX HRA Model.

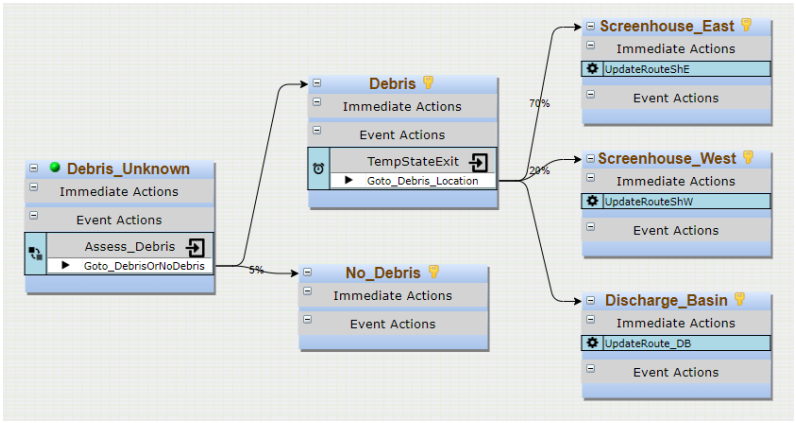

Note: Even though a location is available it still contains debris that must be cleared. It is simply the selected location for the simulation run.

Figure 6-4. Component Model of Debris That Determines Which of the FLEX Staging Locations is Usable to Stage the FLEX Equipment.

Since this is the initial effort to examine and demonstrate the use of EMRALD for HRA FLEX activities, there are many simplifications made to the model. During an ELAP scenario resulting from LOOP, the operators perform a number of activities to restore their instrumentation within the MCR. For the sake of simplicity, this modeling effort assumed those activities occurred successfully and simply assigned a time distribution to the length of time required to perform them. This impacts the model by adding a time delay before the actual FLEX deployment activities (which occur within the FLEX procedure) take place. Specifically, this time delay reduces the amount of time the operators have to perform the actual FLEX deployment.

Once the FLEX response is initiated from the main model, the operator model is invoked. The operator model is comprised of the critical procedure steps required for the operator to make the decision to deploy the FLEX equipment due to the unavailability of the auxiliary feedwater system and then begin clearing debris from the route to the staging location (see Figure 6-5). The operator model performs two critical functions. First, it tracks the sequence of procedure steps and ensures that the operator performs them in the correct order. The second function serves to track when the operator is engaged performing a step and when the operator becomes available to perform a step. This is important to ensure that only one procedure step is performed at a time.

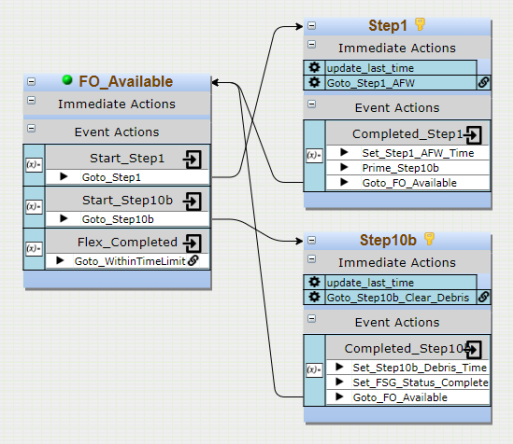

Figure 6-5. Model of the Operators' Actions Comprised of Procedure Steps That Must Be Executed to Complete the FLEX Deployment.

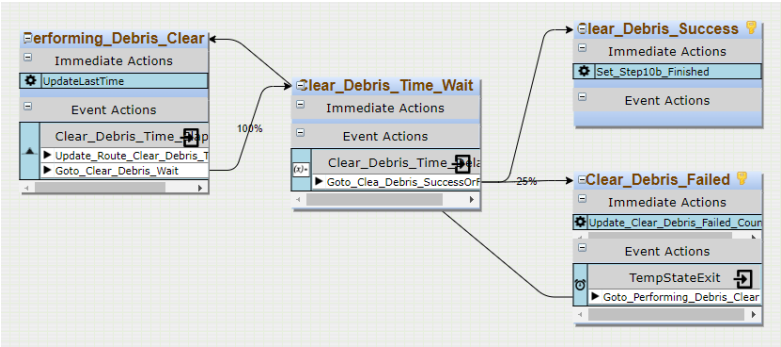

Note: The operator attempts to clear debris, and succeeds or fails. If the operator fails, he or she must repeat the step and incur time that may lead to an overall failure in which the time limit for deploying FLEX is exceeded.

Figure 6-6. Individual Procedure Step Model.

As the operator performs a procedure step, the model invokes an individual procedure model associated with that specific procedure step (see Figure 6-6). The individual procedure step model contains the Goals, Operators, Methods, and Selection (GOMS) HRA elements (Boring and Rasmussen, 2016; Boring et al., 2017; Ulrich et al., 2017; Ulrich and Boring, 2018), which include the probability of successfully completing the procedure steps based on the relevant subtask primitive and performance-shaping factors in addition to the timing distribution for the time required to perform the subtask primitives. For a given procedure step, if the step fails, the operator repeats the step until a successful outcome is achieved. Each repetition adds to the total time taken for the procedure step execution. Within this first modeling effort, only one GOMS-HRA primitive was included. During the scenario, the operator performs a check to determine if auxiliary feedwater is available. If the check succeeds, the operator proceeds to the next task. If it fails, the operator checks the status again. Currently no performance-shaping factors are integrated into the model when sampling the probability estimate for the check primitive subtask. Future work will investigate the best practices to integrate performance shaping factors into the model.

6.3.3.3 Insight from the Model

The results are secondary to the proof of concept of developing the model. The model evaluates the likelihood of exceeding the hypothetical time limit for establishing FLEX equipment to provide auxiliary feedwater before the steam generators run dry. Specifically, the model evaluates the likelihood of exceeding the time when

different staging areas are available and covered by debris that must be cleared. As expected, the lower priority items incur longer timespans for FLEX deployment, since it takes additional time to clear the longer path to the staging area. The overall failure probability for performing the FLEX staging of the makeup pump across different staging locations was found to be 1E-05 (see Figure 6-7). Ultimately, the model is very simple. As such, the results should not be taken as realistic, representative probabilities. Instead, the results are intended to demonstrate that the EMRALD tool can generate data useful for both PRA and HRA FLEX activities to inform utilities of potential risks. More accurate results will be obtained as a more comprehensive set of contexts are modeled and results are validated to operational performance data.

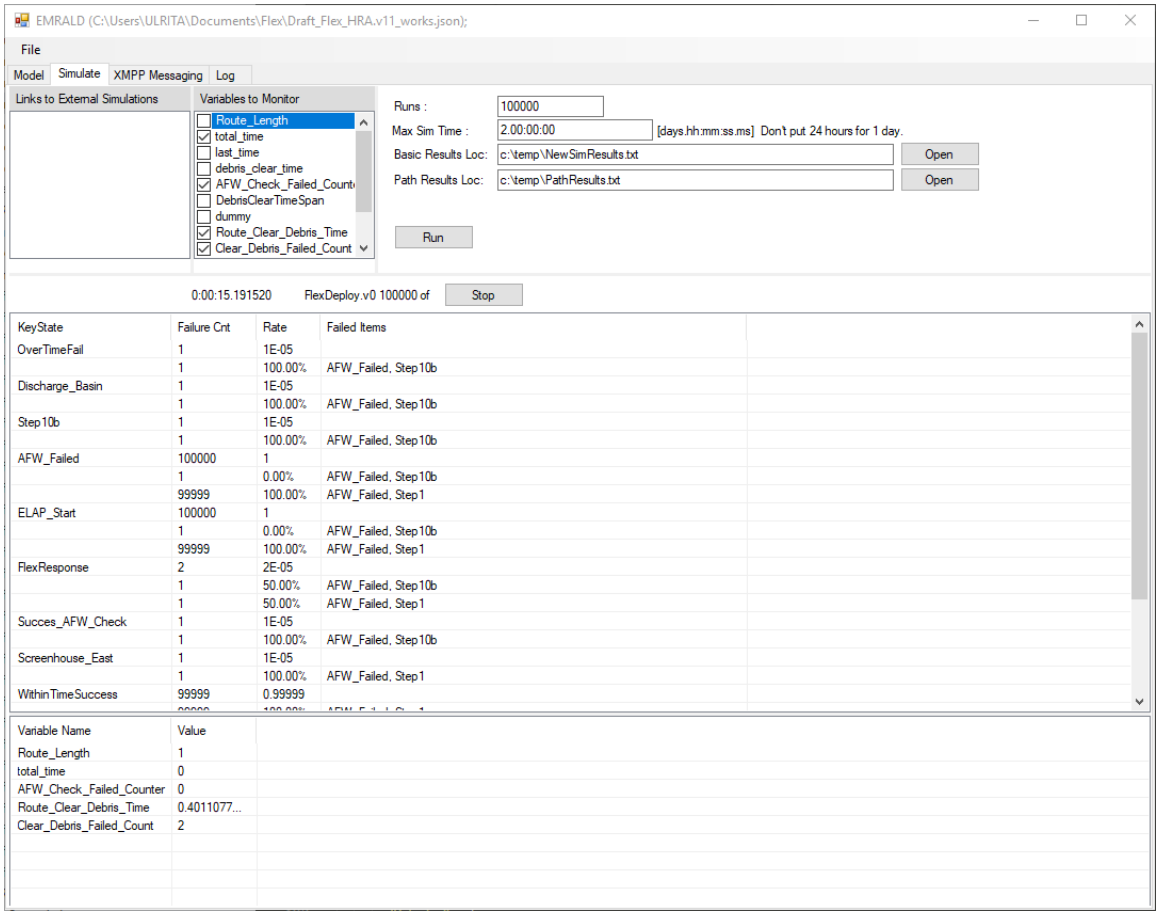

Figure 6-7. EMRALD Analysis Results as Displayed Using the Computation Engine.

This result has been analyzed to identify which insights could be obtained from the model. In this study, rather than getting a new value for dynamic HRA, it was the more focused on whether we can complement the PRA/HRA modeling by observing the new human failure types that have not considered in traditional HRA. To achieve the goal, this study considered relative conservative timing assumptions as introduced in Section 6.3.4.1. It contributed to deriving a relatively large number of human errors especially for the overtime failures as shown in Table 6-6 and Table 6-7. In future research, the approach needs to be validated using the more reliable timing assumptions or actual plant data. In addition, what the outputs (i.e., the HEPs in Table 6-7), mean also needs to be investigated to support dynamic PRA/HRA modeling.

6.3.4 PRA/HRA-Based FLEX HRA Modeling

6.3.4.1 Modeling Overview

This modeling work assumes a simplified SBO FLEX scenario based on the ETs and FTs introduced in Section 3 of INL-EXT-19-53556 (Ma, et al., 2019a). The scenario context is almost identical with the procedure context-based FLEX HRA model described in the previous section, but it mainly focuses on FLEX activities outside of the MCR. This model treats FLEX equipment failure events normally considered in FTs and HFEs related to FLEX.

Figure 6-8 shows a timeline for the FLEX SBO scenario model. The timeline includes two events, three HFEs, and failure of FLEX DGs and FLEX steam generator pumps (SGPs). The two human actions are (1) ELAP declaration and (2) debris removal. The three HFEs are (1) operators failing to stage/start/run FLEX DG, (2) operators failing to stage/run/supply FLEX SG pump, and (3) operators failing to supply an alternative water source to FLEX SGP. In the timeline, the two events and three HFEs have time distributions, respectively. Table 6-5 and Table 6-6 indicate a summary of timing information for the two events and three HFEs. In the timing information, most of the mean time values are informed on the basis of previous research (Park et al., 2019) and FLEX-related literature (Nuclear Energy Institute, 2016), while the standard deviation and minimum and maximum values are provided as best estimates due to data scarcity:

- Standard deviation: 50% of mean value
- The number of samples: Four
- Minimum: 5% value within 95% confidence interval
- Maximum: 95% value within 95% confidence interval.

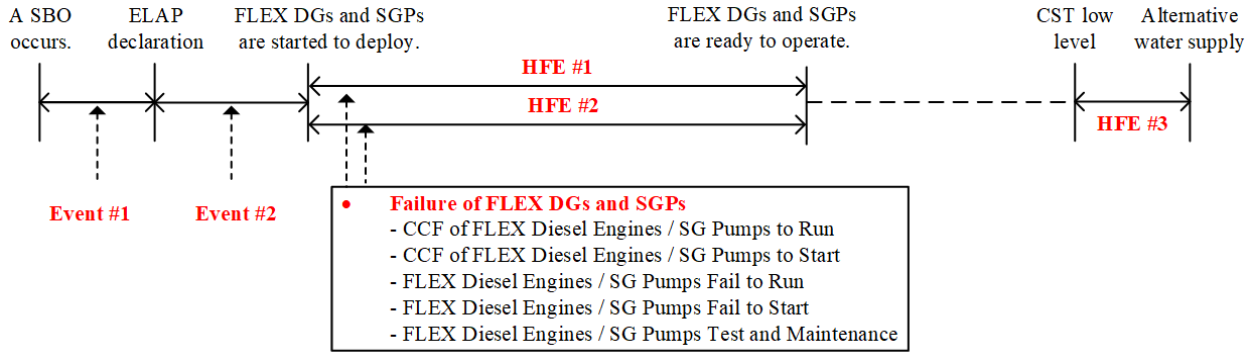

Figure 6-8. Timeline for a Simplified FLEX SBO Scenario.

Table 6-5. Timing Information for Event #1 and #2.

Event No.		Event # 1	Event # 2
Event		ELAP Declaration	Debris removal
Time Information [min]	Mean	5.00	60.00
	Std.	2.50	30.00
	Min.	2.55	30.60
	Max.	7.45	89.40

Table 6-6. HRA-Specific Information and Timing Information for HFE #1, #2, and #3.

HFE No.			HFE # 1	HFE # 2	HFE # 3
Description			Operators Fail to Stage/Start/Run FLEX Diesel for SG Pump.	Operators Fail to Stage/Run/Supply FLEX SG Pump.	Operators Fail to Supply Alternative Water Source to FLEX SG Pump
Cue			ELAP Declaration	ELAP Declaration	FLEX Diesel and FLEX SG Pump are ready to start
Diagnosis	Actor		MCR Operators	MCR Operators	MCR Operators
	Work Device		MCR Boards	MCR Boards	MCR Boards
Execution	Actor		Plant Staff	Plant Staff	Local Operators
	Work Device		FLEX Diesel	FLEX SG Pump	FLEX SG Pump
Time Information [min]	$T_{Time\ Window}$		240.00	240.00	1320.00
	T_{Delay}	Mean	0.00	0.00	1200.00
		Std.	-	-	600.00
		Min.	-	-	612.00
		Max.	-	-	1788.00
	$T_{Diagnosis}$	Mean	10.00	10.00	5.00
		Std.	5.00	5.00	2.50
		Min.	5.10	5.10	2.55
		Max.	14.90	14.90	7.45
	$T_{Execution}$	Mean	120.00	120.00	60.00
		Std.	60.00	60.00	30.00
		Min.	61.20	61.20	30.60
		Max.	178.80	178.80	89.40

The difference between the events in Table 6-5 and the HFEs in Table 6-6 depends on whether each event is credited in the PRA or HRA. Based on the assumptions shown in Table 6-6, the HEP information for the HFEs is estimated as shown in Table 6-7. The HEPs are informed from previous research (Park et al., 2019) that estimated the HEPs based on Standardized Plant Analysis Risk-Human Reliability Analysis (SPAR-H) (Gertman et al., 2005) and observation and experience in stress tests performed by the Korean Utility in the earlier study.

Table 6-7. HEP Information for three HFEs.

HFE No.	Type	HEP for Diagnosis or Execution	Final HEP
HFE #1	Diagnosis	4.8e-2	5.0e-2
	Execution	2.0e-3	
HFE #2	Diagnosis	4.8e-2	5.0e-2
	Execution	2.0e-3	
HFE #3	Diagnosis	4.8e-2	6.0e-2
	Execution	1.2e-2	

For the failure of FLEX DGs and FLEX SGPs, 10 equipment failure events are considered in the model. The list for the events and the error probabilities are shown in Table 6-8. These are based on the FTs introduced in Section 3 of INL-EXT-19-53556 (Ma, et al., 2019a).

Table 6-8. Information of Equipment Failure for FLEX DGs and FLEX SGPs.

Equipment Type	Equipment Failure	Failure Probability/Rate
FLEX DGs	CCF of FLEX DGs to run	2.826e-4
	CCF of FLEX DGs to start	5.750e-5
	FLEX DGs fail to run	1.250e-3
	FLEX DGs fail to Start	8.180e-6
	FLEX DGs unavailable due to test and maintenance	2.250e-4
FLEX SGPs	CCF of FLEX SGPs fail to run	1.434e-3
	CCF of FLEX SGPs fail to start	6.380e-4
	FLEX SGPs fail to run	2.197e-3
	FLEX SGPs fail to start	4.840e-4
	FLEX SGPs unavailable due to test and maintenance	2.560e-4

6.3.4.2 Model Details

The PRA/HRA-based FLEX HRA model has been developed based on the inputs introduced in the previous section. Similar to the other procedure-based approach, the simulation model relies on a main model and supporting component. In this case, there is one main model and five component models as described below:

- One Main Model for PRA/HRA-based FLEX HRA Model (Figure 6-9)
- Component Model Describing Equipment Failure Related to FLEX DGs and SGPs (Figure 6-10)
- Component Model Describing Operator Failure Related to HFE #1 (Figure 6-11)
- Component Model Describing Operator Failure Related to HFE #2 (Figure 6-12)
- Component Model Describing Operator Failure Related to HFE #3 (Figure 6-13).

As a conservative modeling approach, recovery actions or equipment recovery cases are not assumed. For each HFE, an overtime failure is evaluated by comparing the time window and total time required for operators, so that we can see the effect of time uncertainty for each HFE.

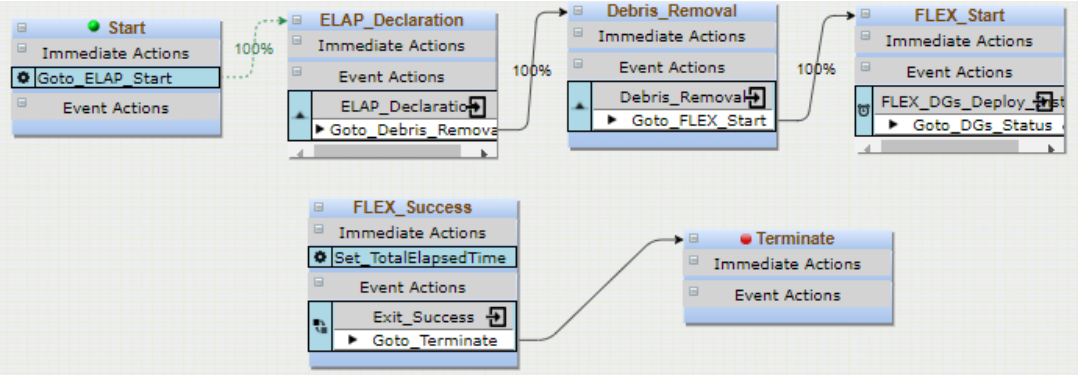

Figure 6-9. Main Model for PRA/HRA-based FLEX HRA Model.

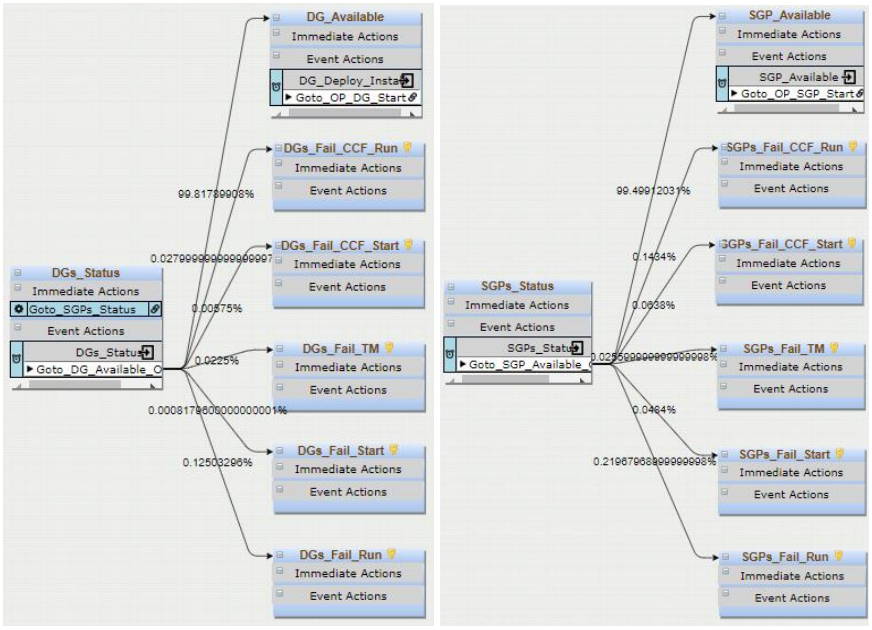

Figure 6-10. Component Model Describing Equipment Failure Related to FLEX DGs / FLEX SGPs.

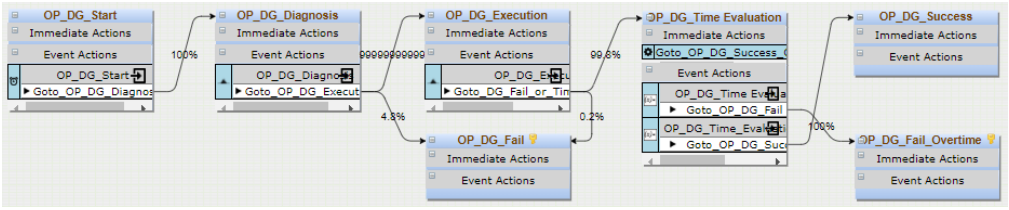

Figure 6-11. Component Model Describing Operator Failure Related to HFE #1.

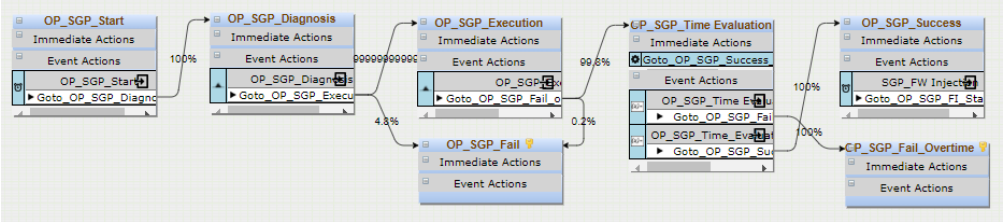

Figure 6-12. Component Model Describing Operator Failure Related to HFE #2.

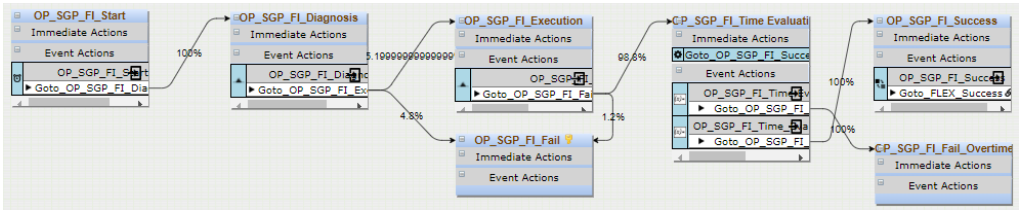

Figure 6-13. Component Model Describing Operator Failure Related to HFE #3.

6.3.4.3 Insights from the Model

The PRA/HRA-based FLEX HRA model was simulated for 100,000 trials. As shown in Table 6-9, 71.2% of the entire cases failed due to human error (69.8%) or equipment failure (0.4%), while 29.8% demonstrated a successful FLEX deployment. Specifically, Table 6-10 indicates the number of cases and the ratio in respect to error types in human error and equipment failure categories with 100,000 trials. Human-error category, "OP_SGP_FI_Fail_Overtime," which means that HFE #3 fails due to overtime, constitutes the highest number (25,892, 37.1%), while "DGs_Fail_Run" shows the highest number (126, 32.4%) within the equipment failure category.

Table 6-9. The Number of Cases and The Ratio for Success and Failure with 100,000 Trials.

Category		The number of cases	The ratio
Success		29,845	29.8%
Failure	Human Error	69,766	69.8%
	Equipment Failure	389	0.4%

Table 6-10. The Number of Cases and the Ratio in Respect to Error Types in Human Error and Equipment Failure with 100,000 Trials.

Category	Error Type		The Number of Cases	The Ratio
	Event ID in EMRALD Software	Description		
Human Error	OP_DG_Fail	HFE #1 fails.	4,977	7.1%
	OP_SGP_Fail	HFE #2 fails.	3,785	5.4%
	OP_SGP_FI_Fail	HFE #3 fails.	3,543	5.1%
	OP_DG_Fail_Overtime	HFE #1 fails due to overtime.	19,189	27.5%
	OP_SGP_Fail_Overtime	HFE #2 fails due to overtime.	12,380	17.7%
	OP_SGP_FI_Fail_Overtime	HFE #3 fails due to overtime.	25,892	37.1%
Sum		69,766		100.0%
Equipment Failure	SGPs_Fail_TM	FLEX SG Pumps Fail Due to Test and Maintenance	12	3.1%
	SGPs_Fail_CCF_Run	CCF of FLEX SG Pumps Fail to Run	53	13.6%
	SGPs_Fail_Run	FLEX SG Pumps Fail to Run	80	20.6%
	SGPs_Fail_CCF_Start	CCF of FLEX SG Pumps Fail to Start	25	6.4%
	SGPs_Fail_Start	FLEX SG Pumps Fail to Start	21	5.4%
	DGs_Fail_Run	FLEX Diesel Engines Fail to Run	126	32.4%
	DGs_Fail_CCF_Start	CCF of FLEX Diesel Engines to Start	14	3.6%
	DGs_Fail_TM	FLEX Diesel Engines Fail Due to Test and Maintenance	26	6.7%
	DGs_Fail_Start	FLEX Diesel Engines Fail to Start	1	0.3%
	DGs_Fail_CCF_Run	CCF of FLEX Diesel Engines to Run	31	8.0%
Sum		389		100.0%

Figure 6-14 compares the time window and total time required for HFE #1, #2, and #3 as mean values. For example, the total time required for HFE #1 is calculated as 195 min by summing 5 min (time to declare ELAP), 60 min (time to remove debris), and 130 min (time to perform HFE #1). The time required is compared with the time window of HFE #1 (i.e., 4 hrs). In summary, all the comparisons show that the time required values are less than the time windows. In the traditional HEP calculation in HRA, the failure probability caused by overtime is not considered. However, in this EMRALD model, human errors caused by overtime (i.e., "OP_DG_Fail_Overtime," "OP_SGP_Fail_Overtime," and "OP_SGP_FI_Fail_Overtime," show much higher error probabilities than the normal human failures like "OP_DG_Fail," "OP_SGP_Fail," and "OP_SGP_FI_Fail").

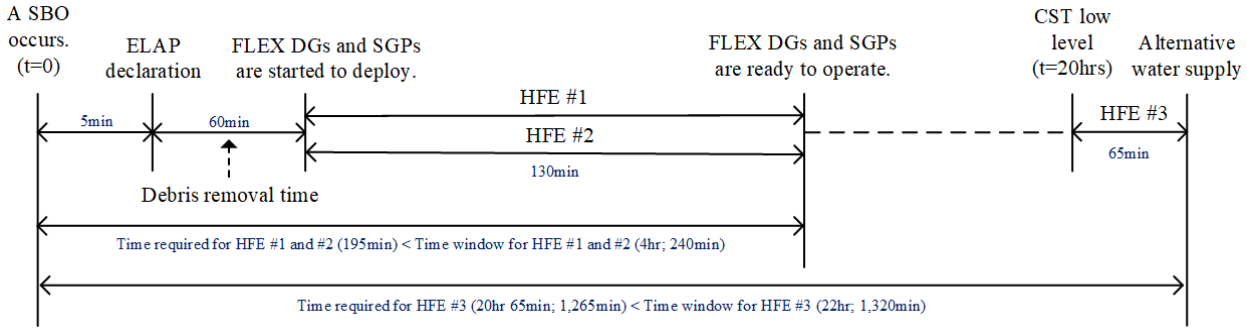

Figure 6-14. A Comparison between Time Window and Time Required with Mean Value.

This result has been analyzed to identify which insights could be obtained from the model. In this report, rather than getting a new value for dynamic HRA, it was the more focused on whether we can augment existing PRA/HRA modeling by observing the new human failure types that have not been considered in traditional HRA. To achieve the goal, this study considered relatively conservative timing assumptions as introduced in Section 6.3.4.1. It identified a relatively large number of human errors especially for the overtime failures as shown in Table 6-9 and Table 6-10. In future research, the approach needs to be validated using more reliable timing assumptions or actual plant data. Additionally, how to interpret the dynamic PRA/HRA modeling outputs must be reconciled with the traditional error probability view to identify a comprehensive representation of system risk that can be readily incorporated into the PRA. A single error percentage cannot be calculated from this data as can be achieved in a traditional static HRA, and a method for synthesizing the results into a compatible format must be identified.

6.3.5 Discussion

6.3.5.1 Initial Modeling Effort Success

The current study demonstrates the feasibility of modeling human operator FLEX activities dynamically with EMRALD. These first efforts were purely for proof of concept and require additional fidelity to accurately capture realistic conditions during a FLEX event. EMRALD was designed for PRA for hardware systems and, as a result, it was not initially clear whether it would prove feasible to model human activities. This demonstration shows that it is feasible, but that there are still challenges to overcome to better reflect unique aspects of human actions.

For example, EMRALD conceptualizes components as individual objects within the model. Each component can be instantiated in only one instance within the model such that any component exists only once within the model. It can be referenced from different elements within the model; however, it is only a single instance. This works well for PRA since the physical world represents the function of a component as one entity. Human actions, however, may be used repeatedly at different times in the simulation and on different components that might be easier or more challenging to assess. The assessed action therefore exists as separate instantiations of that particular human action type. For example, a human action may consist of assessing the state of a valve multiple times during the simulation. The assessed action is not the same across time spans since the state of the operator might change due to performance-shaping factors and the context at that time. Therefore, the conceptualization of a generic action type is needed to eliminate the tedious process of manually redefining the action each time it is invoked in a particular context. Instead, a generic action component could be invoked and populated with the context of its use, including the performance-shaping factors that govern the human operator's ability to perform the assessment. Since humans repeatedly perform various actions, this would greatly reduce the amount of modeling time required to accommodate the unique human operator aspects when they are performing basic human actions. Furthermore, it would be useful to chain together individual human action components into

more sophisticated generic actions to further reduce the level of effort required for capturing repeatedly used and more complicated human actions.

6.3.5.2 Benefits of EMRALD HRA Modeling versus Traditional HRA

A distinguishing feature of EMRALD HRA modeling versus traditional HRA is its ability to evaluate HRA uncertainty considering error possibilities, time-related factors, and equipment failures all in a single simulation. EMRALD modeling is especially useful to evaluate time uncertainty, a factor that is largely missed in existing static HRA analysis. In HRA, timing information such as the time window or time required is essential to estimate HEPs. Especially for the time required, a time distribution should be assumed, because it is highly context specific and represents a source of individual variability. However, in traditional static HRA, median or average values are used. These are based on experimental observation, operator interviews, or expert judgement. Because of the challenge of HRA data scarcity—particularly for BDBEEs—it is common to resort to expert judgement to complete static HRAs.

Notwithstanding a lack of data to inform the estimate, the major problem is that the calculation approach in traditional HRA is not adequate to consider the dynamic context between human actions with statistical time distributions. In contrast, the EMRALD HRA models consider statistical distributions for HRA timing information and capture the variability in human actions due to different contexts. Using Monte Carlo simulation, the EMRALD model compares the time window and time required for human actions, and then evaluates the failure type caused by an overage in time required.

In addition, EMRALD provides HRA analysts more options to model operator actions in a more nuanced and realistic manner. As introduced in the previous sections, EMRALD models time-related factors that may affect time or HRA uncertainty such as different staging areas, delay time due to debris removal, or simultaneous human actions during FLEX situations. Such factors, which are not readily modeled in static HRA, are important to realistically model human actions during BDBEEs such as FLEX.

6.3.6 Future Directions

1. Expansion of Model

   Since this is the initial iteration of the modeling effort, significant simplifications were made to test the modeling adequacy of EMRALD for FLEX activities. For example, the distance to the different staging locations was assigned magnitudes of 1, 1.5, and 2 for the first, second, and third priority locations. An accurate model would require using actual route distances in conjunction with some type of metric to capture the likelihood of debris actually occurring along each route. In the current model, an equal amount of debris was assumed to exist across all routes, and the total debris that must be cleared is a function of this equal debris and distance of the route. Many other areas of the modeling effort can include greater fidelity. In particular to HRA, the largest gain could be made from including a more accurate depiction of the performance-shaping factors and applying changes to these as the simulation unfolds.

2. Refinement of Operator Decision Probabilities

   In future iterations, a more complete rendition of the GOMS-HRA framework will need to be implemented in addition to real data from simulated FLEX scenarios by plant crews. There are opportunities for further validation of specific task probabilities in the context of a FLEX event. Due to the assumed high stress and low-time characteristics of these instances, the scenarios will not occur at a normal baseline. Operators and crew will be operating at a performance decrement in all instances, and that error impact requires further research to quantify.

   An additional modification to the HRA modeling that has been discussed in other projects, but has yet to receive full attention, is the quantification of the effects of recovery on increasing the probabilities of successful task completions. FLEX situations exemplify the reason human operators are a huge benefit to nuclear power. The impacts of human creativity and reasoning in the face of novel situations could yield

substantive gains in these emergency situations. There are large potential benefits to better include recovery functions in these models and in HRA in general.

A final angle for further research is the use of cognitive modeling applications and tools to better capture the decision-making steps of a human operator. The suitability of these tools is currently unknown for this application, but the authors believe that linking EMRALD to an external simulation that is better designed to handle the spectrum of human actions and cognition may be a beneficial step to constructing more dynamic HRA models that could be applied to FLEX scenarios and other HRA efforts across the industry.

3. Development Toolkits for Computation-Based HRA

   To the best of the authors' knowledge, there are currently very few easy-to-use modeling tools available to construct and evaluate dynamic HRA models. EMRALD has the ability to couple with external simulations to augment its current simulation capability. The authors have an existing reduced order model (ROM) of a nuclear power plant, the Rancor Microworld Simulator, that could be coupled to EMRALD to run full plant scenarios. Doing so would be fruitful because the simplified model contains both the primary coolant loop and secondary plant systems. RELAP5-3D is a phenomenal tool to couple to EMRALD for evaluating CDF within the primary loop; however, it is possible to capture dynamics of the secondary systems in tandem with the primary coolant loop using ROMs.

   Another future direction the authors intend to pursue is developing a tool that would allow for rapid model creation via the already existing procedure structure for many human actions within nuclear power. Indeed, the authors used existing FLEX procedures in the development of the scenario and the model itself for the procedure-based approach. Since nuclear power has developed procedures, and therefore scripted a large volume of human activities, both in the MCR and, to a more limited extent, in the field, it would vastly simplify the modeling effort if the native format of these actions could be fed directly into a dynamic HRA modeling and simulation tool.

4. Crediting FLEX Gear for Non-BDBEE Operations

   Static HRA provides an approximation of human activities in using FLEX equipment during BDBEEs. Dynamic HRA, such as the current EMRALD modeling example, allows simulation across a range of possible outcomes to more accurately represent the complex nature of BDBEEs. A final use of dynamic FLEX HRA simulation is to support the consideration of the benefits of FLEX equipment for non-BDBEE situations, such as using FLEX equipment to enhance safety margins during outage work. Creating a realistic simulation for FLEX equipment deployment allows modeling of these scenarios beyond what is capable by current PRA models.

6.3.7 Summary of FLEX HRA

This effort demonstrates a dynamic simulation approach to account for contextual and time uncertainties that have been missing in existing HRA. Two FLEX HRA models with different approaches were developed using EMRALD software. One FLEX HRA model is mainly developed on the basis of procedure contexts, while the other one depends on PRA/HRA modeling approaches. The major insights coming from each model were discussed.

FLEX actions occur on a different timescale than those considered in typical PRA/HRA context, in which the bulk of operator actions occur within the main control room. The activities modeled in these approaches occur primarily outside of the control room, in the field. These two dynamic modeling approaches demonstrate more realistic modeling of FLEX actions and include evaluations of the time uncertainty that may be missed by existing static analysis of FLEX activities.

7. MULTICRITERION BENEFIT EVALUATION FOR FLEX DEPLOYMENT

This section proposes an MCBE methodology for evaluating costs and benefits of safety enhancements in NPPs. The MCBE methodology establishes a comprehensive evaluation scope using multiple evaluation criteria (including public risk, occupational risk, plant revenue, and plant cost) and multiple contexts (including plant normal operations, incidents, and accidents). The MCBE methodology also incorporates a decision maker's preferences toward hazard likelihood and consequence into cost and benefit estimations using cumulative prospect theory. As a case study, this section presents the application of the MCBE methodology to the implementation of FLEX in a generic PWR.

7.1 Overview

As one of the lessons learned from the Fukushima Daiichi accident, attention has been drawn to preparedness and mitigation of unanticipated events such as BDBEEs. The U.S. NRC required a series of post-Fukushima safety enhancements, first issued as NRC orders and later incorporated as part of NRC regulations to U.S. commercial NPPs (U.S. Nuclear Regulatory Commission, 2012a; U.S. Nuclear Regulatory Commission, 2018a; U.S. Nuclear Regulatory Commission, 2019a). The enhancements were dedicated to FLEX, spent fuel pool instrumentation, containment venting systems, seismic and flooding defense, and emergency preparedness (U.S. Nuclear Regulatory Commission, 2018a).

These safety enhancements can undoubtedly make NPPs safer, but an accompanying concern is whether they will become heavy financial burdens for NPPs. An example is FLEX, which has been implemented at the majority of U.S. NPPs. Each NPP incurred a startup expense on purchasing and installing FLEX equipment, building protected structures to store FLEX equipment, developing associated procedures and trainings, conducting associated calculations, etc. Besides the one-time startup expense, each NPP needs to spend a portion of its annual budget on FLEX equipment testing and maintenance (TM) in order to maintain equipment operability. Besides pursuance of enhanced safety, competitiveness of economic performance is also a key for NPP sustainability. There is a timely need to evaluate the impacts of these enhancements on plant safety and economics so that plants can have a better idea on the efficacy of these enhancements and plan on how to strategize their usages for better efficiency.

Plant safety and economics are most often competing against each other. This is mostly true if we confine the scope of economic impact analysis (EIA) to startup and periodic TM costs. But if we expand the scope of EIA, there is a potential that efforts to reduce risk could bring economic benefits in the form of plant revenue increases or cost savings. This research, as part of the ERP Project, intends to develop an MCBE methodology for evaluating NPP safety enhancements. The MCBE methodology features the adoption of multiple criteria for cost and benefit evaluations and modeling underlying relationships between plant safety and economics. For NPP enhancements, MCBE methodology quantifies costs and benefits and then calculates a benefit-to-cost ratio (BCR). The methodology adopts two criteria to evaluate plant safety—public risk and occupational risk—and two criteria to evaluate plant economics: plant revenue and plant cost. Before conducting BCR calculations, safety-related criteria are converted to monetary values so as to be comparable with economics-related criteria. The MCBE methodology also incorporates the risk preference of a decision maker toward hazard likelihood and consequence into cost and benefit estimation using cumulative prospect theory (CPT). The outputs of MCBE methodology could be provided to plant DMs for a variety of strategic planning, such as evaluating the necessity of implementing a new enhancement, comparing different enhancement alternatives, and seeking for best use of an in-place enhancement.

This section demonstrates the feasibility of MCBE methodology using FLEX as a case study. FLEX is selected considering it is already in place in most U.S. NPPs, rendering an urgent need to develop plans for crediting, testing, and maintaining FLEX equipment to achieve a good balance between plant safety and economics. It should be noted that MCBE methodology is expected to be applicable to other NPP safety enhancements, such as ATF, as well as enhancements in other industrial systems with severe accident consequences. Literature review and contributions of this research are presented in Section 7.2. The MCBE

methodology is explained in Section 7.3, and a computational application for FLEX is provided in Section 7.4. Section 7.5 summarizes this section and discusses candidate topics of future research.

7.2 Literature Survey and Research Contributions

This section first provides a review on existing studies which considered both plant safety and economics in NPP decision making. It should be noted that, although plant safety can be measured by a broad variety of metrics, this review focuses on research adopting the same safety metric as the one used in MCBE methodology (i.e., risk estimated using PRA). This section then compares MCBE methodology with reviewed studies and explains its methodological contributions.

Formulated in the 1970s, PRA is a well-established technique that has been widely used by the nuclear power industry and other industries, such as aerospace. PRA models are already developed for most reactors worldwide. Compared to the maturity of PRA applications, integration of PRA and EIA for NPP decision-making is relatively less well explored. Still, there is a considerable body of existing studies exploring such integration. This review finds that integration methods in existing studies fall in one of two broad categories:

1. Correlation-type integration: This type of integration does not establish direct connection between PRA and EIA, but identifies common ground that affects or is affected by both. A representative example is studies on maintenance-schedule optimization such as (Zhang, Du, Tong, & Li, 2019) which adopts a maintenance schedule for feedwater systems in a multi-unit NPP site as common ground—maintenance schedule acted as a shared input parameter affecting both site-wide risk (a PRA output) and maintenance cost (an EIA out). Another example is studies on benefit evaluation of risk-informed applications, such as (Pence, et al., 2018) in which completion times of NPP equipment were adopted as a common ground—extension of completion times, if with risk (a PRA output) still falling below risk threshold, could help avoid plant shutdowns and associated production losses as well as bringing regulatory cost savings (EIA outputs).
2. Causation-type integration: This type of integration establishes a direct causal relationship between PRA and EIA and utilizes outputs of PRA as an input of EIA. PRA develops scenarios and estimates their likelihood of occurrence. For a scenario of interest, EIA then estimates its "expected" cost or benefit by multiplying occurrence likelihood by resultant economic impact. NUREG-1530 provided a dollar per person-rem conversion method to estimate expected costs of scenarios with CD (U.S. Nuclear Regulatory Commission, 2015). Other studies also estimated expected costs of non-core-damage scenarios, such as (Electric Power Research Institute, 2004) estimating production losses; (Dube, Albinson, Wolfgang, Saunders, & Krueger, 2017) quantifying property loss, production loss, and regulatory cost given a variety of events, including turbine trip and forced manual plant shutdown; (Zeng & Zio, 2018) quantifying post-accident SG refurbishment costs and production losses; (Mandelli, et al., 2019) quantifying replacement cost, inspection costs, and production losses using different battery replacement options; and (Schumock, et al., 2020) quantifying tornado-induced property losses.

The above reviewed studies are capable of explicitly modeling correlations and causations between plant safety and economics. However, they differ in their evaluation scope of decision-making criteria. Most of reviewed studies focused on avoiding interruptions to plant normal operation and preventing occurrence of scenarios with CD (referred as "incidents" hereinafter). In addition, as a measure of plant safety, metrics related to public risk such as CDF and LERF were adopted in most reviewed studies, but occupational risk was still excluded from evaluation. These two missing parts were considered and modeled in (Smith C. L., 2002), which developed a methodology of evaluating decision-making criteria during NPP incidents. The MCBE methodology adopts an evaluation scope in line with (Smith C. L., 2002), uses both public and occupational risk as plant-safety measures, and targets a variety of contexts, including plant normal operations, incidents, and accidents.

(Smith C. L., 2002) focused on decision-making during an incident, such as a leaking SG tube, then evaluated and compared incident-management alternatives using disutility as a performance indicator. The performance indicator is a weighted sum of disutility values of five evaluation criteria, including cost, CD, industrial accidents, radiological dose, and external attention. Two criteria—cost and radiological dose—were formulated as continuous numbers, and the other three criteria appeared as nonquantifiable, discrete states such as core damage or none. Each criterion was then mapped to a disutility value residing between 0 and 1. Compared with (Smith C. L., 2002), MCBE methodology quantifies each evaluation criterion and converts non-monetary criteria to monetary values as a common scale to facilitate adding all criteria.

The approach of using monetary value as a common ground was also adopted in NUREG/BR-0058, Revision 5 (U.S. Nuclear Regulatory Commission, 2017a), guidance used by the U.S. NRC to evaluate the costs and benefits of proposed regulatory actions. But an issue emerges when aggregating expected (potential) monetary values and non-expected (realized) ones such as capital costs. Expected values are formulated as a product of scenario likelihood and resultant economic impact, while non-expected values can be taken as a special case of expected ones where occurrence probability is one. As a result of such mathematical formulations, expected monetary values are usually much lower than non-expected ones, which may render a misleading impression that drivers of expected monetary values are not as important as those driving non-expected monetary values. To tackle this nonequivalence issue, MCBE methodology borrows from decision science (Tversky & Kahneman, 1992; Cha & Ellingwood, 2013; Cha & Ellingwood, 2019) and utilizes CPT as the decision method to facilitate incorporation of preferences toward both scenario occurrence likelihood and economic consequence and establishes common ground to evaluate expected and non-expected monetary values.

To summarize, this section develops a new MCBE methodology for evaluating costs and benefits of safety enhancements in NPPs. The MCBE methodology falls in the intersection of cost-benefit analysis (CBA) and multicriterion decision analysis (MCDA) realms. Similar to CBA, MCBE methodology expresses costs and benefits in monetary terms; similar to multicriterion decision analysis, it evaluates costs and benefits using multiple criteria, not necessarily monetary ones, and calculates their values perceived by DMs. Compared to existing studies combining PRA and EIA in NPP decision-making, MCBE retains the capability of explicitly modeling correlations and causations between plant safety and economics and makes the following methodological contributions: (1) establishing a comprehensive evaluation scope using multiple evaluation criteria (including public and occupational risk and plant revenue, and cost) and multiple contexts (including plant normal operations, incidents, and accidents) and (2) providing quantification methods for each evaluation criterion, converting non-monetary criteria to monetary values, and ensuring equivalences of expected and non-expected monetary values using CPT.

7.3 MCBE Methodology

Figure 7-1 demonstrates the proposed MCBE methodology, consisting of three methodological steps: (1) characterization of safety-enhancement alternatives, (2) quantification of cost-benefit evaluation criteria, and (3) CBA.

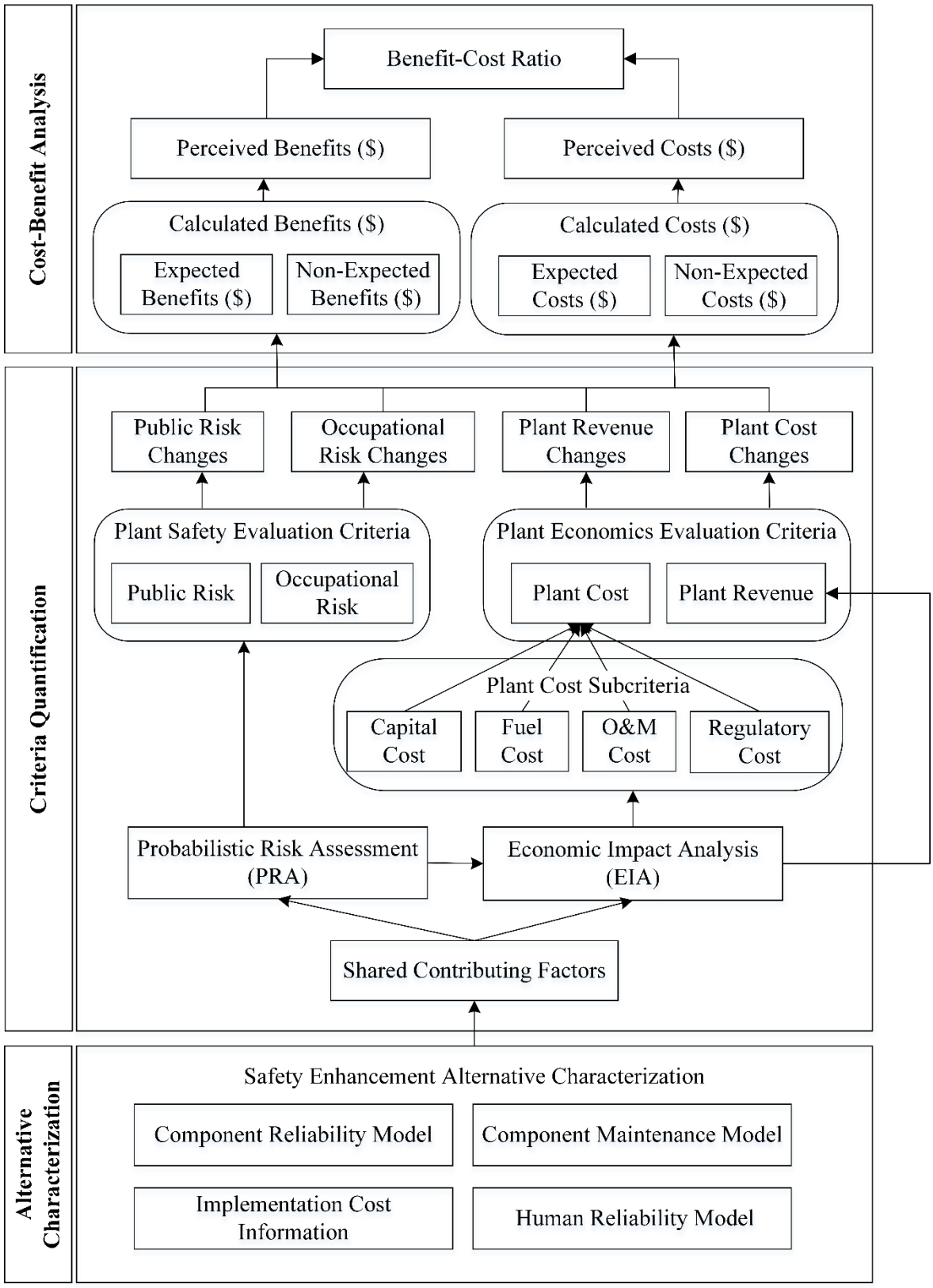

Figure 7-1. MCBE Methodology for Evaluating Safety Enhancements in NPPs.

One safety enhancement could have more than one alternative (referred as "safety-enhancement alternative" or "alternative" thereinafter). It is also possible that multiple safety enhancements, each of which has more than one alternative, need to be evaluated. The MCBE methodology evaluates one alternative at a time and uses BCR as PI. For cases involving multiple alternatives, MCBE methodology can run multiple times, equal to total number of alternatives, to compare alternatives based on their BCRs. Introduction of each methodological step is provided as follows.

7.3.1 Step 1: Alternative Characterization

This step characterizes safety-enhancement alternatives and sets up analysis conditions. If the alternative introduces new hardware components to a plant, the characterization should include information such as component types (e.g., pumps and valves), number of components of each type, expected functions (e.g., providing additional cooling), deployment circumstances (e.g., during accidents), TM plans (e.g., conducting preventive maintenance once per quarter), and associated human actions (e.g., manual activation). This information defines the analysis condition of implementing the alternative in a target plant. A baseline analysis condition without alternative implementation must also be defined in this step.

7.3.2 Step 2: Criteria Quantification

This step defines and quantifies criteria for evaluating costs and benefits of safety-enhancement alternatives. Evaluation criteria include two points related to plant safety (public and occupational risk) and two points related to plant economics (plant revenue and cost). These criteria are selected based on a logical analysis of potential plant scenarios, which is visualized in the event-sequence diagram below (Figure 7-2).

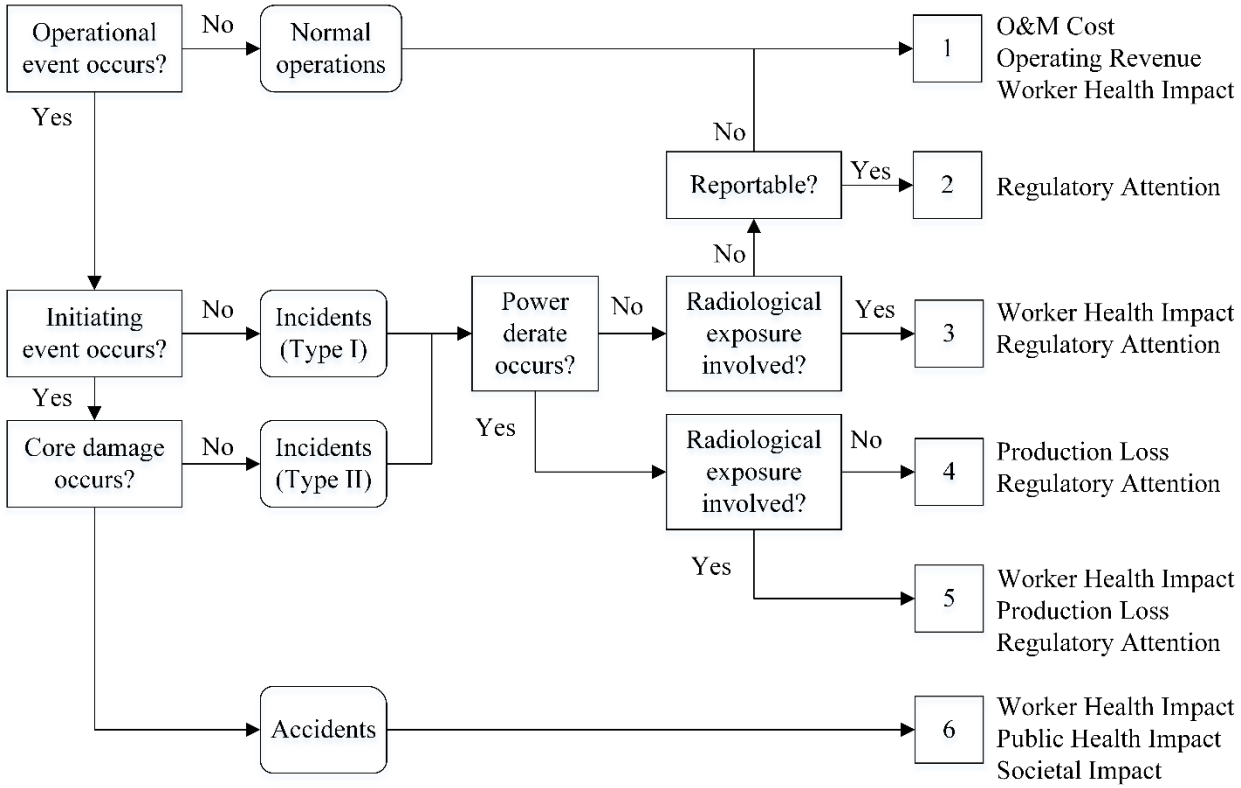

Figure 7-2. Event-Sequence Diagram for NPP Scenarios.

Figure 7-2 starts with examining whether an operational event occurs in an NPP. An operational event refers to either an initiating event or a degraded condition (U.S. Nuclear Regulatory Commission, 2017b). If a degraded condition occurs, it does not trigger a reactor-trip demand, but still could bring negative impacts to a plant. If an initiating event occurs, it will trigger a reactor-trip demand and call upon a series of mitigation measures to prevent CD; this process can be modeled using ET analysis, leading to scenarios with or without CD. This section defines degraded-condition-led scenarios as "incidents (Type I)," initiating event-led scenarios without core damage as "incidents (Type II)," and initiating event-led scenarios with core damage as "accidents."

Figure 7-2 ends with six scenario categories. If no operational event occurs, a plant remains in normal operations (i.e., Scenario Category 1). Under such scenarios, a plant incurs operation and maintenance (O&M) costs, receives revenue from electricity production, and imposes occupational-health impact on plant workers who perform routine tasks. Type I or II incidents can fall into one of five scenario categories, depending on whether each involves power derate or radiological exposure. If an incident involves neither and is not reportable to NRC per regulation (U.S. Nuclear Regulatory Commission, 2017c), it falls into Scenario Category 1. If an incident involves neither, but is reportable, it belongs to Scenario Category 2 and draws regulatory attention. If an incident involves radiological exposure only, it belongs to Scenario Category 3, imposes occupational-health impact, and draws regulatory attention. If an incident involves power derate only, it falls into Scenario Category 4, leads to production loss, and draws regulatory attention. If an incident involves both, it is categorized as Scenario Category 5, imposes occupational-health impact, leads to production loss, and draws regulatory attention. An accident falls into Scenario Category 6, imposes worker and public-health impact as well as societal impact.

By analyzing the impacts of plant-scenario categories, four evaluation criteria are selected: public risk measured in annual public doses, occupational risk measured in annual occupational doses, plant revenue measured in U.S. dollars, and plant cost measured in U.S. dollars. Criterion "plant cost" is broken down into four sub-criteria: capital cost, fuel cost, O&M cost, and regulatory cost. These evaluation criteria are not independent from one another, but are grounded on a shared set of contributing factors, and connected by complex correlations and causations. One example is that, by implementing a plant-safety enhancement, both public risk and regulatory cost could be reduced. This is because risk significance of an incident can become lower due to reduction in public risk, and an incident with lower risk significance draws less regulatory attention. Another example is that a component, originally designed for accident prevention only, is used to support normal O&M. Such extended usage could streamline O&M schedules and reduce O&M costs; however, it could also render a public risk increase. This is because additional usage could accelerate component degradation. When called upon under accidental circumstances, the component may have a lower reliability and lead to a higher public risk. To explicitly model correlations and causations among evaluation criteria, this step develops models of safety-related evaluation criteria using PRA, develops models of economics-related evaluation criteria using EIA, and integrates PRA and EIA in a holistic modeling framework using a shared set of contributing factors. This step quantifies evaluation criteria for analysis conditions with or without safety-enhancement implementation and calculates changes in each evaluation criterion using the following equations:

$$\Delta PR_{SE} = PR_B - PR_{SE} \quad (7\text{-}1)$$

$$\Delta OR_{SE} = OR_B - OR_{SE} \quad (7\text{-}2)$$

$$\Delta R_{SE} = R_B - R_{SE} \quad (7\text{-}3)$$

$$\Delta C_{SE} = C_B - C_{SE} \quad (7\text{-}4)$$

where:

SE = Analysis condition with implementation of safety-enhancement alternative

B = Baseline analysis condition without implementation of safety-enhancement alternative

ΔPR_{SE} = Public risk changes after implementing safety-enhancement alternative

ΔOR_{SE} = Occupational risk changes after implementing safety-enhancement alternative

ΔR_{SE} = Plant revenue changes after implementing safety-enhancement alternative

ΔC_{SE} = Plant cost changes after implementing safety-enhancement alternative

$(\cdot)_B$ = Value of an evaluation criterion under analysis condition B

$(\cdot)_{SE}$ = Value of an evaluation criterion under analysis condition SE

7.3.3 Step 3: CBA

This step quantifies costs and benefits of implementing safety-enhancement alternatives and calculates BCR as the performance indicator for the alternative. Changes in each evaluation criterion, calculated in Step 2, are assigned to either benefit or cost. Benefits can take the form of public-risk reduction (positive ΔPR_{SE}), occupational-risk reduction (positive ΔOR_{SE}), plant-cost reduction (positive ΔC_{SE}), or plant-revenue increase (negative ΔR_{SE}); costs can take form of public-risk increase (negative ΔOR_{SE}), occupational-risk increase (negative ΔOR_{SE}), plant-cost increase (negative ΔC_{SE}), or plant-revenue reduction (positive ΔR_{SE}). To establish a common scale for cost and benefit measurement, ΔPR_{SE} and ΔOR_{SE} are first converted to equivalent monetary values. For public risk and occupational risk, health impacts (mortality and morbidity) on public and plant workers are monetized as dollars per person-rem of collective dose (U.S. Nuclear Regulatory Commission, 2015). For public risk, societal impact (land contamination, long-term relocation, loss of productive farm area, loss of industrial production, and loss of electric capacity) is monetized as dollars per large early release (LER) accident (Denning & Mubayi, 2017). These results, using monetary value as a common scale, are referred as "calculated costs" or "calculated benefits" in this section and converted to "perceived costs" and "perceived benefits" based on CPT (Tversky & Kahneman, 1992). This step then calculates BCR as a ratio of perceived benefits and perceived costs.

7.4 Case Study: Deploying FLEX in PWR

This section explains the application of MCBE methodology for FLEX in NPPs. FLEX implementation, as a mandatory regulatory requirement, is now complete at a majority of U.S. NPPs, each of which incurred tremendous startup costs and continues to pay for routine TMs of FLEX equipment. Besides prevention and mitigation for BDBEEs, plants are seeking other possibilities to credit FLEX. A few commonly asked questions include, what benefits FLEX can bring to a plant, whether FLEX benefits can outweigh its costs, and how a plant can credit FLEX to maximize or increase FLEX benefits. These questions have been explored in a considerable body of studies. Multifaceted FLEX benefits were demonstrated such as in increasing safety margin (Yang, Wang, Shih, & Chiang, 2019), reducing CDF (Ma, et al., 2019a; Ma, et al., 2019b), and reducing plant O&M cost (Yadav & Biersdorf, 2019). Compared to existing studies, the case study presented in this section evaluates costs and benefits of FLEX implementation using MCBE methodology, adopts a broader evaluation scope (public risk,

occupational risk, plant revenue, and plant cost), includes more plant scenarios (normal operations, incidents, and accidents), and converts calculated costs and benefits to values perceived by plant DMs. This case study should be taken as a generic study, as it is based on the PRA model of a generic PWR plant and obtains a significant amount of parameter estimates based on the industry-average performance of the U.S. power reactor fleet. This case study is used to demonstrate the feasibility of the MCBE methodology, which can also be applied to conduct plant-specific analysis.

7.4.1 Step 1: FLEX Deployment Alternative Characterization

This step characterizes FLEX deployment alternatives and defines analysis conditions for the case study. A FLEX deployment alternative can be characterized by what FLEX equipment is deployed and where. "What" clarifies which FLEX equipment is credited, and "where" refers to credit contexts such as utilizing FLEX equipment to prevent and mitigate LTSBOs, to expedite scheduled activities during a planned outage, to back up inoperable equipment during an incident, to back up a component being maintained either online (during plant operation) or offline (during plant outage), or a combination of part or all of these contexts. Table 7-1 describes a FLEX deployment alternative, presumed in previous ERP research (Ma, et al., 2019a) and also adopted for this case study, in a generic PWR plant (referring as "the reference plant" hereinafter). This alternative utilizes four pieces of FLEX equipment, including two FLEX DGs and two FLEX pumps, to support normal O&M, incidents, and accidents. It should be noted that FLEX DGs and pumps are different from plant DGs and pumps, which refer to existing plant equipment. Two analysis conditions are then established with and without implementation of FLEX deployment alternative, respectively.

Table 7-1. FLEX Deployment Alternative Characterization.

No.	Equipment	Location	Connection	Scenarios and Functions
1	FLEX-DG1	On-site	Pre-staged	Accidents (providing AC power during LTSBOs)
				Incidents (backing up inoperable plant DGs)
				Normal O&M (backing up plant DGs under maintenance)
2	FLEX-DG2	On-site	Pre-staged	Same as those of FLEX-DG1
3	FLEX-P1	On-site	Pre-staged	Accidents (providing SG makeup water during LTSBOs)
				Incidents (providing backup for inoperable plant pumps)
				Normal O&M (providing backup for unavailable plant pumps under maintenance)
4	FLEX-P2	On-site	Portable	Same as those of FLEX-P1

7.4.2 Step 2: Criteria Quantification With and Without FLEX Deployment

This step quantifies each evaluation criteria for each of two analysis conditions and calculates changes in each criteria. The evaluation criteria are grounded on a shared set of contributing factors and connected by correlations and causations visualized in a causal-loop diagram (CLD) in Figure 7-3.

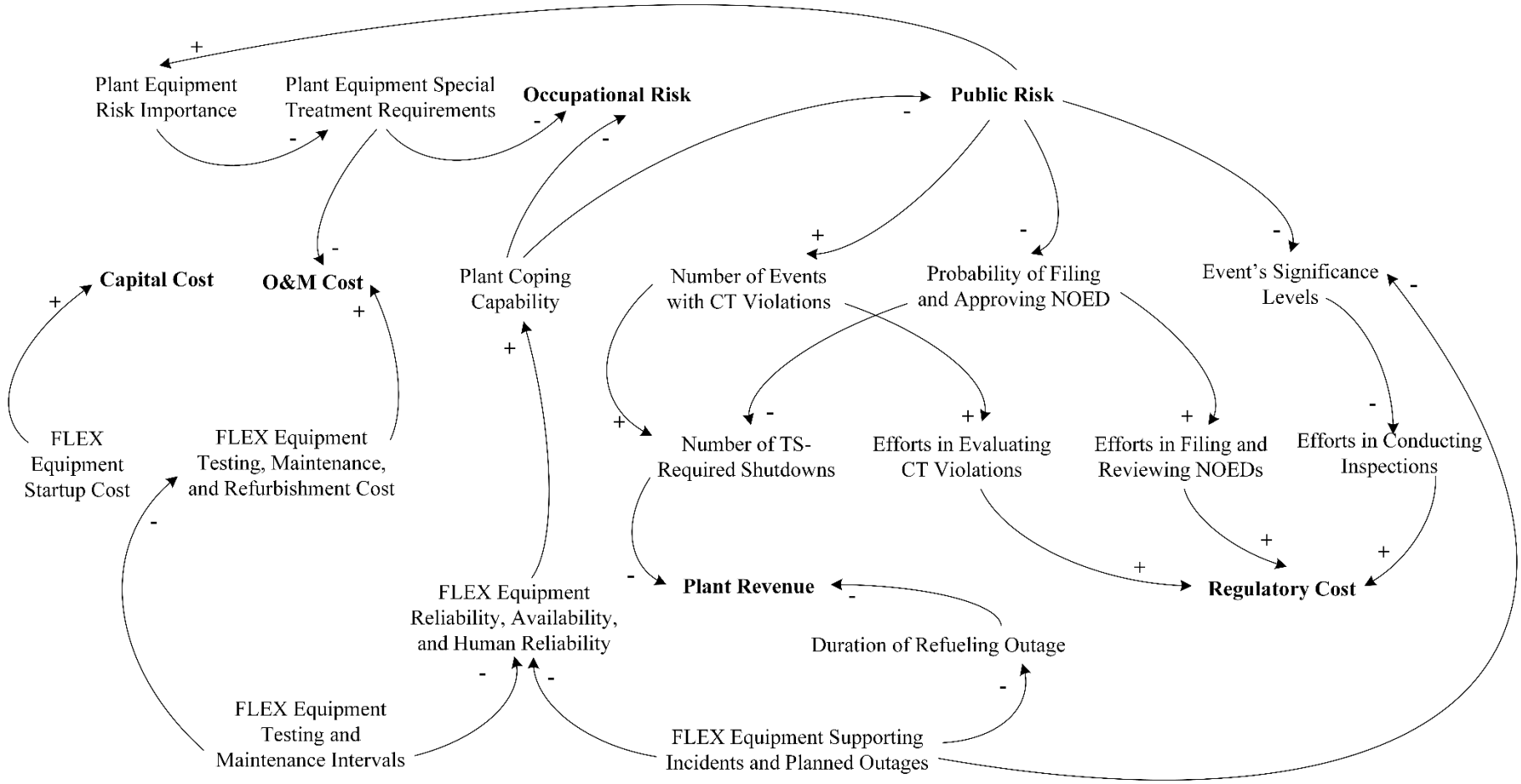

Figure 7-3. CLD of Cost-Benefit Evaluation Criteria for FLEX Implementation in NPPs.

The CLD (Figure 7-3) consists of a set of nodes and links. Nodes represent both evaluation criteria (bold texts (e.g., "Capital Cost") and underlying contributing factors (non-bold texts such as "FLEX Equipment Startup Cost"). Links, visualized as line arrows and marked either positive ("+") or negative ("–"), represent a relation between the two nodes (such as the line arrow marked positive between "FLEX Equipment Startup Cost" and "Capital Cost"). A positive link means the two nodes change in the same direction (e.g., if the FLEX equipment reliability, availability, and human reliability increases, the plant coping capability will also increase). A negative link means the two nodes change in opposite directions (e.g., if the FLEX equipment TM intervals become shorter, the FLEX equipment testing, maintenance, and refurbishment cost will increase).

The evaluation criteria and contributing factors are connected by complex relationships shown in Figure 7-3. Implementation of FLEX deployment alternative leads to increases in capital and O&M costs and decreases in public and occupational risk due to enhanced plant coping capability. The reduced public risk will, in turn, affect the results of several risk-informed activities, including the SDP, CT extension to avoid technical specification-required reactor shutdown (TSSD), and risk-informed categorization and treatment of SSCs. Besides, utilizing FLEX equipment to support non-accident scenarios could facilitate more-flexible maintenance schedule and shorten refueling outages (RFOs); however, such additional usage could escalate FLEX-equipment degradation. It should be noted that fuel cost, although included in the MCBE methodology (Figure 7-1), is not included in the CLD because fuel cost does not change before or after FLEX deployment to the authors' knowledge. Quantifications of evaluation criteria are then partitioned into five processes summarized in Table 7-2 and explained in detail in the following subsections.

Table 7-2. Processes of FLEX Deployment Alternative Cost-Benefit Evaluation Criteria Quantification.

No.	Process	Contributing Factors	Evaluation Criteria
1	FLEX implementation	FLEX equipment startup cost; FLEX equipment TM intervals; FLEX equipment testing, maintenance, and refurbishment cost.	Capital cost. O&M cost.
2	Plant coping-capability enhancement	FLEX equipment TM intervals; FLEX equipment supporting incidents and planned outages; FLEX equipment reliability, availability, and human reliability; plant coping capability.	Public risk, Occupational risk.
3	SDP	Events' significance levels; efforts in conducting inspections.	Regulatory cost.
4	TSSD	Number of events with CT violations; probability of filing and approving notice of enforcement discretion (NOED); number of TSSDs; efforts in evaluating CT violations; efforts in filing and reviewing NOEDs.	Plant revenue. Regulatory cost.
5	SSC TM schedule	Plant equipment risk importance; plant equipment TM interval; FLEX equipment supporting incidents and planned outages; duration of RFO;	O&M cost. Occupational risk. Plant revenue.

1. Criteria Changes Associated with FLEX Implementation

   This subsection calculates changes in plant capital and O&M costs after implementing a FLEX-deployment alternative. The reference plant incurs a one-time expense on purchasing and installing FLEX equipment, building protected structures to store FLEX equipment, developing associated procedures and trainings, conducting associated calculations, etc. Such expense, denoted as $C_{FLEX\ IM}$, can be viewed as an increase of capital cost and is assumed $25 million per reactor lifetime, based on expert elicitation as a U.S. reactor fleet-wide average estimate. Besides the one-time expense, the plant periodically incurs expenses on surveillance test, preventive maintenance, and corrective maintenance for FLEX equipment. Such periodic expense with a unit of dollars per reactor year, can be viewed as an increase of plant O&M cost.

   Based on (Ma, et al., 2019a), the unavailability of a FLEX DG due to TM outages is assumed as 1.50×10^{-2}, and the unavailability of a FLEX pump is assumed as 1.60×10^{-2}. Then, in one year, a

FLEX DG will be under TM for $1.50 \times 10^{-2} \times 365 \times 24 = 131.4$ hours, and a FLEX pump will be under TM for $1.60 \times 10^{-2} \times 365 \times 24 = 140.2$ hours. Assuming a FLEX DG or FLEX pump TM is completed by two workers, the yearly labor of a FLEX DG TM can be calculated as $131.4 \times 2 = 262.8$ person hour per year, and the yearly labor of a FLEX pump TM is $140.2 \times 2 = 280.4$ person hour per year. The yearly FLEX TM labor cost, which is the increase in plant O&M cost due to FLEX implementation, can be estimated using the following equation:

$$C_{FLEX\,TM} = (140.2 \times n_{FLEX\,DG} + 131.4 \times n_{FLEX\,P}) \times MP_{RZ} \times c_{LR} \times MP_{EB} \quad (7\text{-}5)$$

where:

$n_{FLEX\,DG}$	=	Number of FLEX DGs in the FLEX deployment alternative
$n_{FLEX\,P}$	=	Number of FLEX pumps in the FLEX deployment alternative
MP_{RZ}		Multiplier on TM labor to account for extra labor in the radiation zone
c_{LR}	=	Average hourly earnings of TM workers
MP_{EB}	=	Multiplier on average hourly earnings to account for employee benefits

Parameters $n_{FLEX\,DG}$ and $n_{FLEX\,P}$ are both two per reactor in this case study. MP_{RZ} is suggested in (U.S. Nuclear Regulatory Commission, 2017a) as an adjustment factor to account for extra labor due to exposure limits and lower worker efficiency; this study assumes MP_{RZ} as one because FLEX equipment is usually stored in non-radiation zones. Parameter c_{LR} is \$39.46 per person hour, assumed equal to 2019 median hourly pay of nuclear technicians released by U.S. Bureau of Labor Statistics (U.S. Bureau of Labor Statistics, 2020). Parameter MP_{EB} is 1.5, suggested in (U.S. Nuclear Regulatory Commission, 2017a) to account for employee benefits (pension, insurance premiums, and legally required benefits). Calculated $C_{FLEX\,TM}$ is \$3.2E+04 per reactor year. The change in plant capital cost (denoted as $\Delta C_{CP} = -C_{FLEX\,IM}$) and the change in plant O&M cost due to FLEX implementation (denoted as $\Delta C_{O\&M,IM} = -C_{FLEX\,TM}$) are then calculated and shown in Table 7-3.

Table 7-3. Changes in Evaluation Criteria Associated with FLEX Implementation.

No.	Evaluation Criteria	Changes in Evaluation Criteria	
		Value	Unit
1	Capital cost	-2.5E+07	\$ per reactor lifetime
2	O&M cost	-3.2E+04	\$ per reactor year

2. Criteria Changes Associated with Plant Coping-Capability Enhancement

FLEX implementation could enhance a plant's capability to cope with accidents. The FLEX deployment alternative of this case study has been incorporated into the reference plant PRA model using SAPHIRE, and the associated CDF reduction was calculated and presented in (Ma, et al., 2019a). This subsection converts CDF reduction to reductions in public and occupational risk, measured in yearly radiological doses received by public and plant workers and their monetized values.

(Ma, et al., 2019a) credited FLEX equipment in the PRA model by adding new top events into the existing ET for LTSBO, also referred to as ELAP. The first top event is for an operator failing to deploy FLEX equipment for ELAP scenario; the second top event represents whether at least one of two redundant FLEX DGs is successfully deployed to provide ac power; the third top event represents whether at least one of two redundant FLEX pumps is successfully deployed to provide secondary cooling to SG. FTs were developed for each top event. For FLEX equipment, both independent and CCFs for failure modes of fail-to-start and fail-to-run were modeled. Unavailability of FLEX equipment due to TM outages as well as human actions to use FLEX equipment were also modeled. Human-error probabilities for all human actions related to FLEX-equipment deployment were assumed as 0.1.

FLEX-equipment reliability and unavailability data were obtained by adjusting industry-average performance data (U.S. Nuclear Regulatory Commission, 2017d) according to FLEX equipment-specific data collected by PWR Owners Group (Linthicum & Powell, 2019). After crediting FLEX, plant CDF was reduced from 3.12×10^{-5} per reactor year (denoted as CDF_B) to 3.06×10^{-5} per reactor year (denoted as CDF_{FLEX}) (Ma, et al., 2019a).

Changes in public risk and occupational risk can be calculated using the following equations:

$$\Delta PR_{FLEX} = (CDF_B \cdot CP_{LER.B} - CDF_{FLEX} \cdot CP_{LER.FLEX}) \cdot N_{D,P} \quad (7\text{-}6)$$

$$\Delta OR_{FLEX} = (CDF_B \cdot CP_{LER.B} - CDF_{FLEX} \cdot CP_{LER.FLEX}) \cdot N_{D,O} \quad (7\text{-}7)$$

where:

$CP_{LER.B}$ = Conditional probability of LER without FLEX

$CP_{LER.FLEX}$ = Conditional probability of LER with FLEX

$N_{D,P}$ = Population dose around the reference plant (public)

$N_{D,O}$ = Population dose around the reference plant (plant workers)

Parameters $CP_{LER.B}$ and $CP_{LER.FLEX}$ are both assumed 0.1 in this case study. Regarding population doses, NUREG/CR-6349 (Mubayi, Sailor, & Anandalinam, 1995) provided average doses of five U.S. power reactors (Zion, Surry, Sequoyah, Peach Bottom, and Grand Gulf) received by the total population within 10-mile, 50-mile, 100-mile, and 1000-mile in radius around a plant. This case study selects the average population dose within 50-mile radius, which is 1.99×10^5 person rem, as the sum of $N_{D,P}$ and $N_{D,O}$, considering that a 50-mile zone around a plant is the NRC-defined ingestion-pathway emergency-planning zone and is used by NRC in regulatory action CBAs (U.S. Nuclear Regulatory Commission, 2017a). The sum of ΔPR_{FLEX} and ΔOR_{FLEX} is then calculated as 1.19E+02 person-rem per reactor year and monetized using the following equation (U.S. Nuclear Regulatory Commission, 2017a):

$$\Delta PR_{FLEX,\$,H} = \Delta PR_{FLEX} \cdot CF_H \quad (7\text{-}8)$$

$$\Delta OR_{FLEX,\$,H} = \Delta OR_{FLEX} \cdot CF_H \quad (7\text{-}9)$$

where:

$\Delta PR_{FLEX,\$,H}$ = Monetized public risk changes (public-health impact)

$\Delta OR_{FLEX,\$,H}$ = Monetized occupational risk changes (occupational-health impact)

CF_H = Dollar per person-rem conversion factor for health impact

Regarding parameter CF_H, (U.S. Nuclear Regulatory Commission, 2015) provided an estimate of $5,100 (August 2015 dollars) per person-rem as monetary equivalent. This case study adopts this estimate and inflates it to $5,523.70 (March 2020 dollars) using the consumer price index inflation calculator provided by (U.S. Bureau of Labor Statistics, 2020). Besides health impacts, this case study also monetizes societal impact using the following equation:

$$\Delta PR_{FLEX,\$,S} = (CDF_B \cdot CP_{LER.B} - CDF_{FLEX} \cdot CP_{LER.FLEX}) \cdot CF_S \quad (7\text{-}10)$$

where:

$\Delta PR_{FLEX,\$,S}$ = Monetized public-risk changes (societal impact)

CF_S = Dollar per accident-conversion factor for societal impact

Regarding parameter CF_S, (Denning & Mubayi, 2017) provided an estimate of $38 billion (June 2012 dollars) per accident. This case study adopts this estimate and inflates it to $42.74 billion (March 2020 dollars) per accident. The sum of $\Delta PR_{FLEX,\$,H}$, $\Delta OR_{FLEX,\$,H}$, and $\Delta PR_{FLEX,\$,S}$ is estimated as $2.6E+03 per

reactor year. The changes in public risk and occupational risk associated with plant coping-capability enhancement and their monetized values are summarized in Table 7-4.

Table 7-4. Changes in Evaluation Criteria Associated with Plant Coping-Capability Enhancement.

No.	Evaluation Criteria	Changes in Evaluation Criteria		Changes in Evaluation Criteria (monetized)	
		Value	Unit	Value	Unit
1	Public risk and occupational risk	1.2E+02	person rem per reactor year	2.6E+03	$ per reactor year

3. Criteria Changes Associated with SDP

This subsection calculates changes in SDP-associated regulatory cost due to plant-risk reduction. SDP is a representative risk-informed process in which the NRC staff determine safety significance of inspection findings by assessing their impacts on plant CDF or conditional core damage probability (CCDP) (U.S. Nuclear Regulatory Commission, 2016b). The significance of an inspection finding, characterized using delta CDF or delta CCDP, is represented by one of four colors (i.e., green, white, yellow, red) and could act as an input of the reactor oversight process where the NRC staff determine the appropriate responses to inspection findings based on their significances (U.S. Nuclear Regulatory Commission, 2014). The SDP color zones and associated NRC actions are shown in Table 7-5 (U.S. Nuclear Regulatory Commission, 2014; U.S. Nuclear Regulatory Commission, 2016b).

Table 7-5. SDP Color Zones and Associated NRC Actions.

	SDP Color Zone			
	Green	White	Yellow	Red
Delta CDF (per reactor year)	$\leq 1 \times 10^{-6}$	$(1 \times 10^{-6}, 1 \times 10^{-5}]$	$(1 \times 10^{-5}, 1 \times 10^{-4}]$	$\geq 1 \times 10^{-4}$
Safety significance	Very low	Low to moderate	Substantial	High
NRC action matrix	Column I	Column II	Column III	Column IV
NRC increased oversight/inspection	None	Special inspection	Augmented inspection	Incident investigation

It can be observed from Table 7-5 that the NRC action level increases with the increase of safety significance, which will, in turn, result in higher regulatory costs. FLEX implementation could help lower this cost by enhancing plant coping capability and lowering plant baseline CDF (explained in Section 0). For the same inspection finding, delta CDF would decrease with the decrease in plant baseline CDF and the safety significance will either remain in the current or move to a less-severe color zone. The impact of baseline CDF on finding significance has been demonstrated in (Ma, et al., 2019a), analyzing the significance of a degraded condition (an emergency diesel generator failed to start and was inoperable for 9 days) in a generic plant and found that, due to a reduction of plant baseline CDF (from 3.12×10^{-5} per reactor year to 3.06×10^{-5} per reactor year), the significance of this degraded condition was reduced from "low to moderate (white)" to "very low (green)." This case study assumes that, by crediting FLEX equipment and reducing plant baseline CDF, the significance of each SDP finding could be reduced one level (e.g., a finding in the red zone is moved to the yellow zone). Changes in regulatory cost associated with SDP, denoted as $\Delta C_{Reg,SDP}$, are then calculated using the following equations:

$$\Delta C_{Reg,SDP} = C_{Reg,SDP,B} - C_{Reg,SDP,FLEX} \quad (7\text{-}11)$$

$$C_{Reg,SDP,B} = \sum_{i=R,Y,W} f_{ISP,i,B} \cdot (c_{ISP,i} + c_{prior-ISP,i} + c_{post-ISP,i}) \cdot (1 + F_{PPE}) \quad (7\text{-}12)$$

$$C_{Reg,SDP,FLEX} = \sum_{i=R,Y,W} f_{ISP,i,FLEX} \cdot (c_{ISP,i} + c_{prior-ISP,i} + c_{post-ISP,i}) \cdot (1 + F_{PPE}) \quad (7\text{-}13)$$

$$f_{ISP,i,B} = N_{SDP,i,B}/(T_{SDP} \cdot n_{R,SDP}) \quad (7\text{-}14)$$

$$f_{ISP,i,FLEX} = N_{SDP,i,FLEX}/(T_{SDP} \cdot n_{R,SDP}) \quad (7\text{-}15)$$

$$c_{ISP,i} = c_{prior-ISP,i} + c_{post-ISP,i} = c_{REG} \cdot S_i \cdot L_i \quad (7\text{-}16)$$

where:

$C_{Reg,SDP,(\cdot)}$ = Annual regulatory costs associated with SDP

(B = before crediting FLEX; FLEX = after crediting FLEX)

i = Color index of SDP zones (R = Red, Y = Yellow, W = White)

$f_{ISP,i,(\cdot)}$ = Frequency of inspection in response to findings in color zone i

F_{PPE} = Factor of associated plant personnel efforts vs. NRC inspector efforts

$c_{ISP,i}$ = Inspection cost per inspection in response to a finding in color zone i

$c_{prior-ISP,i}$ = Preparation cost per inspection in response to a finding in color zone i

$c_{post-ISP,i}$ = Assessment and documentation cost per inspection for a finding in color zone i

c_{REG} = Average inspection cost per professional staff hour

S_i = Team size for an inspection in response to a finding in color zone i

L_i = Duration of inspection in response to a finding in color zone i

T_{SDP} = Time horizon of SDP finding statistics

$n_{R,SDP}$ = Number of operating reactor units within time horizon T_{SDP}

$N_{SDP,i,(\cdot)}$ = Number of SDP findings in color zone i within time horizon T_{SDP}

This case study conducts a statistical analysis on the notices of violation (NOVs) issued by NRC to reactor licenses and finds that, between 1996 and 2019, NRC has issued seven NOVs for red SDP finding, 17 NOVs for yellow SDP finding, and 218 NOVs for white SDP finding (U.S. Nuclear Regulatory Commission, 2017e). These results are assigned to parameters $N_{SDP,R,B}$, $N_{SDP,Y,B}$, and $N_{SDP,W,B}$, respectively. Parameter T_{SDP} is assigned 24 years calculated from the time period between 1996 and 2019. Parameter $n_{R,SDP}$ is assigned 109, which is the number of operating reactor units within time horizon T_{SDP}. As this case study assumes the significance of each SDP finding can be reduced one level by crediting FLEX, parameters $N_{SDP,R,FLEX}$, $N_{SDP,Y,FLEX}$, $N_{SDP,W,FLEX}$ are assumed as 0, 7, 17, respectively.

When calculating labor per NRC action in response to SDP finding, this case study breaks down the efforts of NRC inspectors into three parts (inspection, pre-inspection preparation, and post-inspection documentation) and assumes that inspection effort equals the sum of pre- and post-inspection efforts. This case study further assumes that an inspection in response to white SDP finding requires a team of $S_W = 5$ staff with a duration of $L_W = 16$ hours; similarly, S_Y and L_Y are assumed 10 staff and 24 hours, and S_R and L_R are assumed 15 staff and 40 hours. Average inspection cost per professional staff hour, c_{REG}, is $281.51 per staff hour (March 2020 dollars), which is inflated from $275 per staff hour (August 2018 dollars) provided in (U.S. Nuclear Regulatory Commission, 2018b). Besides NRC inspectors' efforts, this case study also accounts for the efforts of plant personnel in response to the NRC inspection, which is assumed five

times of NRC inspectors' efforts and addressed using parameter $F_{PPE} = 5$. The changes in regulatory cost associated with SDP are calculated and shown in Table 7-6.

Table 7-6. Changes in Evaluation Criteria Associated with SDP.

No.	Evaluation Criteria	Changes in Evaluation Criteria	
		Value	Unit
1	Regulatory cost	2.9E+04	$ per reactor year

4. Criteria Changes Associated with TSSDs

This subsection calculates changes in plant revenue and regulatory cost associated with TSSDs. If an equipment in an NPP becomes unavailable or inoperable, the equipment must be restored or repaired within the equipment-specific CT according to plant-specific technical specification (TS); if not restored or repaired within CT, the plant must take actions required by TSs such as to proceed to plant down-power or shutdown. Completion times may be permanently or temporarily extended if it can be justified that a proposed CT extension could meet all the five key principles specified in Regulatory Guide 1.177, one of which requires that the impact of proposed CT extension on plant risk should be small (for permanent extension) or acceptable (for temporary extension) (U.S. Nuclear Regulatory Commission, 2011b). Besides such risk-informed CT extensions, NOED request is another way of seeking temporary CT extensions given unanticipated CT noncompliance if it can be demonstrated that a proposed CT extension will result in no net increase in plant risk (U.S. Nuclear Regulatory Commission, 2012b).

The above two processes are both informed by plant risk. As FLEX implementation could reduce plant risk, this case study assumes that, by crediting FLEX, more CT extension requests can be approved and the annual average number of events with violated completion times can be reduced. This case study further assumes that, given an unanticipated, temporary CT-violation event, the conditional probability of qualifying and filing an NOED request can be increased. In addition, it is assumed that, given a filed NOED request, conditional probability of granting a NOED can be increased. Based on these assumptions, FLEX implementation could potentially bring plant revenue increase (denoted as ΔR_{TSSD}) by avoiding TSSDs and regulatory cost savings (denoted as $\Delta C_{Reg,NOED}$) by reducing efforts in evaluating CT-violation events, and filing and reviewing NOED requests.

The changes in plant revenue are calculated using the following equations:

$$\Delta R_{TSSD} = \left(f_{TSSD,B} - f_{TSSD,FLEX}\right) \cdot T_{SD} \cdot P \cdot ER \quad (7\text{-}17)$$

$$f_{TSSD,B} = N_{TSSD,B}/(T_{TSSD} \cdot n_{R,TSSD}) \quad (7\text{-}18)$$

$$f_{TSSD,FLEX} = N_{TSSD,FLEX}/(T_{TSSD} \cdot n_{R,TSSD}) \quad (7\text{-}19)$$

where:

$f_{TSSD,x}$ = Frequency of TS-required reactor shutdowns

T_{SD} = Average reactor downtime per TS-required shutdown

P = Reactor electrical capacity

ER = Unit electricity sales revenue

T_{TSSD} = Time horizon of TS-required reactor shutdown statistics

$n_{R,TSSD}$ = Number of operating reactor units within T_{TSSD}

$N_{TSSD,x}$ = Number of TS-required reactor shutdowns within T_{TSSD}

This case study assumes that a CT-violation event will lead to one of three situations: (1) no NOED request is filed and TS-required reactor shutdown is performed, (2) NOED request is filed and approved and reactor

shutdown is avoided, (3) NOED request is filed and approved; however, equipment restoration or repair cannot be completed within extended CT, and reactor shutdown is performed. Based on these situations, $N_{TSSD,B}$ is calculated as:

$$N_{TSSD,B} = N_{CTV,B} - N_{NOED,B} + N_{TSSD,NOED,B} \quad (7\text{-}20)$$

where:

$N_{CTV,B}$ = Number of events with violated completion times within T_{TSSD} before crediting FLEX

$N_{NOED,B}$ = Number of issued NOEDs within time horizon T_{TSSD} before crediting FLEX

$N_{TSSD,NOED,B}$ = Number of TS-required shutdowns with approved NOEDs within T_{TSSD} before crediting FLEX

Given a CT-violation event, a plant will first evaluate whether the event's risk impact meets the requirements for filing a NOED request; if not, the plant may directly perform the TS-required actions, such as reactor shutdown. If a NOED request is filed out, it is still subject to NRC's approval. This case study calculates conditional probabilities of filing and approving NOED requests as:

$$CP_{NOEDF,B} = 1 - \frac{(N_{TSSD,B} - N_{TSSD,NOED,B}) \cdot f_1}{N_{CTV,B}} \quad (7\text{-}21)$$

$$CP_{NOEDA,B} = N_{NOED,B} / (N_{CTV,B} \cdot CP_{NOEDF,B}) \quad (7\text{-}22)$$

where:

$CP_{NOEDF,B}$ = Conditional probability of filing a NOED, given an event with violated CT before crediting FLEX

$CP_{NOEDA,B}$ = Conditional probability of approving a received NOED request before crediting FLEX

f_1 = Fraction of shutdowns without filing NOED in all TS-required shutdowns

The impacts of FLEX implementation on the annual average number of CT-violation events and probabilities of qualifying and filing NOED request are formulated are reduction factor and improvement factors, respectively, and shown in the following equations:

$$N_{CTV,FLEX} = (1 - RF_1) \cdot N_{CTV,B} \quad (7\text{-}23)$$

$$CP_{NOEDF,FLEX} = IF_1 \cdot CP_{NOEDF,B} \quad (7\text{-}24)$$

$$CP_{NOEDA,FLEX} = IF_2 \cdot CP_{NOEDA,B} \quad (7\text{-}25)$$

where:

$N_{CTV,FLEX}$ = Number of events with violated completion times within T_{TSSD} after crediting FLEX

$CP_{NOEDF,FLEX}$ = Conditional probability of filing a NOED, given an event with violated CT after crediting FLEX

$CP_{NOEDA,FLEX}$ = Conditional probability of approving a received NOED request after crediting FLEX

RF_1 = Reduction factor of events with violated completion times by crediting FLEX

IF_1 = Improvement factor of filing NOED conditional probability after crediting FLEX

IF_2 = Improvement factor of approving NOED conditional probability after crediting FLEX

$N_{TSSD,FLEX}$ is then calculated as:

$$N_{TSSD,FLEX} = N_{CTV,FLEX} \cdot [1 - CP_{NOEDF,FLEX} + CP_{NOEDF,FLEX} \cdot (1 - CP_{NOEDA,FLEX})] \quad (7\text{-}26)$$

where:

$N_{CTV,FLEX}$ = Number of events with violated completion times within T_{TSSD} after crediting FLEX

$N_{NOED,FLEX}$ = Number of issued NOEDs within time horizon T_{TSSD} after crediting FLEX

The changes in plant revenue can then be estimated by substituting Equations (7-18) to (7-26) into Equation (7-17). And the changes in regulatory cost can be calculated using the following equations:

$$\Delta C_{Reg,NOED} = C_{Reg,NOED,B} - C_{Reg,NOED,FLEX} \quad (7\text{-}27)$$

$$C_{Reg,NOED,B} = f_{CTV,B} \cdot c_{CTVE} + f_{NOEDF,B} \cdot (c_{NOEDF,B} + c_{NOEDA,B}) \quad (7\text{-}28)$$

$$C_{Reg,NOED,FLEX} = f_{CTV,FLEX} \cdot c_{CTVE} + f_{NOEDF,FLEX} \cdot (c_{NOEDF,FLEX} + c_{NOEDA,FLEX}) \quad (7\text{-}29)$$

$$f_{CTV,B} = N_{CTV,B}/(T_{TSSD} \cdot n_{R,TSSD}) \quad (7\text{-}30)$$

$$f_{CTV,FLEX} == N_{CTV,FLEX}/(T_{TSSD} \cdot n_{R,TSSD}) \quad (7\text{-}31)$$

$$f_{NOEDF,B} = f_{CTV,B} \cdot CP_{NOEDF,B} \quad (7\text{-}32)$$

$$f_{NOEDF,FLEX} = f_{CTV,FLEX} \cdot CP_{NOEDF,FLEX} \quad (7\text{-}33)$$

where:

$f_{CTV,x}$ = Frequency of events with violated completion times

$f_{NOEDF,x}$ = Frequency of filing NOEDs

c_{CTVE} = Labor cost of evaluating an event with CT-violation

c_{NOEDF} = Labor cost of filing an NOED request

c_{NOEDA} = Labor cost of reviewing an NOED request

The parameters used for calculation of TSSD-associated changes in evaluation criteria are listed in Table 7-7. The changes in evaluation criteria are shown in Table 7-8.

Table 7-7. Parameters for Calculations of ΔR_{TSSD} and $\Delta C_{Reg,NOED}$.

Parameter	Unit	Value*	Reference
T_{SD}	hour	72	-
P	MWe per reactor	1,000	-
ER	$ per MWh	106**	(U.S. Energy Information Administration, 2020)
T_{NOED}	year	19	(U.S. Nuclear Regulatory Commission, 2019c) (start: 2000, end: 2018)
$n_{R,NOED}$	reactor	103	(U.S. Nuclear Regulatory Commission, 2019c)
$N_{NOED,B}$	-	169	(U.S. Nuclear Regulatory Commission, 2019c)
$N_{TSSD,B}$	-	209	(U.S. Nuclear Regulatory Commission, 2019d)
$N_{TSSD,NOED,B}$	-	4	(U.S. Nuclear Regulatory Commission, 2019d)
f_1	-	0.5	-
RF_1	-	0.5	-
IF_1	-	1.2	-
IF_2	-	1.2	-
c_{CTVE}	$ per CT-violation event	5,000	-
c_{NOEDF}	$ per NOED request	5,000	-
c_{NOEDA}	$ per NOED request	5,000	-

* Assumed if not specified.

** Average price of electricity to ultimate customers, all end-use sectors (residential, commercial, industrial, transportation), 2019 annual total.

Table 7-8. Changes in Evaluation Criteria Associated with TSSDs.

No.	Evaluation Criteria	Changes in Evaluation Criteria	
		Value	Unit
1	Plant revenue	-5.5E+05	$ per reactor year
2	Regulatory cost	1.1E+03	$ per reactor year

5. Criteria Changes Associated with Plant SSC TM Schedule

This subsection calculates changes in plant revenue, plant O&M cost, and occupational risk associated with changes in TM schedule of plant SSCs. Crediting FLEX could help streamline SSC TM schedule in multiple ways. By crediting FLEX, RFO duration could be reduced because (1) TMs for plant SSCs with extended completion times may be shifted from offline to online, (2) delays in core offloading could be reduced because FLEX equipment could act as a redundant safety-function success path and reduce outage-risk level, and (3) cooldown process at the beginning of refueling could be accelerated as FLEX equipment could be utilized to improve boration capability (Powell & Graham, 2014). This case study assumes that, by crediting FLEX, an RFO can be reduced by 2 days so that plant revenue can be increased. The changes in plant revenue due to shorter RFO, denoted as ΔR_{RFO}, are calculated as:

$$\Delta R_{RFO} = \Delta RFO \cdot 24 \cdot (\frac{1}{RI}) \cdot P \cdot ER \quad (7\text{-}34)$$

where:

ΔRFO = Reduced duration of a RFO by crediting FLEX, assumed as 2 days

RI = Refueling interval assumed as 1.5 years, which is a typical worldwide refueling interval (World Nuclear Association, 2017)

Additionally, crediting FLEX could enhance plant coping capability and reduce plant baseline CDF; this could lead to reduction in risk importance and risk-informed safety class (RISC) of plant SSCs specified in 10 Code of Federal Regulations (CFR) Part 50.69 (U.S. Nuclear Regulatory Commission, 2017f). Some RISC-1 and RISC-2 SSCs could potentially be recategorized as RISC-3 or 4 and be exempt from a set of special treatment requirements. Westinghouse Owners Group provided a generic estimate that the implementation of 10 CFR 50.69 could lead to savings in multiple areas, such as in-service inspection (ISI), in-service testing (IST), maintenance-rule efforts, procurement and administrative savings, with a total of $1.1E+06 per reactor year (2002 dollars) reduction in plant O&M cost (Westinghouse Owners Group, 2002). This case study assumes that, by crediting FLEX and recategorizing plant SSCs, the plant O&M cost can be further reduced by 5%, which is $7.86E+04 per reactor year (2020 dollars) denoted as $\Delta C_{O\&M,RISC}$. It is to be noted that the implementation of 10 CFR 50.69 could lead to reduction in occupational doses as well due to less-frequent ISIs and ISTs. Southern Nuclear provided an example that, due to implementation of 10 CFR 50.69, the containment spray pump was categorized as RISC-3, and the IST interval was changed from 18 months to 54 months (Mulvehill, 2015). This case study assumes that, by crediting FLEX and recategorizing plant SSCs, ISI and IST frequencies for 10 plant SSCs can be reduced to one third. The associated reduction in occupational risk (denoted as ΔOR_{RISC}) is calculated as:

$$\Delta OR_{RISC} = (\frac{1}{T_{ISIT}}) \cdot ET_{ISIT} \cdot DR_{ISIT} \cdot S_{ISIT} \cdot 10 \cdot (1 - \frac{1}{3}) \quad (7\text{-}35)$$

where:

T_{ISIT} = Average interval of ISI or testing, assumed as 1.5 years

ET_{ISIT} = Average exposure time per ISI or testing, assumed as 2 hours

DR_{ISIT} = Average dose rate per ISI or testing, assumed as 0.1 rem per hour

S_{ISIT} = Average team size per ISI or testing, assumed as 2

The calculated changes in plant revenue, O&M cost, and occupational risk are shown in Table 7-9.

Table 7-9. Changes in Evaluation Criteria Associated with Plant SSC TM Schedule.

No.	Evaluation Criteria	Changes in Evaluation Criteria		Changes in Evaluation Criteria (monetized)	
		Value	Unit	Value	Unit
1	Plant revenue	-3.4E+06	$ per reactor year	-	-
2	O&M cost	7.9E+04	$ per reactor year	-	-
3	Occupational risk	1.8E+00	person rem per reactor year	9.8E+03	$ per reactor year

7.4.3 Step 3: CBA for FLEX Deployment

7.4.3.1 BCR Estimation

This subsection estimates two types of BCRs of implementing FLEX, including a calculated BCR based on calculated costs and benefits and a perceived BCR based on perceived costs and benefits, using the following equations adapted from (Cha & Ellingwood, 2019):

$$BCR_{Calc.} = \frac{\sum_i C_{L,i} \cdot (p_{0,L,i} - p_{1,L,i})}{\sum_j C_{I,j} \cdot (p_{0,I,j} - p_{1,I,j})} \quad (7\text{-}36)$$

$$BCR_{Perc.} = \frac{\sum_i |V(C_{L,i})| \cdot (w(p_{0,L,i}) - w(p_{1,L,i}))}{\sum_j |V(C_{I,i})| \cdot (w(p_{0,I,j}) - w(p_{1,I,j}))} \quad (7\text{-}37)$$

where:

$BCR_{Calc.}$ = Calculated BCR

$BCR_{Perc.}$ = Perceived BCR

i = Benefit element index

j = Cost element index

C_I = Cost of implementing FLEX

C_L = Potential loss that can be avoided by implementing FLEX

$p_{(\cdot)}$ = Probability of potential loss

(0 = without FLEX implementation; 1 = with FLEX implementation)

$V(\cdot)$ = Value function

$w(\cdot)$ = Probability weighting function

$|\cdot|$ = Absolute value

Estimation of $BCR_{Calc.}$ is based on the sum of multiple economic consequences, each weighted by its likelihood change; such estimation presumes a linear relationship between calculated and perceived values of likelihood or consequence. In practical cases, however, such ideal linear relationships may not hold. (Tversky & Kahneman, 1992) found that people tend to overweight low probabilities and underweight moderate and high probabilities, perceive losses and gains differently, and exhibit diminishing sensitivity when losses or gains increase; the CPT was then proposed to reflect the nonlinearities between calculated and perceived likelihood or consequence due to a DM's risk preference in his or her perception. Estimation of $BCR_{Perc.}$, developed from CPT, separately examines hazard likelihood and consequence and converts their calculated values to perceived values through probability weighting function and value function, respectively, using the following equations adapted from (Tversky & Kahneman, 1992) and (Rieger, Wang, & Hens, 2017):

$$\left|V\left(C_{(\cdot)}\right)\right| = \left|-\lambda \cdot {C_{(\cdot)}}^{\beta}\right| = \lambda \cdot {C_{(\cdot)}}^{\beta} \quad (7\text{-}38)$$

$$w\left(p_{(\cdot)}\right) = \frac{{p_{(\cdot)}}^{\delta}}{[{p_{(\cdot)}}^{\delta} + (1 - p_{(\cdot)})^{\delta}]^{1/\delta}} \quad (7\text{-}39)$$

where:

λ = Parameter describing the amount of losses being perceived as larger than gains

β = Parameter describing the amount of diminishing sensitivity for losses

δ = Parameter describing the amount of overweighting small probabilities and underweighting moderate and high probabilities

The cost and benefit elements of implementing FLEX for a 20-year period are estimated in Section 7.4.2 and are summarized in Table 7-10 and Table 7-11, respectively. Except for the one-time FLEX startup cost, all the cost and benefit elements are assumed to have the potential of occurring in each of 20 years with element-specific, constant annual probabilities p_0 and p_1. The element-specific economic consequences C_I and C_L are also assumed constant each year and are converted to present value with a discount rate of 0.04. The values $|V(C_I)|$ and $|V(C_L)|$ are the sums of values of each annual-occurring cost and benefit element, respectively. CPT parameters λ, β, and δ are assigned 1.36, 0.49, and 0.71, respectively, which are the U.S. nation-level CPT parameter estimates (Rieger, Wang, & Hens, 2017). Using Equations (7-36) to (7-39), $BCR_{Calc.}$ is estimated to be 2.3 and $BCR_{Perc.}$ is estimated to be 5.4. These greater-than-one BCRs indicate that, implementing FLEX at the reference plant for 20 years creates benefits that are expected to outweigh costs.

Table 7-10. Cost Elements of Implementing FLEX for a 20-Year Period.

j	Criterion	Process	$C_{I,j}{}^*$	$\lvert V(C_{I,j})\rvert$	$p_{0,I,j}$	$w(p_{0,I,j})$	$p_{1,I,j}$	$w(p_{1,I,j})$
1	Capital cost	FLEX startup	2.5E+07	5.7E+03	0.0E+00	0.0E+00	1.0E+00	1.0E+00
2	O&M cost	FLEX TM	3.2E+04	3.7E+03	0.0E+00	0.0E+00	1.0E+00	1.0E+00

* Units for $C_{I,1}$ and $C_{I,2}$ are $ per reactor lifetime and $ per reactor year, respectively.

Table 7-11. Benefit Elements of Implementing FLEX for a 20-Year Period.

i	Criterion	Process	$C_{L,i}{}^*$	$\lvert V(C_{L,i})\rvert$	$p_{0,L,i}$	$w(p_{0,L,i})$	$p_{1,L,i}$	$w(p_{1,L,i})$
1	Public risk and occupational risk	Coping capability	4.4E+10	3.7E+06	3.1E-06	1.2E-04	3.1E-06	1.2E-04
2	Regulatory cost	SDP (Red)	2.0E+06	2.8E+04	2.7E-03	1.5E-02	0.0E+00	0.0E+00
3	Regulatory cost	SDP (Yellow)	8.1E+05	1.8E+04	6.5E-03	2.7E-02	2.7E-03	1.5E-02
4	Regulatory cost	SDP (White)	2.7E+05	1.1E+04	8.3E-02	1.5E-01	6.5E-03	2.7E-02
5	Plant revenue	TSSD	7.6E+06	5.4E+04	1.1E-01	1.7E-01	3.5E-02	8.4E-02
6	Regulatory cost	TSSD (NOED)	1.0E+04	2.1E+03	1.4E-01	2.0E-01	7.2E-02	1.3E-01
7	Regulatory cost	TSSD (CT)	5.0E+03	1.5E+03	1.9E-01	2.5E-01	9.6E-02	1.6E-01
8	Plant revenue	TM schedule	3.4E+06	3.6E+04	1.0E+00	1.0E+00	0.0E+00	0.0E+00
9	O&M cost	TM schedule	7.9E+04	5.7E+03	1.0E+00	1.0E+00	0.0E+00	0.0E+00
10	Occupational risk	TM schedule	9.8E+03	2.1E+03	1.0E+00	1.0E+00	0.0E+00	0.0E+00

* Units for all $C_{L,i}$ are $ per reactor year.

7.4.3.2 Discussions

This subsection discusses identification of cost and benefit drivers and the impact of CPT and implementation period on BCR of implementing FLEX at the reference plant.

1. Identification of Cost and Benefit Drivers

   As shown in Table 7-10 and Table 7-11, the costs and benefits of implementing FLEX consist of two and 10 elements, respectively. The elements are ranked according to their contributions in total costs and benefits in Table 7-12 and Table 7-13.

   .

Table 7-12. Cost Element Rankings of Implementing FLEX for a 20-Year Period.

j	Criterion	Process	Calculated Cost		Perceived Cost	
			% in Total	Ranking	% in Total	Ranking
1	Capital cost	FLEX startup	98.2%	1	60.9%	1
2	O&M cost	FLEX TM	1.8%	2	39.1%	2

Table 7-13. Benefit Element Rankings of Implementing FLEX for a 20-Year Period.

i	Criterion	Process	Calculated Benefit		Perceived Benefit	
			% in Total	Ranking	% in Total	Ranking
1	Public & occupational risks	Coping capability	0.1%	6	0.0%	10
2	Regulatory cost	SDP	0.1%	6	0.8%	6
3	Regulatory cost	SDP (Yellow)	0.1%	6	0.4%	7
4	Regulatory cost	SDP (White)	0.5%	4	2.5%	5
5	Plant revenue	TSSD	13.6%	2	9.4%	3
6	Regulatory cost	TSSD (NOED)	0.0%	9	0.3%	8
7	Regulatory cost	TSSD (CT)	0.0%	9	0.3%	8
8	Plant revenue	TM schedule	83.5%	1	71.1%	1
9	O&M cost	TM schedule	1.9%	3	11.2%	2
10	Occupational risk	TM schedule	0.2%	5	4.1%	4

It can be observed that, when shifting from calculated to perceived values, rankings of cost elements remain the same, and the one-time FLEX startup cost is identified as a more-critical cost driver than the FLEX equipment TM cost over 20 years. Rankings of benefit element change only slightly, and the top three benefit drivers, under both cases, include plant-revenue increase due to shortened RFO duration (Element 8), plant-revenue increase due to avoided TSSDs (Element 5), and plant O&M cost reduction due to SSCs recategorized as lower RISCs (Element 9). Recall that FLEX is primarily designed to mitigate accidents. If limiting FLEX credit to accident mitigation, only the benefits due to CDF reduction or through risk-informed activities can be achieved. Except for Element 8, all benefit elements are either directly or indirectly a result from CDF reduction with a total contribution of 29% in perceived benefits. This indicates that exploring additional FLEX credit to streamline plant SSC TM schedule and shorten RFO duration could bring substantial additional benefits, which can be 2.5 times the benefits of crediting FLEX for accident mitigation only. It can also be observed that the benefits directly due to risk reduction are relatively small (Element 1, contributing less than 0.1% in total perceived benefit) and the benefits associated with risk reduction are mainly indirectly achieved through implementing risk-informed activities (Elements 2–7, 9, and 10, contributing 29% in total perceived benefit).

2. Impacts of Implementation Time Period and CPT on BCR

   The BCR of implementing FLEX depends on how long the FLEX implementation is and whether CPT is utilized. The BCRs with implementation time from 1 to 40 years, with or without CPT, are estimated and shown in Figure 7-4.

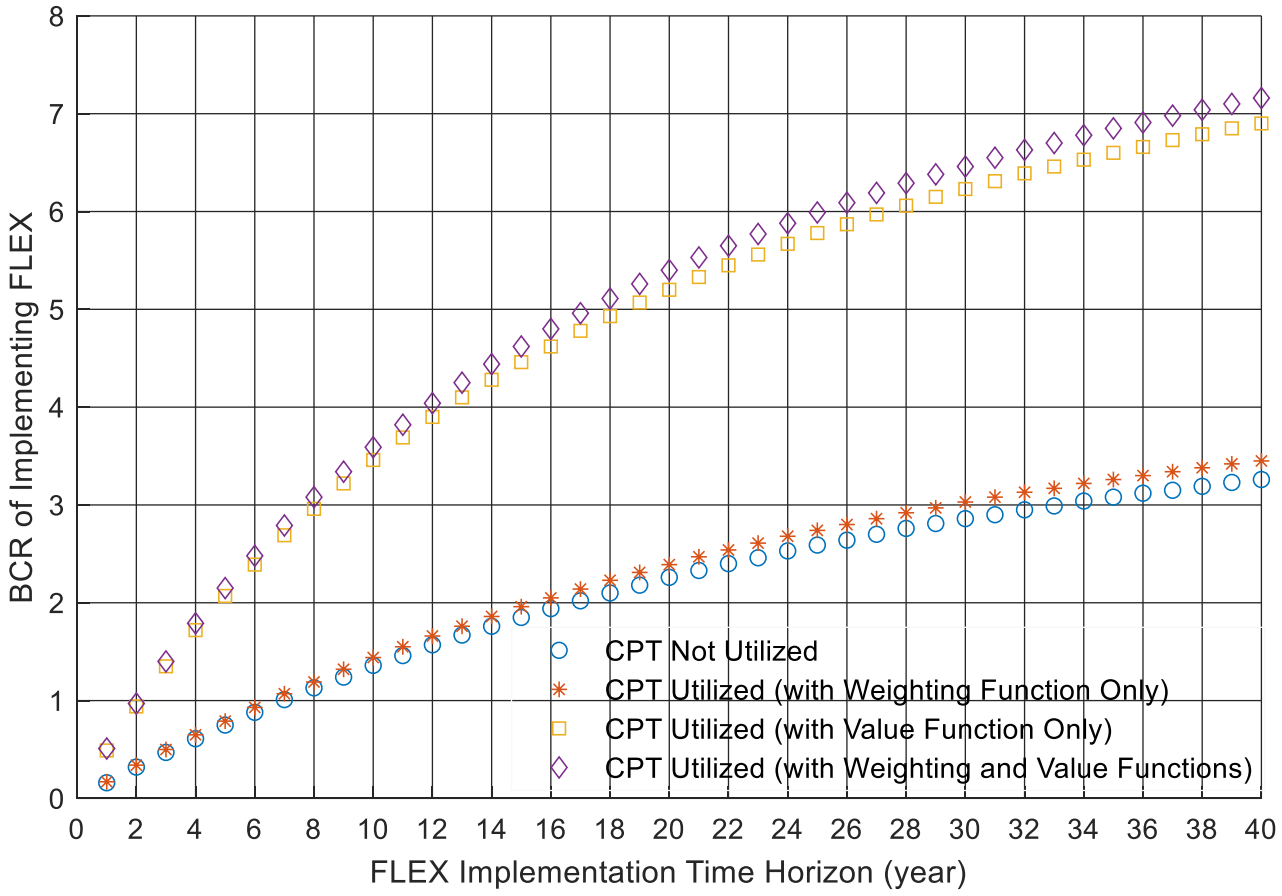

Figure 7-4. BCRs of implementing FLEX with and without CPT over different implementation times.

It can be observed that the BCR of implementing FLEX increases when the implementation time increases. The payback period to reach the break-even point where benefit equals cost is between 6 and 7 years, based on calculated BCR (without CPT utilization), and the payback period, based on perceived BCR (with CPT utilization), is between 2 and 3 years. In other words, if FLEX can be implemented at the reference plant for a period longer than the payback period, the benefit of implementing FLEX is projected to outweigh its cost. The maximal calculated and perceived BCRs are 3.3 and 7.2, both of which are obtained from a 40-year implementation period. It can also be observed that perceived BCRs are greater than calculated BCRs at all times. This difference is dominated by the impact of value function, which reflects a DM's diminishing sensitivity as losses increase. Weighting function, which reflects a DM's overweighting small probabilities and underweighting moderate and high probabilities, also affects the BCR, but the impact is relatively small.

7.5 Summary of Multicriterion Benefit Evaluation

This section proposes the MCBE methodology for conducting multicriterion, multicontext cost and benefit evaluations for safety enhancements in NPPs. The MCBE methodology provides a way to quantify safety and economic benefits and explicitly model the correlations and causations between these two. The MCBE methodology is also capable of quantitatively reflecting a DM's risk preferences toward hazard likelihood and consequence using CPT. The case study of implementing FLEX at the reference plant demonstrates the feasibility of proposed MCBE methodology and the BCRs, given that different implementation time periods with and without CPT are calculated. The case study results indicate that:

- FLEX implementation costs: The dominant cost of implementing FLEX is the one-time, startup expense for purchasing and installing FLEX equipment, building protected structures to store FLEX equipment, developing associated procedures and trainings, conducting associated calculations, etc. Besides the one-time expense, the reference plant will incur annual expenses for FLEX equipment TM, but such annual cost is estimated to be substantially outweighed by the annual benefits of implementing FLEX.
- FLEX implementation benefits: It is observed that over 70% of benefits are achieved by crediting FLEX to streamline the plant TM schedule and shortening RFO duration. Other benefits are achieved from plant risk reduction due to plant accident coping-capability enhancement. These results suggest that, although FLEX is primarily designed to cope with accidents, it would be beneficial to explore additional FLEX credit in plant O&M efficiency improvement.
- FLEX implementation BCR: The BCR of implementing FLEX increases as the implementation time period increases. If FLEX can be implemented at the reference plant for a period longer than the payback period, the benefits of implementing FLEX is expected to outweigh the costs. The payback periods to reach the break-even point where benefits equal costs are estimated to be between 2 and 3 years if utilizing CPT and between 6 and 7 years if not utilizing CPT. If using 40 years as the maximal implementation time horizon, the maximal BCRs that can be achieved are estimated to be 7.2 if utilizing CPT and 3.26 if not utilizing CPT.

Also, note that the research presented in this section is subject to the following two limitations. Future research efforts will be dedicated to relaxing these limitations:

- Data limitation: The case study results in this section are generic results based on the PRA model of a generic PWR plant, and a significant portion of the parameters are estimated based on industry-average performance of U.S. power reactor fleet. This limitation could be relaxed by replacing generic data with plant-specific data, if available.
- Time resolution limitation: In this section, MCBE methodology demonstrates its capability to address the long time-frame impacts on BCR estimation (i.e., safety-enhancement implementation time periods, measured in years), but does not address the short time-frame impacts (i.e., accident progression timing, measured in hours, minutes, or even seconds). To relax this limitation, an interface between MCBE methodology and dynamic PRA needs to be developed to drive TH calculations and simulate plant responses and human actions.

8. BWR FUEL ROD BURSTING POTENTIAL EVALUATION USING BISON

8.1 Introduction

Fuel-rod behavior during accidents and transients is one of the major safety issues for LWRs. ATF fuel rods such as FeCrAl cladding have been designed to have similar or improved thermo-mechanical behavior in normal operation and provide increased coping time during design-basis accidents (DBAs) and beyond DBAs. A key aspect in the assessment of the ATF designs is the determination of potential increases in coping time with respect to traditional UO_2 fuel and Zircaloy cladding materials. Assessing the time to failure for FeCrAl cladding during an accident provides a means of comparing the failure or burst performance of FeCrAl and Zircaloy under the same or similar accident conditions.

After the Fukushima Daiichi NPP accident, SBO has been widely recognized as one of the most severe postulated events and the fuel-rod behavior should be effectively evaluated in the operations of NPPs. However, the studies on fuel-rod performance such as the cladding failure under SBO are still scarce. In this study, simulations are carried out using FeCrAl and Zircaloy claddings to facilitate comparisons between traditional cladding and the proposed accident tolerant FeCrAl cladding under an STSBO.

This section presents the fuel performance analysis for the ATF design with the BISON code. BISON is currently being validated against a wide variety of integral LWR fuel-rod experiments. Unlike the simplified fuel-rod deformation model used in RELAP5-3D, BISON provides more mechanistic modeling of the fuel-rod bursting. For instance, BISON has been developing the capability to model ATF fuel rods, including FeCrAl cladding, Cr-coated cladding and U_3Si_2 fuel. In this report on the ATF fuel modeling and simulations with the BISON code, the focus is on the FeCrAl cladding. In fact, BISON's capability for the FeCrAl cladding includes models for thermophysical properties as a function of temperature, volumetric swelling, and oxidation. Thermophysical properties include the thermal conductivity, specific heat, Young's modulus, Poisson's ratio, yield stress, ultimate tensile strength (UTS), and coefficient of linear thermal expansion. These empirical models are based upon the existing data for the either C35M or APMT^{TM} alloy (Gamble, K.A., et al., 2017).

8.2 Cladding Failure Models in BISON

During an accident situation such as SBO or LOCA, internal pressurization and high temperature are anticipated to eventually induce cladding overstress. The combination effect of the outward creep deformation of the cladding tube leading to cladding ballooning and the overstress under the effect of internal pressurization and high temperature may eventually drive failure due to burst. There are also other thermo-mechanical mechanisms which may lead to cladding burst. However, regardless of the type of the adopted thermo-mechanical model, a failure criterion for clad during transient conditions is required to analyze the fuel-rod behavior under accident conditions. Due to the large uncertainty affecting the experimental data, the choice of the criterion may not be unique. BISON offers four different options for failure criterion for Zircaloy cladding and two different options for failure criterion for FeCrAl cladding.

8.2.1 Zircaloy Cladding Failure Models in BISON

The traditional cladding for fuel rods is Zirconium-based alloys. Criteria to determine the occurrence of cladding failure or burst (rupture) of this cladding material are available in BISON (Pastore, G., et al., 2015). More precisely, the cladding burst of Zircaloy claddings during accident conditions such as SBO or LOCA can be predicted by use of four different burst criteria: overstrain, overstress (OS), plasticity instability (PI), and the combination of OS/PI. These four correlations are described in paragraphs below.

1. Overstress criterion

When the overstress burst criterion is used, it is assumed that failure will occur when the local hoop stress (or tangential stress) σ_θ exceeds a limiting burst stress σ_b (Erbacher, F.J., et al., 1982):

$$\sigma_\theta \geq \sigma_b \tag{8-1}$$

The burst stress σ_b depends on the temperature and oxygen concentration in the cladding, which is defined as:

$$\sigma_b = a * e^{(-bT)} * e^{[-(\frac{\eta-\eta_0}{9.5*10^{-4}})^2]} \tag{8-2}$$

where T (K) is temperature, η is the current weight fraction of oxygen picked up in the cladding, and a and b are material dependent constants. A set of constants based on an evaluation of Zircaloy-4 high-temperature burst data by Erbacher et al. (Erbacher, F.J., et al., 1982) is listed in Table 8-1. The values for the parameters a and b are given in the table for material parameters depending on phase. In the mixed phase (α+β) region, linear interpolations of ln(a) and b are made between the values for pure α and middle of α+β (50%α 50%β) phase, and between 50%α 50%β and pure β phase.

Table 8-1. Material parameters used to calculate the burst stress of Zircaloy-4.

Zr Phase	Temperature region (K)	a (MPa)	b (K^{-1})
α	$< T_\alpha = 1085$	830	$1 \cdot 10^{-3}$
50%α–50%β	$T_{\alpha\beta} = 1166$	3000	$3 \cdot 10^{-3}$
β	$> T_\beta = 1248$	2300	$3 \cdot 10^{-3}$

The current oxygen weight fraction η may be determined through:

$$\eta = \frac{2r_{clad,\,outer}}{\rho_{Zy*}\left(r^2_{metal,\,outer} - r^2_{clad,\,inner}\right)} \times g + \eta_0 \tag{8-3}$$

in which η_0=1.2·10^{-3}, is the oxygen weight fraction at fabrication. Note that the burst stress depends on temperature and oxygen content and may change significantly under accident conditions.

Under low-stress situations, cladding burst may still occur due to plastic instability such as high strain rate or large augmented strain, in which the overstress criterion may lead to unsafe predictions, as stated by Marcello et al. (Di Marcello, V., et al., 2014). To overcome this drawback with the overstress failure criterion, a plastic instability criterion was developed.

2. Plastic Instability Criterion

The plasticity instability criterion is based on the strain rate limitation. It can be triggered upon attaining a limiting value for the effective plastic (including creep and plasticity) strain rate:

$$\dot{\varepsilon}_{pl,eff} \geq \dot{\varepsilon}_b \tag{8-4}$$

in which $\dot{\varepsilon}_{pl,eff}$ is the effective plastic strain rate and $\dot{\varepsilon}_b$is the limiting strain rate. In BISON, the limiting value $\dot{\varepsilon}_b = 100\ h^{-1} \cong 2.78 * 10^{-2} s^{-1}$ is adopted from data by Marcello et al. (Di Marcello, V., et al., 2014).

3. Combined Failure Criterion

A combination of overstress and plastic instability criteria establishes that cladding burst occurs when either condition of overstress or plastic instability is fulfilled. The combined failure criterion is recommended, especially in low-stress situations when the load on the cladding changes relatively suddenly such as during a power ramp or scram. Thus, the prediction of failure occurrence avoids unsafe predictions in low-stress situations as a consequence of non-negligible strain rate. These three ballooning/burst models implemented in BISON have been validated to several separate effects of ballooning/burst tests (Pastore, G., et al, 2016;

Pastore, G., et al., 2017). In general, the combination of OS/PI criteria is recommended as the failure criterion for Zircaloy cladding during transient conditions.

4. Overstrain Burst Criterion

   In postulated accident conditions, the mechanical deformation of the cladding can be large due to large strain, which is another kind of plastic instability. Cladding burst can also be studied through an overstrain criterion, in which cladding burst occurs once the permanent engineering total hoop strain (i.e., creep) exceeds 40%. In BISON, the true strain is used and therefore the permanent engineering hoop strain limit is converted through:

$$\varepsilon_{hoop,limit} = ln(1.0 + 0.4) = 33.6\% \quad (8\text{-}5)$$

   where burst occurs if $\varepsilon_{hoop} \geq \varepsilon_{hoop,limit}$. Note that this overstrain burst criterion for Zircaloy cladding is overly too simplified and the effect of temperature is not considered. For more realistic studies of the burst mechanism, the overstrain model is not recommended.

8.2.2 FeCrAl Cladding Failure Models in BISON

1. UTS Criterion

   For the UTS criterion for FeCrAl cladding, failure occurs when the hoop stress in any finite element within the cladding exceeds the UTS. The UTS burst criterion of FeCrAl alloy C35M as a function of temperature is illustrated as piecewise functions in Figure 1. The plot is adapted from (Gamble, K.A., et al., 2017). At low temperatures, the UTS provides a good failure criterion as compared to experimental data. As the temperatures is higher than 800K, failure will occur in a brittle fashion since little ductility remains. It is also apparently that in the mid-range temperature (800–1050 K), the prediction from the UTS burst criterion is conservative. However, at high temperature above 1050 K, it is observed that the prediction is overestimated with respect to experimental data.

2. INL Burst Criterion

   In order to overcome the deficit of UTS burst model and more suitably to capture the failure behavior of FeCrAl observed in experiments, a more realistic cladding failure criterion model was developed at INL (Gamble, K.A., et al., 2017) for BISON. Correspondingly, this novel model will be utilized to study the thermo-mechanical behavior of full-length fuel rods with the FeCrAl cladding. The INL burst criterion of FeCrAl alloy C35M as a function of temperature is shown as piecewise functions in Figure 8-1.

   Unlike the simplified fuel-rod deformation model used in RELAP5-3D which is based on the melting point of cladding material, BISON provides more mechanistic modeling of the fuel-rod bursting. Note that these failure criteria implemented in BISON are purely empirical, which means that they are either too simplified as with the overstrain failure criterion for Zircaloy cladding or derived by fitting correlations to different set of experientially measured data on cladding burst as with other three criteria. The choice of the criterion should not be unique among those burst criteria, since it is inevitable that there are a large amount of uncertainty affecting the experimental data. The evolution of thermo-mechanical behavior for full-length BWR fuel rods under an STSBO condition is simulated and the point in time when cladding burst occurs is evaluated through the BISON simulations.

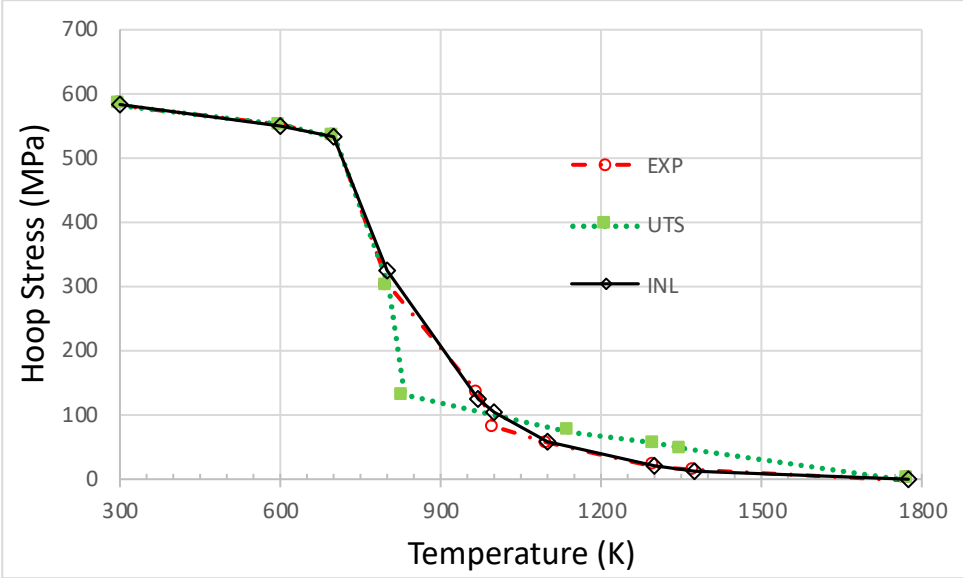

Figure 8-1. UTS and INL burst criteria as a function of temperature for FeCrAl alloy C35M along with the experimental data. Zero hoop stress at the melting point (1773 K) of C35M was used.

8.3 Methods and Boundary Conditions

The main parameters to simulate full-length BWR fuel rods of UO_2 fuel with Zircaloy cladding and FeCrAl cladding are listed in Table 8-2. Specifically, UO_2 fuel is used in this generic BWR NPP design. The total active fuel column length is 3.6891 m, which is slightly distinguished from the commonly used value 3.658 m. As listed in Table 8-2, the cold plenum length is 177.8 mm. The enrichment used here is 4.8%. Cladding thickness is 0.63 mm and 0.315 mm for Zircaloy cladding and FeCrAl cladding, respectively. Note that due to the high neutron absorption of FeCrAl, the cladding thickness of FeCrAl is reduced by half compared to that of Zircaloy. The fuel pellet diameter for FeCrAl is increased correspondingly to keep the same gap width and rod diameter. Correspondingly, the pellet outer radius is 4.38 mm and 4.698 mm for Zircaloy cladding and FeCrAl cladding, respectively. As a result, the fuel cross-sectional area for FeCrAl is larger than that of Zircaloy.

Table 8-2. Fuel-rod parameters used in BISON.

Parameter	Zircaloy cladding	FeCrAl cladding
Pellet outer radius (mm)	4.38	4.698
Pellet quantity	375	375
Pellet height (mm)	9.832	9.832
Cladding thickness (mm)	0.63	0.315
Top/bottom cladding thickness (mm)	2.24	2.24
Gap thickness (side) (mm)	0.12	0.12
Gap thickness (bottom) (mm)	1	1
Total (active) fuel column length (m)	3.6891	3.6891
Cold plenum length (mm)	177.8	177.8
Enrichment (%)	4.8	4.8
Pellet density (%TD)	94.5	94.5
Cladding type	Zirlo	FeCrAl

In order to reliably predict the thermo-mechanical behavior and integrity of the full-length nuclear fuel rods during accidents, it is a requirement to first complete BISON simulation during normal reactor operation. The final outputs from these BISON simulations will serve as the initial inputs for the followed SBO simulations. It is noted that the SBO scenario simulated using BISON is the STSBO scenario (SBO-2) analyzed in Section 4.2.5. In addition, in order to perform a realistic fuel-rod analysis under SBO, specific user inputs to control the BISON simulations are also required. In particular, five BCs are generated by RELAP5-3D for steady state and for SBO as user inputs. The first BC is the power, which is associated with an LWR fuel rod and is typically given as rod-averaged linear power (or linear heat rate) in units of kW/m or W/m and a function of time. During the SBO, the power is switched into the decay heat. The power should vary in time and space which leads to the second BC, the axial variation in power. It is given as a scaling factor as a function of distance from the bottom of the rod and time, and it is fixed in the BISON simulations during both normal reactor operation and SBO. Fast neutron flux is the third BC which is supplied by RELAP5-3D for steady state and set to zero during SBO scenario. The last two BCs are coolant temperature and pressure, which are as a function of distance from the bottom of the rod and time. The corresponding BCs are shown in Figure 8-2 and Figure 8-3 for steady state and SBO, respectively.

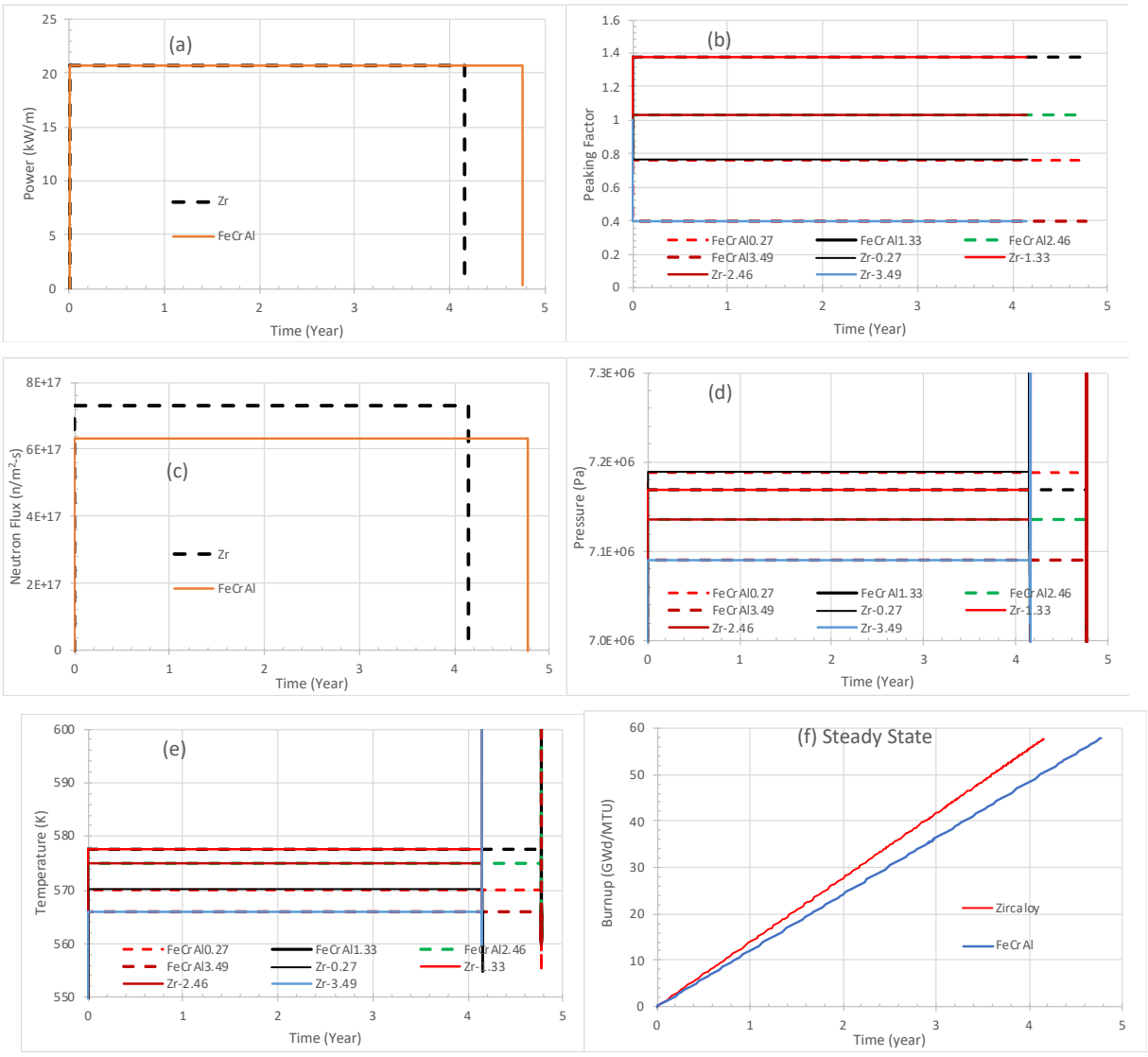

Figure 8-2. Five BCs are generated based on RELAP5-3D for steady state for the full-length fuel rod for (a) average linear power (heat rate); (b) axial peaking factor; (c) fast neutron flux; (d) coolant pressure; (e) coolant temperature; and (f) the corresponding burnups as a function form BISON simulations.

The magnitudes of average linear heat rate supplied to the fuel rod are same for Zircaloy and FeCrAl cladding, with a linear ramp to 20.7 kW/m over 1000 seconds and a hold at constant power at steady state for 4.15 and 4.77 years for Zircaloy and FeCrAl, respectively. Note that this power level is similar to typical average operating power for PWR rods. With the same linear heat rate, the choice of longer operation time at steady state for FeCrAl which has a larger fuel cross section is made in order to achieve same burnup for both Zircaloy and FeCrAl claddings. The use of the same linear heat rate also leads to a slightly lower fast neutron flux for FeCrAl cladding due to relatively larger fuel cross section of the corresponding fuel rodlet. In the end of the steady state, a burnup of 57.9 GWd/MTU will be achieved for both fuel claddings as shown in Figure 8-2 (f) from the corresponding BISON simulations.

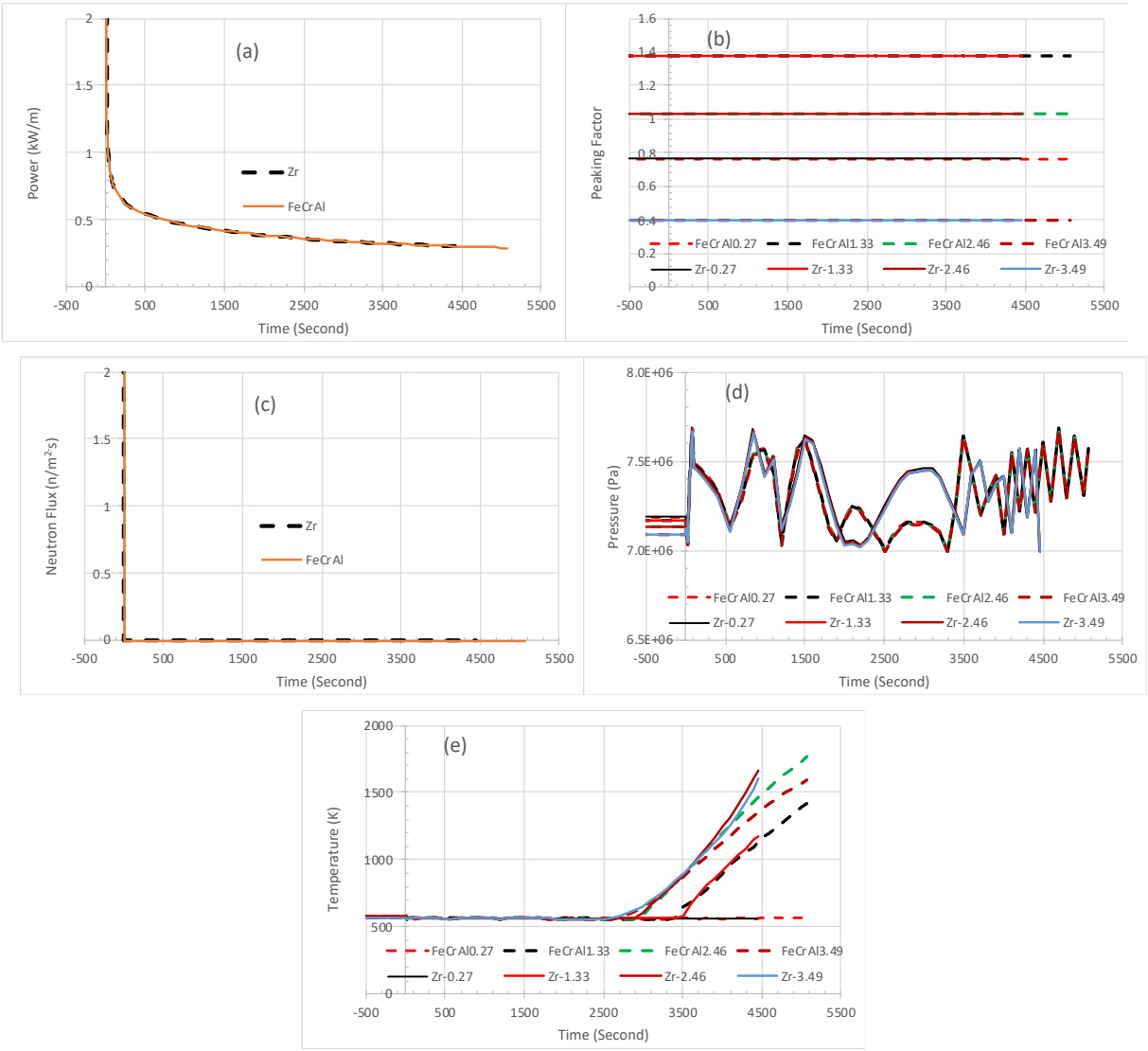

Figure 8-3. Five BCs for SBO for (a) the power; (b) peaking factor; (c) fast neutron flux; (d) coolant pressure; and (e) coolant temperature. Zero in the SBO time is the beginning of SBO and the end of steady state. Four BCs are generated by RELAP5-3D except the BC of neutron flux (0 at SBO).

Several preparatory BISON simulations were completed to investigate fuel-rod behaviors under steady state/normal reactor operating conditions and SBO accident conditions. The evolution of the full-length fuel-rod behavior during normal reactor operation is a prerequisite investigating the SBO and determining the available time, or the so-called coping time, for NPP operators for mitigation measures to prevent fuel failures.

8.4 Fuel Rod Burst Evaluation Results and Discussion

8.4.1 Fuel-Rod Evolution

8.4.1.1 Fuel-Rod Evolution of Temperature

Fuel temperature is a primary factor determining the thermal and mechanical performance of a fuel rod. Figure 8-4 shows the maximum temperature evolution of fuel and cladding in the steady state and SBO.

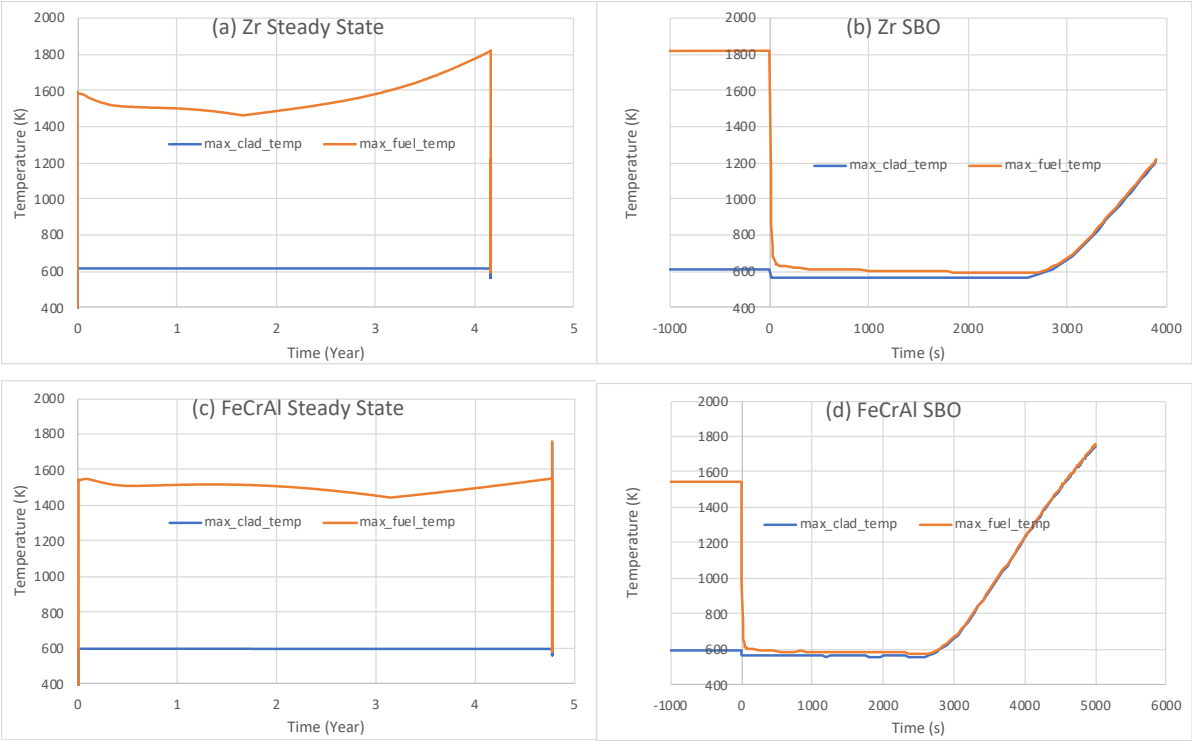

Figure 8-4. (a) Maximum temperature evolution of fuel and cladding in the steady state and (b) SBO for the fuel rod with Zircaloy cladding; (c) Maximum temperature evolution of fuel and cladding in the steady state and (d) SBO for the fuel rod with FeCrAl cladding. Zero in the SBO time is the beginning of SBO and the end of steady-state operation.

For the fuel rod with Zircaloy cladding, it can be seen that, in the steady state as shown in Figure 8-4 (a), the maximum cladding temperature around 614 K is quite stabilized in the whole steady state operation. For the fuel rod with FeCrAl cladding in the steady state as shown in Figure 8-4 (c), the maximum cladding temperature is ~ 596 K being quite stabilized in the whole steady state operation. This indicates the BC of coolant (or outer-cladding surface) temperature as shown in Figure 8-2 (e) carries away the heat generated by the fuel well. Meanwhile, for the fuel rod with Zircaloy cladding in the steady state as shown in Figure 8-4 (a), the maximum fuel temperature decreases from ~1578 K to ~1459 K in ~1.73 years then increases to ~1816 K in the end (~4.15 years) of the steady state operation. For the fuel rod with FeCrAl cladding in the steady state as shown in Figure 8-4 (c), the maximum fuel temperature decreases from ~1541 K to ~1441 K in ~3.24 years then increases to ~1546 K in the end (~4.77 years) of steady state operation. It is interesting to note that the maximum fuel temperature profile for FeCrAl cladding is lower than that of Zircaloy cladding. Specifically, the temperature for FeCrAl cladding is significantly lower (~270 K) than that of Zircaloy cladding in the end of steady state, which may indicate that the fuel rodlet with FeCrAl cladding can operate safer in the steady state than Zircaloy cladding. Among five BCs, since same level of power (averaged linear power and axial peaking factor), external pressure and coolant temperature are applied to both cladding as shown in Figure 8-2, it suggests that the lower fuel and cladding temperatures for FeCrAl cladding are determined by the lower fast neutron flux strongly as shown in Figure 8-2 (c).

As SBO starts after the reactor scram, the maximum fuel temperature for the Zircaloy cladding drops rapidly from ~1816 K at the steady state to ~620 K in about 100 seconds, then stays below 620 K for about 2700 seconds as shown in Figure 8-4 (b). Meanwhile, the maximum cladding temperature initially decreases from about 614 K to ~566 K in a few of seconds. This is opposite to that in an LOCA event in which the cladding temperature rises abruptly in a few second due to the blow-down phase as the initial stored energy in the fuel pellets is transferred to the cladding. The time to failure can be determined as 3900 seconds with the maximum cladding temperature 1208 K.

As SBO starts for the fuel rod with FeCrAl cladding, the maximum fuel temperature drops rapidly from ~1546 K at the steady state to ~600 K in about 100 seconds, then stays below 600 K for about 2700 seconds as shown in Figure 8-4 (d). Meanwhile, the maximum cladding temperature initially decreases from about 596 K to ~566 K in a few seconds, which is very similar behavior with that of Zircaloy cladding under SBO and is opposite to that in an LOCA event in which the cladding temperature rises abruptly in a few second. The time under SBO transients lasts much longer than LOCA transients as shown in Figure 8-4 (b) and (d). After 2700 seconds, both fuel and cladding are almost equal and increase significantly. The time to failure for FeCrAl cladding is determined as 5000 seconds with the maximum cladding temperature 1754 K in the ballooning region. Thus, the potential increase in coping time with respect to FeCrAl cladding is about 1100 seconds under SBO.

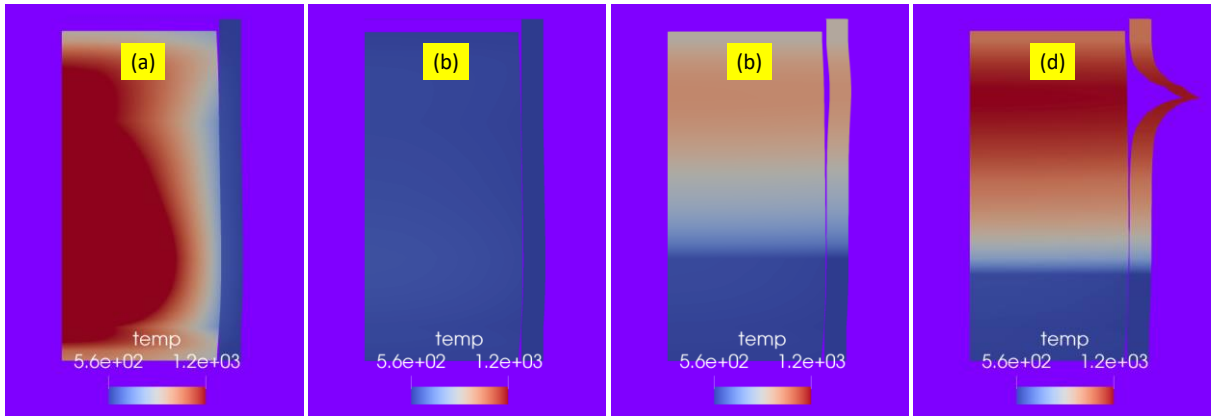

Figure 8-5. Snapshots of temperature evolution for the fuel rod with Zircaloy cladding from a BISON SBO simulation. (a) Middle of steady state; (b) beginning of SBO; (c) middle of SBO; and (d) end of simulation. 400× in the radial direction for visualization.

Without any mitigation measures, it is anticipated that the fuel rod will be deformed and failure eventually under significantly high fuel temperature. Figure 8-5 shows the snapshots of a BISON simulation for the temperature evolution for the fuel rod with Zircaloy cladding. Figure 8-5 (a) shows the fuel rodlet temperature distribution in the middle of the steady state. It is found that the hottest spots for the fuel and cladding are located near the bottom of fuel rod. Meanwhile, fuel-cladding contact also occurs in the hottest zone. As SBO starts, the contact of fuel-cladding is separated as shown in Figure 8-5 (b) and there is no more fuel-cladding contact in the whole SBO period as shown in Figure 8-5 (b)–(c). In the end of simulation, the hottest spots for the fuel and cladding are shifted to the region near the top fuel rod with significant ballooning.

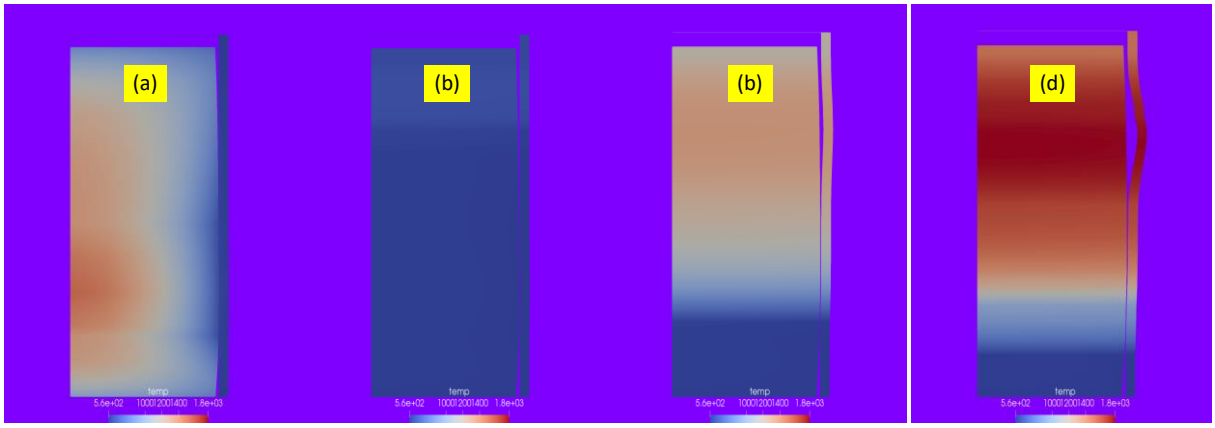

Figure 8-6. Snapshots of temperature evolution for the fuel rod with FeCrAl cladding from a BISON SBO simulation. (a) Middle of steady state; (b) beginning of SBO; (c) middle of SBO; and (d) end of simulation. 400× in the radial direction for visualization.

Figure 8-6 shows the snapshots of a BISON simulation for the temperature evolution for the fuel rod with FeCrAl cladding. Figure 8-6 (a) shows the temperature distribution in the fuel and cladding in the middle of the steady state. It is observed that the hottest spots for the fuel and cladding are located below the middle of the fuel rod. Meanwhile, fuel-cladding contact also occurs in the hottest zone. As SBO starts, the contact of fuel-cladding is disappeared as shown in Figure 8-5 (b) and there is no more fuel-cladding contact in the whole SBO period. In the end of simulation, the hottest spots for the fuel and cladding are shifted to the region near the top fuel rod with significant ballooning. However, the magnitude of ballooning for FeCrAl is less than that of Zircaloy. Note that the coolant temperature is peaked at the top toward the final times in the boundary condition file as shown in Figure 8-3 (e). That would force the peak temperature of cladding to be at that location.

8.4.1.2 Fuel-Rod Evolution of Mechanical Properties

Due to the significantly higher fuel and cladding temperatures, it is likely that a number of fuel properties will be affected. Cladding hoop stress and hoop strain are another two critical factors determining the thermal and mechanical performance of a fuel rod. The evolution of the maximum cladding hoop stress and hoop strain for the fuel rod with Zircaloy cladding in the steady state and SBO is shown in Figure 8-7 (a) and (b), respectively. In the steady state, the maximum cladding hoop stress slowly reduces to about -3.06 MPa from zero for ~1.6 years, then increases to the peak value of ~153 MPa in the end of the steady state. Meanwhile, the maximum hoop strain increases to ~0.18% in ~100 seconds, then slowly decrease to –0.016% in the 2.17 years, then slowly increases to 1.27% in the end of the steady state as shown in Figure 8-7 (a).

As SBO starts, the maximum drops from ~153 MPa in the end of the steady state to ~30 MPa in about 50 seconds, increases to ~ 40 MPa in 3450 second, then decreases to ~3 MPa in the end of simulation at the point of 3900 seconds. Meanwhile, the maximum cladding hoop strain initially decreases from about 1.27% to ~1.05% in ~20 seconds, remains ~1.05% for about 3430 seconds, then increases to ~28.9% in the end of simulation at the point of 3900 seconds.

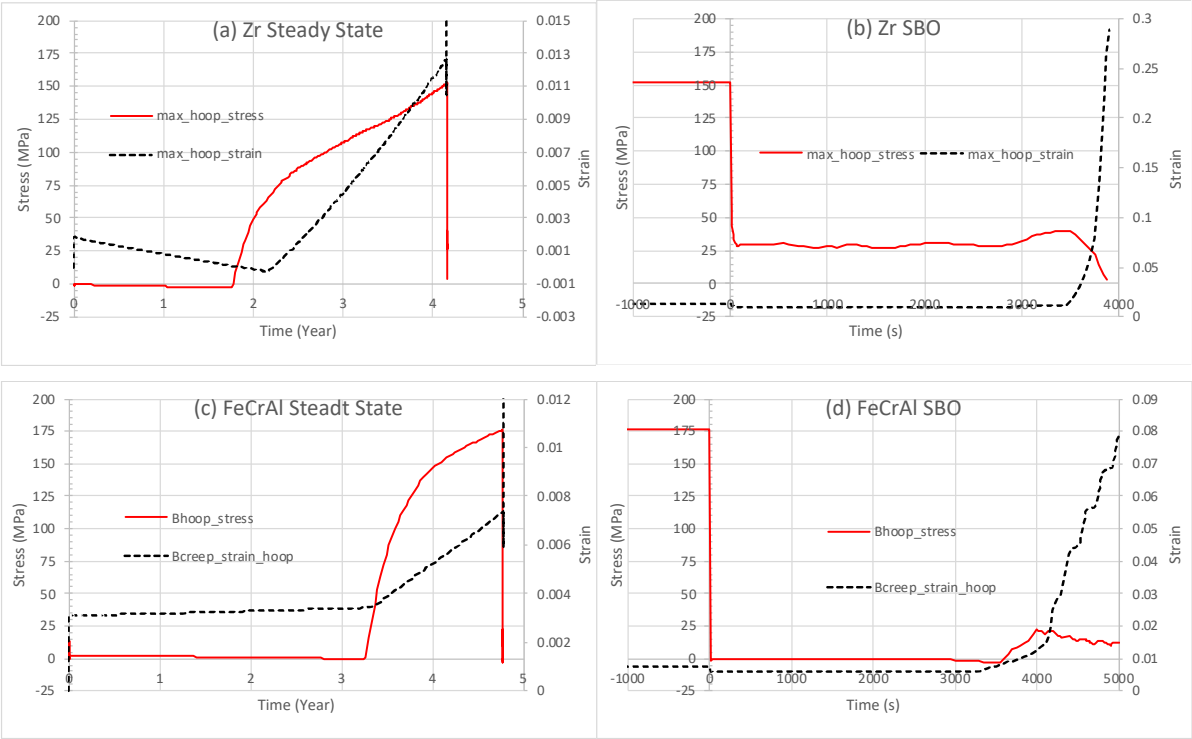

Figure 8-7. (a) Evolution of maximum hoop stress and maximum hoop strain of fuel and cladding in the steady state and (b) SBO for the fuel rod with Zircaloy cladding; (c) evolution of maximum hoop stress and maximum hoop strain of fuel and cladding in the steady state and (d) SBO for the fuel rod with FeCrAl cladding. Zero in the SBO time is the beginning of SBO and the end of steady-state operation.

The evolution of the maximum cladding hoop stress and hoop strain for FeCrAl in the steady state and SBO is shown in Figure 8-7 (c) and (d), respectively. The maximum cladding hoop stress in the steady state slowly reduces to about –0.58 MPa from zero for ~3.24 years, then increases to the peak value of ~178 MPa in the end of the steady state in ~4.77 years. Meanwhile, the maximum hoop strain increases slowly from 0.31% to ~0.34% for ~3.6 years, then increases slightly rapid to 0.74% in the end of the steady state as shown in Figure 8-7 (c).

As SBO starts, the maximum rapidly decreases from ~178 MPa in the end of the steady state to about –2.06 MPa in about 10 seconds, remains with a negative value of the maximum hoop stress for about 3600 seconds, then increases to about –12.1 MPa in the end of simulation at the point of 5000 seconds. Meanwhile, the maximum cladding hoop strain initially decreases from about 0.74% to below 0.6% in ~20 seconds, remains below 0.6% for about 3300 seconds, then increases to ~28.9% in the end of simulation at the point of 3900 seconds. It is apparent that under SBO, for this BWR design with FeCrAl cladding, the maximum hoop stress and hoop strain are significantly lower than those of fuel rod with Zircaloy cladding.

Under SBO conditions, it is anticipated to observe significantly higher rod internal pressure (i.e., plenum pressure). In particular, at transient, more fission gas is expected to release from the fuel pellet, and the internal pressurization of the fuel rod will be excessive as extensive fission gas is released from the fuel pellet to the free volume within a fuel rod. As one can see from Figure 8-8, with current BWR design, such behavior under SBO for both claddings is not observed from BISON simulations. The maximum plenum is below 13 MPa and 10 MPa in the whole SBO scenario for Zircaloy and FeCrAl, respectively.

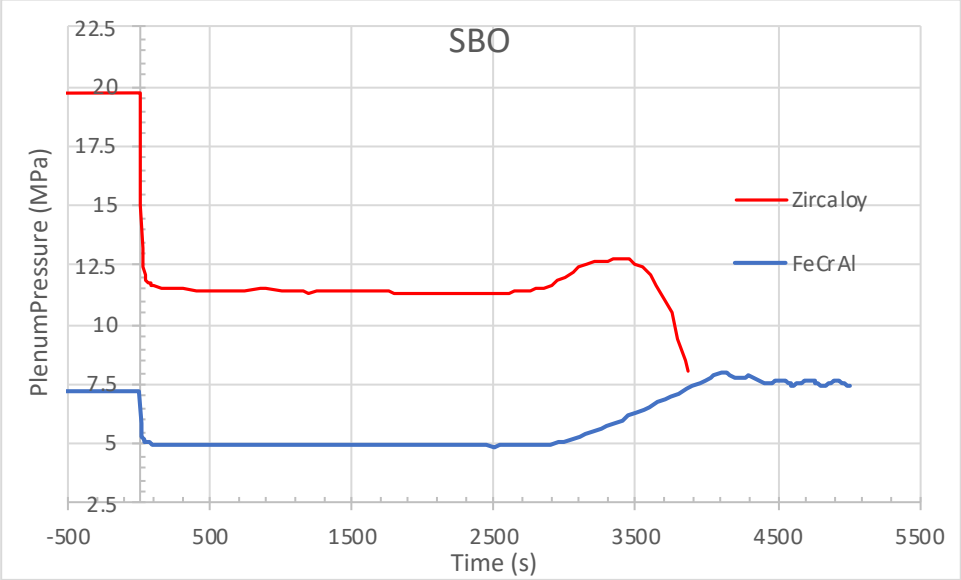

Figure 8-8. Evolution of plenum pressure at SBO for the fuel cladding of Zircaloy and FeCrAl. Zero in the SBO time and the beginning of SBO and the end of steady-state operation.

Meanwhile, it is observed that in the end of the steady state, the computed internal pressure for FeCrAl (~7.4 MPa) is significantly lower than that of Zircaloy (~19.5 MPa). Since same burnup with a value of 57.9 GWd/MTU is achieved for both fuel claddings as shown in Figure 2 (f) and same level of power as shown in Figure 2 (a) for linear hate rate (b) for axial power peaking factor, and thermal hydraulic BCs as shown in Figure 8-2 (d–e), it is apparently that an increase in fast neutron flux by a factor of 1.15 from FeCrAl to Zircaloy significantly shifts the onset of gas release by a factor of 5.9, which is evident in Figure 8-8. Thus, the correlation between internal plenum pressure (akin fission gas release) is non-linear. The lower fast neutron flux will benefit the NPP in the normal steady-state operation in the point view of internal plenum pressure.

8.4.2 Fuel-Rod Burst Mechanisms

Under SBO, extreme hoop stress or hoop strain may occur at some locations and lead to rod burst as local hoop stress or hoop strain exceeds burst stress. Although cladding burst was predicted by RELAP5-3D with this BWR design for both claddings, bursting was not observed using BISON with BCs provided through RELAP5-3D. Specifically, BISON simulations were exited with some kind of numerical instability and failure criteria could be triggered for both claddings.

The hoop stress and hoop strain may strongly depend on the cladding temperature. Under SBO, it may reach an extremely high value, leading to rod burst as local hoop stress exceeds a limiting burst stress. As an example, Figure 8-9 shows the evolution of the maximum cladding temperature, maximum hoop stress, and the corresponding failure hoop stress based on INL burst criteria for FeCrAl.

This data clearly indicates that at 4125 seconds, the increased maximum hoop stress reaches 20.37 MPa and the corresponding burst hoop stress is 20.11 MPa with a maximum cladding temperature of 1298 K. However, bursting was not observed using BISON with BCs provided through RELAP5-3D, although cladding burst was predicted by RELAP5-3D with this BWR core design under SBO. Thus, it is speculated that the location of the maximum hoop stress is not at the same location of the maximum cladding temperature or the maximum hoop strain. The relevant cladding temperature and hoop stress in the maximum ballooning zone are analyzed for both claddings, and the results are shown in Figure 8-10. As shown in Figure 8-10 (a) and (c), the location of the maximum cladding temperature and the maximum hoop strain is overlapped for both claddings. For the Zircaloy cladding, the maximum hoop strain is also anchored in the same location as the maximum cladding temperature and the maximum hoop strain. However, overstress, plasticity instability and overstrain failure criterion cannot be triggered.

For the FeCrAl cladding, the maximum hoop strain is not found within the maximum ballooning zone because the hoop stress in that zone remains negative (compressive) and is slightly positive around 4000 seconds. With such low tensile or even compressive hoop stress in the ballooning zone, the overstress burst criterion is not met.

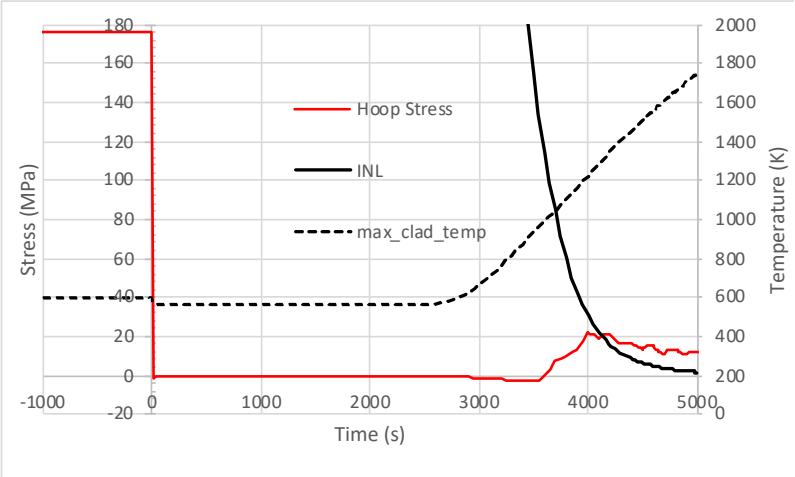

Figure 8-9. Evolution of the maximum cladding temperature, maximum hoop stress and the corresponding failure hoop stress based on INL burst criterion. Zero SBO time and the beginning of SBO and the end of steady-state operation.

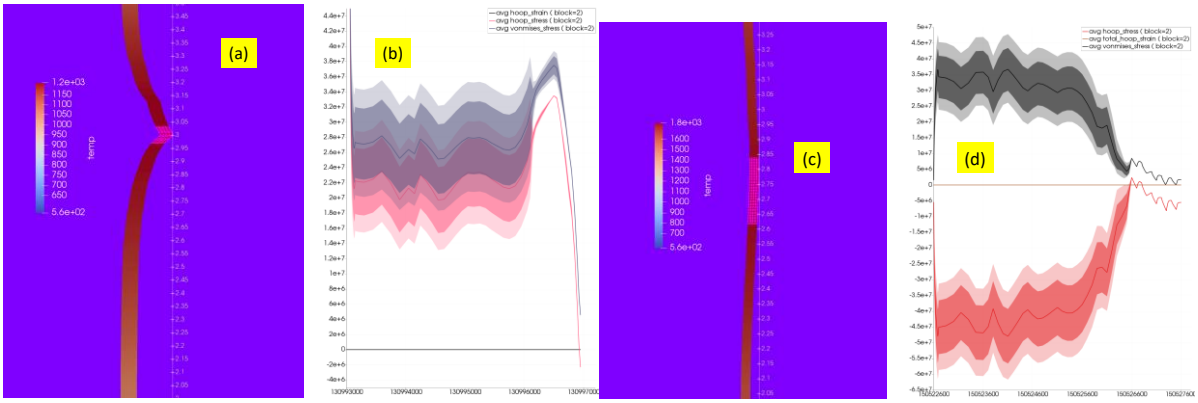

Figure 8-10. Fuel rod with FeCrAl cladding: (a) Snapshot of temperature in the end of simulation for the maximum ballooning zone; (b) Evolution of hoop stress and von Mises stress; Zircaloy cladding (c) Snapshot of temperature; (d) Evolution of hoop stress and von Mises stress in the end of simulation for the maximum ballooning zone.

The hoop stress (akin tangential stress) is the stress around the circumference of the fuel rod due to a pressure gradient between the external coolant pressure and the internal plenum pressure. It can be positive or negative depending on the direction of the pressure gradient between the external coolant pressure and the internal plenum pressure. In SBO condition, the external system coolant pressure oscillates between 7.5 and 7.7 MPa, as shown in Figure 8-3 (d). For the FeCrAl in SBO, the plenum pressure is less than 7.5 MPa on most occasions, as shown in Figure 8-8. Thus, most of the time, a negative hoop stress is expected to observe for FeCrAl in the ballooning zone under SBO because of the negative pressure gradient. With a compressive or very low tensile hoop stress, the overstress burst criterion cannot be initiated. Driven by the temperature boundary condition, the cladding temperature approaches the melting point of 1773 K of C35 FeCrAl alloy. At that high temperature, Young's modulus becomes 5% of its original value. With such a low stiffness, the cladding turns

marshmallow-like and begins to balloon with a compressive hoop stress, preventing the reason why the overstress burst criterion. In contrast, a positive hoop stress should be observed for Zircaloy in the ballooning zone until near the end of postulated accident condition because of the positive pressure gradient because the plenum pressure is larger than 7.5 MPa.

8.5 Summary of Fuel Rod Burst Evaluation

The SBO event has been widely recognized as one of the most severe conditions that an NPP can experience. Through BISON fuel performance simulations of a short-term SBO (i.e., SBO-2) accident without any mitigation measures, it is suggested that the evolution of the full-length BWR fuel-rod behavior is mainly determined by the cladding or coolant temperatures. Though the clad melting temperature or PCT may be a direct indicator of the failure of fuel rods, our results from BISON modeling and simulations strongly suggest that it is more realistic to use a cladding failure criterion based on cladding burst to determine the coping time. In particular, four fuel-rod burst criteria for Zircaloy cladding and two criteria for FeCrAl cladding were used in this comparative study, in which cladding failure times are predicted by BISON simulations. As SBO starts after the reactor scram, fuel temperature drops rapidly, which is opposite of an LOCA event in which the peripheral fuel temperature rises abruptly first. Fuel temperature reduces to about the same temperature as that of the cladding for 2700 seconds, and eventually cladding and fuel temperatures increase quickly as the coolant boils off. Meanwhile, significant fuel-cladding contact is observed only in the steady state for both claddings near the bottom of fuel rod. This is due to the outward fuel thermal expansion driven by the power boundary condition in this BWR reactor primary system. As the SBO starts, the fuel-clad contact recedes immediately, which is a benefit from large gap distance between fuel and cladding in the initial BWR design. The time to failure is about 5000 and 3900 seconds for FeCrAl and Zircaloy cladding, which is much longer than the typical few hundred seconds under the LOCA scenario. Thus, an increase 1100 seconds of coping time may be reached by using FeCrAl cladding. The fuel ballooning spot is in the high-temperature region. Remarkably, the BISON simulations found that none of cladding-burst criterion can be satisfied and hoop stress is significantly low in this BWR SBO design for both claddings, a stark difference from LOCA or PWR SBO events where the phenomenon is common and was demonstrated (Pastore, G., et al., 2015; Pastore, G., et al., 2017; Yu, J., C. Blakely, and H. Zhang, 2019).

9. CONCLUSIONS AND FUTURE WORK

This report documents the FY 2020 activities on ERP R&D, with one of the focus areas being to extend the analyses conducted in FYs 2018 and 2019 for a PWR to a BWR. These activities used integrated evaluation approaches that combine the plant PRA models with multiphysics best-estimate analyses and performed detailed risk and benefit assessments of ATF designs, and FLEX for the current fleet of BWRs. These studies will help achieve both safety and operational performance enhancements.

Risk analysis was conducted for the FeCrAl and Cr-coated cladding design impact on a generic BWR model based on a GE BWR/4 design with Mark I containment for SBO and MLOCA accident scenarios using the generic SAPHIRE and RELAP5-3D models. The FLEX analysis was presented as an overview of FLEX equipment and strategies implemented in the nuclear industry after the Fukushima accident. A FLEX model was developed and incorporated into the generic BWR SAPHIRE model to assess the risk impact. A FLEX HRA was performed, which suggested a dynamic approach to HRA with FLEX strategies. An MCBE framework for FLEX deployment was developed. It demonstrated the safety and economic improvement with FLEX to enhance the resilience of existing NPPs. Finally, a fuel-rod bursting evaluation was performed using BISON.

In the ATF SBO analysis, the RELAP5-3D simulation results show that the gain of coping time, or the delay of time-to-core-damage due to the ATF designs, is less than 20 minutes for most SBO scenarios. For FeCrAl, eight of the nine analyzed SBO scenarios have a gain of coping time from 4 to 20 minutes. The other scenario has a gain of coping time of 50 minutes. These times are relatively short when compared to core damage with Zircaloy in the associated scenarios. For Cr-coated cladding, eight of the nine analyzed SBO scenarios have a gain of coping time from 1 to 15 minutes, with the other scenario gaining a coping time of 42 minutes. The coping time gains at MOC and EOC are a bit less that those at BOC.

With these relatively small increases of the time-to-core-damage, the risk-benefit on behalf of the CDF brought by the ATF designs would be very small. The PRA quantification results show that the marginal coping time increase would lead to about ~3–5% and ~1–3% reductions in the CDF induced by weather-related LOOP, respectively. For both ATF designs, the CDF reductions vary during the fuel cycle, exhibiting the greatest reduction at BOC and the lowest reduction at EOC. However, the RELAP5-3D simulation results show a clear benefit in adopting ATFs with much less hydrogen produced at the time of CD, which can be a few times lower for Cr-coated cladding or two orders of magnitude lower than that of the Zircaloy-clad cases.

Sensitivity analyses were performed for traditional fuel design and near-term ATF designs under SBO scenarios to examine how the combination of ATF and certain advanced technologies or operations could postpone the time to CD and increase the coping time. Three sensitivity calculations were conducted, including increased RCIC operation time, FLEX equipment startup time, and RCIC blackstart operations. The results show an almost linear relationship between the time to CD and the RCIC operation time, significant effects from the FLEX startup time on the SBO mitigation, and considerable coping time gains provided by the combination of RCIC blackstart and ATF.

In the ATF MLOCA analysis, the RELAP5-3D simulation results show that for Chromium-coated cladding, the gain of coping time, or the delay of time to CD, ranges from 2 minutes to 4 minutes for MLOCA-4, and less than 2 minutes for other MLOCA scenarios. For FeCrAl cladding, the gain on coping time ranges from 3 minutes to 11 minutes for all the MLOCA scenarios. Although the relatively small increase in time to CD from the RELAP5-3D simulation results suggests that there could have some additional time for associated operator actions, a change to the general MLOCA PRA model is not warranted. The ATF designs would bring risk benefits to plants even though the benefits are small and unquantified for MLOCA. Also, the RELAP5-3D simulation results show the clear benefit in adopting ATFs with much less hydrogen produced at the time of CD, which can be a few times lower for the Cr-coated cladding, and up to two orders of magnitude lower for FeCrAl cladding than with Zircaloy cladding.

In the FLEX PRA analysis, FLEX equipment and associated human actions were modeled and incorporated into the generic BWR SAPHIRE model. The results show that the total LOOP CDF with FLEX from the generic model is 1.45E-6 per year, which is a 15% reduction when compared with the total LOOP CDF with no FLEX

(1.71E-6 per year). In the FLEX HRA analysis, dynamic simulation approaches were explored to account for contextual and time uncertainties that have been missing in existing HRA. Two FLEX HRA models with different approaches were developed using EMRALD. One FLEX HRA model is mainly developed on the basis of procedure contexts, while the other one depends on PRA/HRA modeling approaches. These first efforts were for proof of concept and still require added fidelity to accurately capture realistic conditions; however, initial modeling effort success was observed in demonstrating the feasibility of modeling FLEX-related human actions dynamically using EMRALD.

In the MCBE analysis, a comprehensive costs and benefits evaluation scope was established using multiple evaluation criteria and multiple contexts. The MCBE method also reflects a decision maker's preferences toward hazard likelihood and consequence into cost and benefit estimations using CPT. The MCBE was applied to the FLEX implementation in a generic PWR plant. Preliminary, proof-of-concept results indicated that if FLEX were implemented at the reference plant for 20 years, the benefits of FLEX implementation could be expected to outweigh the costs. The results also suggested that although FLEX was originally designed to cope with accidents, it would be beneficial to explore additional FLEX credit in plant operation and maintenance-efficiency improvement.

In the fuel rod bursting potential evaluation using Bison, simulations were carried out for Zircaloy and FeCrAl claddings under the SBO-2 scenario. The simulation results indicate that the evolution of the full-length BWR fuel-rod behavior is mainly determined by the cladding or coolant temperature. The results also strongly suggest that, though the clad melting temperature or peak cladding temperature may be a direct indicator of fuel-rod failures, it is more realistic to use a cladding failure criterion based on cladding burst to determine the coping time. The simulated time to failure is about 5000 and 3900 seconds for FeCrAl and Zircaloy cladding, respectively. Thus, an increase of 1100 seconds in coping time may be reached using FeCrAl cladding.

For future work, we recommend the following activities for ERP research:

- Perform risk-informed ATF analyses for BWR in other accident scenarios such as large LOCA, small LOCA, loss of main feedwater, and general transients.
- Continue to explore the dynamic HRA method and using EMRALD to credit FLEX operations in accident mitigation.
- Investigate approaches that could maximize the benefits from the industry investment of FLEX and collaborate with industry to conduct plant-specific FLEX analysis.
- Collaborate with industry on methods to enhance plant-safety features and reduce plant operating costs, for example, by optimizing plant performance index.
- Extend the benefits evaluation (i.e., MCBE) to other plant resilience enhancement technology, for example, collaboration with industry leading institutions (e.g., Exelon) to apply MCBE to the new battery technologies with increased battery capacity.

10. REFERENCES

Boring and Rasmussen. (2016). GOMS-HRA: A method for treating subtasks in dynamic human reliability analysis. *Risk, Reliability and Safety: Innovating Theory and Practice, Proceedings of the 2016 European Safety and Reliability Conference*, (pp. 956-963).

Boring et al. (2015). Applicability of simplified Human Reliability Analysis methods for severe accidents. *In Proceedings of the 7th International Conference on Modelling and Simulation in Nuclear Science and Engineering (7ICMSNSE).*

Boring et al. (2017). Task and procedure level primitives for modeling human error. *Advances in Intelligent Systems and Computing, 589*, 30-40.

Cathcart, J. V., & et al. (1977). *Reaction Rate Studies, IV, Zirconium Metal-Water Oxidation Kinetics.*

Cha, E., & Ellingwood, B. R. (2013). The role of risk aversion in nuclear plant safety decisions. *Structural safety, 44*, 28-36.

Cha, E., & Ellingwood, B. R. (2019). The relation between cost-benefit analysis and risk acceptance in regulatory decision-making. *International Journal of Risk Assessment and Management, 22*, 44-62.

Denning, R., & Mubayi, V. (2017). Insights into the Societal Risk of Nuclear Power Plant Accidents. *Risk Analysis, 37*(1), 160-172.

Di Marcello, V., et al. (2014). The TRANSURANUS mechanical model for large strain analysis. *Nuclear Engineering and Design, 276*, 19-29.

Dube, D., Albinson, B., Wolfgang, R., Saunders, M., & Krueger, G. (2017). Exelon economic enterprise risk modelling of a BWR. *Proceedings of ANS International Topical Meeting on Probabilistic Safety Assessment (PSA 2017).* Pittsburgh, PA.

Eide, S., Gentillon, C., Wierman, T., & Rasmuson, D. (2005). *Reevaluation of Station Blackout Risk at Nuclear Power Plants - Analysis of Loss of Offsite Power Events: 1986-2004.* Nuclear Regulatory Commission.

Electric Power Research Institute. (2004). *Generation Risk Assessment (GRA) Plant Implementation Guide (Product 1008121).*

EPRI. (2012, April 16). *Modular Accident Analysis Program: A Software Toll for Analyzing Nuclear Plant Accident Scenarios.* Electric Power Research Institute. Retrieved April 16, 2018, from https://www.epri.com/#/pages/product/000000000001025795

EPRI. (2014). *Incorporating Flexible Mitigation Strategies into PRA Models: Phase 1: Gap Analysis and Early Lessons Learned.*

EPRI. (2018). *Human Reliability Analysis (HRA) for Diverse and Flexible Mitigation Strategies (FLEX) and Use of Portable Equipment: Examples and Guidance, EPRI 3002013018.*

Erbacher, F.J., et al. (1982). Burst criterion of Zircaloy fuel claddings in a loss-of-coolant accident. *American Society for Testing and Materials, Special Technical Publication*, 271-283.

Field, K. G., Snead, M. A., Yamamoto, Y., & Terrani, K. A. (2017). *Handbook on the Material Properties of FeCrAl Alloys for Nuclear Power Production Applications.* Oak Ridge National Laboratory, Nuclear Technology R&D.

Gamble, K.A., et al. (2017). An investigation of FeCrAl cladding behavior under normal operating and loss of coolant conditions. *Journal of Nuclear Materials, 491*, 55-66.

Gauntt, R. O., Cash, J., Cole, R. K., Erickson, C. M., Humphries, L., Rodriguez, S. B., & Young, M. F. (2005). *MELCOR Computer Code Manuals.* Nuclear Regulatory Commission.

Gertman et al. (2005). *The SPAR-H human reliability analysis method (NUREG/CR-6883).* U.S. Nuclear Regulatory Commission.

Global Nuclear Fuel. (2006). *GE14 for ESBWR Fuel Rod Thermal-Mechanical Design Report, Licensing Topical Report (NEDO-33242).* Global Nuclear Fuel.

Hales, J. D. et al. (2015). *BISON Theory Manual, The Equations behind Nuclear Fuel Analysis.* Idaho National Laboratory.

Holzwarth, U., & Stamm, H. (2002). Mechanical and thermomechanical properties of commercially pure chromium and chromium alloys. *Journal of Nuclear Materials, 300*, 161-177.

Idaho National Laboratory. (2018). *Light Water Reactor Sustainability Program Integrated Program Plan.* Idaho National Laboratory.

Idaho National Laboratory. (2020). *MARMOT.* Retrieved from https://moose.inl.gov/marmot/SitePages/Home.aspx
Idaho National Laboratory. (2020). *MOOSE.* Retrieved from https://moose.inl.gov/SitePages/Home.aspx
Johnson, N., & Ma, Z. (2019). *Analysis of Loss-of-Offsite-Power Events: 1987-2018.* Idaho Falls: Idaho National Laboratory.
Kichline, M. (2018). Human Reliability Analysis for Using Portable Equipment. *EPRI FLEX Workshop.*
Linthicum, R., & Powell, M. (2019). FLEX Equipment Reliability Data. *PSA 2019* (pp. 458-461). Charleston: American Nuclear Society.
Ma et al. (2018). *Plant-Level Scenario-Based Risk Analysis for Enhanced Resilient PWR – SBO and LBLOCA.* Idaho National Laboratory.
Ma, Z. (2019). *Enhanced Component Performance Study: Emergency Diesel Generators 1998-2018.* Idaho Falls: Idaho National Laboratory.
Ma, Z., & al., e. (2018). *Plant-Level Scenario-Based Risk Analysis for Enhanced Resilient PWR – SBO and LBLOCA.* Idaho National Laboratory.
Ma, Z., Davis, C., Parisi, C., Dailey, R., Wang, J., Zhang, S., . . . Corradini, M. (2019b). *Evaluation of the Benefits of ATF, FLEX, and Passive Cooling System for an Enhanced Resilient PWR Model (INL/EXT-19-56215).* Idaho National Laboratory.
Ma, Z., Parisi, C., Davis, C., Park, J., Boring, R., & Zhang, H. (2019a). *Risk-Informed Analysis for an Enhanced Resilient PWR with ATF, FLEX, and Passive Cooling (INL/EXT-19-53556).* Idaho National Laboratory.
Mandelli, D., Wang, C., St. Germain, S., Smith, C., Morton, D., Popova, I., & Hess, S. (2019). *Combined Data Analytics and Risk Analysis Tool for Long Term Capital SSC Refurbishment and Replacement (INL-EXT-19-55819).* Idaho National Laboratory.
Matev, A. (2006). Analysis of Operator Response to Station Blackout. *International RELAP5-3D User Group Meeting* . West Yellowstone: Idaho National Laboratory.
Mubayi, V., Sailor, V., & Anandalinam, G. (1995). *Cost-Benefit Considerations in Regulatory Analysis (NUREG/CR-6349).*
Mulvehill, J. (2015). Implementation of 10 CFR 50.69 at Southern Nuclear. *27th Annual EQ Technical Meeting.* Clearwater, FL.
Nuclear Energy Institute. (2016). *Diverse and Flexible Coping Strategies (FLEX) Implementation Guide (Revision 4).*
Nuclear Engineering International. (2007, September). Fuel Design Data. *Nuclear Engineering International, 52*(638), p. 32.
Park et al. (2019). Remaining and emerging issues pertaining to the human reliability analysis of domestic nuclear power plants. *Nuclear Engineering and Technology, 51*, 1297-1306.
Park et al. (2019). Treatment of human and organizational factors for multi-unit HRA: Application of SPAR-H method. *Annals of Nuclear Energy, 132*, 656-678.
Pastore, G., et al. (2016). Modelling of LOCA Tests with the BISON Fuel Performance Code. *Proceedings of the Enlarged Halden Programme Group Meeting – EHPG 2016.* Fornebu, Norway.
Pastore, G., et al. (2015). Modeling of Fuel Behavior during Loss-of-Coolant Accidents using the BISON Code. *Proceedings of the Reactor Fuel Performance Meeting – Top Fuel 2015.* Zurich, Switzerland.
Pastore, G., et al. (2017). LOCA Demonstration with Experimental Assessment (IFA-650.10).
Pence, J., Abolhelm, M., Mohaghegh, Z., Reihani, S., Ertem, M., & Kee, E. (2018). Methodology to evaluate the monetary benefit of Probabilistic Risk Assessment by modeling the net value of Risk-Informed Applications at nuclear power plants. *Reliability Engineering & System Safety, 175*, 171-182.
Powell, M., & Graham, K. (2014). The Impact of FLEX on Outage Risk. *Nuclear Engineering International*.
Prescott, S., Smith, C., & Vang, L. (2018). EMRALD, Dynamic PRA for the Traditional Modeler. *In Proceedings of the 14th International Probabilistic Safety Assessment and Management Conference.* Los Angeles, CA.
Prosek, A., & Cizelj, L. (2013, April). Long-Term Station Blackout Accident Analyses of a PWR with RELAP5/MOD3.3. *Science and Technology of Nuclear Installations, 2013*.
Reid, M. (2018). Human reliability assessment for 'Flex' equipment. *In Proceedings of the Probabilistic Safety Assessment and Management Conference (PSAM 2018).* Los Angeles, CA.

RELAP5-3D Code Development Team. (2018). *RELAP5-3D Code Manual Volume I.* Idaho National Laboratory. Idaho Falls: Idaho National Laboratory.
Rieger, M., Wang, M., & Hens, T. (2017). Estimating cumulative prospect theory parameters from an international survey. *Theory and Decision, 82*(4), 567-596.
Robb, K. R., Howell, M., & Ott, L. J. (2017). *Parametric and Experimentally Informed BWR Severe Accident Analysis Using FeCrAl.* Oak Ridge National Laboratory, Nuclear Technology R & D.
Schultz, R. R. (2015). *RELAP5-3D(c) Code Manual Volume V: User`s Guidelines.* Idaho National Laboratory. Idaho Falls: Idaho National Laboratory.
Schumock, G., Zhang, S., Farshadmanesh, P., Owens, J., Kasza, N., Stearns, J., . . . Mohaghegh, Z. (2020). Integrated Risk-Informed Design (I-RID) methodological framework and computational application for FLEX equipment storage buildings of Nuclear Power Plants. *Progress in Nuclear Energy, 120*, 103186.
Smith, C. L. (2002). Risk-informed incident management for nuclear power plants.
Smith, C. L., & Wood, S. T. (2011). *Systems Analysis Programs for Hands-on Integrated Reliability Evaluations (SAPHIRE).* Idaho National Laboratory. Idaho Falls: US NRC.
Tversky, A., & Kahneman, D. (1992). Advances in prospect theory: cumulative representation of uncertainty. *Journal of Risk and Uncertainty, 5*(4), 297-323.
U.S. Bureau of Labor Statistics. (2020). *Consumer Price Index Inflation Calculator*. Retrieved from https://www.bls.gov/data/inflation_calculator.htm/
U.S. Bureau of Labor Statistics. (2020). *Occupational Outlook Handbook - Nuclear Technicians*. Retrieved from https://www.bls.gov/ooh/life-physical-and-social-science/nuclear-technicians.htm
U.S. Energy Information Administration. (2020). *Electric Power Monthly with Data for February 2020.*
U.S. Nuclear Regulatory Commission. (2010). *Draft Guidance for Use of Containment Accident Pressure in Determining the NPSH Margin of ECCS and Containment Heat Removal Pumps (ML13015A437).* U.S. Nuclear Regulatory Commission. Retrieved August 2020, from https://www.nrc.gov/docs/ML1301/ML13015A437.pdf
U.S. Nuclear Regulatory Commission. (2011). *General Electric Systems Technology Manual Chapter 2.2 Fuel and Control Rods System (ML11258A302).* U.S. Nuclear Regulatory Commission. Retrieved August 2020, from https://www.nrc.gov/docs/ML1125/ML11258A302.pdf
U.S. Nuclear Regulatory Commission. (2011b). *An Approach for Plant-Specific, Risk-Informed Decisionmaking: Technical Specifications (Regulatory Guide 1.177, Revision 1).*
U.S. Nuclear Regulatory Commission. (2012). *Reactor Concepts Manual -- Boiling Water Reactor Systems (ML120970422).* U.S. Nuclear Regulatory Commission.
U.S. Nuclear Regulatory Commission. (2012). *State-of-the-Art Reactor Consequence Analyses Project Volume 1: Peach Bottom Integrated Analysis, NUREG/CR-7110, Vol. 1.*
U.S. Nuclear Regulatory Commission. (2012). *TRACE V5.0 Theory Manual: Field Equations, Solution Methods, and Physical Models*. (N. R. Commission, Producer) Retrieved April 16, 2018, from https://www.nrc.gov/docs/ML0710/ML071000097.pdf
U.S. Nuclear Regulatory Commission. (2012a). *Order Modifying Licenses with regard to Requirements for Mitigation Strategies for Beyond-Design-Basis External Events (EA-12-049).*
U.S. Nuclear Regulatory Commission. (2012b). *NRC Inspection Manual Chapter 0410, Notices of Enforcement Discretion.*
U.S. Nuclear Regulatory Commission. (2014). *NRC Inspection Manual Chapter 0308, Reactor Oversight Process.*
U.S. Nuclear Regulatory Commission. (2015). *Reassessment of NRC's Dollar Per Person-Rem Conversion Factor Policy (NUREG-1530, Rev. 1) (Draft Report for Comment).*
U.S. Nuclear Regulatory Commission. (2016b). *NRC Inspection Manual Chapter 0308 Attachment 3, Significance Determination Process Technical Basis.*
U.S. Nuclear Regulatory Commission. (2017). Acceptance criteria for emergency core cooling systems for light-water nuclear power reactors, Title 10, Part 50.46, of the Code of Federal Regulations.
U.S. Nuclear Regulatory Commission. (2017). *Industry Average Parameter Estimates 2015 Update.* Nuclear Regulatory Commission. Retrieved from Reactor Operational Experience Results and Databases: https://nrcoe.inl.gov/resultsdb/AvgPerf/

U.S. Nuclear Regulatory Commission. (2017a). *Regulatory Analysis Guidelines of the U.S. Nuclear Regulatory Commission (Draft Report for Comment) (NUREG/BR-0058, Revision 5).*
U.S. Nuclear Regulatory Commission. (2017b). *Risk Assessment of Operational Events Handbook, Volume 1 - Internal Events (Revision 2.02).*
U.S. Nuclear Regulatory Commission. (2017c). *Licensee Event Report System, Title 10, Part 50.73, of the Code of Federal Regulations.*
U.S. Nuclear Regulatory Commission. (2017d). *Industry Average Parameter Estimates, 2015 Update.*
U.S. Nuclear Regulatory Commission. (2017e). *Escalated Enforcement Actions Issued to Reactor Licensees, Notice of Violation associated with Red, Yellow, or White Significance Determination Process (SDP) finding: (NOV).*
U.S. Nuclear Regulatory Commission. (2017f). *Risk-Informed Categorization and Treatment of Structures, Systems and Components for Nuclear Power Reactors, Title 10, Part 50.69, of the Code of Federal Regulations.*
U.S. Nuclear Regulatory Commission. (2018a). *Safety Enhancements After Fukushima.*
U.S. Nuclear Regulatory Commission. (2018b). *Average Cost Per Professional Staff-Hour, Title 10, Part 170.20, of the Code of Federal Regulations.*
U.S. Nuclear Regulatory Commission. (2019a). *Mitigation of Beyond-Design-Basis Events, Title 10, Part 50.155, of the Code of Federal Regulations.*
U.S. Nuclear Regulatory Commission. (2019b). *Flexbible Mitigation Strategies for Beyond-Design-Basis Events (Regulatory Guide 1.226, Revision 0).*
U.S. Nuclear Regulatory Commission. (2019c). *NOEDs Issued to Power Reactor Licensees.*
U.S. Nuclear Regulatory Commission. (2019d). *Search Licensee Event Reports (LERs). Filtered by reportability 50.73(a)(2)(i)(A) "The completion of any nuclear plant shutdown required by the plant's technical specifications".*
Ulrich and Boring. (2018). Expanding GOMS-HRA from analog to digital human-machine interfaces. *In Proceedings of the 14th Probabilistic Risk Assessment and Management Conference (PSAM14).* Los Angeles, CA.
Ulrich et al. (2017). Operator timing of task level primitives for use in computation-based human reliability analysis. *Advances in Intelligent Systems and Computing, 589*, 41-49.
Wang, J., Dailey, M., & Corradini, M. (2019). Performance evaluation of accident tolerant fuels (ATF) and reactor core isolation cooling (RCIC) for boiling water reactor. *In Proceedings of American Nuclear Society Winter Meeting.* Washington, D.C.
Westinghouse Owners Group. (2002). *Generic Cost-Benefit Assessment of the Proposed Draft 10 CFR Part 50.69.*
World Nuclear Association. (2017). *The Nuclear Fuel Cycle*. Retrieved from https://www.world-nuclear.org/information-library/nuclear-fuel-cycle/introduction/nuclear-fuel-cycle-overview.aspx
Wu, X., & Shirvan, K. (2019). System code evaluation of near-term accident tolerant claddings during boiling water reactor short-term and long-term station blackout accidents. *Nuclear Engineering and Design*.
Yadav, V., & Biersdorf, J. (2019). *Utilizing FLEX Equipment for Operations and Maintenance Cost Reduction in Nuclear Power Plants (INL/EXT-19-55445).* Idaho National Laboratory.
Yang, J.-H., Wang, J.-R., Shih, C., & Chiang, Y. (2019). *International Agreement Report, The Analysis and Study of ELAP Event and Mitigation Strategies Using TRACE Code for Maanshan PWR (NUREG/IA-0496).*
Yu, J., C. Blakely, and H. Zhang. (2019). Investigation of Zr-based alloy cladding burst mechanisms under Station Blackout using Bison. *Proceedings of Top Fuel 2019.* Seattle, WA.
Zeng, Z., & Zio, E. (2018). Joint Optimization of Business Continuity by Designing Safety Barriers for Accident Prevention, Mitigation and Emergency Responses. *2018 3rd International Conference on System Reliability and Safety (ICSRS)*, (pp. 316-320).
Zhang, H., Szilard, R., & Hess, S. (2018). *R&D Roadmap for Enhanced Resilient Plant Systems, Metrics, Scenarios, Risk Analysis, and Modeling and Simulation.*
Zhang, S., Du, M., Tong, J., & Li, Y.-F. (2019). Multi-objective optimization of maintenance program in multi-unit nuclear power plant sites. *Reliability Engineering & System Safety, 188*, 532-548.